January 2014

# Optimal Allocation Of Distributed Renewable Energy Sources In Power Distribution Networks

Samir Dahal

# OPTIMAL ALLOCATION OF DISTRIBUTED RENEWABLE ENERGY SOURCES IN POWER DISTRIBUTION NETWORKS

by

Samir Dahal

Bachelor of Science, NYU Polytechnic School of Engineering, 2009

A Dissertation
Submitted to the Graduate Faculty

of the

University of North Dakota

in partial fulfillment of the requirements

for the degree of

Doctor of Philosophy

Grand Forks, North Dakota
August
2014

This dissertation, submitted by Samir Dahal in partial fulfillment of the requirements for the Degree of Doctor of Philosophy from the University of North Dakota, has been read by the Faculty Advisory Committee under whom the work has been done and is hereby approved.

Hossein Salehfar (Chair)

Michael D. Mann (Co-Chair)

William D. Gosnold

Prakash Ranganathan

Brian Tande

This dissertation is being submitted by the appointed advisory committee as having met all of the requirements of the School of Graduate Studies at the University of North Dakota and is herby approved.

Wayne Swisher
Dean of the Graduate School

Date

PERMISSION

Title Optimal Allocation of Distributed Renewable Energy Sources in Power Distribution Networks

Department Electrical Engineering

Degree Doctor of Philosophy

In presenting this dissertation in partial fulfillment of the requirement for a graduate degree from the University of North Dakota. I agree that the library of this University shall make it freely available for inspection. I further agree that permission for extensive copying for scholarly purposes may be granted by the professor who supervised my dissertation work or, in his absence, by the Chairperson the department or the dean of the School of Graduate Studies. It is understood that any copying or publication or other use of this dissertation or part thereof for financial gain shall not be allowed without my written permission. It is also understood that due recognition shall be given to me and to the University of North Dakota in any scholarly use with may be made of any material in my dissertation.

Signature Samir Dahal

Date July 10th, 2014

TABLE OF CONTENTS

LIST OF FIGURES

LIST OF TABLES

## ACKNOWLEDGEMENTS

I would like to express deepest appreciation to my advisor Dr. Hossein Salehfar for trusting me to come up with this fascinating project and being patient, understanding, encouraging, generous and an outstanding role model. I would also like to thank my co-advisor Dr. Michael Mann for constantly encouraging me and always providing a positive feedback when things seemed slow. I am very grateful for having had an opportunity to work with Dr. William Gosnold. Thank you for allowing me to be a part of geothermal power team at UND and teaching me the importance of collaborative work. I appreciate all the comments, suggestions, and thoughtful reviews by my dissertation committee members: Dr. Prakash Ranganathan and Dr. Brian Tande.

I would like to thank my peers, Gahendra Kharel, Jivan Thakare, Mark Mcdonald, Kirtipal Barse, and Dr. Taehee Han for their support. My time at UND would not have been this enjoyable without their invaluable friendship.

I would have not been able to complete my work had it not been for the constant support of my wife Rejwi. She has always inspired me to be an optimist and encouraged me to excel and achieve beyond what I think I am capable of. I am also grateful for the support of my in laws. They have been my second parents and have always supported me in this endeavor. Finally, I want to thank my parents who have been incredibly supportive of this whole process. Thank you for believing in me, for encouraging me to be the best I can be, and providing me with a strong foundation.

To dada and mommy.

## ABSTRACT

In this dissertation study, various methods for optimum allocation of renewable distributed generators (DGs) in both balanced and unbalanced distribution networks have been proposed, developed, and tested. These methods were developed with an objective of maximizing several advantages of DG integration into the current distribution system infrastructure.

The first method addressed the optimal sitting and sizing of DGs for minimum distribution power losses and maximum voltage profile improvement of distribution feeders. The proposed method was validated by comparing the results of a balanced distribution system with those reported in the literature. This method was then implemented in a co-simulation environment with Electric Power Research Institute's (EPRI) OpenDSS program to solve a three phase optimal power flow (TOPF) problem for optimal location and sizing of multiple DGs in an unbalanced IEEE-123 node distribution network. The results from this work showed that the better loss reduction can be achieved in less computational time compared to the repeated load flow method.

The second and third methods were developed with the goal of maximizing the reliability of distribution networks by optimally sitting and sizing DGs and reclosers in a distribution network. The second method focused on optimal allocation of DGs and reclosers with an objective of improving reliability indices while the third method demonstrated the cost based reliability evaluation. These methods were first verified by

comparing the results obtained in a balanced network with those reported in literature and then implemented on a multi-phase unbalanced network. Results indicated that optimizing reclosers and DGs based on the reliability indices increases the total cost incurred by utilities. Likewise, when reclosers and DG were allocated to reduce the total cost, the reliability of the distribution system decreased.

The fourth method was developed to reduce the total cost incurred by utilities while integrating DGs in a distribution network. Various significant issues like capital cost, operation and maintenance cost, customer service interruption cost, cost of the power purchased from fossil fuel based power plants, savings due to the reduction in distribution power losses, and savings on pollutant emissions were included in this method. Results indicated that integrating DGs to meet the projected growth in demand provides the maximum return on the investment.

Additionally, during this project work an equivalent circuit model of a 1.2 kW PEM fuel cell was also developed and verified using electro impedance spectroscopy. The proposed model behaved similar to the actual fuel cell performance under similar loading conditions. Furthermore, an electrical interface between the geothermal power plant and an electric gird was also developed and simulated. The developed model successfully eliminated major issues that might cause instability in the power grid. Furthermore, a case study on the evaluation of geothermal potential has been presented.

# CHAPTER 1

# INTRODUCTION

## 1.1. Background

In recent years, the penetration of intermittent renewable energy sources such as wind and solar into the U.S. energy profile has increased significantly. In fact, most of the States have adopted renewable portfolio standards (RPS) that would require electric utilities to supply at least 20% of their load with the electricity generated from renewable sources by the year 2030 [1]. However, the present electric power system infrastructure is not built to incorporate and accommodate large number of renewable energy systems due to their unpredictable characteristics. The integration of renewable systems into existing power systems requires careful planning and decision making as to their size and intermittent capacity contribution to the production mix of the electric utilities at any given time. The most efficient way to utilize renewable sources of energy is by placing them near load or demand side. Energy sources utilized in this manner are known as distributed generators (DGs). Since most DG systems are intermittent sources and have a potential of inducing power system instability problems, it is essential to determine the appropriate location and penetration of renewable resources into distribution networks. This would result in minimum fluctuations in network stability and maximum profit for utilities while accommodating the time varying demand for electricity. As a result numbers of studies have been performed to determine the optimal size and capacity of DGs into the energy production mix.

## 1.2. Problem Statement

The importance of proper DG integration into the distribution system has been investigated in a number of studies. Authors in [2]–[9] have demonstrated the reduction of power loss by optimally sizing and placing DGs in distribution networks. Similarly, in [10]–[14] optimal sizing and location of DG resulted in improved reliability of the network. As power loss decreases and reliability increases, profit for utility increases as well. Therefore, for utilities, integrating DGs in distribution networks provides the dual advantage of meeting the RPS and strengthening their infrastructure while reducing the cost. However, most of these studies have been performed on balanced distribution systems. Distribution networks in actual power systems are multi-phase unbalanced systems because of unequal three phase loads, untransposed lines and conductor bundling [15]. As a result, existing literatures fail to provide a realistic insight into the actual problem.

Even though a number of studies on the effect of DGs on the reliability of distribution networks are available in the literature, to the best of the author's knowledge none of these studies are conducted in three phase unbalanced distribution networks [10]–[14], [16]–[21]. Furthermore, these studies are conducted with DGs located at a fixed bus and can only supply active power at all times. This assumption ignores the fact that utilities are required to accommodate multiple DGs that can interact with both active and reactive powers in their network. Hence, these studies do not provide an actual insight into the correlation between DG allocation and reliability of the distribution systems.

During the planning phase of DG integration into the present power infrastructure, the goals of utilities must be kept in mind first, namely, providing a reliable and secure

electric supply to customers at the lowest cost while maximizing profits. Once this optimal situation has been described, individual factors to consider for the creation of a model to achieve this ideal can be identified. These factors may include reduction in distribution loss, improvement in reliability, and reduction in pollutants. Thus, a thorough cost benefit analysis must be conducted by including all these factors to maximize the potential benefits that can be achieved by connecting DGs to the distribution networks. This research attempts to provide the framework for such planning while overcoming the aforementioned drawbacks in the DG allocation problem.

### 1.3. Research Objectives

The primary objective of this work is to optimally allocate renewable DGs in a multi-phased unbalanced distribution network. In this research the term "optimal allocation" refers to finding the best sitting and sizing of DGs that would result in:

i) Minimum distribution loss and maximum improvement in feeder voltage profile.

ii) Maximum reliability of the system while reducing the cost in the investment of protective devices.

iii) Minimum cost incurred by the utility as a result of DG integration.

In order to accomplish the primary objective, the following secondary objectives have been established:

1) Investigate the impact of DGs on the distribution power loss and voltage profile of distribution networks.
2) Improve the reliability of distribution systems via the optimal allocation of DGs.

3) Reduce the total cost incurred by the utility due to the integration of DGs in the distribution system.

All of these objectives can be achieved only when the proper power electronics interfaces are available to reduce various instabilities caused by the intermittent nature of renewable DGs. However, development of an effective interface requires an accurate model of these renewable energy systems. Hence, this research has the following two additional objectives.

4) Develop and verify an equivalent circuit model of a 1.2 kW PEM fuel cell.
5) Model and simulate an electrical interface between geothermal power plants and electric grid.

## 1.4. Methodology

Objective 1 has been accomplished by developing a method based on Newton Raphson load flow and Particle Swarm Optimization (PSO) to solve the distribution power flow and optimize the location and sizing of various types of DGs [22]. The proposed method is tested on a balanced IEEE-69 bus distribution system and results are compared with those obtained using Improved Analytical (IA) method and Artificial Bee Colony (ABC) method. After verifying the effectiveness of the proposed PSO method, it is then used in a co-simulation environment with OpenDSS program to solve Three Phase Optimal Power Flow (TOPF) problem for optimal location and sizing of multiple DGs in an unbalanced IEEE-123 node distribution network [23].

Objective 2 has been accomplished by implementing a Discrete Particle Swarm Optimization method (DPSO) for optimal allocation of reclosers and DGs in a distribution network [24]. The first part is focused on optimal allocation with an objective

of improving reliability indices while the second part demonstrates the cost based reliability evaluation. The effectiveness of the proposed method is verified by testing it on a balanced IEEE-90 bus distribution network and comparing the results with those reported in the literature. This method is also implemented and tested on multi-phase unbalanced IEEE-123 node distribution feeder.

Objective 3 has been accomplished by first developing a cost function, also known as objective function, which represents the total capital cost, operation and maintenance cost, cost of the power that needs to be purchased, cost related to the reliability of the system, and cost associated with pollutant emissions. This objective function is then minimized by implementing the PSO method in a co-simulation environment with OpenDSS program. Assuming an annual growth of 2% in power demand, the proposed method is tested on the IEEE-123 node distribution feeder.

Objective 4 has been accomplished by developing a program based on the Levenberg-Marquardt (LM) algorithm to extract the initial values of the components that are to be used in the equivalent circuit model from the Nyquist plots obtained using electrochemical impedance spectroscopy (EIS) [25][26]. The equivalent circuit model is developed by using various electrical components whose values are given by the proposed LM based program. This model is then validated by obtaining impedance plots at various operating conditions and comparing them with the impedance plots obtained from the real fuel cell operation and performance using EIS.

Objective 5 has been accomplished by developing a simulation model of the induction generator based geothermal power plants in a MATLAB/SIMULINK environment with connection to the electric grid through an AC-DC-AC converter. The

voltage obtained from the generator is first rectified by a six pulse diode bridge. The filtered DC voltage is then applied to an IGBT based inverter which generates a 60 Hz AC voltage.

## 1.5. Layout of Dissertation

The remainder of this dissertation includes seven chapters. Chapters 3 through 7 are based upon papers that have been written by the author and have been published or submitted for publications. Chapter 2 discusses renewable distributed generators (DGs) and their impact on stability, distribution power losses, and reliability of distribution networks.

Chapter 3 discusses the impact of location and sizing of DGs on distribution power losses and voltage profile of various distribution networks. Effects of DG integration on power losses of both balanced and unbalanced distribution networks are presented in this chapter. The basis for this chapter are [27] and [159].

Chapter 4 proposes two distinct methods for optimal allocation of reclosers and DGs for reliability improvement of both balanced and unbalanced distribution networks. The first method optimizes the allocation of DGs and reclosers with the objective of improving reliability indices while the second method demonstrates the cost based reliability evaluation. The basis for this chapter is [160].

Chapter 5 proposes a method for optimal allocation of various types of DGs on the distribution system to minimize the total cost incurred by the utility. Here, the planning problem is formulated by converting several factors like, investment cost, OM cost, reliability, pollutant emission, and power purchased by the utility, into a cost function and optimizing this cost function using the PSO method. The basis for this chapter is [161].

Chapter 6 discusses the development of an equivalent circuit model (ECM) of a 1.2 kW PEM fuel cell. A computer program based on Levenberg – Marquardt algorithm is implemented to obtain values of the electrical components used in the ECM of the fuel cell from a Nyquist plot obtained via Electrochemical Impedance Spectroscopy (EIS) method. The basis for this chapter is [162]

Chapter 7 presents the development and simulation of an electrical interface between geothermal power plants and electric grid. A case study on the evaluation of geothermal power potential is also presented in this chapter. This chapter is based on [163] and [164]

Chapter 8 summarizes the work presented in this dissertation and recommends a future research direction.

## 1.6. List of Published Work

Based on the work of this research and related work, the following papers have been written and submitted for the review, presentation, and/or publication at national and international conferences and technical journals.

1. **S. Dahal** and H. Salehfar, "Optimal location and sizing of distributed generators in distribution networks," in *2013 North American Power Symposium (NAPS)*, 2013, pp. 1–6. ***(won third best paper award during 2013 NAPS)***
2. **S. Dahal**, M. Mann, and H. Salehfar, "Development and verification of an Electrical Circuit Model of Proton Electrolyte Membrane (PEM) fuel cell using Impedance spectroscopy," Journal of Power Sources, submitted.

3. **S. Dahal** and H. Salehfar, “Impact of Distributed Generators on the Power Loss and Voltage Profile of Three Phase Unbalanced Distribution Networks”, *International Journal of Power and Energy systems*, submitted.

4. **S. Dahal** and H. Salehfar, “Reliability Evaluation of DG Enhanced Unbalanced Distribution Networks”, in preparation.

5. **S. Dahal** and H. Salehfar, “Cost Minimization Planning for Allocation of Distributed Generators in Unbalanced Distribution Networks”, in preparation.

6. **S. Dahal**, M. R. McDonald, and B. Bubach, “Evaluation of Geothermal Potential of Lightning Dock KGRA, New Mexico,” *Geothermal Research Council transaction*, vol. 36, Sept. 2012

7. R. Klenner, M. R. McDonald, **S. Dahal**, A.M. Crowell, and A. V. Oploo, “Evaluation of the geothermal potential in the Rio Grande Rift: San Luis Basin, Colorado and New Mexico,” *The Mountain Geologist*, v. 48, no. 4, pp. 107-119.

8. **S. Dahal**, H. Salehfar, W. Gosnold, and M. Mann, “Modeling and simulation of the interface between geothermal power plant based on organic rankin cycle and the electric grid,” *Geothermal Research Council transactions*, vol. 34, pp 1011-1016, Oct. 2010.

9. T. Han, T. A. Haagenson, H. Salehfar, **S. Dahal** , and M. D. Mann “An efficient approximation method for an individual fuel cell impedance characterization,” in Proc. ASME Eighth International Fuel cell Science, Eng. and Tech., pp 735-739, June 2010**.**

# CHAPTER 2

# RENEWABLE DISTRIBUTED GENERATION

## 2.1. Introduction

Typical power system design in the United States is radial, with large centers of generation producing hundreds of gigawatts (GW) of power, often delivered across hundreds of miles to the consumers. High voltage lines compose the transmission system, with loads connected at middle and low voltage levels. However, this familiar blueprint is slowly changing. Increasingly, due to a number of factors, alternative sources of generation are being incorporated into the existing power grid. New renewable portfolio standards (RPS) established by many States require certain percentage of retail electricity sold in the State to be obtained from renewable energy sources. Availability of subsidies for renewable energy installations, from State and federal governments, for individuals as well as communities, has also increased the development of sustainable distributed generations (DGs) which are small generation plants, usually with the output of less than 10 megawatts (MW) that are connected directly to the distribution network. Other contributing factors to the growth in DG include concerns over environmental impacts of emissions from traditional modes of power generation and declining costs of manufacturing and materials for various DG technologies.

## 2.2. Impacts of Distributed Generators

In traditional power systems, distribution networks were designed for a unidirectional power flow in which the primary substation was the only source of power.

In those systems, voltage would decrease towards the end of the radial spokes, or feeders, as the load caused a voltage drop. However, addition of DG into the distribution system creates a reverse power flow which can degrade the power system protection system. Additionally, the voltage level at the point of DG connection increases which leads to an altered voltage profile on the feeder. A specific example of the impact that a renewable distribution resource can have on the power system is the case of wind turbines. Induction generator based turbines require reactive power compensation. While this is often balanced by the installation of capacitor banks, it is nonetheless another consideration in an already complex system, and is the type of consideration that should be considered and represented during DG integration planning. Finally, many forms of renewable DG are variable sources - generating at given times, and offline at others, with a relatively unpredictable schedule. Not only do voltage and current profiles require attention in this case, but also the reliability of the supply would be a concern.

Nevertheless, most of the distribution systems are well designed and sufficiently large in capacity. Thus, despite the fact that they were not intended for DGs inclusion, they can still handle some amount of DG as long as the appropriate protection functions are utilized. Furthermore, when such DGs are added in modest quantities and operated at the right time and locations, they can actually improve the performance of the distribution system, rather than degrade it [28]. Following sections examine the significant impacts of DGs on various characteristics of the existing distribution network.

### 2.2.1. Stability

Stability is the ability of the power system to deliver power under relatively stable conditions. Power system stability is heavily dependent on the fluctuation of the voltage

profile and system frequency in the distribution feeders. According to American national standard institute (ANSI) standard C84.1, the range of acceptable customer service voltage is ± 5 percent of the nominal level with +6% or -8% acceptable for occasional short-term events. DGs, however, have a greater impact on the system voltage than they do on the frequency. This is due to DG's ability to change the voltage only at the connection point without changing the voltage across the entire distribution system. Thus, the capacity of DG needs to be relatively significant compared to the total system capacity. Since the largest DG units of 50MW are still less than 0.01% of eastern or western area generation, integration of DGs do not significantly impact the frequency [28]. Numerous studies have been performed to better understand the effect of DGs on voltage fluctuation. Authors in [29] have investigated the impacts of changing the location, size and loading condition of DGs on the voltage profile of a distribution system. Effects of DG on distribution losses and voltage regulations including voltage flicker and harmonics have been presented in [30].

A novel method of locating and sizing DG units to improve the voltage stability margin has been presented in [31]. By considering the probabilistic nature of load and renewable DG, authors in [31] proposed a method to first select candidate buses to install the DG units, prioritizing those buses which are sensitive to voltage profile and thus improving the voltage stability margin. Similarly, [32] investigated the application of DGs as voltage regulators. Here, the output of DG was controlled in such a way that acceptable level of power quality is achieved with a reasonable operating cost. The relationship between the location and sizing of DG and their effect on voltage fluctuations has been discussed in [33]. This paper addressed a possible under-voltage

condition when DGs are installed on a feeder with load-tap changing (LTC) transformer. Additionally, several studies have proposed a method to control and improve the voltage profile by integrating DGs into the distribution system [33-35]. In [34], authors proposed a DG control method to improve the voltage profile. A simple analytical method to estimate the voltage profile of a radial distribution feeder while connecting DG whose active and reactive power generations were constrained by the permissible voltage level is presented in [35]. The authors of [36] proposed a voltage coordination method of DGs for proper voltage regulation in distribution system using load-tap changing transformers and line drop compensators. Here, the distribution system voltage is coordinated by controlling the reactive power of DGs according to their real power output.

### 2.2.2. Distribution Losses

The U.S. transmission and distribution systems have an estimated 8-10 percent total loss [28]. Even though, this loss percentage is small, it still accounts for almost 7 billion megawatt hours of lost electricity [37]. Almost 70% of these losses occur in distribution networks [38]. The optimal placement and dispatch of DGs can significantly reduce these losses. Ideally, to get the maximum reduction in losses, DGs must be located at correct points on the feeder system, dispatched around the time of peak system losses and operated at the optimal output power levels. However, a DG that is too large for a given feeder location creates a reverse power flow and increases the total distribution losses [39], [40].

Placement of DGs to optimize losses in power systems is similar to the capacitor placement for the same purpose. The only difference is that capacitors can only supply reactive power while DGs can impact both real and reactive power flows. Minimizing

distribution losses has an added benefit of reducing the voltage drop and improving the voltage profile of the distribution network [41].

Numbers of studies have validated the effectiveness of optimal allocation of DGs on distribution loss reduction. Authors in [2]–[9] have demonstrated the reduction in power losses by optimally sizing and placing DGs in distribution networks. An analytical method based on exact loss formula is proposed in [4]. This method can optimally site and size a single DG in a distribution network. In [42], an analytical method in combination with Kalman filter algorithm is proposed to optimize the location and sizing of DGs for loss reductions.

A summary of the studies that propose various optimal DG allocation methods for distribution loss reductions is presented in Table 1. The Table lists the method used by authors to optimize the allocation of DGs, the number of DGs integrated in the system, and the load profiles used for calculating distribution losses.

Table 1. Summary of the studies that propose optimal DG allocation for distribution loss reduction

| Reference | Method Used | Number of DGs | Load Profile |
|---|---|---|---|
| Rao et. el, [9] | Harmony Search Method | Multiple | Multi level |
| Hung et. el, [8] | Improved analytical method | Multiple | One load level |
| Arya et. el, [7] | Differential Evolution | Multiple | One load level |
| Atwa et. el, [41] | Mixed Integer non linear programming | Multiple | Time varying |
| Ochoa et. el, [43] | Multi period optimal AC power flow | Multiple | Multi-level |
| Willis [44] | The “2/3” rule | Single | One load level |
| Wang et. el [45] | Analytical method | Single | Time varying |
| Acharya et. el [4] | Analytical method | Single | One load level |
| Mouti et. el [6] | Artificial bee colony | Multiple | One load level |
| Mouti et. el [46] | Heuristic curve fitting | Single | One load level |
| Hedayati et. el [47] | Continuation power flow | Multiple | One load level |
| Costas et. el [48] | Analytical method | Single | One load level |
| Alhajri et. el [49] | Improved sequential quadratic programming | Multiple | One load level |
| Hamedi et. el [50] | CYMEDIST software application | Multiple | Multi-load level |

### 2.2.4. Reliability

Reliability plays an important role in the success of DG integration activities. Addition of DGs into the distribution networks is only appreciated when service interruptions that impact the distribution system customers are reduced. DGs can negatively affect service reliability because, as has been discussed earlier, they generate bi-directional power flows which can confuse the operation of grid protection equipments.

However, if the protection equipments are properly placed and coordinated, DGs can improve the overall reliability of the system. This is only possible when DGs are allowed to operate in islanding condition. Islanding is a situation in which DG installations and portions of the distribution system have become isolated from the rest of the system but DGs in the islanded section continue to operate and serve the consumer loads in the section [28]. While unintentional islanding can pose serious dangers like damaging the distribution system equipments, increasing the incidents of energized and downed feeders, delaying service restoration, and violating voltage and frequency requirements for connected loads, properly planned intentional islanding allows DGs to support the islanded section until the service is restored to the whole system. For an effective islanding, DGs must be able to support the islanded load while maintaining the voltage and frequency requirements. They must also be able to handle any transient-starting inrush essential to restart the island.

Numerous studies have shown the effectiveness of DGs in improving the reliability of distribution networks [10]–[14], [16]–[21]. All of the reviewed studies show that with proper allocation of DGs, the reliability of distribution system can be increased significantly while reducing the distribution system losses.

A summary of the reviewed studies on the reliability evaluation of DG enhanced distribution networks is given in Table 2.

Table 2. Summary of the reviewed studies on the effects of DGs on system reliability.

| Reference | Objective |
|---|---|
| Pregelj et. el, [51] | Minimization of various reliability indices by optimally placing reclosers in a DG enhanced feeder using genetic algorithm. |
| Singh et. el, [11] | Minimization of reliability indices by optimally allocating reclosers and DGs using Ant Colony System algorithm. |
| Conti et. el, [12] | Improvement in the system adequacy using analytical methods |
| Li et. el , [14] | Minimization of various reliability indices by optimally placing reclosers in a DG enhanced feeder using multiple population genetic algorithm. |
| Chowdhury et. el, [16] | Maximization of the deferred capital investment by improving the reliability of the system as a result of DGs integration. |
| Brown et. el [17] | Investigation of the positive and negative impacts of DGs on system reliability by using predictive reliability assessment tools. |
| Fotuhi-Firuzabad et. el, [18] | Investigation on the effects of DGs on various reliability indices by analytical methods. |
| Yun et. el, [19] | Development of reliability evaluation methods based on momentary interruptions and cost evaluation which unifies the sustained and momentary interruption costs. |
| Falaghi et. el, [20] | Investigation on the effects of location and sizing of DGs on various reliability indices. |
| McDermott et. el, [21] | Investigation on positive and negative effects of DGs on reliability of the distribution system. |

# CHAPTER 3

# OPTIMAL DG ALLOCATION FOR MINIMUM POWER LOSS AND MAXIMUM VOLTAGE IMPROVEMENT

## 3.1 Optimal Location and Sizing of Distributed Generators in Balanced Distribution Networks.

Using a combination of Particle Swarm Optimization (PSO) and Newton-Raphson load flow methods this section investigates the impact of location and size of distributed generators on distribution systems. Similar to the existing improved analytical (IA) method, the proposed approach optimizes the size and location of distributed generators with both real and reactive power capabilities. However, studies show that the proposed method yields much better results than the IA technique and with less computation times. In addition, compared to other evolutionary algorithms such as Artificial Bee Colony (ABC), the proposed method achieves a better distribution system voltage profile with smaller DG sizes. To show the advantages of the proposed method, the IEEE 69-bus distribution system is used as a test bed and the results are compared with those from IA and ABC approaches.

### 3.1.1 Introduction

In recent years, the penetration of renewable energy sources into the U.S energy profile has increased significantly. According to the United States Energy Information Administration (USEIA), the contribution of renewable energy sources has now reached 13% with a target of reaching 25% by 2020 [52].

Since most of the renewable energy sources are readily available in most part of the world, they reduce the necessity of centralized power generation stations. As a result, renewable sources of energy are being utilized in the form of distributed generation (DG) in distribution systems. In addition to reducing the negative environmental effects, implementing renewable sources of energy as DGs can drastically reduce the distribution system losses and improve voltage regulation, power quality, and the reliability of the power supply [2–4]. However, losses in the distribution system will increase significantly if the location and size of DGs are not properly determined [3–6]. Hence, for a reliable and efficient operation of the electric grid, optimum allocation of DGs is a must task.

Several techniques have been proposed to determine the optimum position and size of DGs. The two-third rule, which is commonly applied in the allocation of capacitors in distribution systems, has been proposed in [56] and [45]. Despite the simplicity of its application, the unrealistic assumption of uniformly distributed loads in a distribution system makes the two-third rule ineffective in applications with DGs included. An analytical method for DGs placement to reduce system losses has been presented in [8]. Although this method determines the location of a single DG in both radial and network distribution systems, it does not provide the optimal size of DGs. Authors in [4] utilize an analytical method to obtain the optimal location and size of a single DG unit. This method is based on an exact loss formula and power flow method and is employed only twice, once with DG and once without DG. Although promising, this method does not account for any constraints such as voltage requirements that the distribution systems must meet. In [6], authors have proposed an artificial bee colony (ABC) algorithm to determine the optimal location, size, and power factor of DGs by

minimizing the total system power losses. Similarly, a combination of genetic algorithm and particle swarm optimization has been used in [57] to optimize the sizing and location of DGs.

Most of the techniques currently available in the literature are based on the assumption that DGs can only deliver real power. This assumption is unrealistic because there are many types of DGs that provide and/or consume both active and reactive powers. The most significant work dealing with all types of DGs has been presented in [58]. Authors in [58] utilize an improved analytical (IA) method, a modification of the method proposed in [4], to obtain the optimal location and size of a single DG unit. Although robust, this method also provides similar results as those of the original analytical method. Moreover, the IA method optimizes the DG size and location separately. Optimal location can only be obtained after determining the optimal size.

To address this issue, the author of the present document uses a combination of particle swarm optimization technique and the Newton- Raphson load flow method to determine the optimal location and size of DGs simultaneously in order to reduce the active power losses in the distribution system. Using the IEEE 69-bus distribution system as a test bed, the results from the proposed method and those from the IA and ABC methods are compared and discussed. Section 3.1.2 of this document summarizes the IA method and the proposed method. For a detailed description of the ABC method, the reader is referred to [6]. Section 3.1.3 discusses and compares the results. Finally, section 3.1.4 presents the conclusions on this work.

### 3.1.2 Methodology

***Improved Analytical Method***. This method is a modification of the analytical method presented in [4] which is based on the exact loss formula given by (1).

$$P_L = \sum_{i=1}^{N}\sum_{J=1}^{N}[\alpha_{ij}(P_iP_j + Q_iQ_j) + \beta_{ij}(Q_iP_j - P_iQ_j)] \quad (1)$$

Where,

$\alpha_{ij} = \frac{r_{ij}}{V_iV_j}\cos(\delta_i - \delta_j)$

$\beta_{ij} = \frac{r_{ij}}{V_iV_j}\sin(\delta_i - \delta_j)$

$V_i$ Voltage magnitude at bus i

$\delta_i$ Voltage angle at bus i

$z_{ij} = r_{ij} + jx_{ij}$ ij$^{th}$ element of the [Zbus] matrix

$P_i\ and\ P_j$ active power injection at buses i and j, respectively

$Q_i\ and\ Q_j$ reactive power injection at buses i and j, respectively

$N$ number of buses.

Equation (1) has been modified to obtain the improved analytical method as given by (2).

$$P_{DGi} = \frac{\alpha_{ii}(P_{Di} + xQ_{Di}) + \beta_{ii}(xP_{Di} - Q_{Di}) - X_i - xY_i}{x^2\alpha_{ii} + \alpha_{ii}} \quad (2)$$

Where,

$P_{DGi}$ : real power injected by DG at bus i

$P_{Di}$ : real load demand at bus i

$x$ : $\tan(\cos^{-1}(PF_{DG}))$

$Q_{Di}$ : reactive load demand at bus i

$X_i$ : $\sum_{\substack{j=1 \\ j\neq i}}^{N}\left(\alpha_{ij}P_j - \beta_{ij}Q_j\right)$ and,

$Y_i$ : $\sum_{\substack{j=1 \\ j\neq i}}^{N}(\alpha_{ij}Q_j - \beta_{ij}P_j)$

Equation (2) provides the optimum size for all types of DGs. The value of *x* turns to be positive and constant for DGs that inject both real and reactive power and it will be negative and constant for DGs that inject real power but consume reactive power [57]. Optimal location of DGs is obtained by comparing the power losses after injecting the optimal size of DGs at various locations in the distribution network. The case which results in minimum losses is considered to be the optimal location.

***Particle Swarm Optimization:*** Particle swarm optimization (PSO) technique has been commonly used to calculate the optimum power flows in power systems [59]–[61]. However, its use in the allocation of DGs is relatively a new topic. In PSO, a set of particles, each representing a potential solution (fitness), moves freely in a multi dimensional search space. The position and velocity of a particle i are represented by vectors $X_i$ and $V_i$, respectively. During the flight, each particle knows its best value *Pbest* and its position up to that point. Moreover, each particle also knows the best value of the group *Gbest* among all the *Pbest* values. Hence, each particle i is continuously updating its velocity and position in a manner given in Equations (3) and (4) [60].

$$V_i^{k+1} = \omega V_i^k + c_1 rand\left(Pbest_i^k - X_i^k\right) + c_2 rand(Gbest_i^k - X_i^k) \quad (3)$$

$$X_i^{k+1} = X_i^k + V_i^{k+1} \quad (4)$$

Where,

$V_i^k$: current velocity of particle i at k[th] iteration

$X_i^k$: current position of particle i at k[th] iteration

$c_1, c_2$: positive constants

$Pbest_i^k$: best position of particle i until k[th] iteration

$Gbest_i^k$: best position of the group until k[th] iteration

*Rand:* random numbers between 0 and 1

$\omega$: inertial weight parameter

In this study, a new inertia weight as proposed by authors in [61] is used. This weighting factor $\omega$ is defined as a function of the local best ($Pbest$) and the global best ($Gbest$) values of the objective function for each generation and is given by (5) as:

$$\omega_i = (1.1 - \frac{Gbest_i}{Pbest_i}) \tag{5}$$

Where, i is the i[th] iteration.

Although the value of the acceleration constants $c_1 \; and \; c_2$ ranges from 1.0 to 2.0, higher values of them decrease the solution time [60]. Hence $c_1 \; and \; c_2$ are set as 2.

***Objective function:*** The main objective of the proposed method is to reduce the real power losses in the distribution system as given by equation (1). For IA, equation (2) is used as an objective function. The following constraints must be satisfied during the optimization process:

1) The voltage at every bus in the network should be within the acceptable range of ± 5% [62].

2) The network power flow equation must be satisfied

### 3.1.3 Results and Discussion

Using a combination of the particle swarm optimization techniques and the Newton- Raphson method, the proposed PSO has been implemented in the MATLAB program environment as shown in Figure 1. The proposed methodology is tested using the IEEE 69-bus radial distribution system with a total load of 3.8 MW and 2.69 MVAR [63]. A single line diagram of the test system is shown in Figure 2. Although, the proposed method can be used for all forms of renewable DGs, results of only those DGs that are capable of supplying both real and reactive powers are presented here. The power factor of the DGs used in this study is arbitrarily set to 0.82 lagging.

***Size allocation:*** Figure 3 shows the optimal size of DGs at the respective locations for the IEEE 69-bus test system. In this Figure, the black and gray color bars represent the optimum sizes obtained using the IA and the proposed PSO methods, respectively. One can easily see that the sizes of DGs obtained from the PSO method are smaller than those obtained from IA.

***Location selection:*** The IA method requires the calculation of optimal sizes before determining the optimal locations. The PSO method, on the other hand, calculates the optimum sizes and locations simultaneously. The optimal location of DGs is where the total power loss of the system is minimum. Using the optimum sizes found in the previous section, the total power loss of the test system is calculated. Figure 4 compares the total power losses of the system obtained by using both the proposed PSO and IA methods. The total power loss by IA is much higher compared to that of PSO. Notice that the loss pattern of the test system is similar in both IA and PSO. Although the

minimum loss occurs at bus 61 for both methods, the minimum loss for IA is 83 kW whereas the minimum loss for PSO is 43 kW.

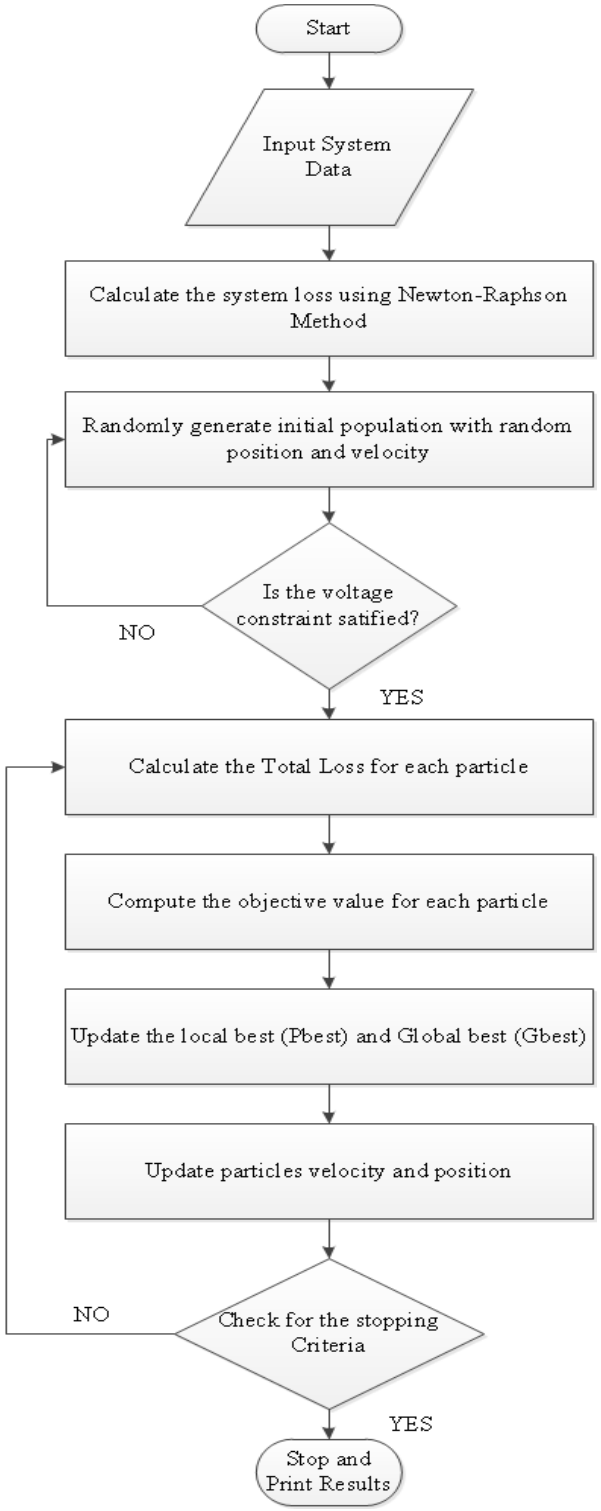


Figure 1: Flow chart of the proposed PSO method for DG allocation

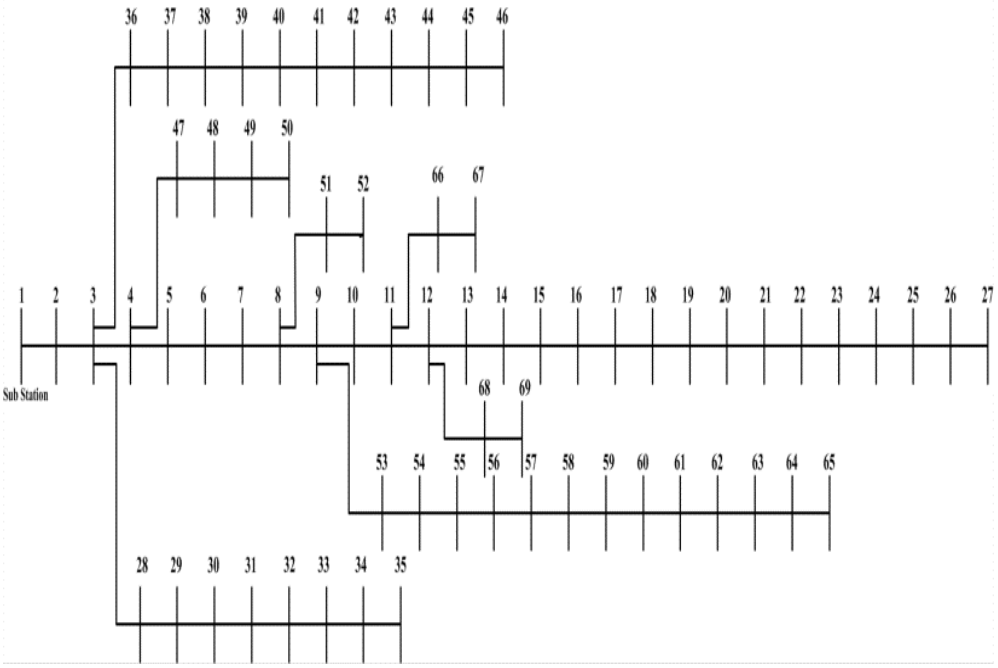


Figure 2. One line diagram of IEEE-69 bust distribution system

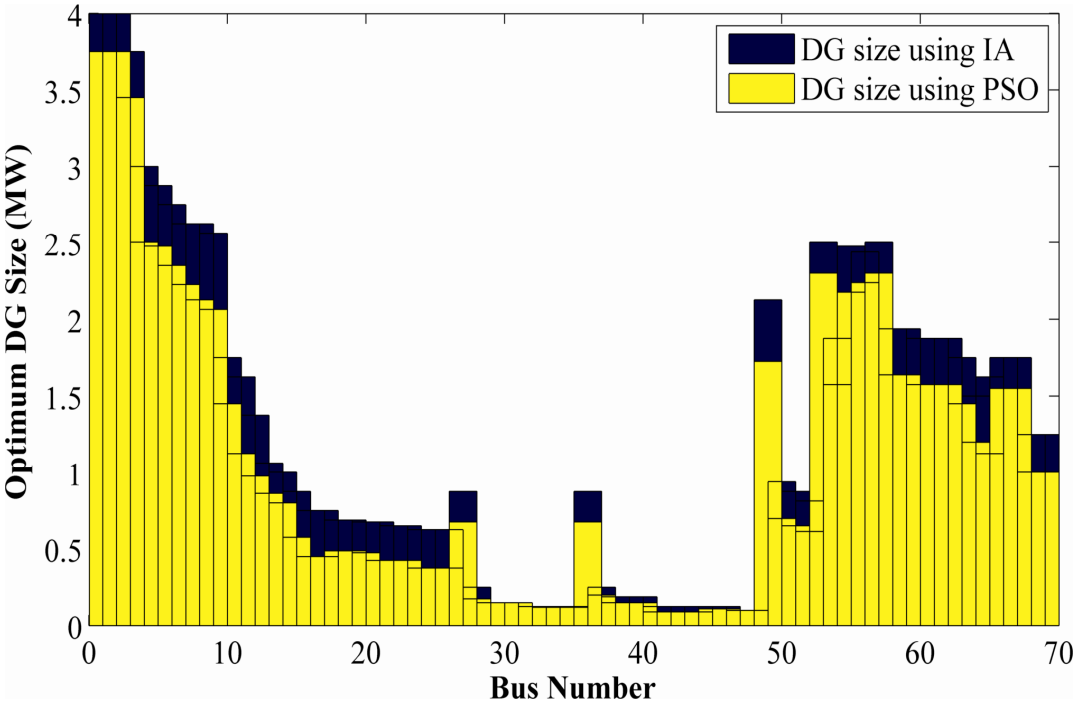


Figure 3. Optimum size of DG at respective buses

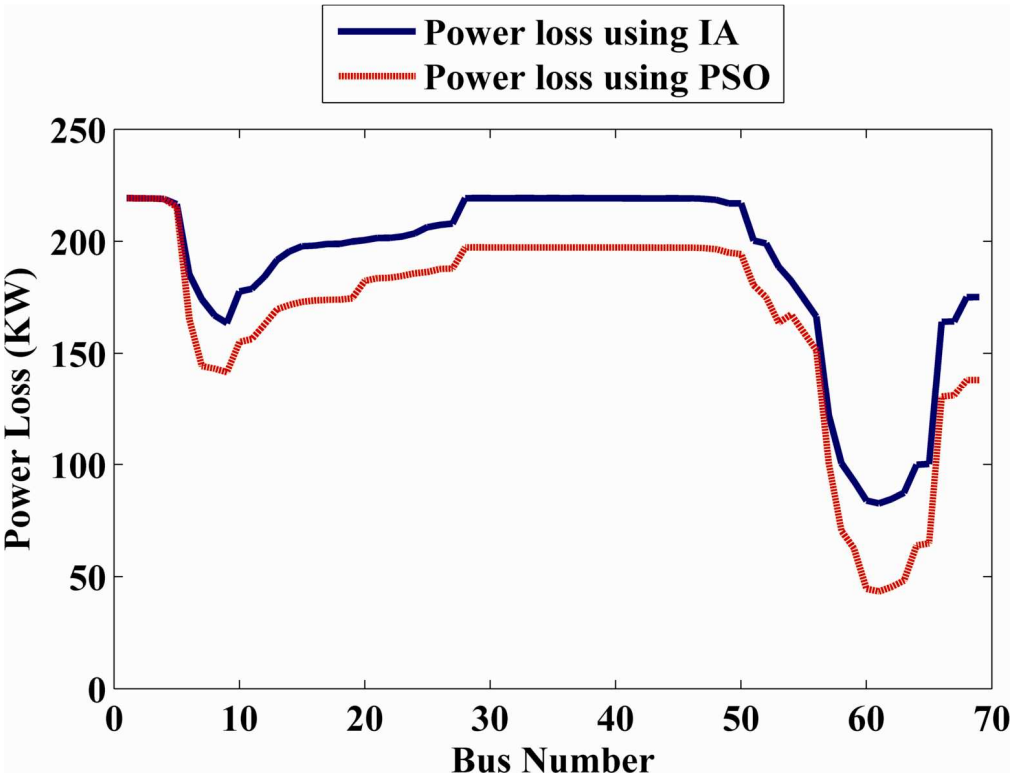


Figure 4. Power loss at each bus after insertion of DGs with 0.82 lagging power factor.

***Voltage profile*:** Figure 5 shows the improvement in voltage profiles at each bus of the test system with DGs included. The Figure also shows the voltage profile before DGs installation. While both IA and PSO improve the system voltage and provide a more uniform and stable profile, a better improvement is achieved by the proposed PSO method.

Compared to IA, the PSO method can significantly reduce the optimum size of DGs and power losses in a distribution network. In addition, the computational time for the PSO is significantly lower than that of IA. This is because IA requires a step wise optimization whereas PSO is able to optimize both size and location simultaneously. Also, PSO is very efficient in finding the global minimum [61]. Note that since capacitor

banks only supply reactive power, the proposed PSO method can be used for the allocation of capacitor banks as well.

In order to show the advantages of the proposed method and for comparison purposes, Table 3 shows a summary of the results including optimum location, corresponding optimum size of DGs and the total power losses obtained from the IA, PSO and ABC methods. From this Table, it can be concluded that the proposed PSO can achieve better results compared to the IA method and the ABC algorithm. Also, if optimally sized DGs are located at their optimal locations, not only the total losses in the distributed system are reduced significantly but voltage profiles are improved as well.

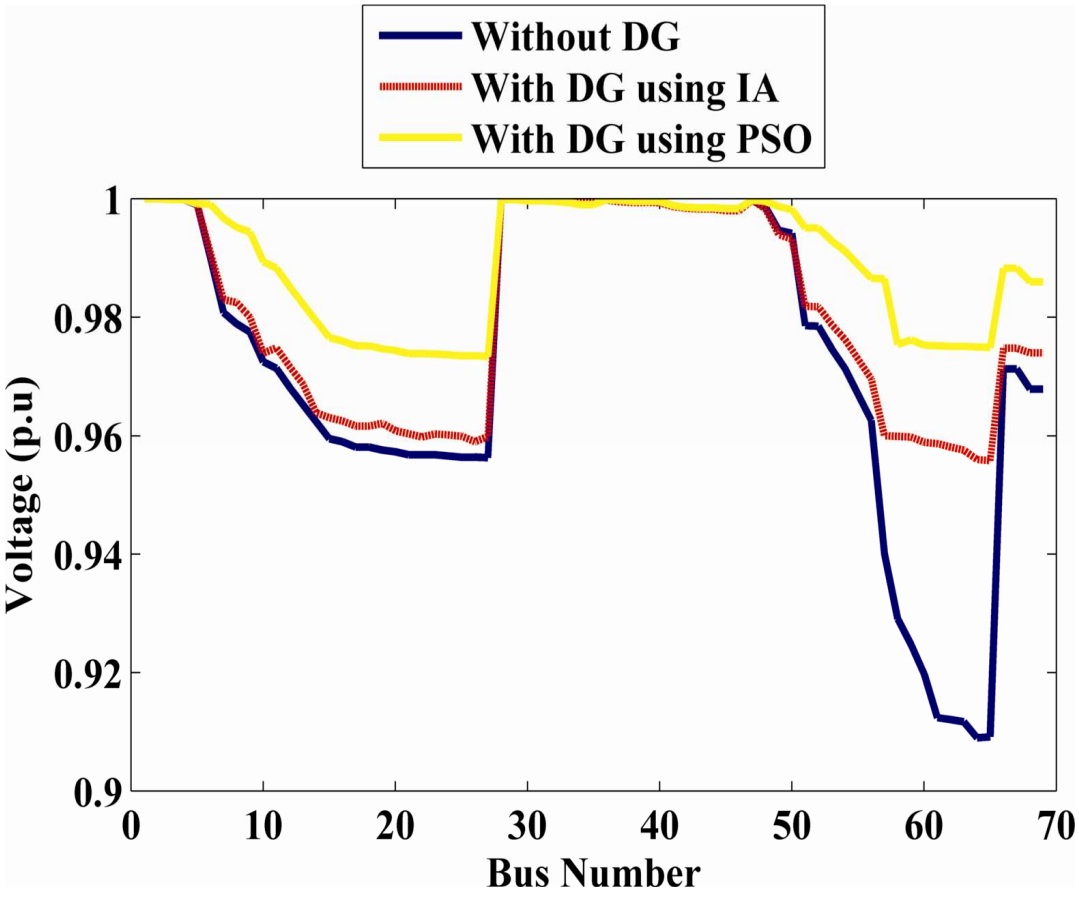


Figure 5. Voltage Profile at various buses

Table 3. Comparison of results between IA, ABC and PSO.

| | IA | ABC [6] | PSO |
|---|---|---|---|
| Optimum location | Bus # 61 | Bus #61 | Bus # 61 |
| Optimum size(MW) | 2.2 | 2.2 | 1.3 |
| Real Power loss (KW) | 83 KW | 24 KW | 43KW |
| Min. Voltage (p.u) | 0.9558 | 0.972 | 0.975 |

### 3.1.4 Conclusions

A combination of the particle swarm optimization (PSO) technique and Newton-Raphson load flow method is used to determine the optimal size and location of distributed generators in a distributed network. Effectiveness of the proposed method in solving the DG allocation problem is verified by comparing its result with those from the improved analytical (IA) and the artificial bee colony (ABC) approaches. Results from this work show that the PSO method can allocate DGs more effectively and in less time compared to IA and ABC. Also, PSO's ability to simultaneously find the optimal size and location makes it more attractive for large-scale distribution systems. Even though the optimal locations obtained from the proposed method are the same as those obtained using other algorithms [6,10,12], the size of DGs that will lead to minimum power loss is smaller than the sizes reported in the literature. Analysis shows that if optimally sized DGs are located at their optimal locations, the total losses in the distributed system are reduced significantly with improvement in voltage profile.

## 3.2 Optimal Location and Sizing of Distributed Generators in Multi-Phase Unbalanced Distribution Networks.

In this section, a particle swarm optimization (PSO) based method is developed to determine the optimal allocation of distributed generators (DGs) in multi-phase unbalanced distribution networks. The PSO algorithm has been programmed in MATLAB using an open source software called OpenDSS in a co-simulation environment to solve the unbalanced three-phase optimal power flow (TOPF) problem and to find the optimal location and sizing of different types of distributed generators. Using the IEEE 123 node distribution feeder as a test bed, results from the proposed method are compared to those from the repeated load flow (RLF) method. For a realistic study, mixes of all type of DGs are considered. Results indicate that integrating optimally sized DGs at the optimal locations not only reduces the total power loss in the distribution system but improves the voltage profile as well.

### 3.2.1 Introduction

In recent years, development of “Smart Grid” has influenced the primary focus of research on the electric power production, transmission, and distribution. Among the various attributes of smart grids, flexibility and resiliency of distribution systems [1] and integration of distributed generators (DGs) into the power grid [65] are classified as an advanced distribution management system (DMS) [66]. Even though DMS was created as a simple extension of supervisory control and data acquisition (SCADA) from transmission system, it must be equipped with all the methodologies and capabilities that are currently used to analyze the transmission systems. Since DMS is the brain of the smart distribution grid, methods such as optimal DG placement, integrated voltage/var

control, distribution power flow (DPF), and contingency analysis must be adapted to the characteristics of common distribution systems [3,4].

The importance of proper DG integration into the distribution system has been investigated in a number of studies. Authors in [2]–[9] have demonstrated the reduction of power loss by optimally sizing and placing DGs in distribution networks. Similarly, in [10]–[14] optimal sizing and location of DG resulted in improved reliability of the network. As power loss decreases and reliability increases, profit for electric utility increases as well. Therefore, for utilities integration of DGs in distribution networks provides the dual advantage of meeting the renewable portfolio standard (RPS) and strengthens their infrastructure while reducing cost. However, most of the above studies have been performed on balanced distribution systems. Distribution networks in actual power system are multi-phase unbalanced systems because of unequal three phase loads, un-transposed lines and conductor bundling [15]. As a result, studies performed on balanced distribution systems fail to provide a realistic insight into the actual problem.

One of the reasons for conducting optimal allocation studies in balanced networks is the simplicity of solving the optimal power flow problem. Although numbers of studies have suggested methods for solving the distribution load flow (DLF) problem [68]–[72], they require complex, expensive calculations and thus are time consuming. A much simpler and effective method for solving three phase optimal power flow (TOPF) problems has been proposed in [67]. Authors in [67] make use of a quasi-Newton method which requires the numerical evaluation of gradients. However, a gradient based method has a higher possibility of converging to a local minima making the results inaccurate [24], [25]. Furthermore, Newton-based techniques rely heavily on the value of initial

conditions and thus may never converge to a solution due to the inappropriate initial conditions [75]. In the present study the particle swarm optimization (PSO) algorithm is used in a co-simulation environment with OpendDSS program to solve the unbalanced TOPF problem for optimal location and sizing of multiple DGs. Unlike the gradient based optimization methods, the PSO based method is a heuristic global optimization technique with no overlapping and mutation calculations. This not only makes the proposed method effective but also results in lower computational times [76].

The remainder of the chapter is organized as follows. Section 3.2.2 presents and describes the objective function, application of PSO, and its parameter tuning. The implementation of the proposed method along with its validation is presented in section 3.2.3. In section 3.2.4, results are discussed and then conclusions are drawn in section 3.2.5.

### 3.2.2 Methodology

***Objective Function :*** PSO has long been used to solve OPF problems [75], [77]–[79]. In these references, authors have developed methods for single phase OPF problems. However, the same method of single phase systems can be modified for the unbalanced TOPF. In the present work the method proposed by authors in [4] and [31] have been modified with a goal of achieving both optimal location and sizing of DGs, simultaneously.

The unbalanced TOPF problem can be formulated as follows [4]:

$$\text{Min} \quad F(x,u) \tag{1}$$

Subject to:

$$g(x,u) = 0 \quad (2)$$

and

$$h(x,u) \leq 0 \quad (3)$$

where $F$ is the objective function which needs to be minimized, $x$ is the vector of dependent variables like bus voltages and bus loads, $u$ is the vector of independent variables, mainly the DGs size and location, $g$ is the equality constraints which represent the load flow equations, and $h$ represents the system operating constrains like allowable sizes of DGs and voltage stability.

Since the main focus of this work is to strengthen the unbalanced multi-phase distribution networks while reducing the operating cost by allocating the optimal size and location of DGs, our objective function represents the total power loss of the given distribution network. Hence, the objective function is given as

$$min \sum_{k=1}^{n} P_L(k) \quad (4)$$

Where $P_L$ is the power loss in each of the distribution node (or line) and $n$ is the number of nodes (or lines). In the scope of this work, strengthening a distribution networks means improving the voltage profile of the system. This can be achieved

by enforcing the voltage at every node in the distribution system to be within the acceptable range of 0.95 pu and 1.05 pu . Hence the following inequality constraint is applied to ensure the acceptable voltage profile of the distribution network.

$$V^{min} \leq V_i \leq V^{max}, \qquad i = 1,\ldots n \quad (5)$$

where *n* is the number of nodes. Additionally, availability also dictates the size of the DGs that can be connected to the distribution network. This results in the following constraints:

$$P_G^{min} \leq P_{Gi} \leq P_G^{max} \tag{6}$$

$$P_G^{min} \leq P_{Gi} \leq P_G^{max} \tag{7}$$

Inequality constraints in equations (5), (6) and (7) can be incorporated into the objective function as quadratic penalty terms as follows [75]:

$$\min \sum_{k=1}^{n} P_L(k) + \lambda_p (P_{Gi} - P_{Gi}^{lim})^2 + \tag{8}$$

$$\lambda_v (\sum_{i=1}^{n} (V_{Li} - V_{Li}^{lim})^2 + \lambda_Q (\sum_{i=1}^{NDG} (Q_{Gi} - Q_{Gi}^{lim})^2$$

Where *n* is number of nodes, *NDG* is number of DGs, $\lambda_P$, $\lambda_V$, and $\lambda_Q$ are penalty factors and

$$V_{Li}^{lim} = \begin{cases} V^{max}; V > V^{max} \\ V^{min}; V < V^{min} \end{cases} \tag{9}$$

$$P_{Gi}^{lim} = \begin{cases} P^{max}; P > P^{max} \\ P^{min}; P < P^{min} \end{cases} \tag{10}$$

$$Q_{Gi}^{lim} = \begin{cases} Q^{max}; Q > Q^{max} \\ Q^{min}; Q < Q^{min} \end{cases} \tag{11}$$

In this study, the following types of DGs have been considered.

- Type 1: DGs which can inject only real power such as fuel cells, PV cells, and geothermal power plants.
- Type 2: DGs which can inject both real and reactive power such as synchronous generators.
- Type 3: DGs which can inject real power and absorb reactive power such as induction generators.

***Application of PSO:*** The computational procedures of PSO used in this work are summarized in the following steps:

Step 1: Individual position and velocity initialization: In this step, n particles are randomly generated. Each particle is an m-dimensional vector, where m is the number of parameters to be optimized. In our study, n is a 3 dimensional vector which represents the value of real power, reactive power, and locations. Thus, the position of particle i at iteration 0 is represented by:

$$X_{i,j}(0) = (P_{il},\ldots\ldots P_{im}), (Q_{il},\ldots.Q_{im}), (L_{il},\ldots L_{im}), \quad i = 1,\ldots n, \quad j = 1,2,3 \qquad (12)$$

Here, the $X_{i,j}(0)$ is generated by randomly selecting a value with uniform probability over the $j^{th}$ optimized parameter search space [ $X_j^{min}$, $X_j^{max}$]. Similarly, each particle is randomly assigned an initial velocity by randomly selecting a value with uniform probability over the $j^{th}$ dimension [ $-V_j^{max}$, $V_j^{max}$]. Thus, the velocity of particle i at iteration 0 is given by ;

$$V_{i,j}(0) = (V_{il},\ldots\ldots V_{im}) \quad i = 1,\ldots n, \quad j = 1,2,3 \qquad (13)$$

Where the maximum velocity $V_j^{max}$ has been applied to enhance the local exploration of the problem space [22]. In order to maintain a uniform velocity through all dimensions, the maximum velocity in the jth dimension can be obtained as:

$$V_j^{max} = ( X_j^{max} - X_j^{min}) / N, \qquad N = \text{iteration number} \tag{14}$$

All other parameters, including the local best (Pbest), the global best (Gbest), and the inertial weight parameters are also initialized in this step.

Step 2: Velocity and position updating: During the flight, each particle knows its best value Pbest and its position up to that point. Moreover, each particle also knows the best value of the group Gbest among all the Pbest values. Hence, each particle i is continuously updating its velocity and position in a manner given in Equations (15) and (16) [60].

$$V_i^{k+1} = \omega V_i^k + c_1 \text{rand}\left(\text{Pbest}_i^k - X_i^k\right) + c_2 \text{rand}(\text{Gbest}_i^k - X_i^k) \tag{15}$$

$$X_i^{k+1} = X_i^k + V_i^{k+1} \tag{16}$$

$V_i^k$ : current velocity of particle i at kth iteration

$X_i^k$ : current position of particle i at kth iteration

$c_1, c_2$ : positive constant weighting factors

$\text{Pbest}_i^k$ : best position of particle i until kth iteration

$\text{Gbest}_i^k$ : best position of the group until kth iteration

rand : uniformly distributed random numbers between 0 and 1

ω : inertial weight parameter

As seen in (15), velocity of any particle depends on its local best and global best values. Thus, by learning the knowledge from individual particles and from other members of the particle's neighborhood, velocity drives the optimization process. Furthermore, the second component in equation (15) depends on the value of local best which reflects the change in velocity based on its own thinking and memory and thus can be referred to as the cognitive part. Similarly, third part of the same equation depends on global best which reflects the social influence of particles and therefore, can be referred to as the social cognitive part.

Step 3: Individual best (Pbest) updating: The fitness value of every particle at the current iteration is compared to the best fitness value that it has ever achieved up to the current iteration. The best value that has been resulted from the best fitness is called the individual best (Pbest) value. Pbest is updated as follows:

$$\text{if} \quad Fobj_i^{K+1} < Fobj_i^{K}, \quad \text{Pbest}_i^{K+1} = X_i^{K+1} \tag{17}$$

$$\text{Else} \quad \text{Pbest}_i^{K+1} = \text{Pbest}_i^{K} \tag{18}$$

Step 4: Global best (Gbest) updating: The global best value (Gbest) is the best positions among all the individual best positions achieved so far. Equation (19) shows the calculation of Gbest.

$$Gbest^{K+1} = \min (Pbest_i),\ i = 1,\ldots,\ K+1 \quad (19)$$

Stopping Criteria : PSO algorithm stops when it meets one of the following criteria

i) A good fitness value is obtained. In our study a good fitness value is defined as $|Fobj_i^{K+1} - Fobj_i^{K}| < 0.0001$

ii) Maximum number of iterations is reached.

***Parameter tuning of PSO***

*a) Maximum velocity:* Since the main goal of any given particle is to find its optimum position, it continuously updates its velocity and position as described by equations (15) and (16). To limit the trajectory of particles in the given search space, the maximum velocity that a particle can attain is given in (14).

*b) Weighting Factors:* These parameters contribute to the convergence behavior of the PSO method. Although the value of the weighting factors $c_1$ *and* $c_2$ ranges from 1.0 to 2.0, higher values of them decrease the solution time [60]. Hence $c_1$ *and* $c_2$ are both set as 2.0.

*Inertia weight* : In this study, a new inertia weight as proposed by authors in [61] is used. This weighting factor , ω , is defined as a function of the local best (Pbest) and the global best (Gbest) values of the objective function for each generation and is given by (20) as:

$$\omega_i = (1.1 - \frac{Gbest_i}{Pbest_i}) \quad (20)$$

Where, *i* is the *ith* iteration.

### 3.2.3 Implementation

Open source software developed by the Electric Power Research Institute (EPRI) called OpenDSS has been adapted to solve the unbalanced three phase optimal power flow problem (TOPF) [23]. Using OpenDSS, the overall algorithm has been implemented in MATLAB and is based on a two-way data exchange between MATLAB, which implements the PSO algorithm, and OpenDSS simulation engine, which performs DLF and implements the control variables in the distribution network model. The overall algorithm is summarized in Figure 6.

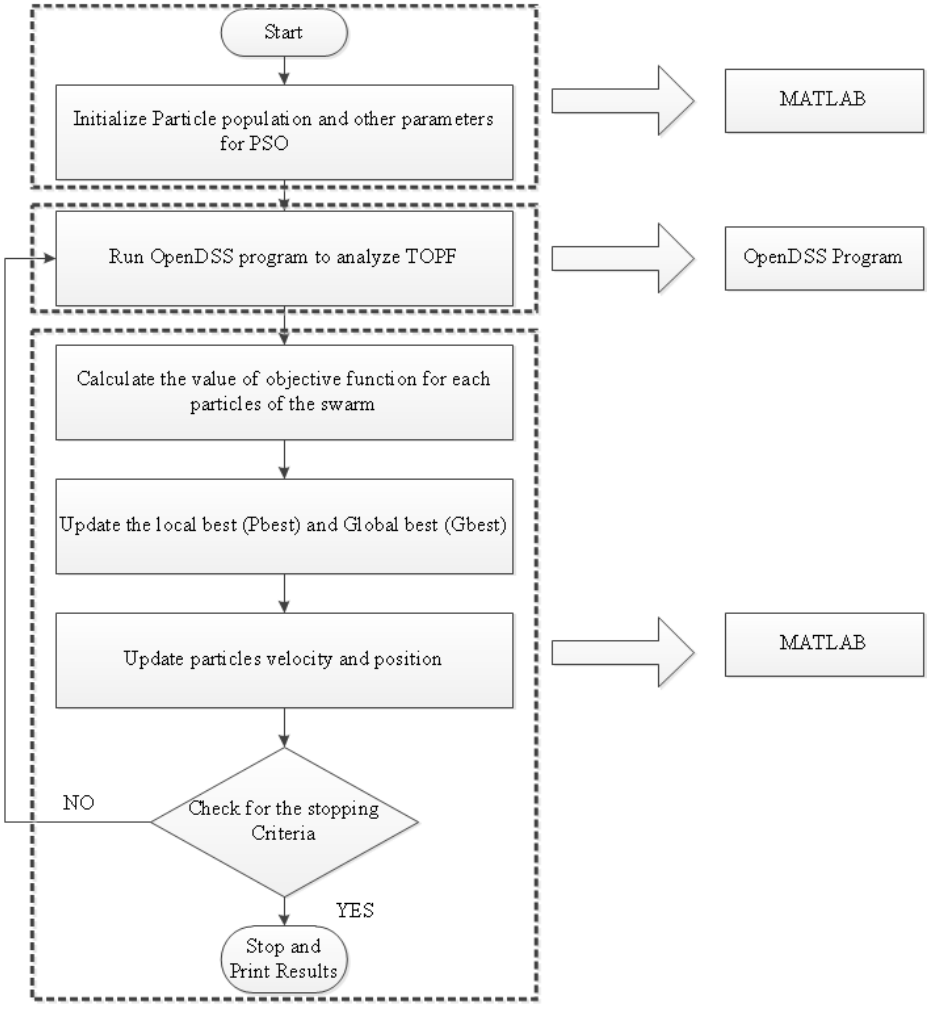


Figure 6. Flowchart of the proposed PSO algorithm.

### 3.2.4 Test System

The proposed method was tested using the IEEE 123 node multi-phase unbalanced distribution feeder as shown in Figure 7. This test feeder consists of four voltage regulators, four capacitor banks, overhead and underground line segments with various phasing, and various unbalanced loading with different load types [80]. The detailed data for this test system can be obtained from [81].

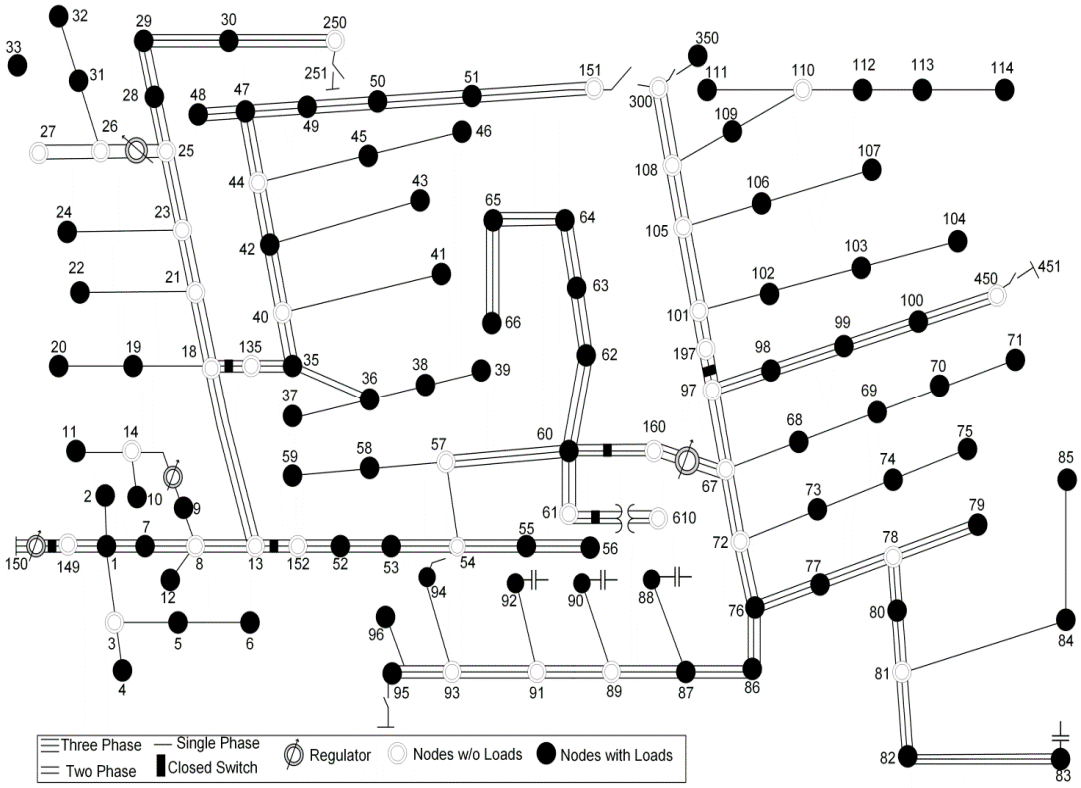


Figure 7. The IEEE 123-node distribution feeder

### 3.2.5 Method Verification

***a) Size allocation:*** Using the repeated power flow method (RPF) reported in [39], the optimal size of DGs at the respective locations in the 123- node distribution feeder are obtained as shown in Figure 8. In order to compare and verify the proposed PSO method,

seven most heavily loaded nodes are selected and the optimal size of DGs at these nodes are obtained using the proposed method. The optimal size of DGs obtained from both RPF and PSO methods are similar as shown in Table 4. This shows that the proposed method is effective in determining the optimal size of DGs in the given distribution network.

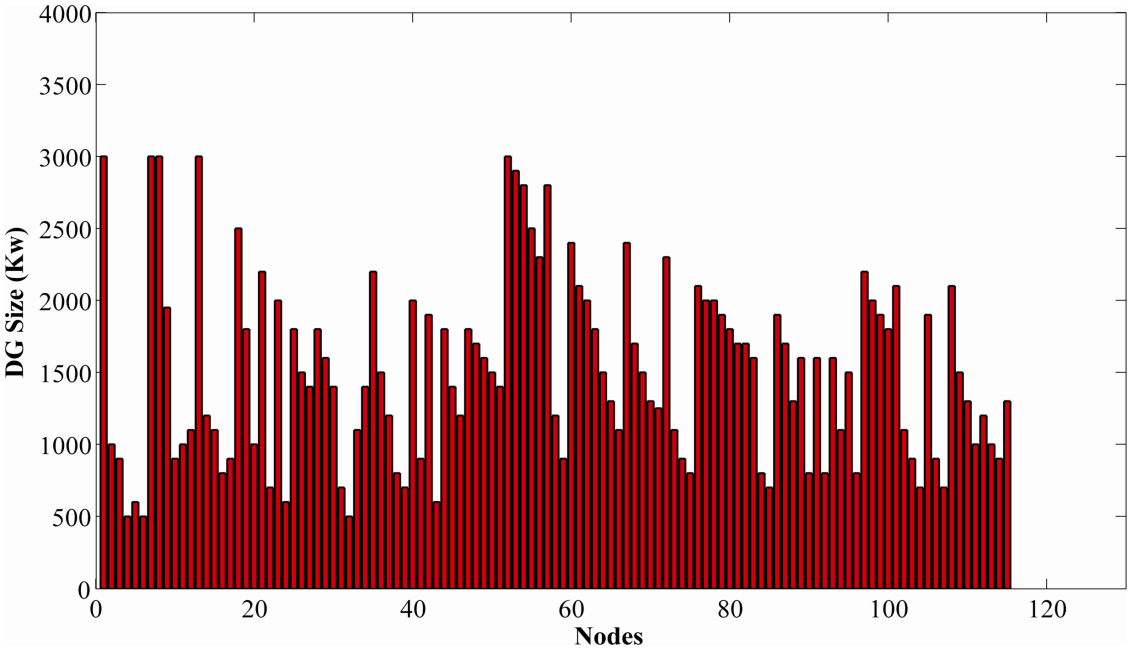


Figure 8. RPF based Optimal size of DGs at respective buses.

Table 4. Comparison of the optimal size sobtained using RLF and PSO methods.

| Node Number | Load (kW) | Optimal size using RFL (kW) | Optimal size using PSO (kW) |
|---|---|---|---|
| 76 | 245 | 2110 | 2105 |
| 48 | 210 | 1715 | 1713 |
| 65 | 140 | 1305 | 1300 |
| 49 | 140 | 1595 | 1597 |
| 47 | 105 | 1800 | 1803 |
| 64 | 75 | 1550 | 1546 |
| 66 | 75 | 1135 | 1135 |

***b) Location Selection:*** Using the optimal DG sizes obtained in the previous section, the optimal location of these DGs which lead to minimal power losses in the distribution system are obtained for each node. Once again, the repeated power flow (RPF) method is used to compared and verify the results obtained from the proposed method. Using RPF method, the total power loss of the system after placing the optimally sized DGs at the respective buses is shown in Figure 9. The optimal location and sizes for four of type 1 DGs and the power reduction achieved is summarized in Table 5.

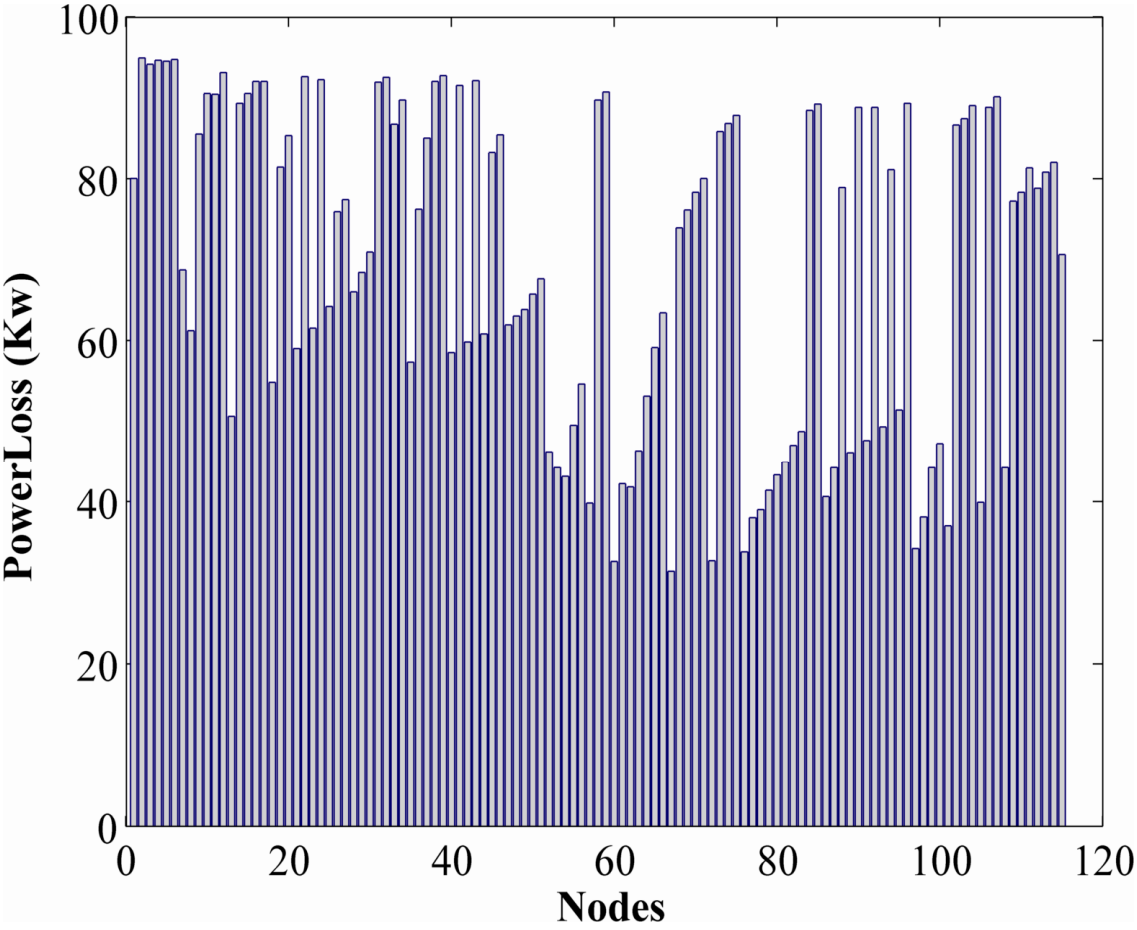


Figure 9. RPF based Power losses at each bus after insertion of optimally sized type1 DGs.

Table 5. Comparison of power loss reductions as a result of optimal location and sizing of Type 1 DGs using RLF and PSO

| DG | Bus no. | Size (MW) | Power Loss reduction RLF (%) | Power Loss reduction PSO (%) |
|---|---|---|---|---|
| 1 | 67 | 2.41 | 36.1 | 37.5 |
| 2 | 67,72 | 1.41, 1.57 | 55.4 | 55.8 |
| 3 | 67,72,47 | 1.08,1.32,0.54 | 69.6 | 69.1 |
| 4 | 67,72,47,114 | 1.49,0.52,0.74,0.25 | 79.1 | 79.4 |

It is found that the Repeated Power Flow (RPF) method is computationally very demanding. The RPF method needs to evaluate $N*[((DG_{max} - DG_{min})/ S) +1)]$ combinations to generate an appropriate answer for this distribution test system. Here, $DG_{max,}$ $DG_{min}$, S, and N are the maximum DG size (2500KVA), minimum DG size (100 KVA), step size (50 KVA) and number of nodes (114), respectively. With an average iteration time of 5 seconds on a PC with speed of 3.20 GHz and 3.49 GB of ram, the total search procedure in RPF takes approximately 396 hours. The proposed PSO method, on the other hands, takes only 20 minutes to reach the optimum solution.

### 3.2.6 Results and Discussion

The proposed PSO based method is applied to three types of DGs. Results obtained for type 1 DGs are shown in Table 5. Table 6 and 7 show the optimum size and location for type 2 and type 3 DGs, respectively, from the proposed PSO method. Installation of multiple DGs with optimal capacity has resulted in significant reduction of

distribution losses. The total losses of the system after allocating Type 1, Type 2, and Type 3 DGs are 19.6 kW, 17.3 kW, and 30.8 kW, respectively. Since Type 3 DGs are induction generators, they consume more reactive power from the distribution network. As a result, the power loss reduction obtained using these types of DGs are smaller.

Table 6. Optimal size allocation of Type 2 DGs calculated by PSO and RPF.

| DG | Bus no. | Size (MVA) | Power Loss reduction using (PSO) (%) | Power Loss reduction using RPF (%) |
|---|---|---|---|---|
| 1 | 67 | 2.43 | 40.1 | 38.4 |
| 2 | 67,76 | 1.43, 1.51 | 53.2 | 45.8 |
| 3 | 67,76,57 | 1.53,0.51,0.92 | 73.4 | 70.1 |
| 4 | 67,76,57,98 | 1.33,0.91,0.31,0.0.43 | 81.7 | 78.5 |

Table 7. Optimal size allocation of Type 3 DGs calculated by PSO and RPF.

| DG | Bus no. | Size (MVA) | Power Loss reduction using PSO (%) | Power Loss reduction using RPF (%) |
|---|---|---|---|---|
| 1 | 60 | 2.4 | 23.4 | 21.5 |
| 2 | 60,72 | 1.49,1.5 | 34.7 | 32.7 |
| 3 | 60,72,58 | 1.19,1.01,0.82 | 47.1 | 43.4 |
| 4 | 60,72,97,102 | 1.06,0.91,0.52,0.51 | 62.5 | 59.8 |

Realistically, utilities must be able to accommodate variety of DGs in their distribution network. In order to address this issue, optimal allocation of five different types of DGs (two type 1, two type 2, and one type 3) was performed and the results are

tabulated in Table 8. This test scenario allows utilities to plan for the percentage of certain type of DGs that can be allowed in a given distribution network. The overall power loss reduction in this study is 18.6 kW which is slightly higher than the ones obtained when only type 2 DGs were used.

Table 8. Optimal allocation of a mix of three types of DGs calculated by PSO and RPF

| DG Type | Bus no. | Size (MVA) | Total Power Loss reduction using PSO (%) | Total Power Loss reduction using RPF (%) |
|---|---|---|---|---|
| 1 | 67, 47 | 0.93,0.45 | 80.42 | 75.29 |
| 2 | 60,72 | 1.19,0.28 | | |
| 3 | 101 | 0.15 | | |

In addition to minimizing distribution losses, optimal allocation of DGs also improves the voltage profile of the distribution system. Since a stable voltage profile affects the stability of the network, the voltage at each node must always be close to 1.0±0.05 pu. Using the proposed method, the calculated voltage profiles of the 123- node distribution feeder with and without DGs are shown in Figures 11 and 10, respectively. In order to demonstrate the maximum impact of DGs, voltage regulators are removed from the distribution network. Figure 11 shows an excellent improvement in the voltage profile of the system after DGs installation. The minimum pu voltage has been improved from 0.936 pu to 0.96 pu.

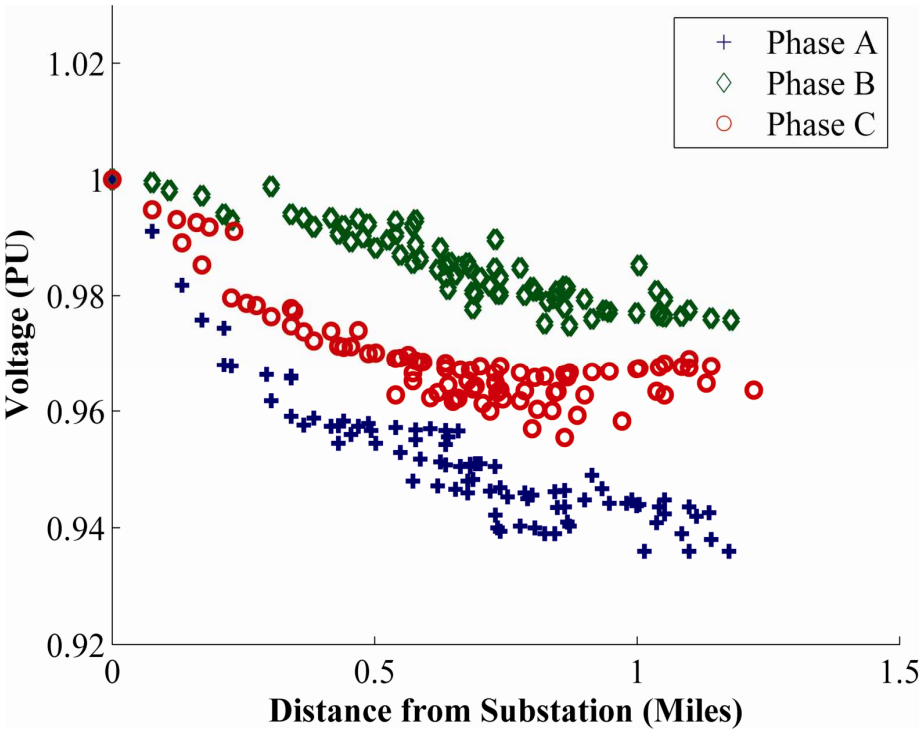


Figure 10. Voltage Profile of distribution network without DG.

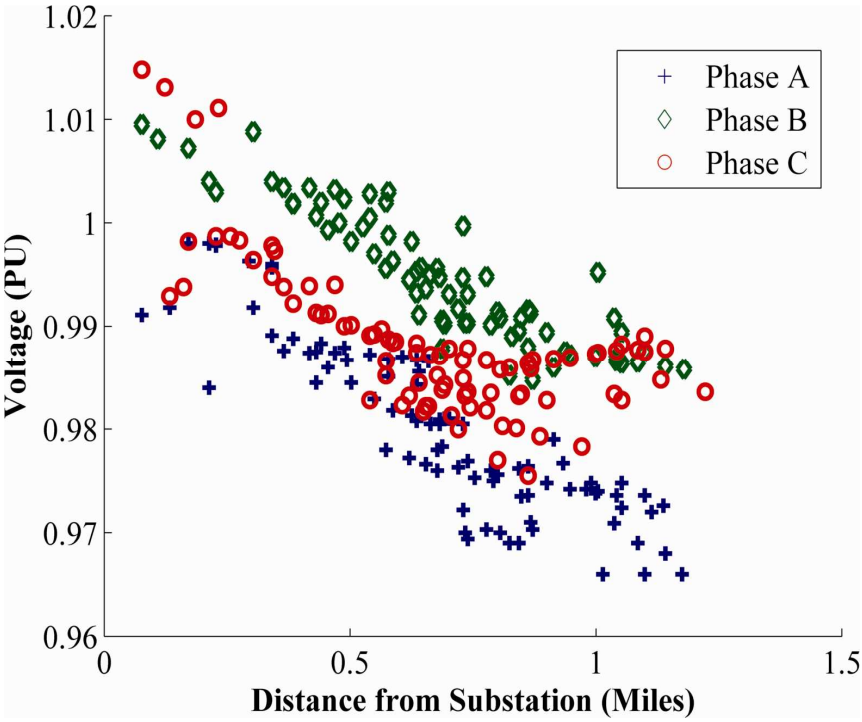


Figure 11. Voltage profile with a mix of different types of DGs.

### 3.2.7 Conclusions

This section proposes a method to determine the optimal size and location of distributed generators in a multi-phase unbalanced distribution networks. A PSO based method has been implemented in MATLAB using the open source software called OpenDSS in a co-simulation environment to solve the distribution power flow and to find the optimal location and size of various types of distributed generators. The effectiveness of the proposed method has been demonstrated by comparing the results with those obtained using the repeated power flow method (RPF). Results indicate that the proposed method can allocate DGs more effectively and in less computational times. Optimal location and generation capacity of all types of DGs are considered and results have been tabulated. Even though the maximum power loss reduction can be achieved by integrating only type 2 (synchronous generators) DGs in the distribution system, this might not be practical because utilities and DMS are required to accommodate various types of DGs in their systems. The results obtained from the proposed method show that if optimally sized DGs are located at their optimal locations, not only the total power loss in the distributed system is reduced significantly but voltage profile will improve as well.

# CHAPTER 4

# RELIABILITY EVALUATION OF DG ENHANCED DISTRIBUTION NETWORKS

In this chapter, discrete particle swarm optimization method is implemented for the optimal recloser and DG placement in both radial and non-radial distribution networks. First part of the chapter proposes a method to minimize various reliability indices of a given distribution system while the second part presents a method to reduce the total cost of protective devices while optimally allocating reclosers and DGs. The proposed method is validated by comparing the results with those obtained using Ant Colony System (ACS) algorithm. Results indicate that a higher reliability, based on composite reliability index, can be achieved with lesser number of reclosers but the customer interruption cost increases significantly. Similarly, minimizing the total cost of protective devices reduces the reliability of the system.

## 4.1 Introduction

Over the past decades, electric demand has increased significantly. This has forced utilities to operate their distribution networks at their full capacity. As a result, distribution systems have become more sensitive towards any kind of power imbalances caused by the improper addition of generators and/or loads. Traditionally, distribution networks were constructed with the sole purpose of delivering electric power from distribution substations to consumers. However, several serious negative effects of traditional fossil fuel based power plants have influenced public opinion toward

renewable energy sources which, in turn, has resulted in the establishment of several renewable portfolio standards (RPS). This has created a provision where electricity generated from renewable resources must account for a certain percentage of utilities' power portfolio. One of the common and efficient ways for utilities to address this mandate is to use renewable energy based distributed generators (DGs). As a result, penetration of DGs into the existing distribution networks has increased significantly [82].

Studies have shown that the proper allocation of distributed generators in distribution networks reduces distribution power losses and improves the voltage profile and reliability of the system [2]–[9], [12], [13], [83], [84]. However, integrating DGs into radial distribution systems creates bidirectional power flows which violate the conventional system protection logic [85]. Hence, a new protection scheme must be implemented to successfully integrate DGs into the existing distribution infrastructure.

In a primary distribution system, reclosers are commonly used as protection devices that improve reliability by isolating a fault, reconfiguring, and restoring the network. Thus, number of reclosers used in any distribution network increases with the expansion of the network and/or loads. Moreover, with an expansion of the distribution network, even an existing recloser may need to be relocated [86]. The selection of adequate number of reclosers and their locations have been presented in [72], [87]–[93]. In these studies, effects on the reliability of distribution networks as a function of the number and location of reclosers without the integration of DGs are discussed. Authors in [83] propose an ant colony system (ACS) algorithm to find the optimal locations of reclosers in a DG integrated distribution system. Similarly, [14] presents a multi-

population genetic algorithm (MPGA) for the optimal numbers and locations of reclosers in similar distribution systems. In both of these studies, the location and sizes of DGs are fixed. In [10], impact on the reliability of the distribution network due to optimal allocation of both reclosers and DGs using genetic algorithm is presented. Authors in [12-14] have formulated objective functions only to reflect various reliability indices and presented their method in a balanced network. Also, improvement in reliability requires an increment in the number of reclosers which increases the financial burden on the utility. Hence it is important to evaluate the reliability of the system while considering the cost associated with the recloser placements.

In this chapter, a discrete particle swarm optimization (DPSO) method has been implemented to calculate the number and location of reclosers and DGs simultaneously in a multi-phase unbalanced distribution system. The first part of this study focuses on optimal allocation with an objective of improving system reliability indices while the second part demonstrates the cost based reliability evaluation.

### 4.2. Discrete particle swarm optimization (DPSO)

In a continuous PSO, as discussed in the previous chapters, n particles are randomly generated. Each particle is an m-dimensional vector, where m is the number of parameters to be optimized. In our study, m is a 3 dimensional vector which represents the position of reclosers, position of DGs, and sizes of DGs. Thus, the position of particle i at iteration 0 is represented by:

$$X_{i,j}(0) = (R_{il},\ldots\ldots R_{im}), (G_{il},\ldots G_{im}), (S_{il},\ldots S_{im}), \quad I = 1,\ldots n, \quad j = 1,2,3 \qquad (1)$$

Here, $X_{i,j}(0)$ is generated by randomly selecting a value with uniform probability over the $j^{th}$ optimized parameter search space [ $X_j^{min}$, $X_j^{max}$]. R, G, and S are location of reclosers and DGs, and sizes of DGs, respectively.

During the flight, each particle knows its best value Pbest and its position up to that point. Moreover, each particle also knows the best value of the group Gbest among all the Pbest values. Hence, each particle i is continuously updating its velocity and position in a manner as given in Equations (2) and (3) [60].

$$V_i^{k+1} = \omega V_i^k + c_1 \text{rand}\left(\text{Pbest}_i^k - X_i^k\right) + c_2 \text{rand}(\text{Gbest}_i^k - X_i^k) \quad (2)$$

$$X_i^{k+1} = X_i^k + V_i^{k+1} \quad (3)$$

$V_i^k$ : current velocity of particle i at kth iteration

$X_i^k$ : current position of particle i at kth iteration

$c_1, c_2$ : positive constants weighting factors

$\text{Pbest}_i^k$ : best position of particle i until kth iteration

$\text{Gbest}_i^k$ : best position of the group until kth iteration

rand : random numbers between 0 and 1

$\omega$ : inertial weight parameter

Discrete particle swarm optimization (DPSO) also uses the same concepts as those of the continuous one. In DPSO, however, the optimal solution can be determined by rounding off the real optimum values to the nearest integer [94], [95]. In the continuous version of PSO method rounding off is performed after the convergence of

the algorithm whereas in DPSO rounding off is performed for all particles during the optimization step of the procedure. Furthermore, results obtained by authors in [96], [97] indicate that the performance of the DPSO method is not affected when the real value of particles is truncated. The velocity vector in DPSO is calculated using the same formula as in the classical PSO as shown in equation (2), but is saturated afterward using the hyperbolic tangent function to obtain a new quantity called the saturated velocity as shown in equation (4).

$$VSAT_i^{K+1} = \frac{1 - \exp(-V_i^{k+1})}{1 + \exp(-V_i^{k+1})} = \tanh\left(\frac{V_i^{k+1}}{2}\right) \quad (4)$$

The position of each particle is then calculated as:

$$X_i^{k+1} = X_i^k + \text{round}(VSAT_i^{k+1}) \quad (5)$$

### 4.2.1. Implementation of DPSO

1) Particle initialization: This is the first step in DPSO. Here, n particles are generated and randomly initialized.

2) Velocity and position updating: In this step, the velocity and position of every particle is updated according to equations (2), (3), (4), and (5). In order to maintain a uniform velocity through all dimensions, the maximum velocity in the jth dimension has been obtained as:

$$V_j^{max} = (X_j^{max} - X_j^{min}) / N, \qquad N = \text{iteration number} \quad (6)$$

$$\text{if} \quad V_i^{K+1} > V_{max}, V_i^{K+1} = V_{max} \tag{7}$$

$$\text{Else if } V_i^{K+1} < -V_{max}, V_i^{K+1} = -V_{max} \tag{8}$$

3) Global best (Gbest) updating: It is the best position among all the particle best positions achieved so far. Equation (9) shows the calculation of Gbest.

$$Gbest^{K+1} = \min (Pbest_i), i = 1,\ldots,K+1 \tag{9}$$

4) Stopping Criteria : DPSO algorithm stops when it meets one of the following criteria

i) A good fitness value is obtained. In our study a good fitness value is defined as $|Fobj_i^{K+1} - Fobj_i^{K}| < 0.001$

ii) Maximum number of iterations is reached.

### 4.2.2. Parameter tuning for DPSO

***Maximum velocity:*** Since the main goal of any given particle is to find its optimum position, it continuously updates its velocity and position. To limit the trajectory of particles in the given search space, the maximum velocity that a particle can attain is given in (6).

***Weighting Factors:*** These parameters contribute to the convergence behavior of DPSO. Although the value of the weighting factors $c_1$ *and* $c_2$ ranges from 1.0 to 2.0,

higher values of them decrease the solution time [60]. Hence $c_1 \; and \; c_2$ are each set as 2.0.

***Inertia weight :*** In this study, a new inertia weight as proposed by authors in [61] is used. This weighting factor ω is defined as a function of the local best (Pbest) and the global best (Gbest) values of the objective function for each generation and is given by (10) as:

$$\omega_i = (1.1 - \frac{\text{Gbest}_i}{\text{Pbest}_i}) \tag{10}$$

Where, i is the *ith* iteration.

The overall implementation of DPSO is shown in Figure 12.

### 4.3. Test Feeders

1. ***IEEE 90 -bus balanced distribution system:*** The first test system is the IEEE - 90 bus with 8- lateral balanced distribution system derived from the portion of the PG&E distribution network as shown in Figure 13. The total load on this system is 3.8MW. There are no protective devices installed in this system.
2. ***IEEE 123- bus multiphase unbalanced distribution network:*** This test system contains 123 nodes with 85 load points. The network contains four voltage regulators, six closed switches and five open switches as shown in Figure 14. There are 114 possible DG and recloser locations.

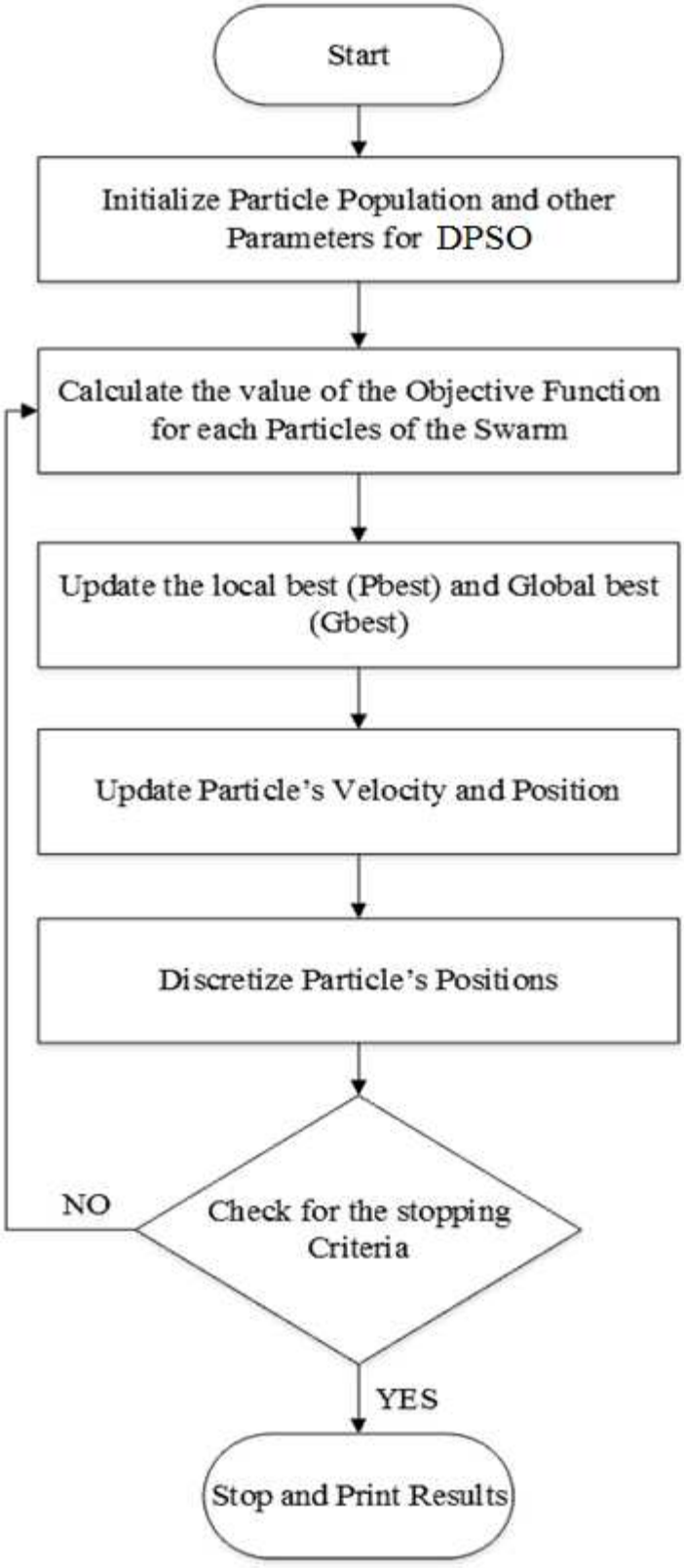


Figure 12. DPSO algorithm

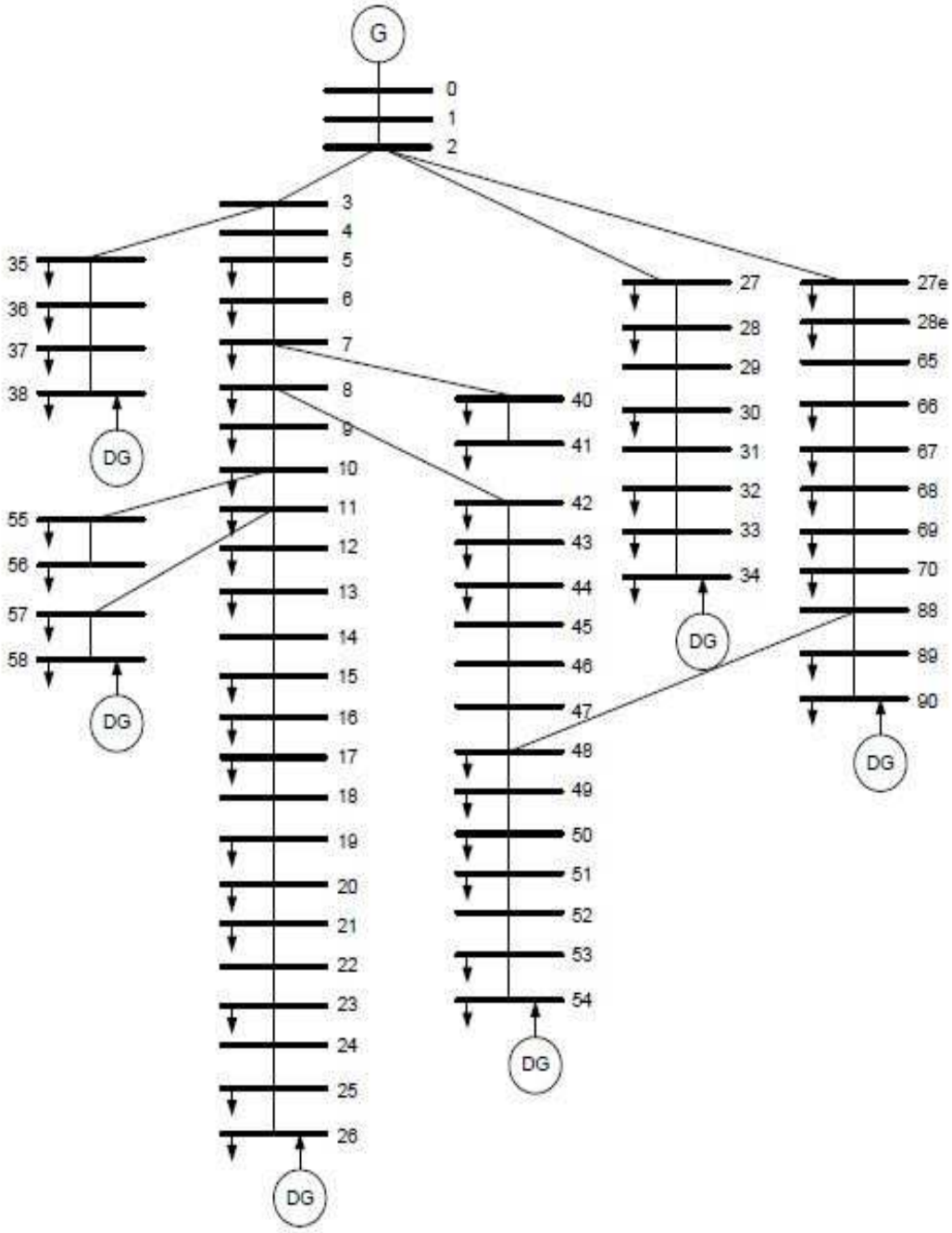


Figure 13. One line diagram of the IEEE 90-bus distribution test system 1

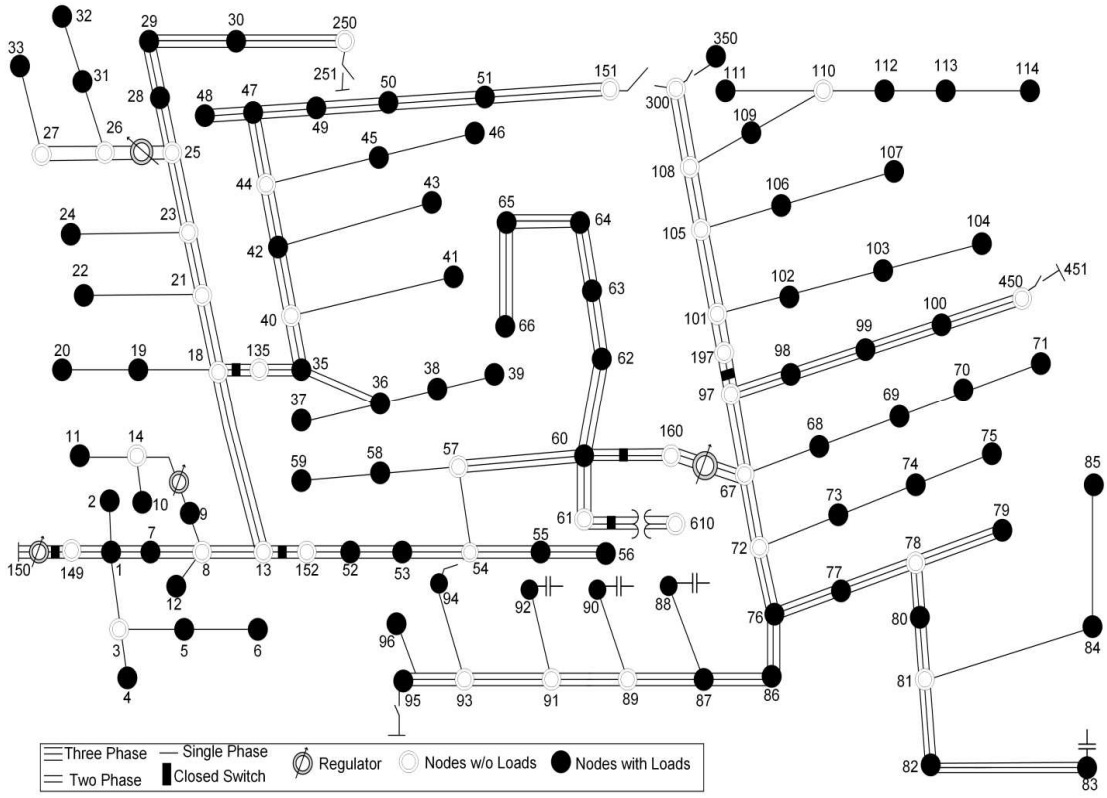


Figure 14. One line diagram of the distribution test system 2.

### 4.4. Part I: Reliability Analysis Based on Composite Reliability Index (CRI)

#### 4.4.1. Problem formulation

It has been reported that service interruptions or failures in distribution systems account for 80% of all customer interruptions [86]. Presence of distributed generators (DGs) in a radial distribution network gives rise to bi-directional power flows which can further degrade the system protections. Figure 15 shows a typical radial distribution system where the power flows from substation transformer to individual customers. The circuit contains four load points with a recloser between each of them.

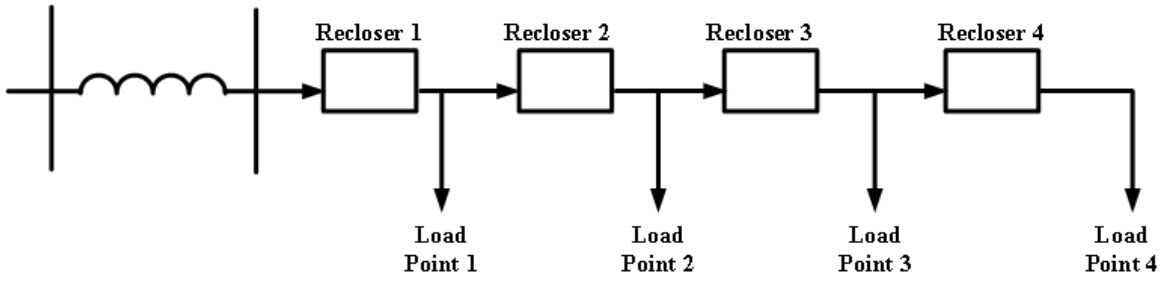


Figure 15. A typical radial distribution feeder

The protection scheme for a typical radial feeder, as shown in Figure 15, is fairly easy. For a fault anywhere on the feeder, only the first recloser upstream from the fault operates. For example, if the fault occurs at load point 3, only recloser 3 will operate. As a result, customers connected to load points 1 and 2 would not be interrupted. In this type of feeder configuration, faults occurring near the substation would affect the maximum number of customers. When a DG is integrated in the feeder system, it can supply power to some customers located downstream from the fault. For a fault occurring at load point 2 in Figure 16, both reclosers 2 and 3 will operate, forming an island with a feeder starting downstream of DG. In this case, DG may be able to supply the power to loads that are connected to load points 3 and 4.

Thus, the location of DGs and protection devices are strongly interdependent. Suboptimal recloser placements may lead to islands with inadequate power generation which can worsen the reliability of the system. Optimal allocation of reclosers and DGs are thus necessary to achieve the maximum reliability in DG integrated distribution networks.

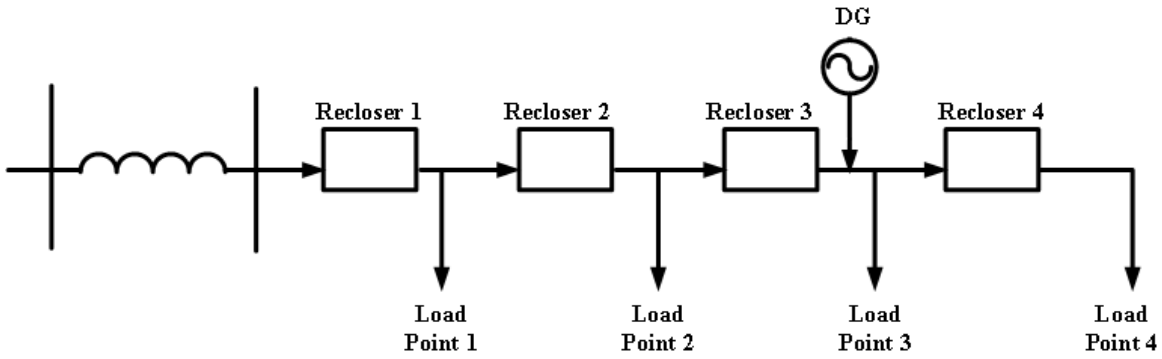


Figure 16. DG integrated radial distribution feeder.

In a distribution network, reliability is evaluated by several indices including system average interruption duration index (SAIDI), system average interruption frequency index (SAIFI), number of customers not supplied (CNS), among others. In this study, SAIDI and SAIFI are used to form an objective function which is optimized to determine the best location of reclosers and DGs.

***Objective function:*** The two most common reliability indices that are used to represent the reliability of the distribution system in the form of a composite reliability index are:

i) System average interruption duration index (SAIDI):

$$\text{SAIDI} = (\sum u_i N_i)/(\sum N_T) \tag{11}$$

Where $u_i$ is the outage time for location $i$, $N_i$ is the number of customers connected to location $i$, and $N_T$ is the total number of customer served.

ii) System average interruption frequency index (SAIFI):

$$\text{SAIFI} = (\sum r_i N_i)/(\sum N_T) \tag{12}$$

Where $r_i$ is the failure rate of power system component $i$.

Now, the objective function called composite reliability index (CRI) is formulated as follows [10]:

$$min\ \{\text{CRI} = W_{SAIDI}\frac{SAIDI-SAIDI_T}{SAIDI_T} + W_{SAIFI}\frac{SAIFI-SAIFI_T}{SAIFI_T}\} \quad (13)$$

Where $W$ is the weight factor associated with reliability indices and $T$ indicates the targeted reliability index. This composite reliability index depends on the values of SAIDI and SAIFI which are the two most commonly used reliability indices for measuring the reliability of distribution systems [98]. Here, the value of CRI decreases when both SAIDI and SAIFI decrease and it becomes negative when index values become lower than the expected targeted values. Since our goal is to minimize the composite reliability index, lowers values of CRI reflect a higher reliability of the system. Constraints in this problem are the number of reclosers and DGs that are available in the system and the number of possible locations for those devices.

### 4.4.2. Calculation of Composite Reliability Index

The objective function given in equation (13) is used to calculate the composite reliability index of the given distribution network. It is assumed that with any fault incident, only a minimal number of reclosers are operated to isolate the smallest possible part of the feeder. In this work, the distribution network has been divided into various sections as suggested by authors in [10] and [84]. A group of line segments between any two adjacent reclosers is defined as a section. Thus, faults occurring in any section will disrupt service to all the customers in that section. If a fault occurs outside the particular section, customers in that section might not be affected if they are still connected to the

substation or if the section operates as an island. Thus, the entire customers within a particular section would experience the same number of interruptions. Figure 17 shows the formation of sections within the distribution network.

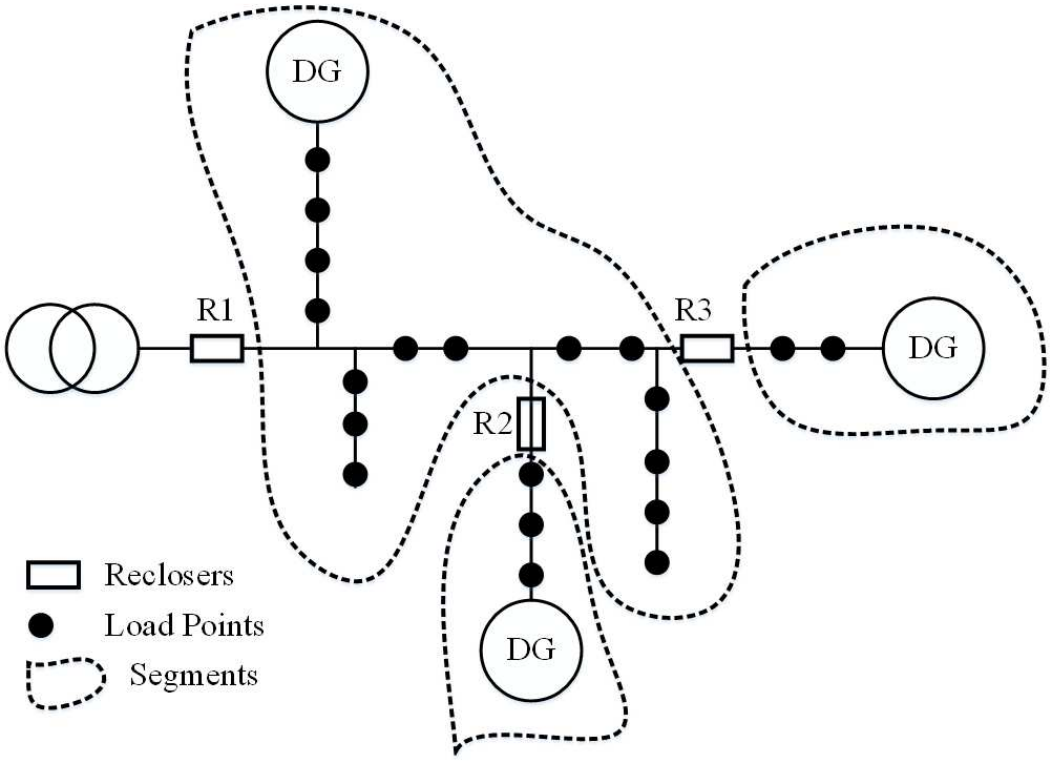


Figure 17. Formation of sections in a distribution system.

The procedure for sectionalizing a single phase distribution network is straight forward as shown in Figure 17. Multi-phase distribution systems, however, require a sophisticated algorithm to sectionalize different phases in the system. The classification method proposed in [10] is adapted in this study. Since sections for different phases do not coincide, each phase of multi-phase sytemts are sectionalized separately as follows [10]:

Let R be the set of all branches, B be the set of all buses and G be the set of all generators in phase A.

i. Open all protection devices present in phase A, i.e. remove all those branches from set R

ii. Pick an aribitarry bus $b_i$ from set B. Determine all buses and generators connected to bus $b_i$ via branches from set R.

iii. Classify all such buses and generators into the same section. Determine all branches connected to the buses in the current section and classify them to be in the same section

iv. Remove all buses, branches, and generators in the current section from their corresponding sets B, R, and G.

v. Repeat steps iii-vi, until set B becomes empty

vi. Repeat steps i-vii for phase B and C.

The procedure for calculating the composite reliability index is shown in Figure 18. For each recloser, the value of objective function is determined by creating sections that are bounded by reclosers, simulating single line to ground faults in each sections, determining the online and offline loads present in the system during the fault at any given section, and finally calculating the value of CRI. For each island (section), the maximum power output of all DGs is calculated. This values is then compared with the load duration curve of this island. The number of faults is then reduced by the percentage of time that the power generation exceeds the load demand of the island. A typical load duration curve and the maximum power output of DGs of a section are shown in Figure 19. In the Figure, the total generation for a section is 1.6 kVA. This is smaller than the load demand at 60% of the time. Hence, for 40% of the faults outside this particular section, loads connected to this section will be disconneted.

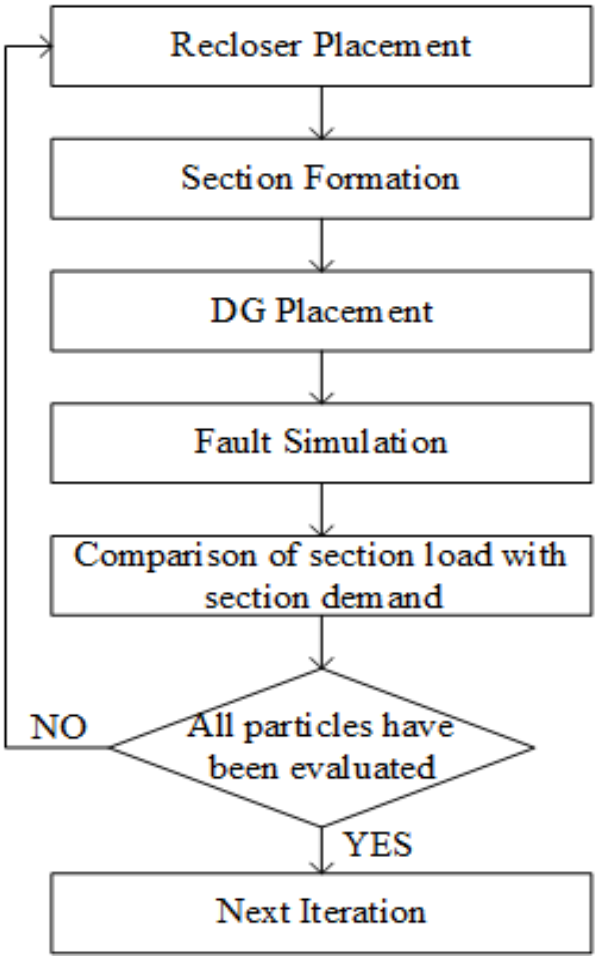


Figure 18. Calculation of the composite reliability index (CRI).

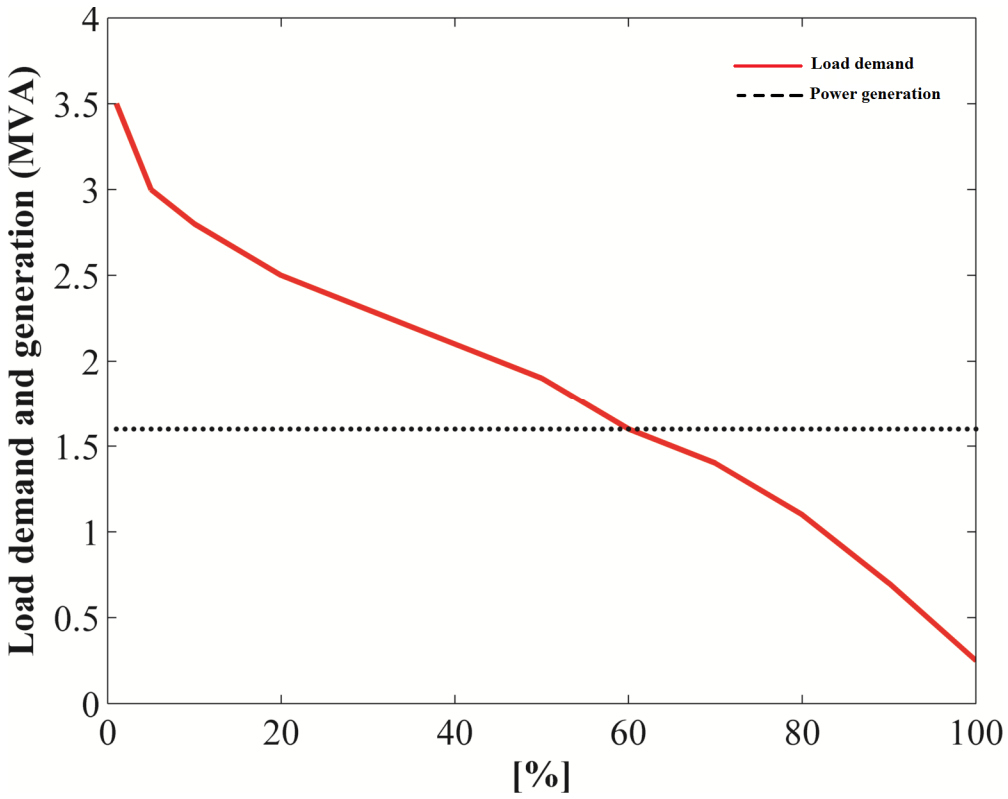


Figure 19. Example of load duration curve of a section [11].

### 4.4.3. Results and discussion

***Test Cases:*** The following cases have been investigated in this study:

i) Optimal recloser allocation in a distribution system without any DG,

ii) Optimal recloser allocation in a distribution system with fixed DG sizes and locations,

iii) Optimal DG allocation in a distribution system with a fix number of reclosers, and

iv) Optimal allocation of reclosers and DGs.

***Method validation:*** Optimal allocation of reclosers in a DG enhanced distribution feeder is shown in [83]. In [82], authors use Ant Colony System (ACS) algorithm to

solve the optimal assignment problem of reclosers in the IEEE 90-bus distribution feeder as shown in Figure 13. The detailed information of this system are obtained from [39] and are also listed in the appendix B for easy reference. In order to validate the proposed method, results from this work, which are obtained by using the same parameter values as used by authors in [83], are compared to those obtained using the methods reported in [83]. The values of these parameters are shown in Table 9. Furthermore, the following assumptions have been made for the method validation:

i) Locations of DGs are fixed and are connected to the end of the six laterals as shown in Figure 13.

ii) All reclosers function identically. In the presence of any type of fault, only the minimum number of reclosers that are close to the fault are activated in order to isolate the fault.

iii) Islanding is permitted in every section.

iv) DGs are always available.

v) Fault incidence rates and the duration of faults are uniform over all feeder branches.

Three different test scenarios, all using type 1 DGs, are used and the results are compared to those obtained using the ACS for validation purpose. These scenarios are: (i) Distribution network without DG, (ii) Type 1 DGs supplying 0.5 MW of constant active power, and (iii) Type 1 DGs supplying 1 MW of constant active power. Simulation results are shown in Tables 10-12.

Table 9. Values of parameters used in the simulation study of the 90-bus test system 1.

| | |
|---|---|
| Damage restoration time (Outage time) | 3 hrs |
| Fault Incidence rate (failure rate (f/yr/miles) | 0.22 |
| Fraction of permanent fault | 0.2 |
| $W_{SAIFI}$ | 0.33 |
| $W_{SAIDI}$ | 0.67 |
| $SAIFI_T$ | 1.0 |
| $SAIDI_T$ | 2.2 |
| Number of particles | 100 |
| Iteration | 100 |

Table 10. Optimum Recloser placement in the distribution system without DG.

| Number of Recloser | CRI | | Recloser locations | |
|---|---|---|---|---|
| | DPSO | ACS | DPSO | ACS |
| 1 | 3.9471 | 3.9560 | 8-9 | 8-9 |
| 2 | 2.8455 | 2.8695 | 30-31 | 8-9,30-31 |
| 3 | 1.9000 | 1.9012 | 3-4,30-31,47-48 | 3-4,30-31,47-48 |
| 4 | 1.6041 | 1.6042 | 3-4,27e-28e,30-31,47-48 | 3-4,27e-28e,30-31,47-48 |
| 5 | 0.9021 | 0.9033 | 3-4,11-12,30-31,47-48,28e-65 | 3-4,11-12,30-31,47-48,28e-65 |

Table 11. Optimum recloser placement in the distribution network with a maximum type 1 DG power of 0.5 MW

| Number of Recloser | CRI | | Recloser locations | |
|---|---|---|---|---|
| | DPSO | ACS | DPSO | ACS |
| 1 | 3.5015 | 3.5022 | 8-9 | 8-9 |
| 2 | 2.3164 | 2.3341 | 8-9,28-29 | 8-9,28-29 |
| 3 | 1.7351 | 1.7432 | 8-9, 27-28,50-51 | 8-9, 27-28,50-51 |
| 4 | 1.1864 | 1.1987 | 3-4,30-31,47-48, 66-67 | 3-4,30-31,47-48, 66-67 |
| 5 | .7058 | 0.7100 | 4-5,10-11,30-31,47-48,67-68 | 4-5,10-11,30-31,47-48,67-68 |

Table 12. Optimum recloser placement in the distribution network with a maximum type 1 DG power of 1 MW

| Number of Recloser | CRI | | Recloser locations | |
|---|---|---|---|---|
| | DPSO | ACS | DPSO | ACS |
| 1 | 3.2856 | 3.3012 | 8-9 | 8-9 |
| 2 | 2.1127 | 2.1455 | 8-9,49-50 | 8-9,49-50 |
| 3 | 1.4752 | 1.5066 | 4-5,27e-28e,47-48 | 4-5,27e-28e,47-48 |
| 4 | 1.0241 | 1.0340 | 8-9,28-29,36-37,49-50 | 8-9,28-29,36-37,49-50 |
| 5 | 0.5974 | 0.5988 | 3-4,10-11,30-31,49-50,67-68 | 3-4,10-11,30-31,49-50,67-68 |

Results listed in Tables 10-12 validate the effectiveness of the DPSO algorithm in finding the optimal location of reclosers for test system 1. The optimal reclosers locations obtained from both ACS and DPSO methods are the same while the composite reliability index values obtained by the proposed DPSO method are slightly lower compared to those obtained using the ACS algorithm. It can also be noticed that for a given capacity

of DGs, reliability of the system increases with the increment in number of reclosers used. Also, for the same number of reclosers used, a larger DG output results in a higher reliability of the system. In all of the cases, the optimal location for a single recloser is between bus 8 and bus 9. This agrees with the observation made by the authors in [51] that the reliability of a radial feeder with a uniformly distributed load can be improved at least by 25% when a single recloser is placed at the middle part of the feeder.

***Implementation on 90-bus test system 1:*** The proposed algorithm is then implemented to find the optimal DG locations in the test system with fixed recloser locations. The optimal sizes of DGs for every bus in the test system has been obtained using continuous particle swarm optimization method as shown in [27]. The maximum penetration of DGs is assumed to be 35% of the total load. It is assumed that five most essential reclosers, based on the results for five recloser placements listed in Tables 10-12, are placed in a system. Here, essentiality is defined by frequency of their appearance. The locations of five reclosers are given in Table 13 and the simulation results are given in Table 14.

Table 13. Locations for the fixed reclosers in the test system 1

| Recloser Number | Location |
|---|---|
| 1 | 3-4 |
| 2 | 10-11 |
| 3 | 30-31 |
| 4 | 47-48 |
| 5 | 67-68 |

Table 14. Effects of type 2 DGs on CRI of a distribution system with fixed reclosers

| DG Number | DG Location | DG size (MVA) | CRI |
|---|---|---|---|
| 1 | 26 | 1.3 | 2.875 |
| 2 | 26, 54 | 1.3, 1.1 | 2.184 |
| 3 | 26,54,34 | 1.3,1.1,0.67 | 1.492 |
| 4 | 26,54,34,90 | 1.3, 1.1,0.67,0.41 | 0.765 |
| 5 | 26,54,34,90, 36 | 1.3, 1.1,0.67,0.41,0.37 | 0.108 |
| 6 | 26,54,34,90,36,58 | 1.3, 1.1,0.67,0.41,0.37,0.12 | 0.093 |

Table 14 shows that for any distribution network, where reallocation of reclosers is not an option, optimizing the location and sizing of DGs can significantly improve the reliability of the distribution system. However, this improvement is smaller compared to the case where DGs were fixed and recloser locations were allowed to be optimized. If the distribution network is being expanded or upgraded, then utilities would have an option in planning the location of DGs and reclosers in order to increase the system reliability. To reflect this case, the proposed method is applied to the test system 1 to optimize the location of both reclosers and DGs and results are presented in Table 15.

Results in Table 15 indicate that the reliability of the system can be improved significantly by properly allocating reclosers and DGs. For example, in test case 1 as shown in Table 10, reliability index improves from 3.9741 to 0. 9021 when the number of reclosers increases from one to five. Similarly, increasing the number for type 2 DGs with a fixed number of reclosers improves the reliability index from 2.875 to 0.093 as shown in Table 14. Additionally, optimizing both the number of reclosers and the type 2 DGs simultaneously results in a significant improvement in the reliability of distribution system as shown in Table 15. Here the value of the composite reliability index is reduced to -0.156, exceeding the targeted CRI of 0.

Table 15. Simultaneous optimal allocation of Reclosers and type 2 DGs in the IEEE 90-bus distribution system

| Number of Reclosers | Number of DGs | Reclosers positions | DG positions | DG size(MVA) | CRI |
|---|---|---|---|---|---|
| 1 | 1 | 8-9 | 26 | 1.31 | 2.875 |
| 2 | 2 | 4-5,47-48 | 26,34 | 1.31,0.95 | 2.343 |
| 3 | 3 | 2-27,8-9,48-49 | 26,54,34 | 1.31,0.95,0.67 | 1.145 |
| 4 | 4 | 7-8,30-31,47-48,67-68 | 26,54,34,90 | 1.31,0.95,0.67,0.98 | 0.235 |
| 5 | 5 | 3-4,10-11,30-31,49-50,67-68 | 26,54,34,90,26 | 1.31,0.95,0.67,0.98,0.84 | -0.156 |

***Implementation on Test system 2:*** In order to demonstrate the effectiveness of the proposed method on a multi-phase unbalanced distribution system, the IEEE 123 node distribution feeder is selected as the second test system. This system has 85 load points as shown in Figure 14. This test feeder consists of four voltage regulators, four capacitor banks, overhead and underground line segments with various phasing, and various unbalanced loading with different load types [80]. The detailed data for this test system can be obtained from [81] and are provided in appendix C for easy reference. This test system is further divided into two cases:

I) Without alternative paths

II) With alternative paths.

In addition, the following assumptions are made during the implementation of the proposed algorithm on this test feeder.

- The distribution network is supplied by only one substation and all normally open switches are removed.
- All reclosers function identically. In the presence of any type of fault, only the minimum numbers of reclosers that are close to the fault are activated in order to isolate the fault.
- Islanding is permitted in every section.
- Fault incidence rate and the duration of faults are uniform over all feeder branches.
- DGs are assumed to be 100% reliable.
- Two alternate paths are considered as shown in Figure 20.
- For the optimization process, lines are named after the nodes that they connect to as shown in Table 16.

Table 16. Line naming procedure

| Node From | Node To | Line Number |
|---|---|---|
| 0 | 1 | 1 |
| 1 | 2 | 2 |
| 1 | 3 | 3 |
| 7 | 8 | 8 |

*Case I: Without alternative paths:* The value of various parameters used in this study are given in Table 17. Results obtained for this case are shown in Tables 18 – 20. Table 18 shows the result obtained when there are no DGs connected to the system. The impact of optimal location of reclosers with fixed locations and sizes of DGs are given in Table 19. Here, the optimal location and size of DGs that resulted in a minimal

distribution power loss have been used. The method for obtaining the optimal location and sizes for this distribution system is described in details in chapter 3. Table 20 shows the result obtained when both reclosers and DGs are optimized.

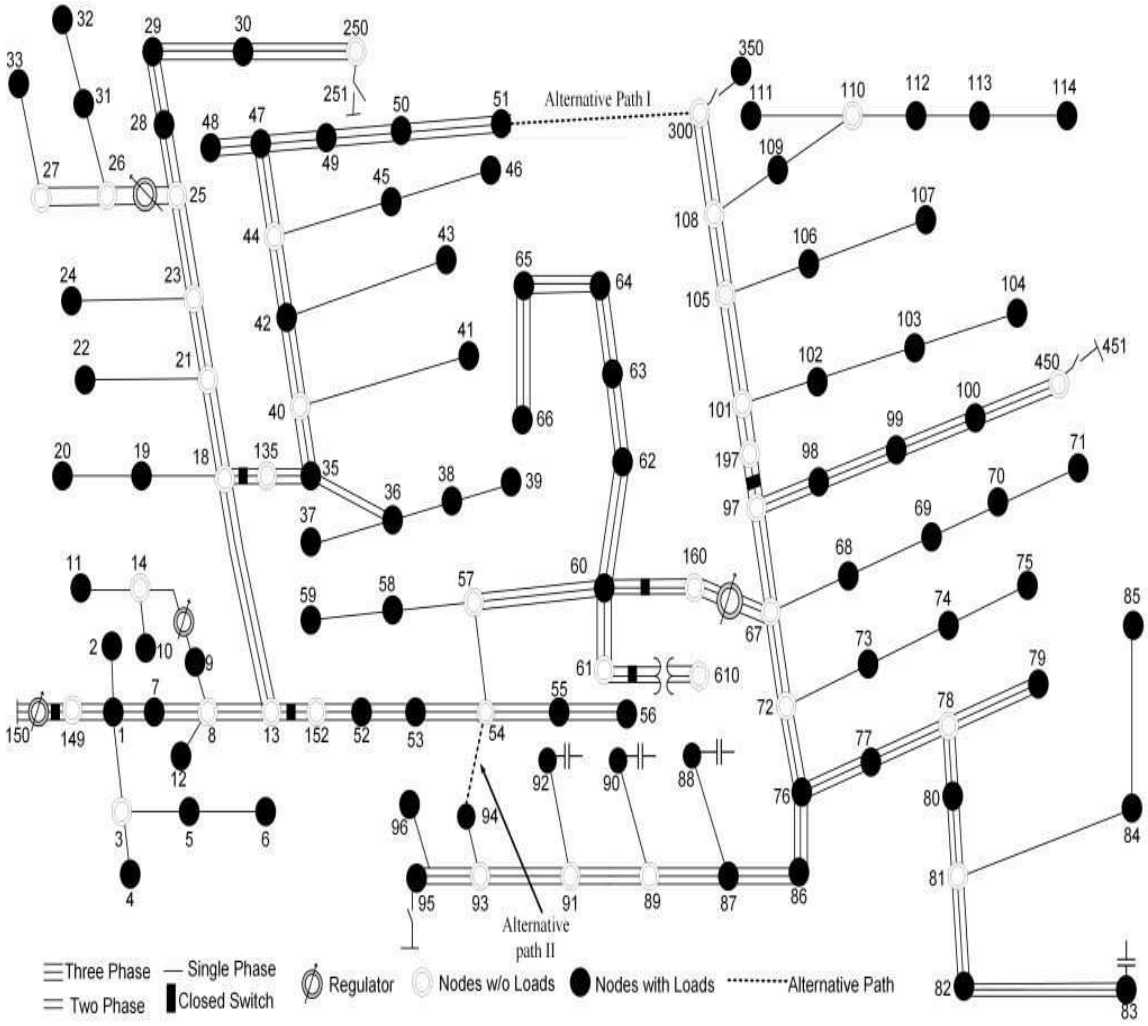


Figure 20. One line diagram of system 2 for case II

Table 17. Values of parameters used in simulation in case I of system 2.

| | |
|---|---|
| Damage restoration time (Outage time) | 3 hrs |
| Fault Incidence rate (failure rate) | 0.22 |
| Fraction of permanent fault | 0.2 |
| $W_{SAIFI}$ | 0.33 |
| $W_{SAIDI}$ | 0.67 |
| $SAIFI_T$ | 1.5 |
| $SAIDI_T$ | 2.7 |
| Number of particles | 100 |
| Iteration | 150 |

Table 18. Optimal recloser location without any DGs in case I of system 2

| Reclosers | Location | CRI |
|---|---|---|
| 1 | 67 | 5.130 |
| 2 | 67,18 | 4.786 |
| 5 | 77,105,87,49,23 | 3.863 |
| 7 | 1,7,54,67,77,44,87 | 3.268 |
| 8 | 7,9,13,60,86,35,18,44 | 2.659 |
| 9 | 7,9,47,25,67,80,87,109,135 | 2.163 |
| 10 | 1,8,13, 21,44, 60,67,77,87,109 | 1.759 |
| 11 | 7,13,18,135,44,57,60,97,76,89,105 | 1.631 |
| 12 | 1,9,21,44,18,60,80,86,102,109,135,25 | 1.619 |

Table 19. Optimal recloser location with five fixed type 2 DGs in case I of system 2.

| Reclosers | Location | DG Location | DG size (MVA) | CRI |
|---|---|---|---|---|
| 1 | 160 | 67 | 1.34 | 3.075 |
| 2 | 40,67 | 67,47 | 1.72 | 2.413 |
| 3 | 52,35,72 | 67,47,72 | 0.873 | 1.284 |
| 4 | 52,72,109,54 | 67,47,72,114 | 1.56 | 0.379 |
| 5 | 87,72,57,109,18 | 67,47,72,114,95 | 0.481 | -0.041 |

Table 20. Optimal location of both reclosers and type 2 DGs in case I of system 2.

| Reclosers | Location | DG Location | DG size (MVA) | CRI |
|---|---|---|---|---|
| 1 | 57 | 60 | 1.43 | 2.851 |
| 2 | 18,35 | 67,50 | 1.16 | 2.148 |
| 3 | 18,52, 72 | 67,47,79 | 0.873 | 0.857 |
| 4 | 35,13,72,54 | 60,48,72,29 | 1.83 | 0.069 |
| 5 | 87,67,52,1,35 | 67,35,86,30,95 | 0.518 | -0.147 |

Results obtained for this case show similar pattern as that of the IEEE 90-bus test system 1. The reliability index of the test distribution system without DG integration decreased with the increment in the number of reclosers. A significant reduction in CRI value is seen when the number of reclosers is increased from one to ten. As has been discussed earlier, smaller values of CRI reflect an improvement in the reliability of distribution networks. There was an additional minimal impact on the CRI value when more reclosers were added as shown in Table 18. Integration of DGs into the distribution system, however, resulted in a significant decrease in the index value. With just five fixed type 2 DGs included, the CRI value is reduced significantly using only five reclosers as shown in Table 19. However, Table 20 shows that simultaneously optimizing for

locations of reclosers and DGs reduced the CRI value but increased the amount of power needed to be produced by DGs compared to that in Table 19.

*Case II with alternative paths:* One line diagram of the test system 2 with alternative paths is shown in Figure 20. The same parameter values as in Case I and shown in Table 17 are used again in this case. Simulation results are shown in Tables 21-22. The presence of alternative paths increases the reliability of the system while increasing the number of reclosers. Compared to case I of system 2, when multiple DGs are integrated in the system, the value of reliability index improves more but the number of reclosers does not reduce significantly as shown in Table 23. The reason being that isolated load points can be serviced through alternative paths. This reduces the service interruption times but more reclosers are required to isolate the loads during faults.

Table 21. Optimal recloser location without DGs in case II of system 2

| Reclosers | Location | CRI |
|---|---|---|
| 1 | 67 | 4.076 |
| 2 | 67,18 | 3.663 |
| 5 | 7,105,68,45,21 | 2.194 |
| 8 | 8,13,21,60,87,35,18,42 | 1.492 |
| 10 | 1,7,11, 21,44, 60,67,77,87,109 | 0.873 |
| 12 | 1,9,21,44,18,60,80,86,102,109,135,25 | 0.549 |
| 15 | 3,8,14,21,35,45,52,57,93,99,110,112,54,77,80 | 0.371 |
| 16 | 1,7,9,40,47,78,86,54,67,94,105,109,68,91,110,52 | 0.304 |

Table 22. Optimal recloser location with five fixed DG in case II of system 2.

| Reclosers | Location | DG Location | DG size (MVA) | CRI |
|---|---|---|---|---|
| 3 | 67,76,108 | 67 | 1.34 | 2.849 |
| 4 | 51,52,40,67 | 67,47 | 1.72 | 2.041 |
| 5 | 94,72,52,35,67 | 67,47,72 | 0.873 | 1.113 |
| 6 | 94,52,72,109,54,67 | 67,47,72,114 | 1.56 | -0.065 |
| 8 | 91,67,72,57,109,18,101, 13 | 67,47,72,114,95 | 0.481 | -0.195 |

Table 23. Comparison of reliability index for case I and case II of system 2.

| Case | Number of Reclosers | Best index value (CRI) | Number of DGs | Optimal DG |
|---|---|---|---|---|
| I | 12 | 1.619 | 0 | |
| I | 5 | -0.041 | 5 | No |
| I | 5 | -0.147 | 5 | Yes |
| II | 16 | 0.0304 | 0 | |
| II | 8 | -0.195 | 5 | No |
| II | 8 | -0.217 | 5 | Yes |

### 4.5. Part II: Reliability Analysis Based on System Disruption Cost (ECOST)

First part of this study provides an insight into the effects of optimization of reclosers and DGs on various reliability indexes. This method is effective when the service provided to customers outweighs the cost incurred by the utility. However, the decision on reliability improvement of any distribution network is highly dependent on the cost to the utility and the value of benefits provided to its customers. Therefore, planning for optimal recloser allocations should include the acceptable level of service provided to customers as a function of utility cost and the costs incurred by customers

due to service interruption. Traditionally, the acceptable level of service has been achieved by comparing indices like SAIFI and SAIDI with arbitrary target values which are based on the perception of the customer tolerance level for service interruptions [99]. However, due to expansion of distribution networks and integration of DGs into these networks, utilities have to make a large number of capital investments and operating decisions. As such, the traditional rule of thumb cannot be used in a consistent manner.

The earliest study of the effect of optimal allocation of switches on expected outage cost (ECSOT) dates back to 1999 [90]. In [90], authors used Bellmann's optimality principal to find the optimal locations of automatic sectionalizing switching devices (ASSAD). The objective of this study was to minimize the total capital investment of switches. In [93], authors suggested simulated annealing algorithm to optimize the switch locations considering investment, outage, and maintenance costs. A value based distribution system reliability planning to minimize the cost of interruptions to both the utility and its industrial customers is discussed in [99]. An Ant colony system (ACS) based algorithm to reduce the customer interruption costs is discussed in [86]. An optimal switch placement in distribution systems using trinary particle swarm optimization algorithm is proposed in [100].

Excluding some exceptions such as [90] and [99], all of the work presented in the literature is based on balanced distribution systems. Effects on the reliability planning due to the integration of DGs in unbalanced distribution systems have not been considered in any study. In the following section of this document, the author proposes the use of DPSO to solve the problem of optimal allocation of reclosers and DGs in three phase unbalanced distribution systems.

### 4.5.1. Objective Function

The objective of this study to optimally allocate reclosers and DGs in three phase unbalanced distribution systems in order to minimize the total system cost which is the sum of expected interruption costs and cost associated with reclosers. The objective function has been derived as shown in equations (16), (17), and (18).

$$\text{ECOST} = \sum_{i=1}^{NC} \sum_{j=1}^{NL} \sum_{k=1}^{CT} \lambda(i) \,.\, C_{i,j}(i,j,k).L(j,k) \quad (16)$$

Where,

| | |
|---|---|
| *NC* | Total number of feeder sections |
| *NL* | Total number of affected load points |
| *CT* | Total number of customer types |
| $\lambda(i)$ | Average failure rate of distribution elements |
| $C_{i,j}(i,j,k)$ | Customer damage function |
| $L(j,k)$ | Average Load of the kth-type customers located at the jth load point |
| ECOST | Expected Interruption cost |

$$\text{I} = \sum_{t=1}^{T} \sum_{r=1}^{N} \big(CC(s) + IC(s) + MC(s)\big) \quad (17)$$

Where,

| | |
|---|---|
| I | Investment Cost |
| *T* | Life period of recloser |

$N$ Number of reclosers

$CC(s)$ Capital cost of recloser

$IC(s)$ Installation cost of recloser

$MC(s)$ Maintenance cost

Hence, the total objective function is:

$$F_{Obj=} ECOST + I \quad (18)$$

Subject to

$$V_i^{min} < V_i < V_i^{max} \quad (19)$$

### 4.5.2. Methodology

The calculation of the total cost of the objective function is performed in following steps:

Step 1) Place a recloser and create a section

Step 2) Integrate DG into the section

Step 3) Simulate single line to ground fault

Step 4) Find all the load points that are disconnected

Step 5) Calculate the type and the amount of lost loads

Step 6) Determine the value of the objective function given by equation (18)

The algorithm stops when one of the following conditions is satisfied:

i) Current iteration number is equal to predefined maximum iteration

ii) If the difference in the value of the objective function is less than 1000.

### 4.5.3. Implementation

The objective function given in equation (18) is optimized using DPSO. A voltage constraint of 1± 5% is enforced by solving the three phase optimal power flow (TOPF). As stated in other parts of this document, the open source software developed by the Electric Power Research Institute (EPRI) called OpenDSS has been adapted to solve this TOPF. The overall algorithm has been implemented in MATLAB and is based on a two-way data exchange between MATLAB, which implements the DPSO algorithm, and OpenDSS simulation engine which performs the TOPF and implements control variables on the distribution network model. The overall implementation of the algorithm is shown in Figure 21. The procedure for solving the three phase optimal power flow (TOPF) has been described in chapter 3.

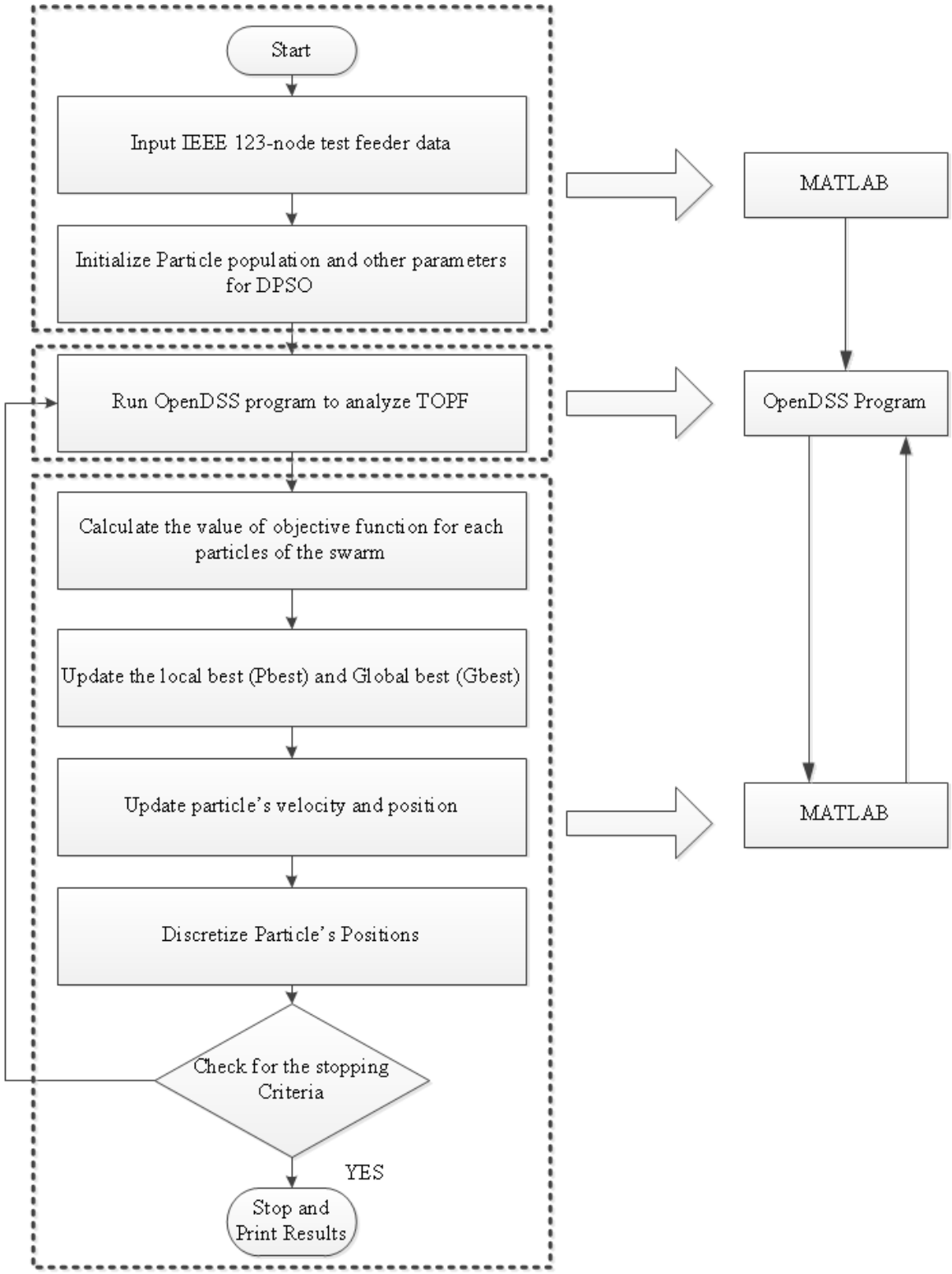


Figure 21. Algorithm to minimize the total cost incurred by the Utility.

### 4.5.4. Results and Discussion

The proposed algorithm is applied to test systems 1 and 2 described earlier. The total investment cost including capital cost and installation cost for each recloser is U.S. $4,700. The annual maintenance cost is 2% of the investment cost. The monetary values associated with customer damage function are taken from [101] and are listed in Table 24. The life period of switches is assumed to be 20 years with an interest rate of 8% and inflation rate of 9% [93]. All the necessary parameters used in the simulation are given in Table 25. The following assumptions are made during the simulation study:

i) The distribution network is powered by only one substation and all normally open switches are removed.

ii) All reclosers function identically. In the presence of any type of fault, only the minimum number of reclosers that are close to the fault are activated in order to isolate the fault.

iii) Islanding is permitted in every section of distribution network.

iv) Fault incidence rate and the duration of faults are uniform over all feeder branches.

v) Since the customer types are not known for the test systems, an assumption has been made that 30% of customers in each section are commercial and the rest are residential.

vi) Each load point is connected to a transformer

vii) Costs of DGs are not considered in this study. It is assumed that utility has decided to integrate DGs and is only planning on maximizing the benefit by optimally allocating them in the distribution system.

viii) It is assumed that DGs connected to any section can supply the power to all loads that are in that section for the duration of the total outage time.

Table 24. Average interruption cost.

| User Type | Interruption Duration | | | |
|---|---|---|---|---|
| | 30 min | 1hour | 4 hours | 8 hours |
| Commercial ($/kW) | 2.78 | 3.73 | 12.29 | 21.73 |
| Residential ($/kW) | 2.2 | 2.6 | 5.1 | 7.1 |

Table 25. Values of parameters used in simulation.

| | |
|---|---|
| feeder restoration time (Outage time) | 4 hrs |
| Fault Incidence rate (failure rate) f/yr/mile | 0.22 |
| Transformer (f/yr) | 0.005 |
| Transformer restoration time | 10 hrs |
| Cost of each recloser (Capital + installation) | $4,700.0 |
| Number of particles | 100 |
| Iteration | 100 |

***Results for the IEEE 90- bus test system 1:*** The proposed method is implemented in test case I and results are tabulated. Table 26 shows the results for the base case where DGs are not connected. Here, five reclosers are allocated one at a time. It can be seen that the value of ECOST decreases and the total cost of reclosers increases as more reclosers are added to the system. The effect of simultaneously optimizing reclosers and DGs locations and sizes on the objective function is shown in Table 27. The Total value of ECOST decreases to $100,241 when five type 2 DGs are integrated in the distribution

system. Since the costs of DGs are not considered in this study, a separate study must be conducted if DGs are being installed just to increase the reliability of the system. As the total ECOST decreases when DGs are integrated in the distribution system, the total optimum cost decreases as well.

Table 26. Optimal recloser allocation without DGs in test system 1

| Number of reclosers | Location | ECOST ($/yr) | Investment cost($/yr) |
|---|---|---|---|
| 0 | --- | 332,769 | --- |
| 1 | 8-9 | 303,934 | 4,700 |
| 2 | 47-48,11-12 | 285,849 | 9,400 |
| 3 | 10-11,27e-28e,47-48 | 260,834 | 14,100 |
| 4 | 3-4,27-28,11-12,42-43 | 247,271 | 18,800 |
| 5 | 3-4,8-9,27e-28e,47-48,3-35 | 240,492 | 23,500 |

From Table 26, it can be seen that the optimal recloser allocation resulted in a significant decrement in the ECOST of the test system. In fact, optimal placement of five reclosers resulted in the reduction of ECOST by 30%. When multiple reclosers and DGs are optimally placed in the system, the total ECOST saving of $208,558 or 62% is achieved.

Table 27. Optimal recloser and type 2 DGs allocation in test system 1

| Number of reclosers | Location | Number of DGs | DG Locations | DG Size (MVA) | ECOST ($/yr) | Investment cost($/yr) |
|---|---|---|---|---|---|---|
| 0 | --- | --- | --- | --- | 332,769 | --- |
| 1 | 8-9 | 1 | 26 | 1.24 | 260,562 | 4,700 |
| 2 | 4-5,47-48, | 2 | 26,34 | 1.15,0.54 | 215,468 | 9,400 |
| 3 | 2-27,8-9,48-49 | 3 | 24,50,34 | 0.98,1.52,0.84 | 183,378 | 14,100 |
| 4 | 7-8,30-31,47-48,67-68 | 4 | 26,34,90,54 | 0.91,1.24,0.87,1.43 | 149,167 | 18,800 |
| 5 | 3-4,10-11,30-31,49-50,67-68 | 5 | 24,50,34,89,58 | 1.04,0.85,0.35,1.52,1.47 | 100,241 | 23,500 |

***Results for the IEEE- 123 node test System 2:*** The following two cases are evaluated using this system.

I. Test system without alternative paths

II. Test system with alternative paths

The results for case I of test system 2 without and with type 2 DGs are presented in Tables 28 and 29. It can be seen from the results that the cost of energy not served

(ECOST) decreases when optimal numbers of reclosers are placed in their optimal locations. The optimal number of reclosers and their locations for the base case are similar to the one reported in literature [92]. Also, integrating type 2 DGs in the system further reduces the total cost incurred by the utility. This is because, sections with DGs act as an island where DG supplies power to all the loads in that particular section during the entire outage time. Furthermore, installing multiple DGs not only decreased the total cost by more than 60% but the number of reclosers decreased as well.

Table 28. Optimum allocation of reclosers for case I of system 2 without DG

| | |
|---|---|
| ECOST for Base case (No recloser) ($/yr) | 473,926 |
| Number of optimal reclosers | 13 |
| Recloser positions | 3,10,14,13,22,47,17,65,79,77,96,103,109 |
| ECOST ($/yr) | 303,719 |
| Switch cost ($/yr) | 61,100 |
| Total Cost ($/yr) | 364,819 |

Table 29. Optimum allocation of reclosers for case I of system 2 with multiple DGs.

| | |
|---|---|
| Number of optimal reclosers | 7 |
| Recloser positions | 13 ,35,47,67,86,77,54 |
| Type 2 DGs | 5 |
| DG locations | 67,95,47,114,74 |
| ECOST ($/yr) | 112,581 |
| Switch cost ($/yr) | 23,500 |
| Total Cost ($/yr) | 136,081 |
| Saving on Total Cost | 63% |

The results obtained for case II are shown in Tables 30 and 31. The ECOST of the system in this case decreases significantly due to the fact that certain load points can be serviced by alternative paths. Because of alternative paths, the number of reclosers required to isolate the loads increases.

Table 30. Optimum allocation of reclosers in case II without DG.

| | |
|---|---|
| ECOST for Base case (No recloser) ($/yr) | 311,102 |
| Number of optimal reclosers | 17 |
| Recloser positions | 3,8,13,21,26,35,42,52,55,57,63,68,73,78,86,93,110 |
| ECOST ($/yr) | 204,043 |
| Switch cost ($/yr) | 79,900 |
| Total Cost ($/yr) | 283,943 |

Table 31. Optimum allocation of reclosers in case II with multiple DGs.

| | |
|---|---|
| Number of optimal reclosers | 11 |
| Recloser positions | 13 ,21,35,47,54,67,86,77,93,109 |
| Number of type 2 DGs | 5 |
| DG locations | 60,51,110,72,91 |
| ECOST ($/yr) | 80,301 |
| Switch cost ($/yr) | 23,500 |
| Total Cost ($/yr) | 103,801 |

From the Tables 28-31, it can be observed that when alternate paths are considered and the locations of reclosers and DGs are simultaneously optimized, the ECOST of the system reduces from $303,719 in Table 28 to $80,301 in Table 31. In

order to demonstrate the economic viability of the proposed system over the life of reclosers, the discount future benefit (DFB) is calculated for the base case without alternative paths as shown in [91].

$$\text{DFB}=\sum_{t=0}^{20}\frac{473{,}926-303{,}719}{(1+0.08)^t}=1{,}841{,}324 \quad (8)$$

Maintenance cost $=0.02*61{,}100*\sum_{t=0}^{20}(1+0.09)^t=69{,}366$

Hence, the DFB is significantly more than the investment and maintenance cost which is $130,466 (61,100 + 69,366). The values of DFB increases significantly for DG integrated distribution system. Therefore, installing switches in this system is a reasonable investment from an economical point of view.

### 4.6. Comparison between CRI and ECOST

In order to compare the effectiveness of the two proposed methods for reliability evaluation, the locations of reclosers and DGs obtained from the first part of the study is used to calculate the total cost (ECOST and investment cost) and results are presented in Table 32. It can be observed that optimizing reclosers and DGs based on the reliability indexes, increases the total cost incurred by utilities. While the number of reclosers needed to obtain the maximum reliability index is less, more money is lost due to the customer interruption cost. This makes sense because reliability indexes depend heavily on number of customers rather than the amount of the load and customer types. Similarly, table 33 shows the effect of minimizing the total cost on reliability index. When reclosers and DG are allocated to reduce the total cost incurred by utility, reliability of the distribution system decreases. This is because of the fact that ECOST depends heavily on the amount of load lost due to fault and type of customer interrupted. The goal in this

case is not to reduce the number of customer affected but to provide more reliable service to industry and commercial consumers.

Table 32. Total cost obtained using the optimal position and number of reclosers and DGs based on minimum CRI index.

| Test System | Case | Number of Reclosers | Number of DGs | Optimal DG | Minimum CRI value | Total Cost ($/yr) |
|---|---|---|---|---|---|---|
| 1 | -- | 5 | 0 | | 0.845 | 511,712 |
| 1 | -- | 5 | 5 | No | -0.019 | 313,597 |
| 1 | -- | 5 | 5 | Yes | -0.156 | 251,391 |
| 2 | I | 12 | 0 | | 1.619 | 313,821 |
| 2 | I | 5 | 5 | No | -0.041 | 250,719 |
| 2 | I | 5 | 5 | Yes | -0.147 | 184,211 |
| 2 | II | 16 | 0 | | 0.0304 | 254,105 |
| 2 | II | 8 | 5 | No | -0.195 | 198,635 |
| 2 | II | 8 | 5 | Yes | -0.217 | 101,122 |

Table 33. CRI obtained using the optimal position and number of reclosers and DG based on minimum total cost value.

| Test System | Case | Number of Reclosers | Number of DGs | Optimal DG | Minimum Total Cost ($/yr) | CRI |
|---|---|---|---|---|---|---|
| 1 | -- | 0 | 0 | | 332,769 | 4.381 |
| 1 | -- | 5 | 5 | No | 240,492 | 1.132 |
| 1 | -- | 5 | 5 | Yes | 100,241 | 0.976 |
| 2 | I | 0 | 0 | | 473,926 | 5.943 |
| 2 | I | 13 | 0 | | 303,719 | 1.864 |
| 2 | I | 7 | 5 | Yes | 112,584 | 1.218 |
| 2 | II | 0 | 0 | | 311,102 | 5.301 |
| 2 | II | 17 | 0 | | 184,043 | 2.708 |
| 2 | II | 11 | 5 | Yes | 80,301 | -.091 |

## 4.7. Conclusion

Integration of DGs in distribution systems has been increasing rapidly over the past decades. An improper allocation of DGs has the potential to degrade the distribution network, but with a proper allocation of DGs and reclosers, significant improvements in system reliability can be achieved. In this chapter, discrete particle swarm optimization based method has been implemented for the optimal allocation of reclosers and DGs. The first part of the study focused on attaining the maximum reliability based on various reliability indexes. A new reliability index called composite reliability index (CRI) has been proposed by combining two mostly used reliability indexes (SAIFI and SAIDI). The proposed method is validated by comparing the results with those obtained using ant colony system (ACS) algorithm. The robustness of the proposed method is demonstrated by solving the optimal allocation problem for both balanced and unbalanced IEEE test distribution systems. The second part of the study proposed a customer interruption cost (ECOST) based objective function for the optimal allocation of reclosers and DGs. This objective function reflects several system properties like failure rate, customer types, and load density. Here, the total cost incurred by utility during the allocation of reclosers and DGs was minimized. Results indicate that simultaneous optimization of the number and location of reclosers and DGs provides the best system reliability. Furthermore, it can be observed that optimizing reclosers and DGs numbers, sizes, and location based on just the reliability indices increases the total cost incurred by utilities. Likewise, when reclosers and DGs are allocated to reduce the total cost incurred by utility, reliability of the distribution system does not improve much. Hence, a careful and detailed planning must be performed to obtain the maximum benefit per dollar invested.

# CHAPTER 5

# COST MINIMIZATION PLANNING FOR ALLOCATION OF DISTRIBUTED GENERATORS

This chapter proposes a method for optimal allocation of various types of distributed generators (DGs) in distribution systems to minimize the total cost incurred by utilities. This planning problem is formulated by converting several issues like, investment cost, operation and maintenance cost, reliability, pollutant emission, and power purchased by the utility, into a cost function. A cost benefit analysis using particle swarm optimization (PSO) algorithm in a co-simulation environment of MATLAB and OpenDSS software is successfully implemented to estimate the most cost-effective allocation of DGs to serve the projected peak demand. The proposed method is tested on the IEEE 123-bus distribution feeder. Results indicate that maximum return on the investment can be achieved when DGs are planned to meet the future load growth.

## 5.1. Introduction

In traditional power systems the electric power generated by centrally located fossil fueled generation plants is transmitted to various substations via transmission lines and then is distributed to consumers through distribution networks. However, with increasing concerns about global warming, various renewable energy policies, like renewable portfolio standard (RPS), have set very ambitious targets for penetration of renewable energy resources in electric power systems. Numerous studies have shown that using renewable energy resources as distributed generators (DG) not only reduces the

already existing weakness, such as distribution power losses, highly sensitive voltage profiles and lower system reliabilities, but also increases network's capacity for power distribution without having to significantly upgrade or expand the system [2], [4]–[7], [9], [12], [83].

Any decision to integrate DGs in distribution systems requires a detailed cost benefit analysis. As such, the foundation of any DG integration planning is to compute cost functions that can accurately represent the operating costs of distribution planning area (DPA). All important issues like lost energy, expected energy not served, reliability, etc., are converted to cost and used to determine the minimum cost investment options [102]. Numerous cost functions have been proposed in literature to reflect particular characteristics of DGs. The effect of changing the penetration level of various DGs on annual energy losses has been discussed in [103]. Authors in [104] have proposed a heuristic approach to DG capacity investment planning with respect to competitive electric market auction. A mixed integer linear program has been proposed in [105] to determine the optimal resource mix of different DG technologies for a particular section of distribution network. Similarly, authors in [41] have used mixed integer linear programming to minimize the system's annual energy losses with numerous constrains including, voltage limits, feeder's capacity, maximum penetration limit, and the discrete size of available DG units.

Most of these works are based on the assumption that DGs can supply fixed and firm power at all times. Only few studies such as [41], [105]–[107] have considered the intermittent nature of DGs output power. Moreover, only one study, [106], has proposed a cost function that represents the major characteristics of DGs such as; actual cost of

DGs, energy loss of distribution system, expected energy not served, and system adequacy as a function of energy cost.

In this study, a cost minimization planning method based on optimal allocation of wind, solar, and geothermal DGs is proposed. An objective function is derived to reflect all aforementioned important issues including the total cost of DGs and the expected savings on pollutant emissions that must be considered during the planning phase. In addition, the price of electricity that must be purchased to supplement DG resources has been included in the formation of the cost function. The adaptive weight particle swarm optimization (AWPSO) method has been used to minimize the objective function. Open source software developed by the Electric Power Research Institute (EPRI) called OpenDSS has been used in a co-simulation environment with MATLAB to solve the unbalanced three phase optimal power flow (TOPF) problem. The proposed method is applied to the multi-phase unbalanced IEEE 123-node distribution feeder. By considering the seasonal load variations, a cost benefit analysis due to the increments in the load is also discussed.

## 5.2. Problem Formulation

Different types of DGs have different impacts on cost, environment, and reliability of the system. For instance, wind turbine generators (WTGs) generate no pollution and they do not consume any fuel. Photovoltaic (PV) systems produce no emission, are durable, and demand minimal maintenance to operate. Biomasses, geothermal, and fuel cell generators, on the other hand, require fuel to generate electrical energy. However, these generators can supply near constant power at all times. Hence, they can be used as dispatchable sources [108].

### 5.2.1. Source and Load representation

WTGs and PV systems are intermittent sources whose output depends on the weather condition. In this study, the intermittent nature of WTGs and PV systems is considered. To make the study realistic, an actual test system is used for simulation. Hourly data of power outputs from an actual WTG are obtained and used from California independent system operator (ISO) [33]. As shown in Figure 22, the power output from WTG varies at each hour. Similarly, hourly data from a PV system are obtained from EPRI's smart grid research center [109]. Since solar energy is only available during the day, the power production starts around 7:00 AM and continues until 7:00 PM as shown in Figure 23. An hourly production data of geothermal energy is obtained from California ISO and is shown in Figure 24.

Instead of constant loads, a seasonal variation in the load profile has been considered in this study. The load data represent the percentage of annual peak load for each hour in a particular season and are shown in Table 34.

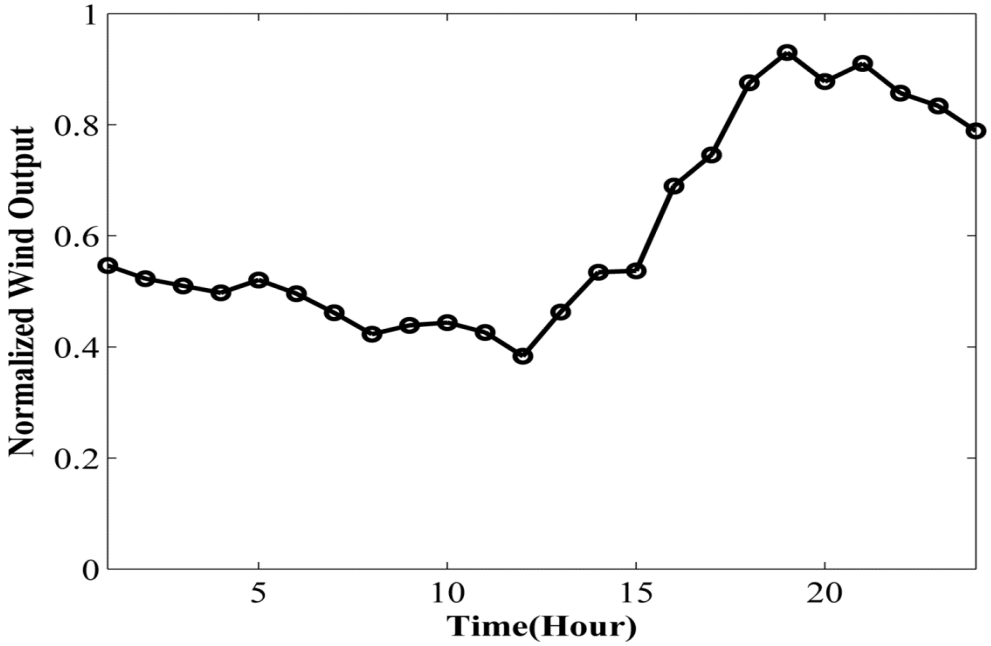

Figure 22. Normalized Wind output data for 24 hours

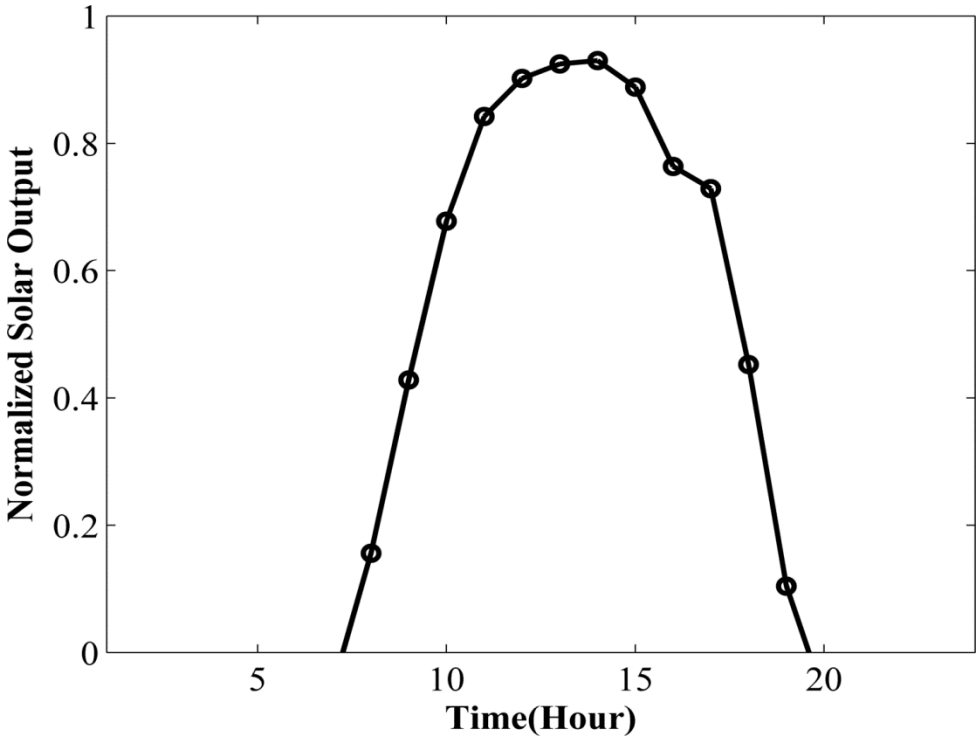


Figure 23. Normalized solar output for 24 hours

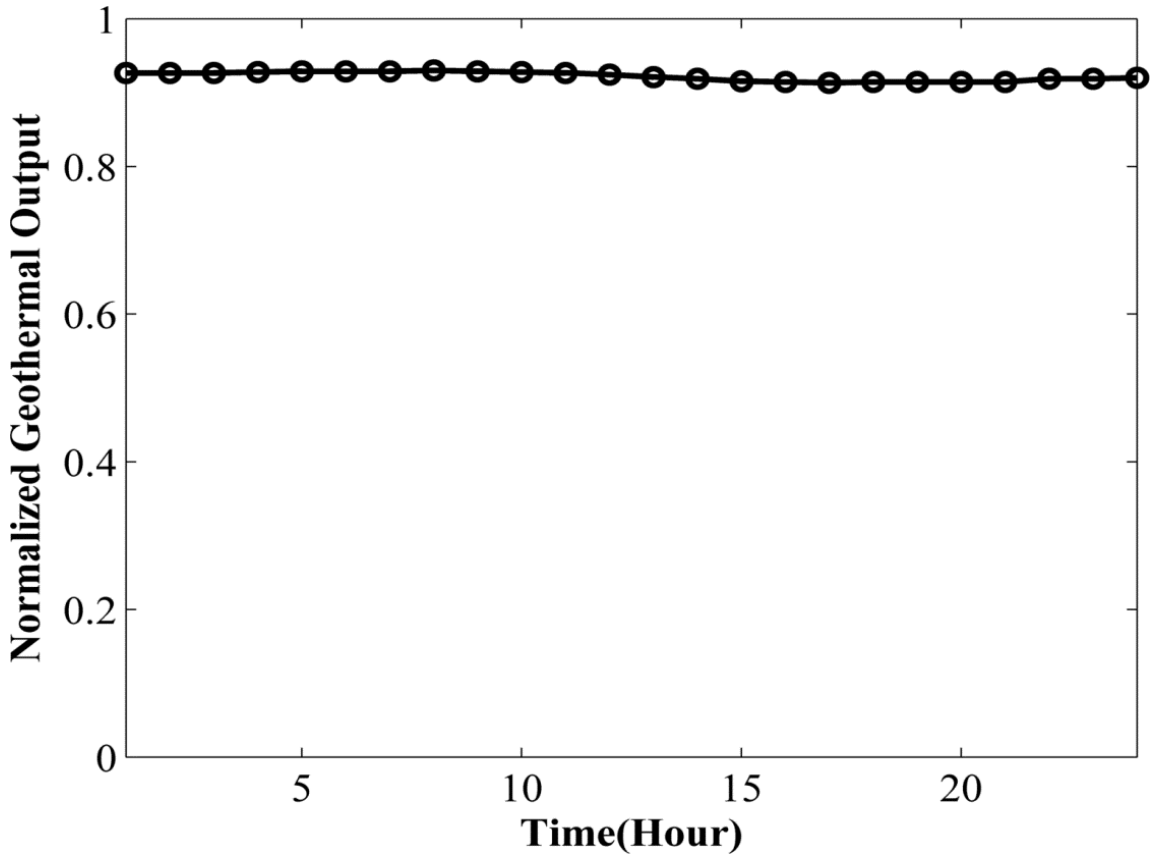


Figure 24. Normalized Geothermal Output for 24 hour.

Table 34. Seasonal load profile.

| Hour | Winter | Spring | Summer | Fall |
|---|---|---|---|---|
| 1 | 0.4757 | 0.3969 | 0.64 | 0.3717 |
| 2 | 0.4473 | 0.3906 | 0.6 | 0.3658 |
| 3 | 0.426 | 0.378 | 0.58 | 0.354 |
| 4 | 0.4189 | 0.3654 | 0.56 | 0.3422 |
| 5 | 0.4189 | 0.3717 | 0.56 | 0.3481 |
| 6 | 0.426 | 0.4095 | 0.58 | 0.3835 |

| | | | | |
|---|---|---|---|---|
| 7 | 0.5254 | 0.4536 | 0.64 | 0.4248 |
| 8 | 0.6106 | 0.5355 | 0.76 | 0.5015 |
| 9 | 0.6745 | 0.5985 | 0.87 | 0.5605 |
| 10 | 0.6816 | 0.6237 | 0.95 | 0.5841 |
| 11 | 0.6816 | 0.63 | 0.99 | 0.59 |
| 12 | 0.6745 | 0.6237 | 1 | 0.5841 |
| 13 | 0.6745 | 0.5859 | 0.99 | 0.5487 |
| 14 | 0.6745 | 0.5796 | 1 | 0.5428 |
| 15 | 0.6603 | 0.567 | 1 | 0.531 |
| 16 | 0.6674 | 0.5544 | 0.97 | 0.5192 |
| 17 | 0.7029 | 0.567 | 0.96 | 0.531 |
| 18 | 0.71 | 0.5796 | 0.96 | 0.5428 |
| 19 | 0.71 | 0.6048 | 0.93 | 0.5664 |
| 20 | 0.6816 | 0.6174 | 0.92 | 0.5782 |
| 21 | 0.6461 | 0.6048 | 0.92 | 0.5664 |
| 22 | 0.5893 | 0.567 | 0.93 | 0.531 |
| 23 | 0.5183 | 0.504 | 0.87 | 0.472 |
| 24 | 0.4473 | 0.441 | 0.72 | 0.413 |

### 5.2.2 Design Variables

***Costs:*** Proper cost estimation of DGs is the most important variable to include during the planning process. In this study, the total cost includes initial capital cost, operational and maintenance costs and the salvage value of the equipment. Also, the power that is needed to be purchased by utility in order to supplement its DG sources has been included. These cost functions are adapted from [110] and [106]. Hence, the total DG cost ($/year) is obtained for each source as follows:

*a. Cost of WTG*: The capital cost of wind turbine is:

$$Capital\ Cost\ (CCw) = \sum_{i=1}^{8760} \alpha_w P_w(i) * \sum_{t=1}^{T} \left(\frac{1+\mu}{1+\varphi}\right)^t \quad (1)$$

where,

| | |
|---|---|
| $\alpha_w$ | Capital cost per kW of wind turbine ($/kWh) |
| $P_w$ | Total rated power (kW) |
| $i$ | Number of operational hours |
| μ | Escalation rate |
| $\varphi$ | Inflation rate |
| T | Life span of the project. |

Operation and maintenance costs during the lifetime of the project is:

$$\mathrm{OMw} = \sum_{i=1}^{8760} [\ \beta_w P_w * \sum_{t=1}^{T} (\frac{1+\mu}{1+\lambda})^t\ ] \qquad (2)$$

where,

| | |
|---|---|
| $\beta_w$ | Operation and maintenance cost per kW of wind turbine ($/kWh) |
| $P_w$ | Total rated power (kW) |
| T | Life of the WTG |
| μ | Escalation rate |
| λ | Interest rate. |

And, the present worth of total salvage value (Salw) is:

$$\text{Salw} = S_w P_w * \left(\frac{1+\varphi}{1+\lambda}\right)^T \quad (3)$$

where,

| | |
|---|---|
| $S_w$ | Salvage value of wind turbine per kW ($/kW) |
| $P_w$ | Total rated power (kW) |
| T | Life of the WTG |
| $\varphi$ | Inflation rate |

Hence , the total cost of Wind turbine is:

$$\text{Cost(WTG)} = N_w * (\text{CCw} + \text{OMw} - \text{Salw}) \quad (4)$$

Where, $N_w$ is the number of installed WTGs.

*b. Cost of PV system*: The capital cost of PV system is given as:

$$\text{Capital Cost (CCs)} = \sum_{i=1}^{8760} \alpha_s P_s (i) * \sum_{t=1}^{T} \left(\frac{1+\mu}{1+\varphi}\right)^t \quad (5)$$

Where,

| | |
|---|---|
| $\alpha_s$ | Capital cost per kW of PV system ($/kWh) |
| $P_s$ | Total rated power (kW) |
| T | Life of the PV system |
| $\mu$ | Escalation rate |

$\varphi$ Inflation rate.

Operation and maintenance cost during the lifetime of the project is:

$$OMs = \sum_{t=1}^{T} [\ \beta_s P_s * \sum_{t=1}^{T} (\frac{1+\mu}{1+\lambda})^t] \quad (6)$$

Where,

$\beta_s$ Operation and maintenance cost per kW of PV system ($/kWh)

$P_s$ Total rated power (kW)

T Life of the PV system

$\mu$ Escalation rate

$\lambda$ Interest rate.

And, the present worth of total salvage value is

$$Ss = S_s P_s * (\frac{1+\varphi}{1+\lambda})^T \quad (7)$$

Where,

$S_s$ Salvage value of PV system per kW ($/kW)

$P_s$ Total rated power (kW)

T Life of the PV system

$\varphi$ Inflation rate.

Hence the total cost of PV system is:

$$\text{Cost(PV)} = N_s * (CCs + OMs - Ss) \quad (8)$$

Where, $N_s$ is the number of PV systems in the distribution network.

*c. Geothermal Power System:* The capital cost of geothermal power system is given as:

$$\text{Capital Cost } (CC_G) = \sum_{i=1}^{8760} \alpha_G P_G(i) * \sum_{t=1}^{T} \left(\frac{1+\mu}{1+\varphi}\right)^t \quad (9)$$

Where,

$\alpha_G$ Capital cost per kW of geothermal system ($/kWh)

$P_G$ Total rated power of geothermal system (kW).

Operation and maintenance cost during the lifetime of the project is:

$$OM_G = \sum_{t=1}^{T} ( \beta_G P_G * \sum_{t=1}^{T} (\frac{1+\mu}{1+\lambda})^t) \quad (10)$$

Where,

$\beta_G$ Operation and maintenance cost per kW of geothermal power ($/kWh)

$P_G$ Total rated power (kW)

T Life of the geothermal power system

μ Escalation rate

λ Interest rate.

And, the present worth of total salvage value is:

$$S_{Geo} = S_G P_G * (\frac{1+\varphi}{1+\lambda})^T \quad (11)$$

Where,

$S_G$ Salvage value of geothermal power per kW ($/kW)

$P_G$ Total rated power (kW)

T Life of the geothermal power system

φ Inflation rate.

Hence the total cost of geothermal power system is:

$$\text{Cost(Geo)} = N_G * (CC_G + OM_G - S_{Geo}) \quad (12)$$

*d. Power purchased:* The annual cost of purchasing power from fossil fuel generators (FFG) is calculated as follows [106]:

$$Cost(FFG) = \sum_{i=1}^{8760} \zeta * P_{FFG}(i) \quad (13)$$

where,

$P_{FFG}$ (i) Power purchased at hour i (kWh)

$\zeta$ FFG power price ($/kWh)

$i$ Hour.

The total cost of DG by combining equations (4), (8), (12), and (13) is:

$$Total\ DG\ cost\ \left(\frac{\$}{year}\right) = \frac{Cost(W) + Cost\ (PV) + Cost\ (Geo)}{T} + Cost(FFG) \quad (14)$$

***Reliability worth:*** Integrating DGs with conventional distribution systems can be useful in supplementing the energy provided to the system and in reducing the expected customer interruption cost (ECOST). ECOST can be calculated as a function of expected energy not supplied (EENS) and annual energy loss (AEL).

Hence,

$$ECOST\left(\frac{\$}{year}\right) = IEAR * \Delta EENS + C_E * \Delta AEL \quad (15)$$

Where IEAR ($/kWh) is the interrupted energy assessment rate of unsupplied energy, $C_E$ ($/kWh) is the average cost of lost electricity, $\Delta EENS$ is the difference in EENS before and after the integration of DGs into the distribution system and is given in equation (16), and $\Delta AEL$ is the net distribution system loss after the addition of DGs and is calculate using equation (17).

$$\Delta EENS = \sum_{i=1}^{8760} (Ptotal(i) - Pdemand(i)) * U(i) \quad (16)$$

$$\Delta AEL = \sum_{i=1}^{8760} (Loss(i)) - DGLoss(i)) \quad (17)$$

Where *Loss(i)* (kWh) is the distribution system loss at time i before DG and *DGLoss(i)* is the distribution system loss at time i after installing DG. The variable *U(i)* in equation (16) takes the following values:

$$\text{U(i)} = \begin{cases} 0 \; if \; (Ptotal - Pdemand) \geq 0 \\ 1 \; if \; (Ptotal - Pdemand < 0 \end{cases}$$

Where *Pdemand(i)* is the load demand during hour i, *Ptotal(i)* is the total power from WTGs, PVs, Geothermal, and Grid during hour i.

$$Ptotal(i) = P_{DG}(i) + P_{FFG}(i) \quad (18)$$

Where,

$$P_{DG}(i) = P_w(i) + P_s(i) + P_G(i) \quad (19)$$

and

$$P_{FFG}(i) = \delta * (Pdemand\ (i) - P_w(i) + P_s(i) + P_G(i)) \quad (20)$$

Where δ is the portion of the insufficient power to be purchased from FFGs. During this study it has been assumed that the failure rates of DGs are 0%. So, sine output power of geothermal plant is fairly constant, EENS depends only on the fluctuation of wind and solar energy.

***Savings on pollutant emissions:*** Adverse effects of pollutants emitted by fossil fuel power plants have been the driving force behind the rapid penetration of renewable sources in the power system. Since DGs have zero emission, the renewable power production index (RPPI) recognizing the environmental benefits of DGs is assumed to \$0.015/kWh. The monetary value of the environmental benefits can be calculated using equation (21).

$$Cost_{env} = P_{DG} * RPPI \tag{21}$$

### 5.2.3. Design Constraints

The Following physical and operational constraints are implemented in this study.

***Power balance constraint:*** The total power in the distribution system should match the total demand within certain reliability criteria [14,19]. Hence for the DG integrated network,

$$P_w(i) + P_s(i) + P_G(i) + P_{FFG}(i) \geq (1 - K)Pdemand\ (i) \tag{22}$$

Where K is the ratio of maximum permissible expected energy not served (EENS) with respect to the total load demand at each time instant.

***DG size constraints:*** In this study, the maximum allowable DG penetration is 30% of the total system load. So, the following constraints must be satisfied.

$$Min\ P_{DG} < P_{DG} < Max\ P_{DG} \tag{23}$$

***Power purchase constraint:*** The amount of power bought from fossil fuel generators should be within a certain range.

$$Min\ P_{FFG} < \sum_{i=1}^{8760} P_{FFG} < Max\ P_{FFG} \tag{24}$$

### 5.3. Problem Statement

Any number of available DGs is considered to be optimally allocated when the financial burden on the utility is at its minimum. Hence, the objective of this study is to minimize the total cost subject to the constraints in (22)-(24). The objective function is formulated by combining equations (14), (15) and (21) as shown in equation (25):

$$f_{obj} = Total\ DG\ cost - ECOST - Cost_{env} \tag{25}$$

The design parameters in this study are the number and size of wind turbines and solar panels and the ratio of the power that needs to be purchased. Only one geothermal power with fixed output connected to a fixed bus is considered in this study. Also, the power outputs from DGs are given the highest priority. Only when the total power supplied by these sources is not sufficient to meet the demand, the certain portion of "unmet" power is purchased.

### 5.4. Test System

The proposed method has been implemented and tested on the IEEE 123-node multi-phase unbalanced distribution feeder as shown in Figure 25. This test feeder consists of four voltage regulators, four capacitor banks, overhead and underground line

segments with various phasing, and various unbalanced loading with different load types [80]. The detailed data for this test system can be obtained from [81] and are reproduced in appendix C for easy reference.

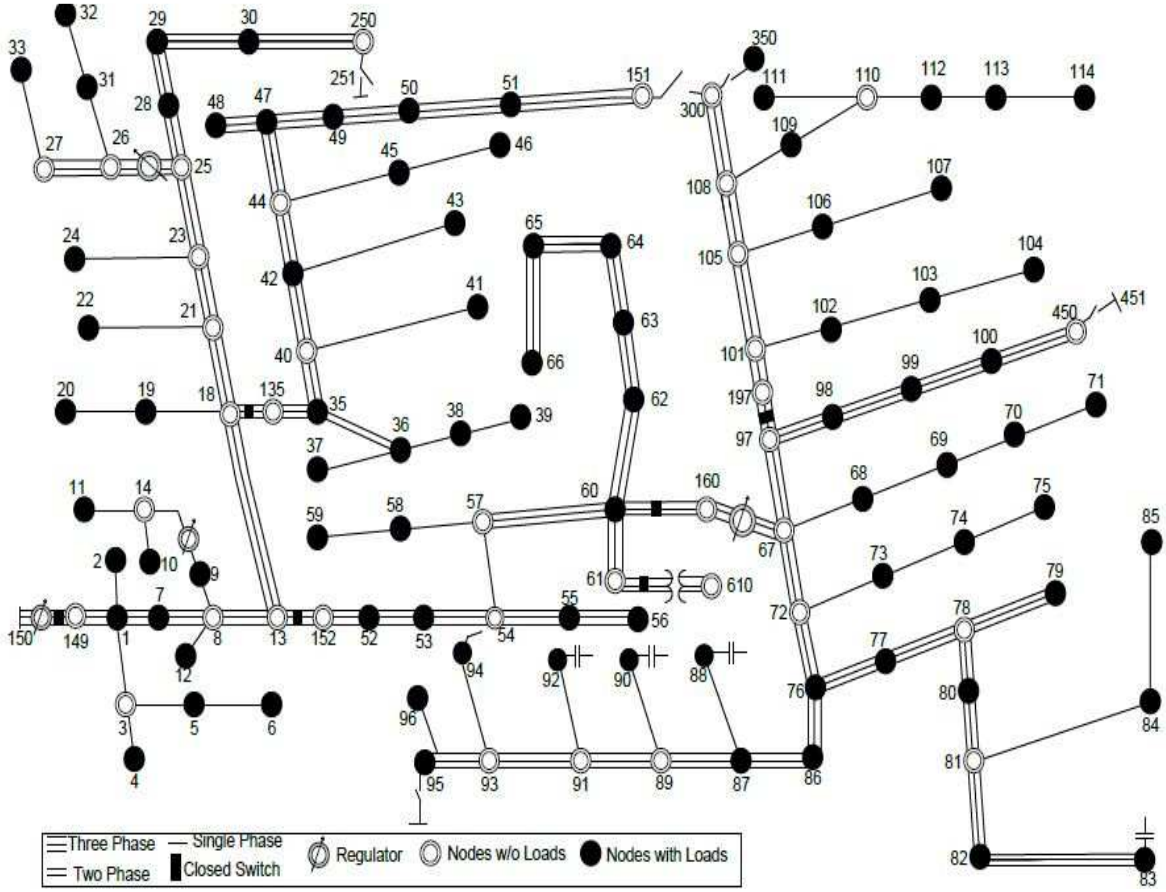


Figure 25. The IEEE 123 node test distribution network

### 5.4.1. System Parameters

Values of various constants required for the application of the proposed method on the test system are listed in Table 35 [110]. The hourly wind, solar, and geothermal power productions as described earlier are used. The peak load profile, which occurs in summer, has been used to determine the optimal allocation of DGs. To show the effectiveness of the proposed method, the seasonal loss of energy has been determined by

considering the load profiles of each season. Capital and operation and maintenance costs are obtained from the U.S. Energy Information Administration (EIA) website [111].

Table 35. Values of Parameters used in the simulation

| | |
|---|---|
| Inflation rate ($\varphi$) | 9% |
| Interest rate ($\lambda$) | 12% |
| Escalation rate ($\mu$) | 12% |
| Life span of the project (T) | 30 years |
| Capital cost for Wind Turbine ($a_w$) | 64.1 $/MWh |
| Capital cost for PV system ($a_s$) | 114.5 $/MWh |
| Capital cost for Geothermal system ($a_G$) | 47.4 $/MWh |
| OM costs for Wind Turbine ($\beta_w$) | 13 $/MWh |
| OM costs for PV system ($\beta_s$) | 11.4 $/MWh |
| OM costs for Geothermal system ($\beta_G$) | 12.2 $/MWh |
| Salvage value of Wind Turbine ($S_w$) | 200 $/kW |
| Salvage value of PV system ($S_s$) | 500 $/kW |
| Salvage value of Geothermal system ($S_G$) | 500 $/ kW |
| Price of purchased electricity ($\zeta$) | 0.15 $/kW |
| Interrupted energy assessment rate (IEAR) | 6 $/ kW |
| Average cost of lost electricity ($C_E$) | 0.06/ kW |
| Percentage of insufficient power to be purchased ($\delta$) | <10% |

## 5.5 Results and Discussion

### 5.5.1. Total Energy Loss

In order to investigate the impact of integrated DG on the annual energy loss of the distribution system, following five scenarios are studied.

I. No DG.

II. Two PV systems.

III. Two Wind Turbines.

IV. Only Geothermal.

***Optimal mix of all three systems connected.***

The procedure for optimal allocation of DGs for minimum power loss has been described in detail in chapter 3. Values obtained in chapter 3 are used in this study. These values are shown in Table 36.

Table 36. Optimal allocation of mixes of various types of DGs

| Scenario | Bus no. | | | Size (MVA) | | |
|---|---|---|---|---|---|---|
| ii | 67, 72 | | | 1.41,1.65 | | |
| iii | 67,76 | | | 1.43,1.51 | | |
| iv | 101 | | | 2.43 | | |
| v | PV | WTG | GEO | PV | WTG | GEO |
| | 67,47 | 60,72 | 101 | 0.93,0.45 | 1.19,0.28 | 0.25 |

Also, since the output power of geothermal plant is fairly constant, a constant value of 250kW at a 0.90 power factor is assumed to be the output power of geothermal power plant. Furthermore, based on the result obtained from the study in chapter 3, this power plant is placed at bus 101.

Results obtained for scenarios that were used to determine the optimal mix of DGs for minimum system energy losses are shown in Figure 26. Results indicate that regardless of the combination of renewable resources used to obtain the optimal fuel mix, there is significant improvement in the annual energy loss reduction compared to the case where DGs were not integrated in the system. Furthermore, between the two intermittent sources, the loss reduction that results in scenario III (only wind based DGs) is higher

than that in scenario II (only PV based DGs). This is because of the fact that solar DGs do not output any power at night. So, for more than twelve hours a day, the distribution system with only solar DGs behaves like the one without any DG. The maximum reduction in loss occurs when a mixture of all types of DGs are integrated into the system. Since, DG systems based on geothermal power produce constant power at all time, they have a significant impact on distribution loss reduction than wind or solar based DGs.

### 5.5.2. Cost evaluation of DG integration

Assuming the lifespan of the project is 30 years, a DG integration plan must be implemented to meet the expected demand for the duration of the project. In this study, it has been assumed that the demand increases by 2% every year. It is also assumed that power generated from DG sources gets priority in meeting the load demand. In a case when DGs cannot meet the demand, power is purchased from the grid to meet the surplus demand. The minimum cost incurred by the utility for every fifth year is shown in Table 37. The optimum location and sizing of DGs mix is shown in Table 38.

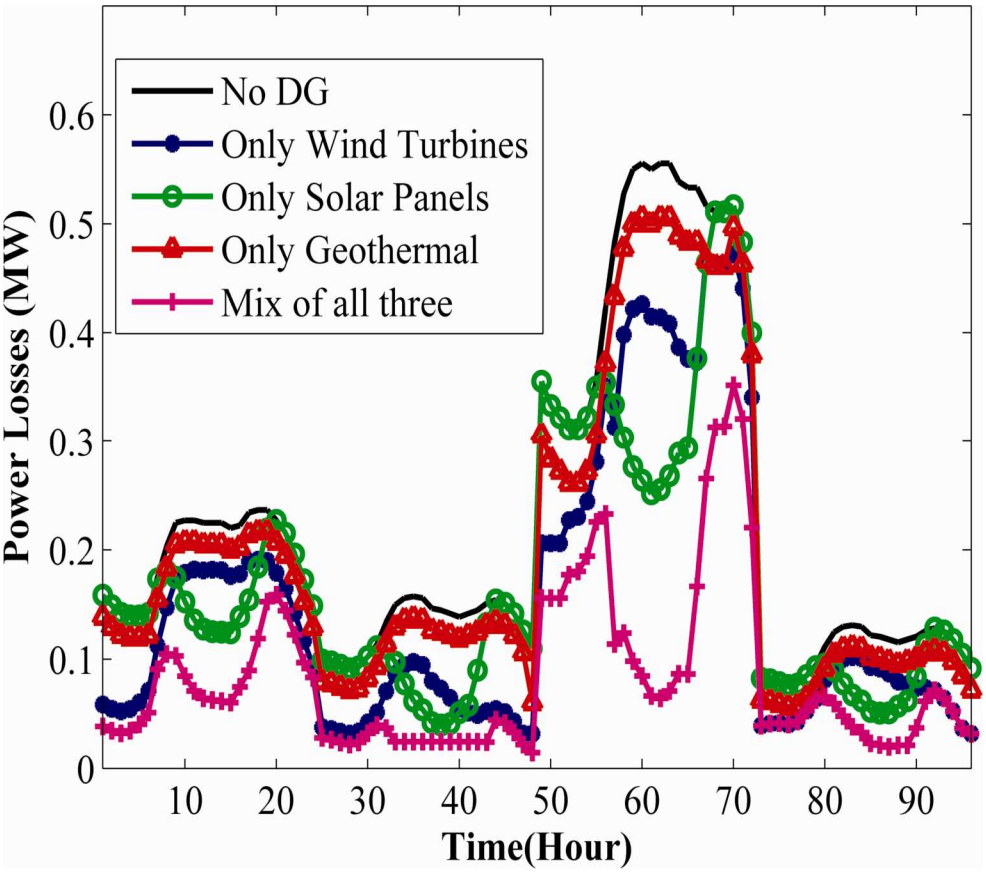


Figure 26. Power losses in a test distribution network

Table 37. Minimum cost incurred by the utility for every fifth year.

| Year | Load Demand (MVA) | Cost ($/year) |
|---|---|---|
| 0 | 4.512 | 45,371 |
| 5 | 4.981 | 38,290 |
| 10 | 5.500 | 25,381 |
| 15 | 6.702 | 17,493 |
| 20 | 6.577 | 11,938 |
| 25 | 7.704 | 5,382 |
| 30 | 8.172 | 2,124 |

Table 38. Optimal allocation of DGs that result in minimum cost.

| Bus Number | Wind Turbine (KVA) | Solar panel (KW) | Geothermal (KVA) |
|---|---|---|---|
| 67 | 755 | 560 | 0 |
| 47 | 570 | 0 | 0 |
| 111 | 0 | 0 | 450 |
| 60 | 0 | 850 | 0 |

From Table 37, it is concluded that as the demand increases, cost incurred by the utility decreases. Also, the minimum cost reduction is not significant during the first five years because the existing substation can supply the demand of up to 5MVA. Figure 27 shows the effectiveness of DGs in improving the reliability of the system. The value of ECOST in (15) is 0 when there are no DGs in the distribution system. But with the increase in demand within a DG integrated network, both distribution losses (DL) and expected energy not supplied (EENS) decrease which results in a significant saving for the utility.

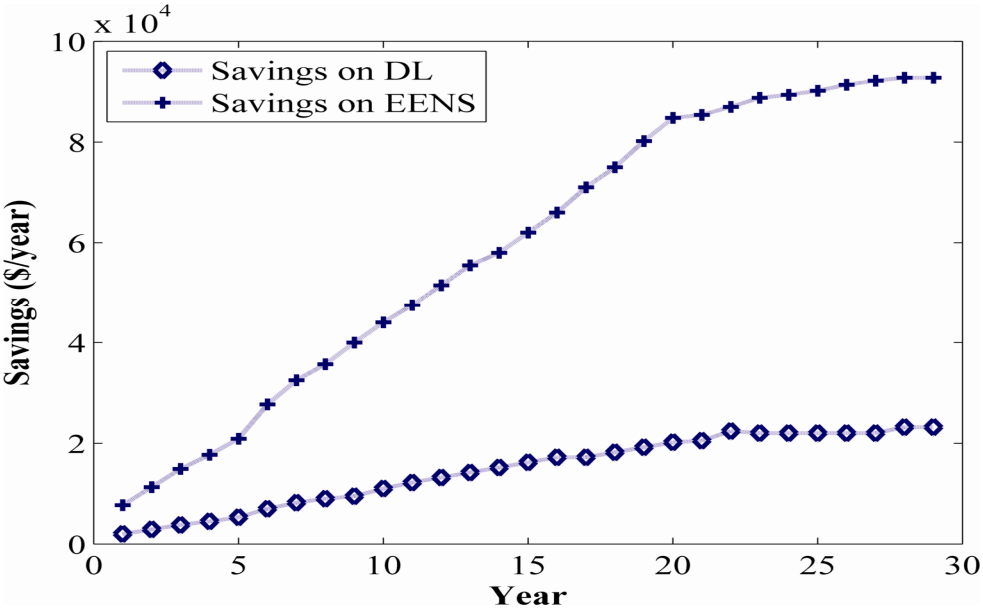


Figure 27. Savings of DL and EENS as demand increases over the years.

The optimal mix of DGs for the 30th year of the project is shown in Figure 28. To investigate the adequacy of the proposed planning method, the summer load profile, which represents the maximum demand during the year, has been chosen. Since the substation is capable of supplying only 5MVA, the rest of the demand should be met by the total output power of DGs and power purchased from FFGs. Results indicate that mixing various types of DGs provides the most economic benefit. Also, integrating base-load DGs with intermittent sources results in a huge reduction in cost. In Figure 28 more than 90% of the load is supplied by the substation and DGs and the surplus demand is met by purchasing power from FFGs.

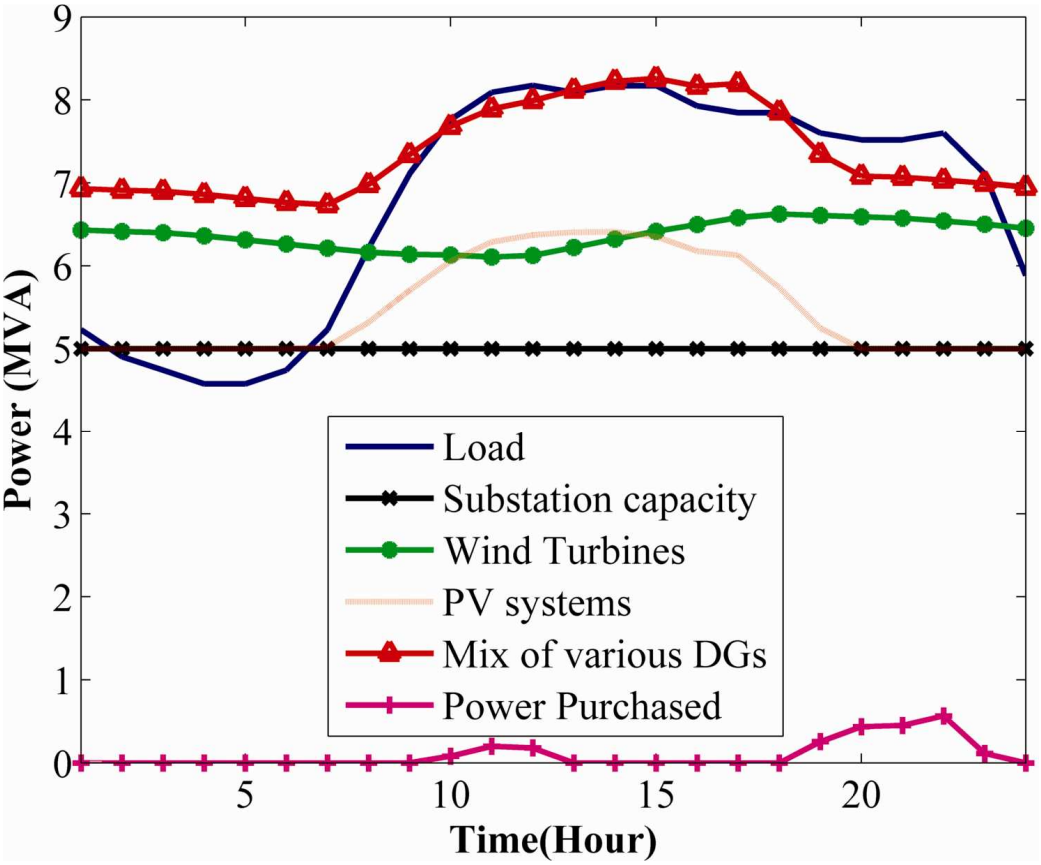


Figure 28. Optimal mix of DGs for 30th year of the project

## 5.6. Conclusion

This chapter introduces a cost minimization planning method for optimal allocation of DGs in a three phase unbalanced distribution network. The proposed cost benefit analysis approach combined with the application of the PSO algorithm in a co-simulation environment of MATLAB and OpenDSS software is successfully implemented to estimate the most cost-effective DGs allocation to serve the projected peak demand. The proposed optimization model minimizes the total investment cost incurred by the utility by taking into account various costs like; investment cost, OM cost, reliability cost, pollution cost, and cost of purchasing power by the utility. The intermittent nature of both wind and PV resources of DGs and load profiles are incorporated in this study. Results indicate that integrating various forms of DG sources results in a minimal investment. Also, base-load DGs must be integrated to achieve the maximum benefit. Although DGs reduce the total distribution loss and increase the reliability of the distribution system, maximum return on the investment can be achieved when DGs are planned to meet the future load growth.

# CHAPTER 6

## DEVELOPMENT AND VERIFICATION OF AN ELECTRICAL EQUIVALENT CIRCUIT MODEL OF PROTON ELECTROLYTE MEMBRANE (PEM) FUEL CELL USING IMPEDANCE SPECTROSCOPY

This chapter presents the development and analysis of an equivalent circuit model of a 1.2kW commercial fuel cell stack. The developed model represents the effects of all major fuel cell electrochemical processes including ohmic, activation, and mass transport and accounts for the low frequency inductive behavior that others have not recognized. Furthermore, only physical elements such as resistors, capacitors and inductors are used in this model. A program based on the Levenberg-Marquardt algorithm [26] is written in MATLAB which extracts the initial values of the components that are to be used in the model from the Nyquist plot obtained using electrochemical impedance spectroscopy (EIS), thus eliminating the need to provide a close initial guess. This program also provides the number of RC branches together with the final values of those circuit elements that are needed to accurately represent the electrochemical behavior of the fuel cell system. Finally, the developed model is validated by obtaining the impedance plots at various operating conditions and comparing them with the impedance plots obtained for the real fuel cell using EIS. The validated model was then used to investigate the transient behavior of the fuel cell.

## 6.1. Introduction

In recent years, smart grid has been getting a lot of attention from the U.S energy sector. One of the important features of the smart grid is its ability to accommodate various renewable distributed sources of energy. Proton Exchange Membrane (PEM) fuel cells are one of those renewable sources of energy that produce electricity as a byproduct of electrochemical reactions between hydrogen and oxygen [112]. Due to their low operating temperature and fast start up characteristics, PEM fuel cells have been extensively researched and used by automobile industries. However, a recent announcement about the successful operation of a 1 Megawatt (MW) PEM fuel cell for power production by Solvay, a PEM fuel cell developer in Belgium, has illustrated the possibility of PEM fuel cells as a viable distributed generator [113]. Before PEM fuel cells can be connected to the electric grid, a series of studies on their impact on the stability of the distribution network must be conducted. These types of studies depend heavily on the simulation model of the system. As a result, numerous attempts have been made to develop accurate model of PEM fuel cells [114]–[121].

Numerous studies have used equivalent circuit diagrams to model PEM fuel cells [4,11–13]. These models represent fuel cells as series and parallel combinations of resistors and capacitors. One of the effective ways to get the accurate values of these resistors and capacitors is from electrochemical impedance spectroscopy (EIS). EIS is an efficient technique to study the dynamic behavior of PEM fuel cells, which depends on the chemical and thermodynamic processes that take place inside the fuel cell. Moreover, EIS has the ability to separate the impedance responses of the various transport processes which occur simultaneously in PEM fuel cells [125]. This allows us to represent the

losses associated with various transport processes by using the simple electrical components like resistors, capacitors, and inductors.

However, using EIS to characterize fuel cells is not a new technique. Authors in [126] developed an equivalent circuit model of alkali fuel cell using resistors to represent solution resistance, charge transfer, and oxygen adsorption, capacitors to represent double layer capacitance and oxygen adsorption capacitance on catalyst, and Warburg impedances to represent oxygen and ion diffusion to catalyst. Similarly, the authors in [127] used EIS to develop an equivalent circuit which allowed them to split the cell impedance into electrode impedance and electrolyte resistance by varying the load current. Instead of using the real value of the elements in the circuit model, authors in [127] relied on the correlation between the impedance of the fuel cell and I-V curve to calculate the voltage loss fraction. An equivalent circuit model of a 500W PEM fuel cells was developed in [124] using resistors and constant phase elements. The value of the fitting diameters together with the values of the resistors and constant phase elements are provided in [124]. However, this model does not account for all the losses that occur within PEM fuel cells.

Furthermore, most of the models that are currently available in literature fail to address the inductive behavior of fuel cells at low frequencies that are caused by the adsorption step during the oxygen reduction reaction [128].The most complete work on modeling this inductive behavior is presented by the authors in [129]. Here, the authors have used constant phase elements (CPE) to model the distributed nature of the double layer charging effects and a Warburg circuit element to represent the mass transport losses in fuel cells. Although CPE and Warburg circuit elements provide a better fitting

result during the extraction of component values for equivalent circuit modeling, they do not physically exist. This creates a problem while designing and testing power controllers for PEM fuel cells. In addition, since CPE and Warburg elements do not contribute towards the transient behavior of PEM fuel cells, they have to be substituted by capacitors and inductor during transient studies [129]. This results in inaccurate developments of fuel cell equivalent circuit models.

An electrical equivalent circuit model of a PEM fuel cell stack without using CPE and Warburg circuit element is presented in [116] and [122]. Although promising, these models do not account for the inductive behavior. Also, these models are insufficient in representing cathode activation and mass transport losses.

Authors in both [116] and [129] have used a computer program to obtain the numerical values for the electrical components that they have used in their models. These programs require users to first create an equivalent circuit model and then provide initial values for the circuit elements. This creates two important difficulties for fuel cell researchers. First, one must know how many RC and RL branches are needed to accurately represent all the losses that take place within the fuel cells. For example, authors in [116] used three parallel branches of resistors and capacitors which are connected in series with a resistor and an inductor, while authors in [129] used two parallel branches of resistors and constant phase elements that are connected in series with one parallel branch of resistors and Warburg elements. Second, the initial values that this software requires must be close to the real values of the components. Guessing initial values that are close to the real ones is difficult if the equivalent circuit model is being developed for the first time. Also, since the PEM fuel cell characteristics vary from

manufacturer to manufacturer and also depend on the operating conditions, the values of the parameters derived for one brand of PEM fuel cells operating under one condition are not the same for fuel cells that are operating under a different condition or are of different brand.

Methods proposed in this chapter remove the aforementioned difficulties. The objective of this study is to develop and analyze an equivalent circuit model of a 1.2kW commercial fuel cell stack. The developed model represents the effects of all major fuel cell electrochemical processes including ohmic, activation, and mass transport; and it accounts for the low frequency inductive behavior that others have not recognized. Furthermore, only physical elements such as resistors, capacitors, and inductors are used in this model. A program based on Levenberg-Marquardt algorithm is written in MATLAB which extracts the initial values of the components that are to be used in the model from the Nyquist plot obtained using EIS, thus eliminating the need to provide a close initial guess. This program will also fit the Nyquist plot curves with numbers of RC branches. The final output of the program contains the results of the curve fitting together with the final values of the circuit elements that are needed to accurately represent the behavior of a fuel cell system. Finally, the developed model is validated by obtaining the impedance plots under various operating conditions and comparing them with the impedance plots obtained for the real fuel cell using EIS empirical measurements. Dynamic response of the validated model is then compared to experimentally obtained measurements.

## 6.2. Experimental setup

The test fuel cell system used in this chapter is a 1.2 kW Nexa$^{TM}$PEM fuel cell. This fuel cell stack contains 47 single cells in series and is capable of producing 1200W of unregulated DC power [130]. This stack can supply a maximum current of 44A with a voltage ranging from 43V at no load to 26V at full load. Although the stack runs with pure dry hydrogen and air, room air is humidified before supplying it to the fuel cell stack to maintain the membrane hydration. The membrane electrode assembly (MEA) is composed of Nafion$^{TM}$112 with a platinum based catalyst. The active area of each MEA is 122 $cm^2$ [131]. The impedance data of this stack is collected using a Solarton® 1250A frequency response analyzer (FRA) and a Chroma 61612 programmable DC electronic load as shown in Figure 29. The Solatron® 1250A has a frequency range from 10µHz to 65 kHz. The programmable DC electronic load has a frequency range up to 50 kHz. The impedance spectrum of the fuel cell was recorded by sweeping frequencies over the range of 40 kHZ to 50mHz with 10 points per decade. Also, since current control is much easier than voltage control, all EIS experiments were carried out in galvanostatic mode [132].

In order to find the optimal amplitude of the AC signal that provides a reasonably good impedance spectrum during the frequency sweeping, various AC signals with amplitudes ranging from 1% to 50% of the DC load current were tested. An AC amplitude of 10% of the DC load current was determined to be optimal [129]. Thus all the EIS tests used in this study are conducted by sweeping the frequency over the range of 40 kHz to 50 mHz using an AC signal with an amplitude of 10% of the operating DC load current.

Also since the reaction between hydrogen and oxygen is exothermic, temperature in the fuel cell increases as the current is drawn from it. As shown in Figure 30, temperature has a significant effect on the performance of PEM fuel cell. Hence care must be taken to maintain the stable temperature while collecting impedance spectroscopy data at respective load currents. In order to achieve a stable temperature, the fuel cell was operated for at least an hour at a corresponding load current before collecting impedance data.

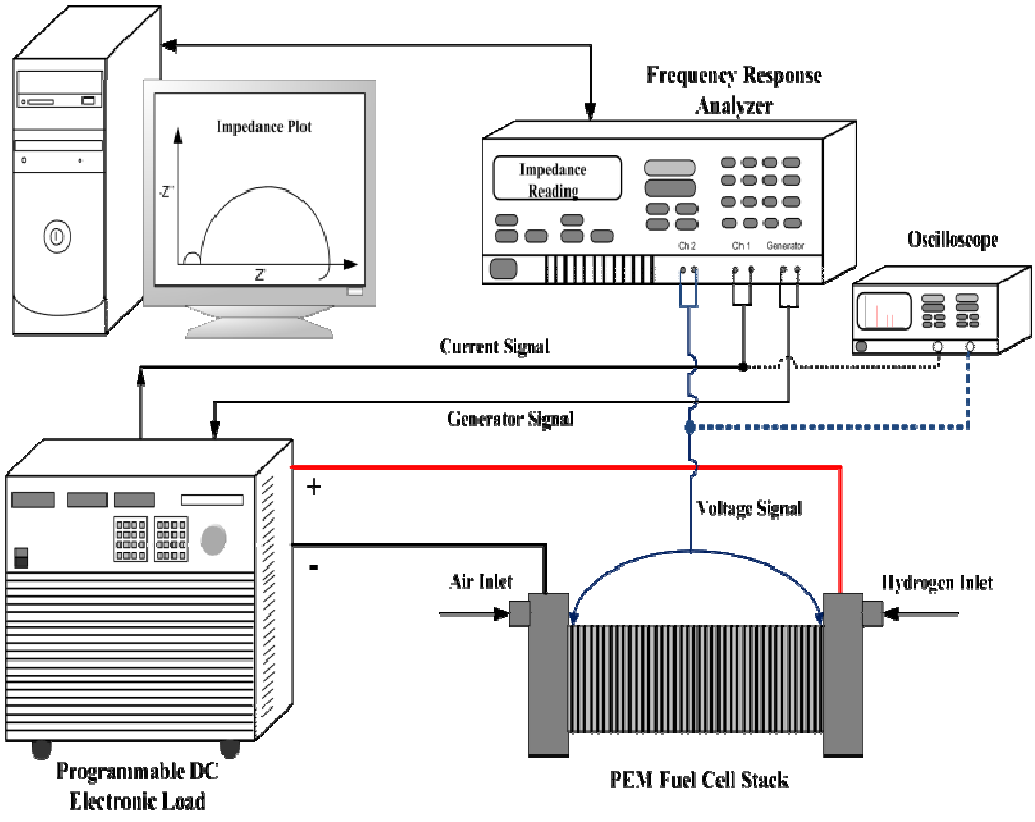


Figure 29. Experimental setup for EIS study of a 1.2 kW PEM fuel cell stack

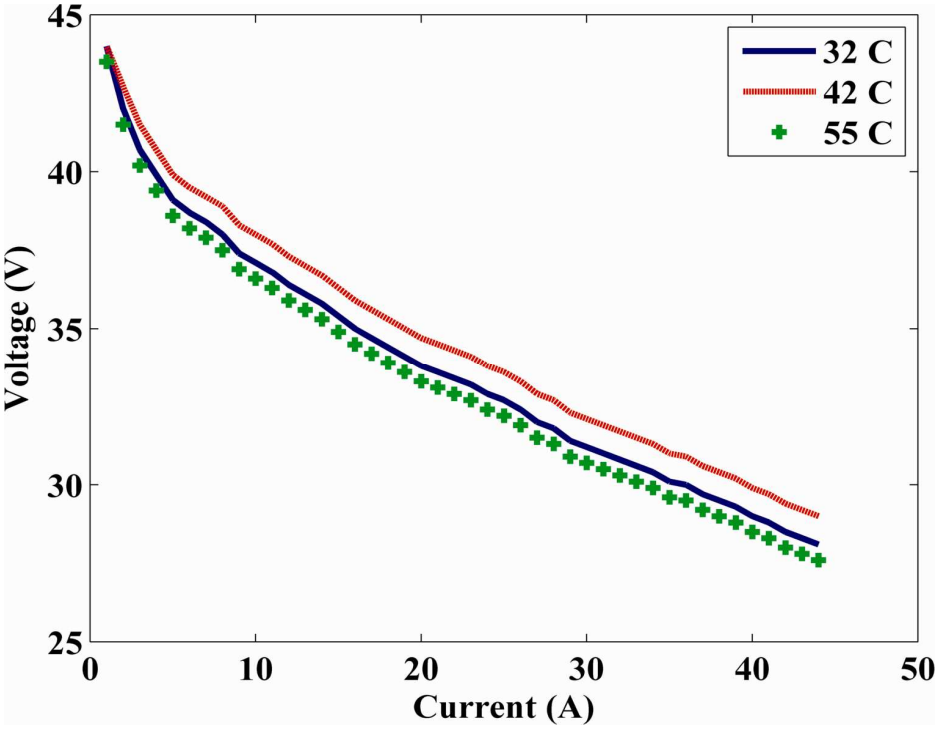


Figure 30. Experimental I-V curves at different temperatures

## 6.3. Model Formation

### 6.3.1. Objective Function

This section explains the development of an objective function which is used for the least square curve fitting. Since this objective function will be used to find the numerical value of electrical components that are used in equivalent circuit model of PEM fuel cells, it should closely represent the real fuel cell characteristics. In other word, since the proposed model will be based on EIS studies, this objective function should represent the impedance behavior of the fuel cell.

A Nyquist plot is the most common and informative way to explain the impedance data obtained from EIS studies [116, 122, 124, and129]. A Nyquist plot of PEM fuel cells consists of various loops representing the major sources of losses. In

[129], authors observe two mid frequency loops representing anode and cathode activation losses and one low frequency loop representing mass transportation losses. These loops can be represented by the combination of several semi-circular loops as shown in Figure 31.

Furthermore, numbers of studies have shown the appearance of semi-circles in a Nyquist impedance response of PEM fuel cells [129]-[131]. Each of the semi-circular loops in a Nyquist plot can be represented by a parallel RC circuit [130]. Therefore, each of the semi circles in Figure 31 can be represented by an electric circuit containing a resistor in parallel with a capacitor. The impedance of this circuit dictates the radius of the semi-circle. In other words, a large impedance of the circuit results in a semi-circle with a large radius. A function describing the impedance of the circuit consisting of various parallel branches as shown in Figure 32 can be obtained as follows.

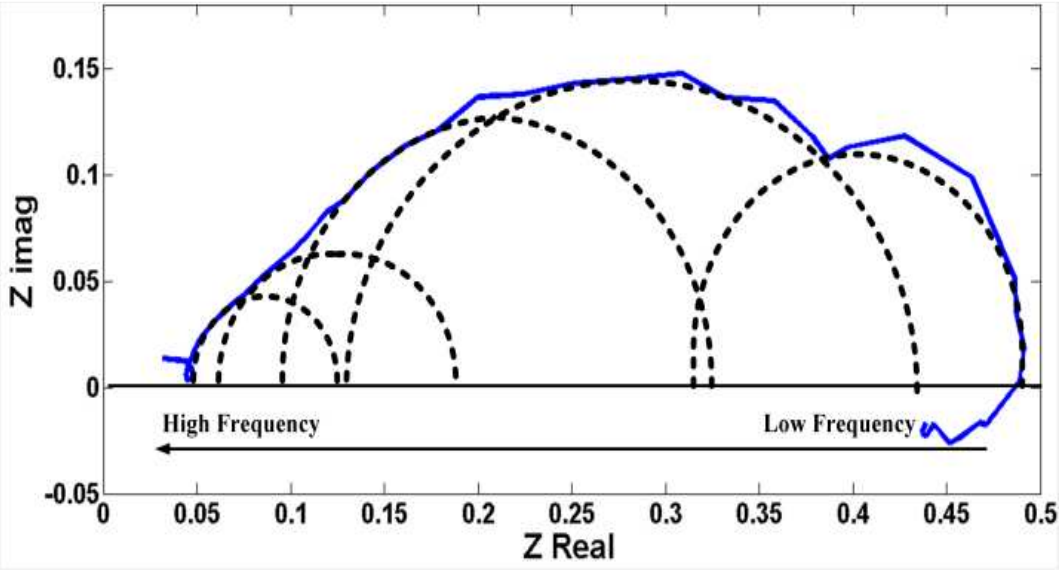


Figure 31. Representation of Nyquist plot of a 1.2kW PEM fuel cell at 10A DC as the combination of several semi-circular loops.

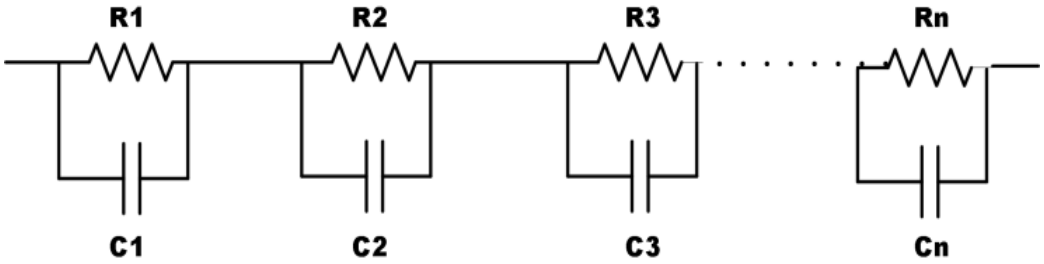


Figure 32. Combination of RC circuits in series

The impedance of the circuit in Figure 32 can be calculated as:

$$Z = \frac{R_1}{1 + j\omega R_1 C_1} + \frac{R_2}{1 + j\omega R_2 C_2} + \frac{R_3}{1 + j\omega R_3 C_3} + \cdots + \frac{R_n}{1 + j\omega R_n C_n} \quad (1)$$

Where,

$R_1 \ldots R_n$ : Resistance

$C_1 \ldots C_n$ : Capacitance

$\omega$ : Angular frequency

$j$ : $\sqrt{-1}$

Equation (1) can be written as:

$$Z = \frac{R_1}{1 + j\omega R_1 C_1} * \frac{1 - j\omega R_1 C_1}{1 - j\omega R_1 C_1} + \cdots + \frac{R_n}{1 + j\omega R_n C_n} * \frac{1 - j\omega R_n C_n}{1 - j\omega R_n C_n}$$

$$Z = \frac{R1 - j\omega {R_1}^2 C_1}{1 + \omega^2 {R_1}^2 {C_1}^2} + \cdots + \frac{R_n - j\omega {R_n}^2 C_n}{1 + \omega^2 {R_n}^2 {C_n}^2}$$

This total impedance $Z$ can be separated into real and imaginary parts as follows:

$$Real(Z) = \frac{R_1}{1 + \omega^2 {R_1}^2 {C_1}^2} + \cdots + \frac{R_n}{1 + \omega^2 {R_n}^2 {C_n}^2} \quad (2)$$

$$Imag(Z) = \frac{-j\omega {R_1}^2 C_1}{1 + \omega^2 {R_1}^2 {C_1}^2} - \cdots - \frac{j\omega {R_n}^2 C_n}{1 + \omega^2 {R_n}^2 {C_n}^2} \quad (3)$$

From (2),

$$Real(Z) = \sum_{i=1}^{n} \frac{R_i}{1 + \omega^2 {R_i}^2 {C_i}^2} \quad (4)$$

From (3),

$$Imag(Z) = -j\omega \sum_{i=1}^{n} \frac{{R_i}^2 C_i}{1 + \omega^2 {R_i}^2 {C_i}^2} \quad (5)$$

Hence, total impedance of the circuit in Figure 32 is:

$$Z = Real(Z) + Imag(Z) \quad (6)$$

Equation (6) gives the impedance of the circuits that represents the anode and cathode activation losses and part of diffusion losses. Since our goal is to formulate an

objective function which can accurately describe the impedance behavior of a PEM fuel cell, impedances representing ohmic losses and diffusion losses must also be considered. Ohmic losses are indicated where the higher frequency loop in a Nyquist plot intersects the real axis and are represented by a real resistor in the circuit model [129]. The diffusion losses observed in the low frequency region is the result of time taken by slow moving reactants to reach the membrane [135]. Since the impedance representing diffusion losses is inductive in nature, it can be represented by a circuit containing a resistor in parallel with an inductor. Hence the circuit which represents all the losses in PEM fuel cells is a series combination of an ohmic resistance, number of branches of resistors in parallel with capacitors, and a branch of diffusion resistance in parallel with an inductor, as shown in Figure 33.

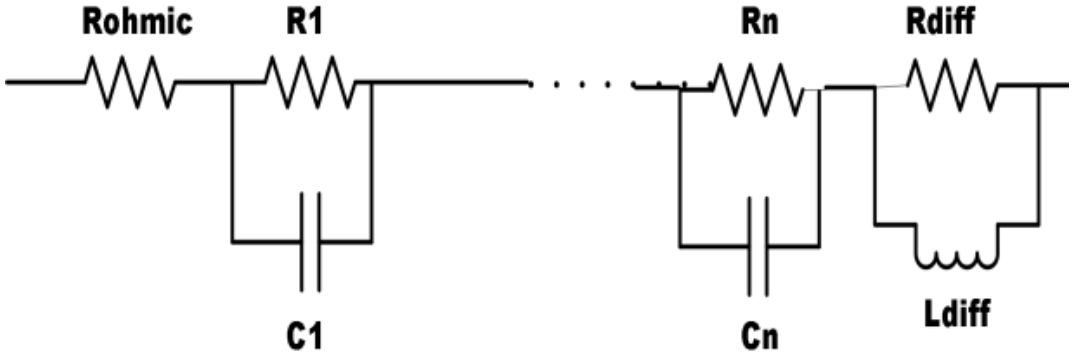


Figure 33. Circuit representing all the losses in a PEM fuel cell

The total diffusion impedance can be calculated as:

$$Zdiff = \frac{j\omega * Rdiff * Ldiff}{Rdiff + j\omega * Ldiff}$$

Where, $diff$ : Diffusion resistance

$Ldiff$ : Diffusion inductance

$\omega$ : Angular frequency

$J : \sqrt{-1}$

Above equation can be written as:

$$Zdiff = Real(Zdiff) + Imag(Zdiff) \quad (7)$$

Where,

(8)

$$Real(Zdiff) = \frac{\omega^2 * Ldiff^2 * Rdiff}{1 + \omega^2 * Ldiff^2}$$

(9)

$$Imag(Zdiff) = \frac{j\omega * Ldiff * Rdiff}{1 + \omega^2 * Ldiff^2}$$

Total real impedance of the circuit in Figure 33 can be obtained by combining (4), (8), and $R_{ohmic}$.

$$Real(Z_T) = R_{ohmic} + \frac{\omega^2 * Ldiff^2 * Rdiff}{1 + \omega^2 * Ldiff^2} + \sum_{i=1}^{n} \frac{R_i}{1 + \omega^2 {R_i}^2 {C_i}^2} \quad (10)$$

Similarly, combining (5) and (9) will give the total imaginary part of the impedance of the circuit in Figure 33.

$$Imag(Z_T) = \frac{j\omega * Ldiff * Rdiff}{1 + \omega^2 * Ldiff^2} - jw \sum_{i=1}^{n} \frac{{R_i}^2 C_i}{1 + \omega^2 {R_i}^2 {C_i}^2} \quad (11)$$

Finally, the objective function which represents the impedance behavior of a PEM fuel

cell is;

$$f(R, C, L, \omega) = Real(Z_T) + Imag(Z_T) \quad (12)$$

### 6.3.2. Extraction of Initial Values

The objective function described by (12) is used to calculate impedance values from the Nqyuist plot which is to be fitted to the one obtained using the EIS method. A Levenberg-Marquardt algorithm is used for the least-square curve fitting. Detailed analysis of the Levenberg-Marquardt algorithm can be found in [26] and [135]. A program written in MATLAB extracts the initial values of the components to be used in the equivalent circuit model of the fuel cell. These initial values are then used in an algorithm to minimize the sum of squares of the deviations of the simulated curve from the experimental EIS plot.

As mentioned earlier, ohmic losses can be represented by a single resistor because the main contributors of these losses are the membrane resistance of individual cells [132]. The diffusion losses which are shown by the low frequency inductive behavior in the Nyquist plot can be represented by a parallel circuit of a resistor and an inductor. The anode and cathode activation losses which are observed in mid frequency range can be approximated by a number of parallel circuits of resistors and capacitors.

Figure 34 shows the approximation of initial value of the Ohmic resistance which is obtained by searching a real impedance value in the high frequency region that corresponds to the zero imaginary impedance. Similarly, the initial value of the resistance representing the diffusion losses is obtained by calculating the length of the real part of the impedance which corresponds to the negative values of imaginary part of the

impedance in low frequency region. This length corresponds to the diameter of a semi-circle which approximates the low frequency loop in the Nyquist plot. The total impedance of the inductor used to represent the diffusion behavior is approximated by the radius of this semi-circle as shown in Figure 35.

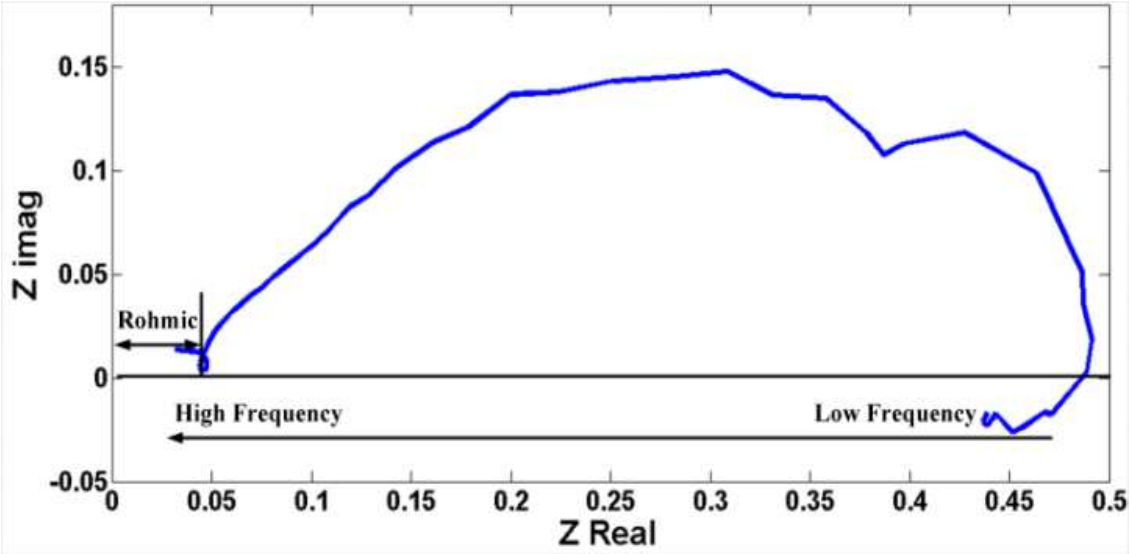


Figure 34. Estimation of Ohmic resistance

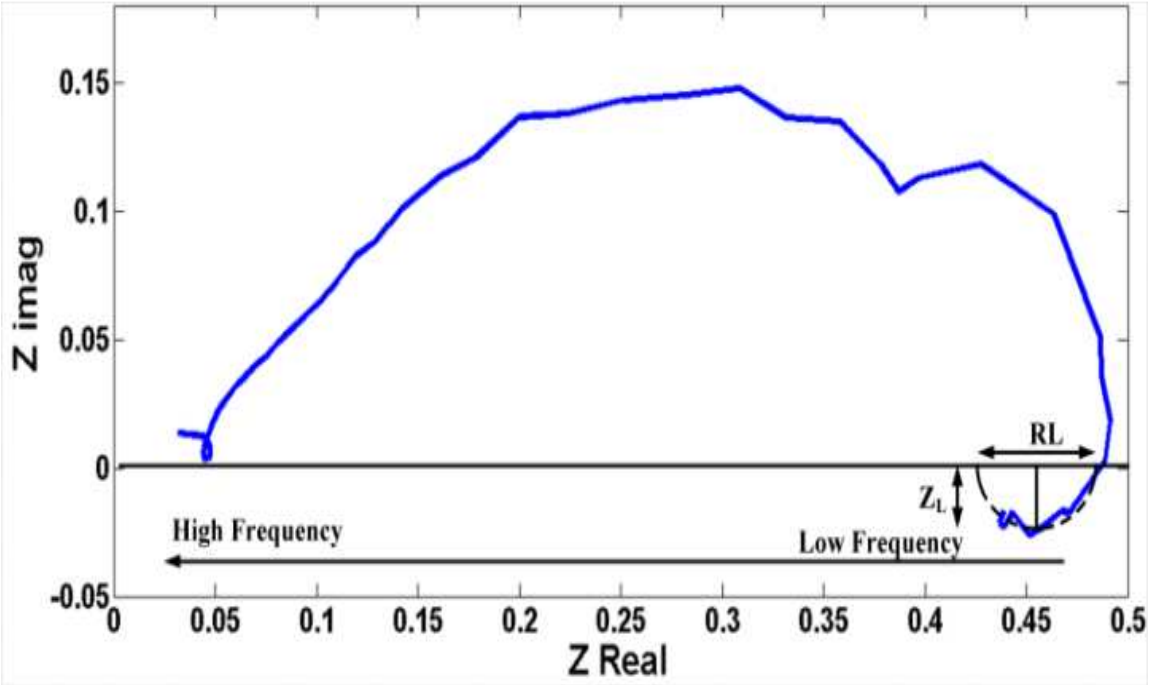


Figure 35. Estimation of parameters that represents diffusion behavior.

Initial values of the circuit components representing the activation losses are approximated as follows:

First only one semi-circular loop is considered to represent the anode and cathode activation losses. This is done by making the value of n in equation (12) to be 1. This implies that there will be only one parallel RC branch that produces the mid frequency loop in the Nyquist plot. In order to find the radius of this loop, the maximum value of the imaginary impedance obtained from the EIS study is extracted. Once the maximum value is obtained, the slope of the tangent line at that point is calculated. If the slope is close to zero then the value of maximum imaginary impedance will represent the radius of a semi-circular loop whose center will be located at a point on the real impedance axis that corresponds to this maximum imaginary impedance. Numerical values of a resistor and a capacitor are then obtained from the diameter and radius of the semi-circle as shown in Figure 36. Using these initial values, the Levenberg-Marquardt algorithm is used to obtain the minimum value of the sum of squares. If the minimum value of the sum of squares is greater than $10^{-3}$, another semi-circular loop will be added to approximate the activation losses.

For n = 2, the same numerical values of R and C that are obtained for n=1 are used to represent the first loop. The radius of the second loop is obtained by finding the first minimum value of the imaginary impedance after the maximum value that was obtained when n = 1. A point on the real impedance axis that corresponds to this minimum imaginary value will be the center of the second semi-circular loop that has just been added. As shown in Figure 37 the diameter and radius of this loop will provide the impedance values for the resistor and capacitor used to represent the second loop.

Another loop will then be added if the minimum value of the sum of squares is greater than $10^{-3}$.

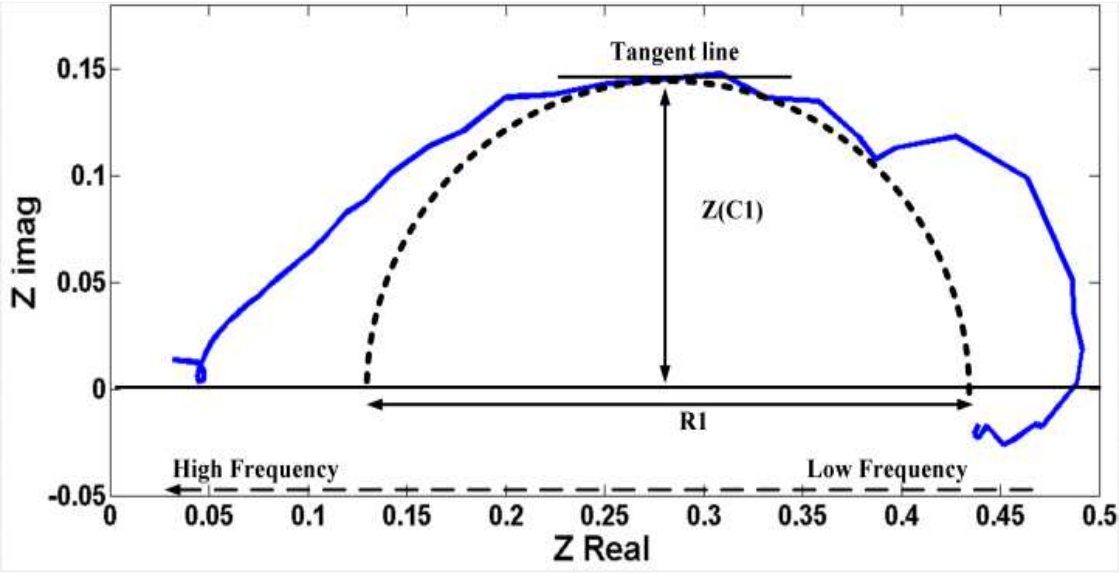


Figure 36. Location of first semi-circular loop to represent the anode and cathode activation losses and estimation of parameters of a circuit that represents the loop

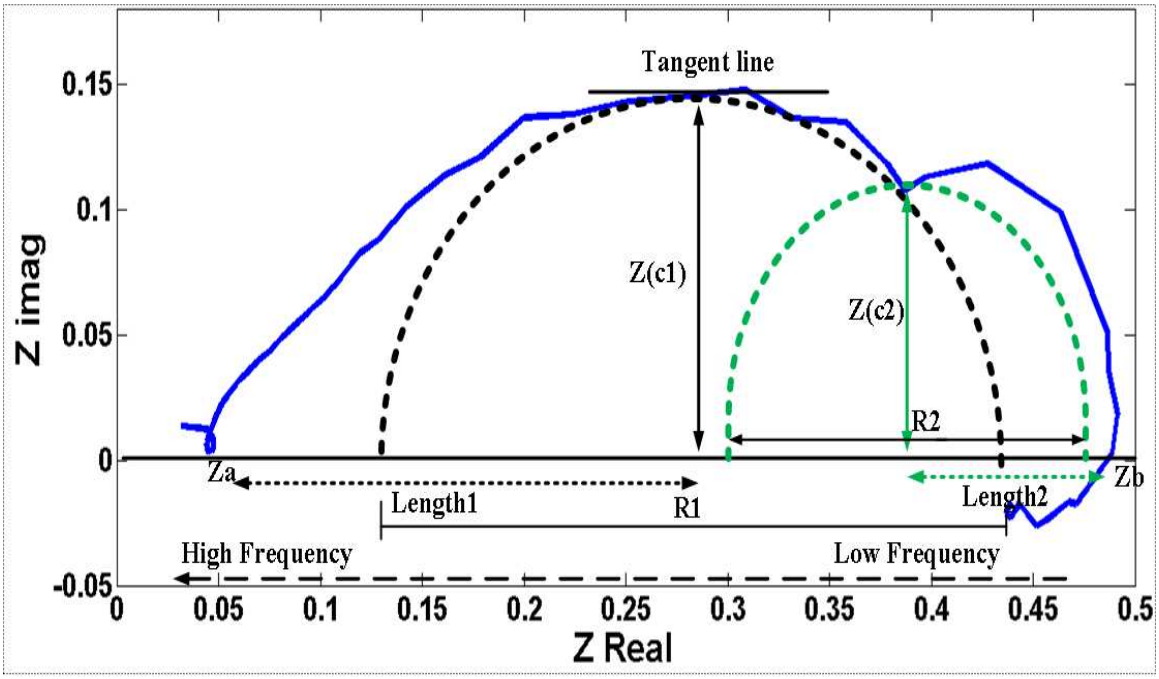


Figure 37. Location of second semi-circle loop and estimation of parameters of a circuit that represents the loop.

For n ≥ 3, the same numerical values of R and C that were obtained from previous steps will be used to represent loops 1 through n-1. The position of the 3rd loop will be determined by examining the distance of the center of the first loop from the point (Za in Figure 38) in the high frequency region where imaginary impedance is zero (length1) and the distance of center of second loop from the point (Zb in Figure 38) in the low frequency region where imaginary impedance is zero (length 2). If length 1 is greater than length 2, the 3rd semi-circle will be placed on the left side of the first loop. But if length 1 is smaller than length 2 then the 3rd semi-circle will be placed on the right side of the second loop. This 3rd loop will be centered at the midpoint of either length 1 or length 2. The diameter and radius of this loop will then provide the impedance value of the resistor and capacitor used to represent the loop. In Figure 38, length 1 is greater than length 2, so a semi-circular loop is placed on the left side of the first loop.

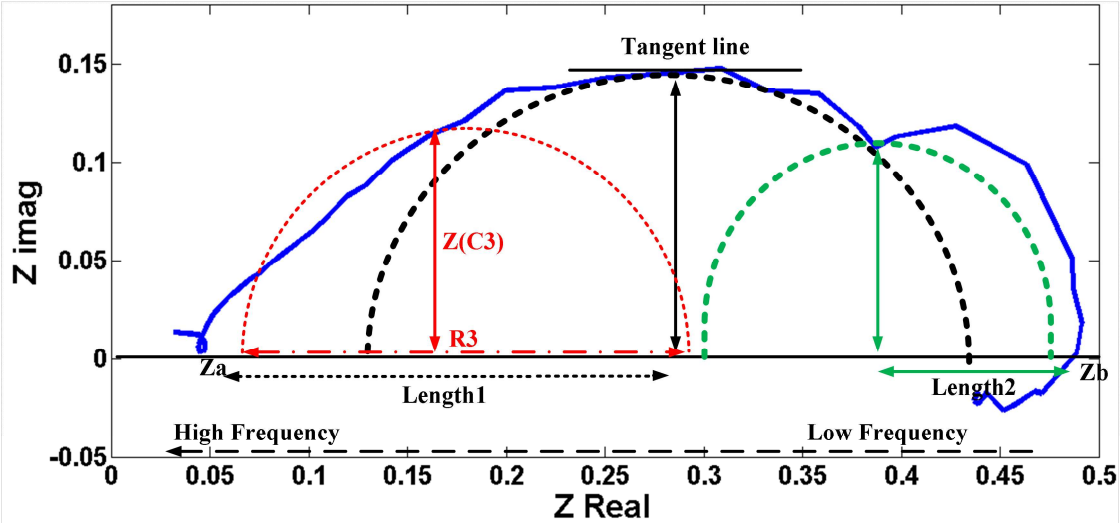


Figure 38. Location of nth activation loss loop and estimation of parameters of the circuit that represents the loop.

For n+1th loop, if the nth loop was placed on the left side of the 1st loop then, the new length1 is the distance between the center of the nth loop and Za as shown in Figure

38. On the other hand, if the $n^{th}$ loop was placed on the right side of the $2^{nd}$ loop, the new length 2 is the distance between the center of the $n^{th}$ loop and Zb.

This process of adding the number of semi-circular loops is continued until the minimum value of the sum of squares is less than $10^{-3}$. Table 39 shows the result of the program where the curve is fitted on a Nyquist plot of a 1.2kW PEM fuel cell at 10A DC with an AC current amplitude of 10% of DC current.

Table 39. Number of activation loss loops in mid frequency level of Nyqyist plot of 1.2 kW PEM fuel cell and corresponding minimum sum of square error.

| Number of loops (n) | Sum of square error |
|---|---|
| 1 | 0.43531 |
| 2 | 0.24635 |
| 3 | 0.08513 |
| 4 | 0.00741 |
| 5 | 0.0008 |

### 6.3.3. Proposed Equivalent Circuit Model of the 1.2kW Nexa™PEM Fuel Cell

Table 39 shows that we need five parallel RC branches to represent the anode and cathode activation loss loops in the mid frequency range of the Nyquist plot of a1.2kW PEM fuel cell. Hence an equivalent circuit model of this PEM cell can be obtained as shown in Figure 39. In the Figure, a DC source represents the open circuit voltage of the PEM fuel cell, Rohmic represents the ohmic losses. Two of the RC parallel circuits (RactA1, CactA1 and RctA2, CactA2) represent the anode activation losses and the other two parallel RC circuits (RactC1, CactC1 and RactC2 and CactC2) represent the cathode

activation losses. The components Cdiff1 and Rdiff1 in the RC parallel circuit represent the time constant of the diffusion process and the components Rdiff2 and Ldiff represent the inductive effect found in the low frequency region.

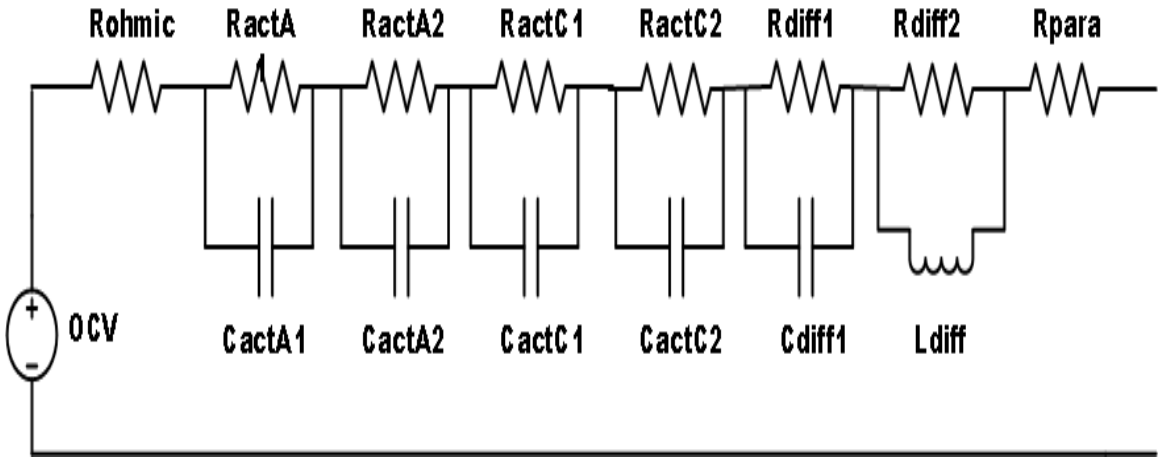


Figure 39. Proposed equivalent circuit model for a 1.2 kW PEM fuel cell Stack

## 6.4. Results and Discussion

### 6.4.1. Validation of the Equivalent Circuit Model

Using the proposed equivalent circuit, Nyquist plots for various current levels are obtained. These plots are then compared with the ones obtained using the EIS method. Figure 40 shows the Nyquist plots of the experimental impedance measurements and their respective fitted curves. As seen in Figure 40, curves obtained from the developed model closely mimic the impedance behavior of those obtained from experimentation.

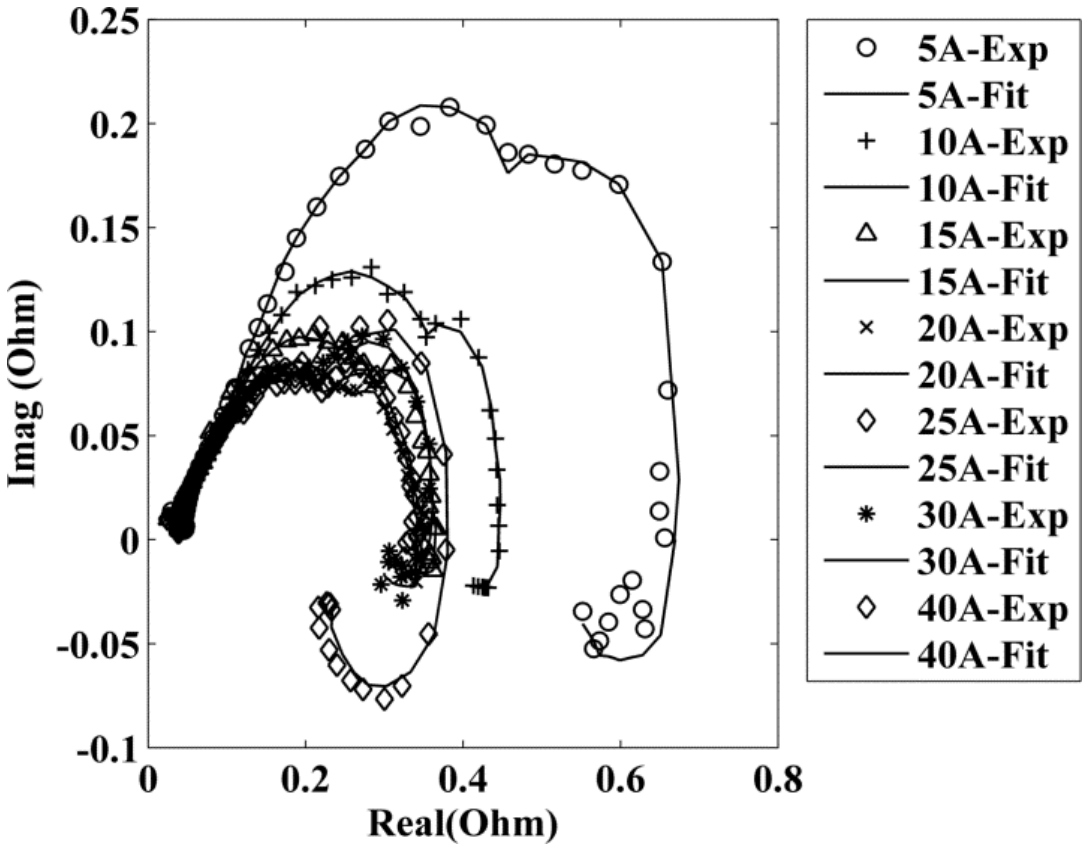


Figure 40. Experimental Nyquist plots for 5-40 Adc with 10% AC amplitude at 45 °C with their fitted curves obtained from the proposed equivalent circuit model

For further validation, the proposed model was simulated in the MATLAB/Simulink environment and an IV plot was obtained. The simulated IV plot closely matches the experimental one as shown in Figure 41.

The numerical values of the electrical components used in the model are given in Table 40.

Table 40. Parameter values for the proposed equivalent circuit of 1.2 kW PEM fuel cell.

| I (A) | Rohmic (Ω) | RctA1 (Ω) | CdlA1 (F) | RctA2 (Ω) | CdlA2 (F) | RctC1 (Ω) | CdlC1 (F) | RctC2 (Ω) | CldC2 (F) | Rdiff (Ω) | Cdiff (F) | RL (Ω) | L (H) |
|---|---|---|---|---|---|---|---|---|---|---|---|---|---|
| 5 | 0.0420 | 0.0529 | 0.0147 | 0.1651 | 0.0683 | 0.0635 | 0.0254 | 0.1854 | 0.0563 | 0.3770 | 0.2220 | 0.008 | 0.0037 |
| 10 | 0.0402 | 0.0460 | 0.0140 | 0.1590 | 0.0610 | 0.0568 | 0.0240 | 0.1758 | 0.0589 | 0.0350 | 0.3390 | 0.1560 | 0.5614 |
| 15 | 0.0390 | 0.0390 | 0.0150 | 0.1400 | 0.0610 | 0.0425 | 0.0189 | 0.1652 | 0.0584 | 0.1150 | 0.4558 | 0.0249 | 0.1670 |
| 20 | 0.0395 | 0.0410 | 0.0160 | 0.1380 | 0.0670 | 0.0325 | 0.0175 | 0.1482 | 0.0489 | 0.0001 | 0.7830 | 0.1120 | 0.1562 |
| 25 | 0.0390 | 0.0400 | 0.0180 | 0.1220 | 0.0720 | 0.0318 | 0.0165 | 0.1352 | 0.0623 | 0.1190 | 0.7060 | 0.0187 | 0.0617 |
| 30 | 0.0388 | 0.0389 | 0.0180 | 0.1177 | 0.0750 | 0.0286 | 0.0154 | 0.1251 | 0.0651 | 0.1100 | 0.6557 | 0.0680 | 0.0360 |
| 35 | 0.0384 | 0.0399 | 0.0185 | 0.1150 | 0.0790 | 0.0258 | 0.0153 | 0.1186 | 0.0684 | 0.0530 | 0.6389 | 0.1470 | 0.0643 |
| 40 | 0.0370 | 0.0390 | 0.0170 | 0.1120 | 0.0780 | 0.0278 | 0.0157 | 0.1114 | 0.0452 | 0.0230 | 0.6740 | 0.1592 | 0.0640 |

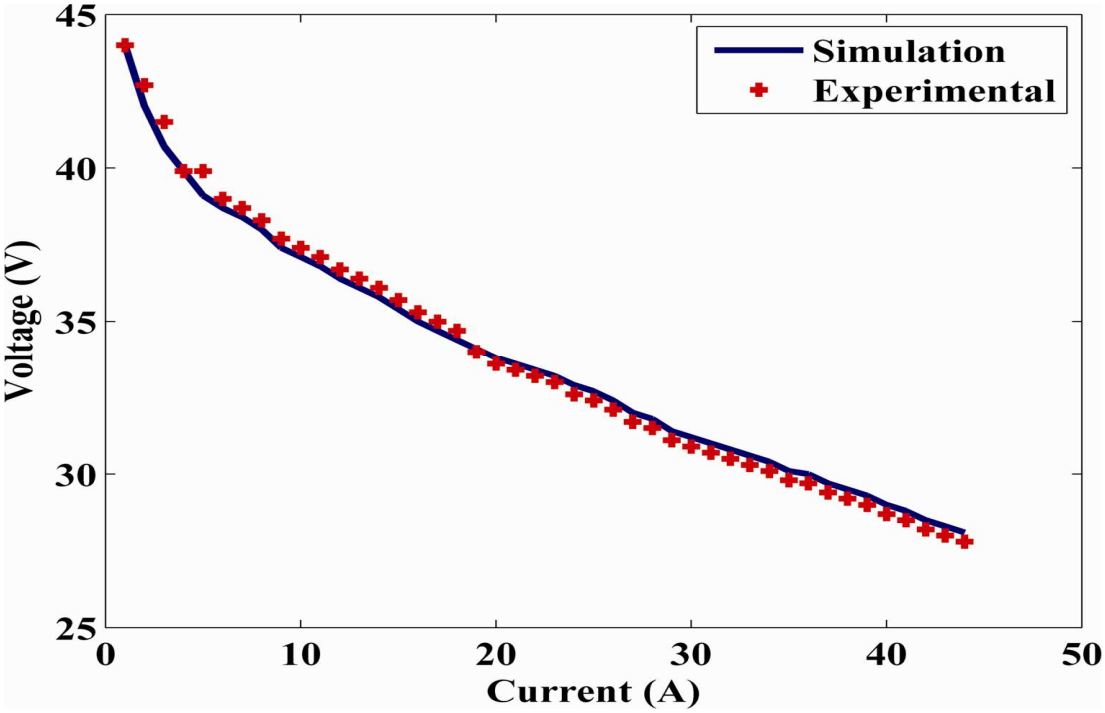


Figure 41. I-V curve obtained from the proposed model and experiment.

### 6.4.2. Transient Analysis

Several studies have suggested that compared to the RC time constant of diffusion processes, capacitance effects associated with activation losses have a significant impact on the transient properties of PEM fuel cells [129], [132], [136]. An inductive response observed at the lower frequency region of the Nyquist plot of PEM fuel cell also contributes towards the transient properties.

The actual transient response of the 1.2kW Nexa$^{TM}$ PEM fuel cell stack is compared to the one obtained from simulation using the proposed model under the same loading conditions. As can be seen in Figure 42, the transient response of the simulated model closely matches the experimental data. The overshoot behavior of voltage in a PEM fuel cell as reported by authors in [137] can also be observed in Figure 42.

Moreover, observance of similar transient responses by authors in [137] and [138] validates the proposed equivalent circuit model.

Several observations of the fuel cell under rapidly load changing conditions were recorded. Using the same load conditions, data from the simulation model are obtained. Figures 43 and 44 show an agreement between the simulation results and those obtained from experimental measurements.

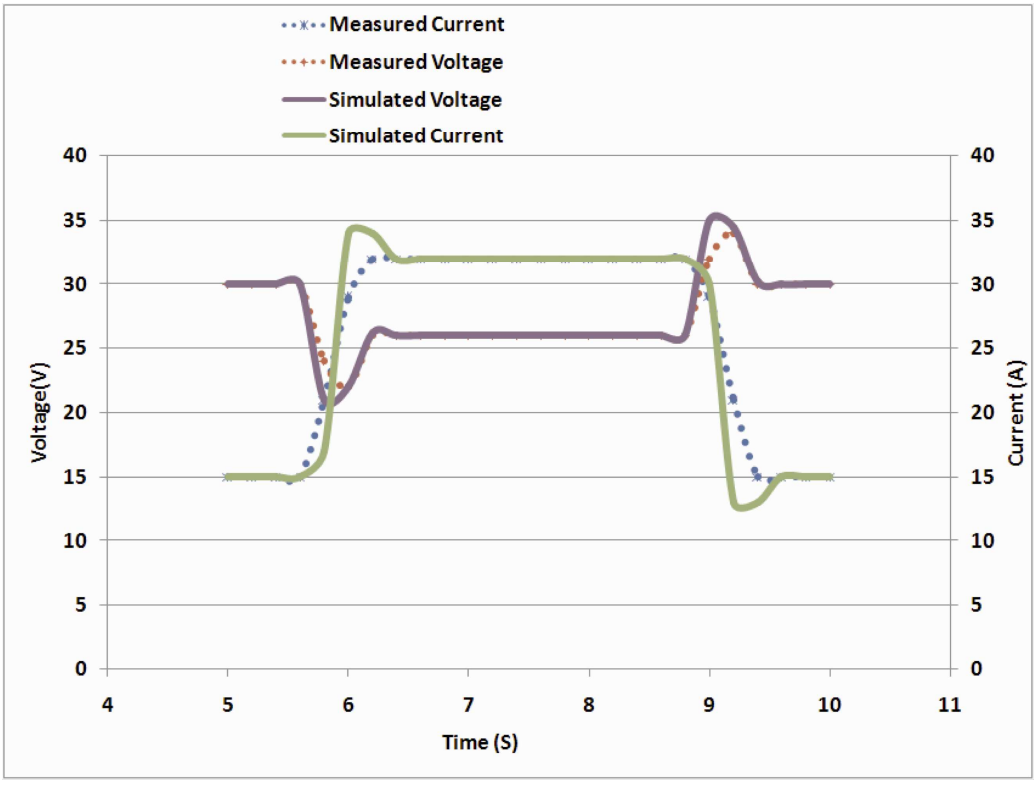


Figure 42. Transient response of the simulation model and actual 1.2 kW Nexa$^{TM}$ PEM fuel cell stack.

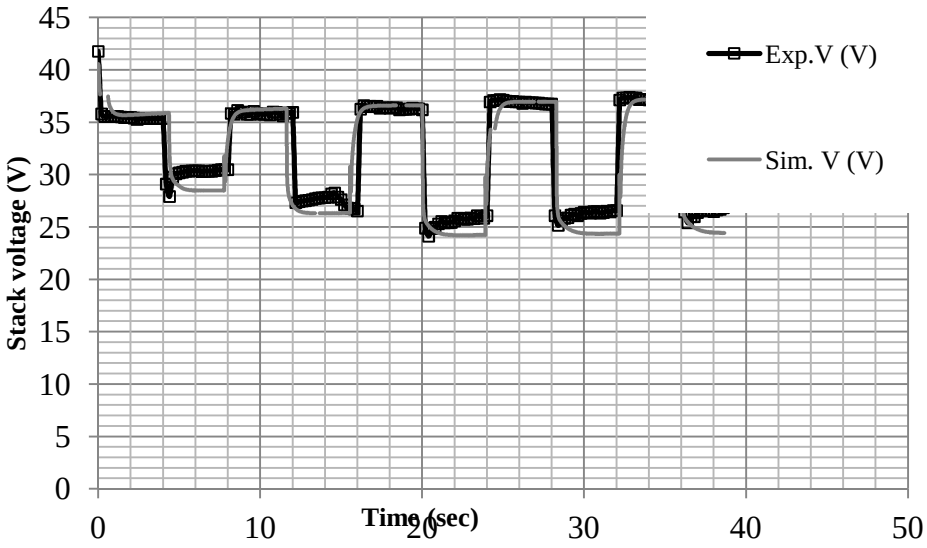


Figure 43. Measured and simulated dynamic voltage response of the PEM fuel cell stack

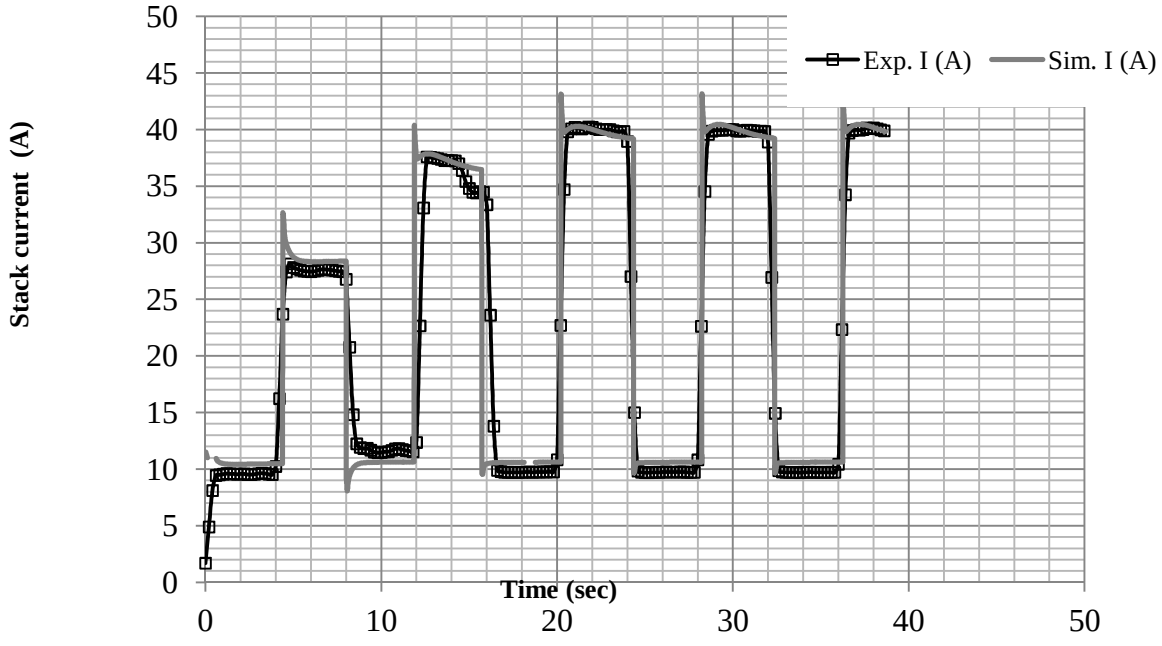


Figure 44. Measured and simulated dynamic current response of the PEM fuel cell stack

## 6.5. Conclusion

The Nyquist plot of any PEM fuel cell can be represented by a number of semi-circular loops. A single loop is obtained from a parallel RC circuit. In order to get the number of loops that can effectively characterize the impedance behavior of a fuel cell stack, a program was written in MATLAB. This program also extracts the initial values of the circuit components which are then used in the Levengberg-Marquardt algorithm for least square curve fitting. An objective function representing the impedance behavior of the PEM fuel cell was also developed. Using this objective function and impedance behaviors of a 1.2kW Nexa$^{TM}$ PEM fuel cell stack, obtained via the EIS technique, an equivalent circuit model was developed. This model was verified by fitting curves to the experimentally obtained impedance measurements. Furthermore, dynamic behavior of the proposed model was compared with the behavior of a real fuel cell stack. Results show that the proposed model behaves much like the real PEM fuel cell stack at similar operating conditions.

# CHAPTER 7

# GEOTHERMAL POWER

Among renewable sources of energy, geothermal sources have potential of supplying more than 100 gigawatts of energy at the constant base load. Hundreds of thousands of oil wells that currently exist in the U.S. have the possibility of becoming one of the major electricity producers. Since most of these plants will be connected to the utility network, their effects on these networks must be studied. The first part of this chapter presents the development and simulation of the electric interface needed to connect geothermal power plant to an electric grid.

The decision to install geothermal power depends on a thorough evaluation of geothermal potential of the targeted site. As such, the second part of this chapter presents a case study on the evaluation of geothermal potential of Lightning Dock, KGRA in New Mexico. Here, several important issues like physiography, geology, tectonics and structure, geothermal, water resources, and infrastructure of the targeted site have been analyzed and an assessment has been made on the viability of this site on being a potential source for geothermal power.

## 7.1. Modeling and Simulation of the Interface between Geothermal Power Plant Based on Organic Rankin Cycle and the Electric Grid

A geothermal power plant is to be designed that uses oil field geothermal fluids with Organic Rankin Cycle (ORC) technology. The ORC engine will use low

temperature (T<150 $^{o}$C) geothermal water to generate electricity which will be sold to a local electric utility. With oil production at the site requiring a significant power load, this plant will be both an electricity generator and a customer. Thus, it will maintain a symbiotic relationship with electric grid at all times. The fewer instabilities and interruptions there are in plant-grid interactions, the more productively and consistently the plant can supply power to consumers. As a result, a complex set of regulatory and unique engineering challenges have to be satisfied while integrating the plant into the grid. This study presents a simulation of the interface between the power plant and electric grid for a stable and reliable flow of power. Using a set of preliminary data, a simulation model of the plant in a MATLAB/SIMULINK environment with connection to the electric grid through an AC-DC-AC converter is developed and tested. The voltage obtained from the generator is first rectified by a six pulse diode bridge. The filtered DC voltage is then applied to an IGBT based inverter which generates a 60 Hz AC voltage. The resulting voltage is connected to the regulated grid.

### 7.1.1. Introduction

Recent national focus on combating global warming and reducing dependence on foreign oil has necessitated the reevaluation of all renewable energy sources and technologies associated with them. In particular, energy resources which are well distributed and have potential to supply constant power are getting more attention. Since geothermal sources have potential of supplying more than 100 gigawatts of energy with a constant base load, new and efficient technologies are emerging every day [139]. Most of these technologies are focused on improving the methods of generating power with no work addressing the transmission of this power to the electric grid.

The proposed geothermal power plant is unique compared to other electric generating plants. It uses the geothermal fluid obtained from the oil well to produce electricity. Since significant power is needed to operate the oil well, this power plant will be both an electricity generator and a customer. Hence, the fewer instabilities and interruptions there are in plant-grid interactions, the more productively and consistently the plant can supply power to the consumers. Moreover, instability in one generating unit has a potential of initiating a chain reaction which can collapse the whole electric grid. As a result, a complex set of regulatory and unique engineering challenges have to be satisfied while integrating the plant into the grid.

In this section a brief overview of the proposed low temperature geothermal power plant and issues concerning its integration into utility grid are presented. Various properties of the power system that will affect its reliability and safety are discussed. Furthermore, presently available set of standards that must be satisfied before connecting the geothermal power plant to the electric grid are summarized. Using a preliminary set of data, a MATLAB/SIMULINK model of an interface between the power plant and the electric grid has been created and its results are presented in this paper.

### 7.1.2. Components of Geothermal Power System

***Geothermal Power Plant:*** The proposed low temperature power plant uses oil field geothermal fluids with Organic Ranking Cycle (ORC) technology to generate electric power. In this technology, the hot fluid which is obtained from the oil well is used to vaporize the organic compound (working fluid). This high pressured vaporized working fluid then enters the power module and drives a turbine to produce electrical power. At the output of the turbine, the low pressured, extended vapor then cycles

through a condenser where it is cooled and condensed into liquid form. This cooled liquid is then sent to the pump, boosted in pressure and sent back to the evaporator to repeat the cycle [140]. Figure 45 shows the schematic of the ORC based geothermal power plant. This Figure is a modified schematic obtained from the webpage of Idaho National Laboratory [141].

A two-pole induction generator is driven by the turbine and generates three-phase AC power at 480V/60 Hz. An induction generator is an asynchronous machine that requires an external source to provide the magnetizing (reactive) current necessary to establish the magnetic field across the air gap between the generator rotor and stator. Without such a source, induction generator cannot supply electric power [62]. Hence, the induction generator is initially started as a motor using a solid-state, phase controlled starter and must always be synchronized to the grid. The reference synchronous speed Ns of an induction machine can be calculated as:

$$Ns = 2*f*60/p \quad rpm \tag{1}$$

$$Ws = (Ns)*\frac{2*\pi}{60} \text{ radians/sec} \tag{2}$$

Where f is the fixed frequency of the induction motor, p is the number of pole in the machine, and rpm is revolution per minute. Synchronous speed Ws and actual speed of the motor W are related to each other by slip parameter of the machine defined as:

$$s = \frac{Ws - W}{Ws} \tag{3}$$

Figure 46 shows the relationship between induction machine's slip, speed, and torque with motoring to generation transition [62].

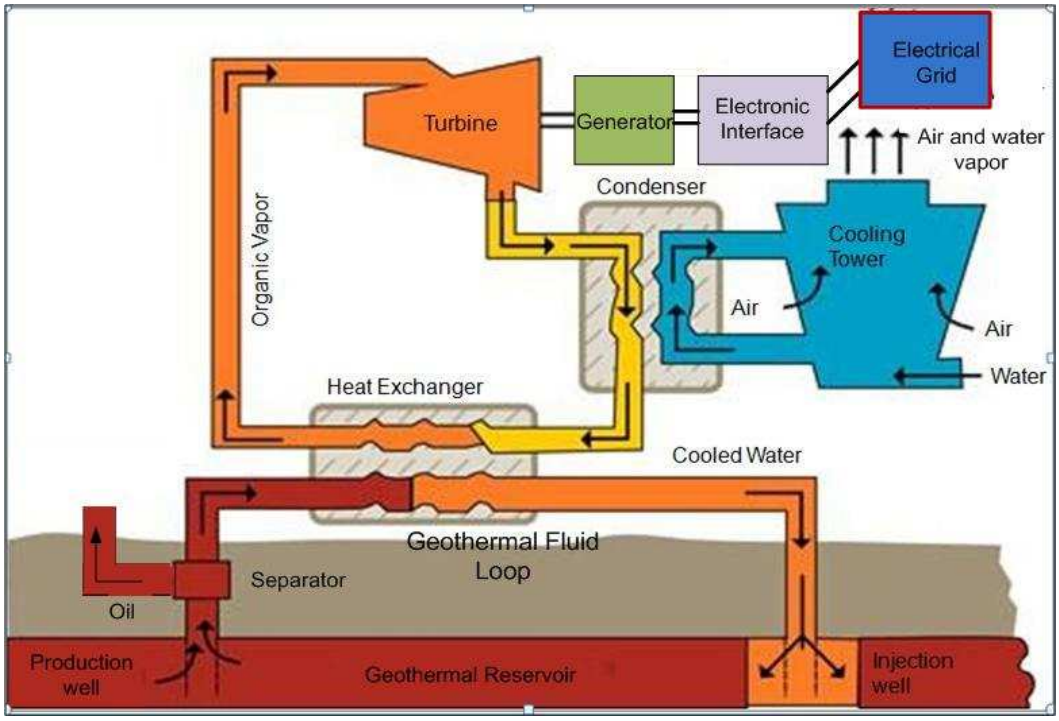


Figure 45. ORC based Geothermal Power Plant

.

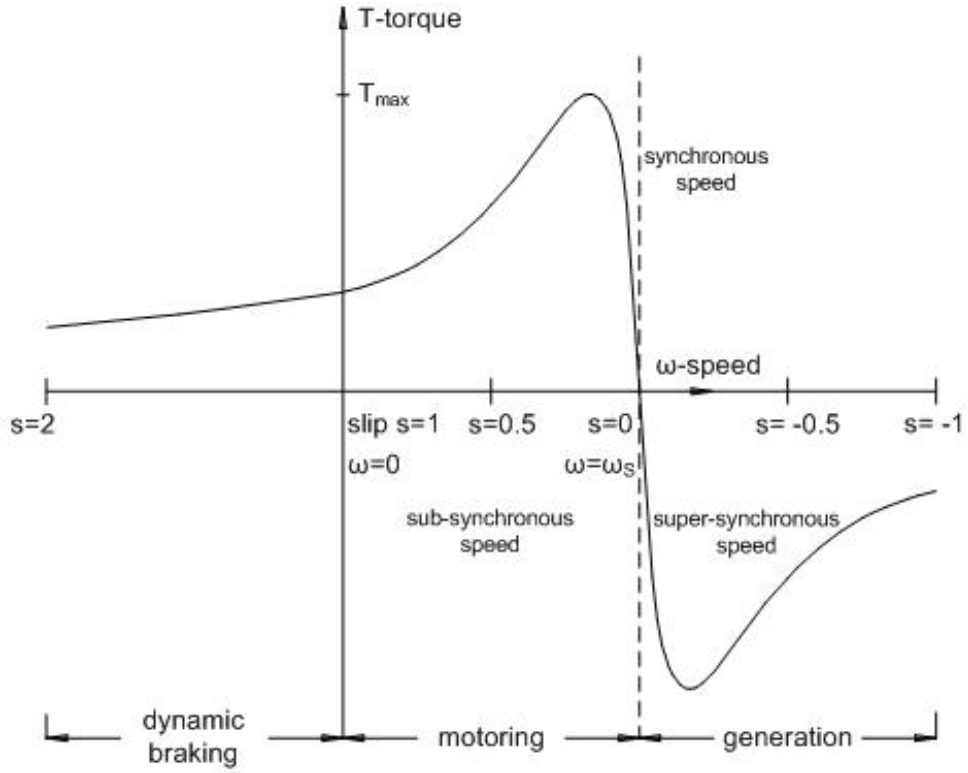


Figure 46. Induction machine speed torque curve with motoring to generation transition.

***Electric Grid:*** Electric grid is a pathway for all the electrical energies to travel from the producers (generators) to the consumers (loads). This grid consists of electric suppliers, transmission, and distribution lines and loads located throughout the country. The electricity generated from all the suppliers are pooled into this grid from which consumers draw their energy. Since the electricity generated from various sources such as solar, wind, coal and hydropower flow in the same grid, they must all be synchronized. Therefore, in a stable grid the frequency and phase of all generating units should be synchronous. Any power plant that is connected to the grid but is not synchronized will experience a large current which is likely to destroy the generator.

Electric supply and demand is balanced at all time by increasing or decreasing the output of the power plants. Power plants whose output power changes to meet the electric demand are said to be operating in the load following mode [141]. The geothermal power plant discussed in this paper will rarely run in this mode. Instead it will provide a constant base load supply of electricity at all time. Hence there must be other power plants in the grid which will run in the load following mode.

An electric grid is generally categorized into either strong or weak grid. Any point O in the grid can be represented as an equivalent circuit as shown in Figure 47. If Va is the voltage at any point A far from point O then voltage at point O is given by,

$$Vo = Va - I*Z_l \tag{4}$$

$$\Delta V = Va - Vo \tag{5}$$

Where I is current in the grid, $Z_l$ is the line impedance, and $\Delta V$ is the voltage variation.

From the above equation, it is clear that as line impedance increases, the voltage at point O decreases. Therefore, at any point O in the grid, if the voltage variation is small, i.e. for small $Z_{l,}$ then the grid is considered to be strong. Similarly, if the voltage variation is large, i.e. for large $Z_{l,}$ then the grid is considered to be weak.

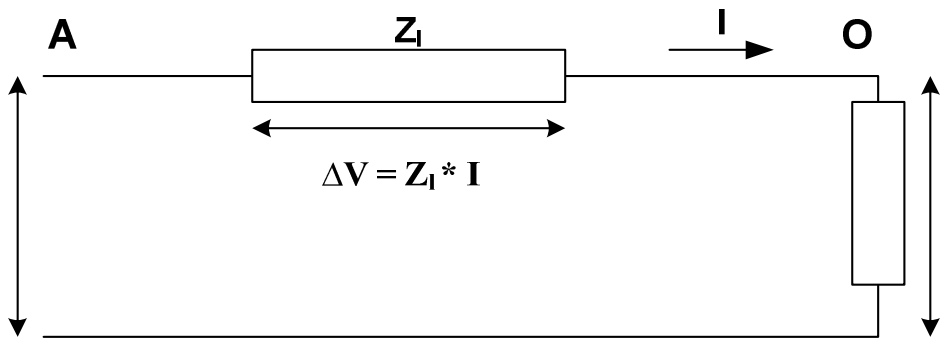


Figure 47. Equivalent circuit of any point O in the electric grid

Variation in voltage is the major cause of instability in the local electric network. Even though the normal tolerances on the voltage levels are ±10%, rapid variations even at a level as lows at 0.5% become problematic. Since the geothermal plant in question will be connected to a weak grid, voltage variations can be a limiting factor on the amount of power that can be supplied to the grid. In addition to voltage variations, other electrical issues that must be resolved before connecting the power plant to the electric grid are discussed in the following sections.

### 7.1.3. Interaction with the Local Electric Network

***Voltage***

*Voltage Flicker:* Voltage flicker is a rapid and frequent change of voltage which can cause serious damage to consumer equipment. In most cases, voltage flicker is a

direct result of the sudden changes in the operating condition of the power generator. These conditions include, but not limited to, starting or stopping of generators, output steps, fluctuation of wind and solar system outputs. Flicker evaluation is based on the IEEE standard 519-1992 [142] ;  It requires the energy producing equipments to not exceed the voltage flicker limits as defined by the maximum permissible voltage fluctuation shown for the borderline of visibility curve shown in Figure48.

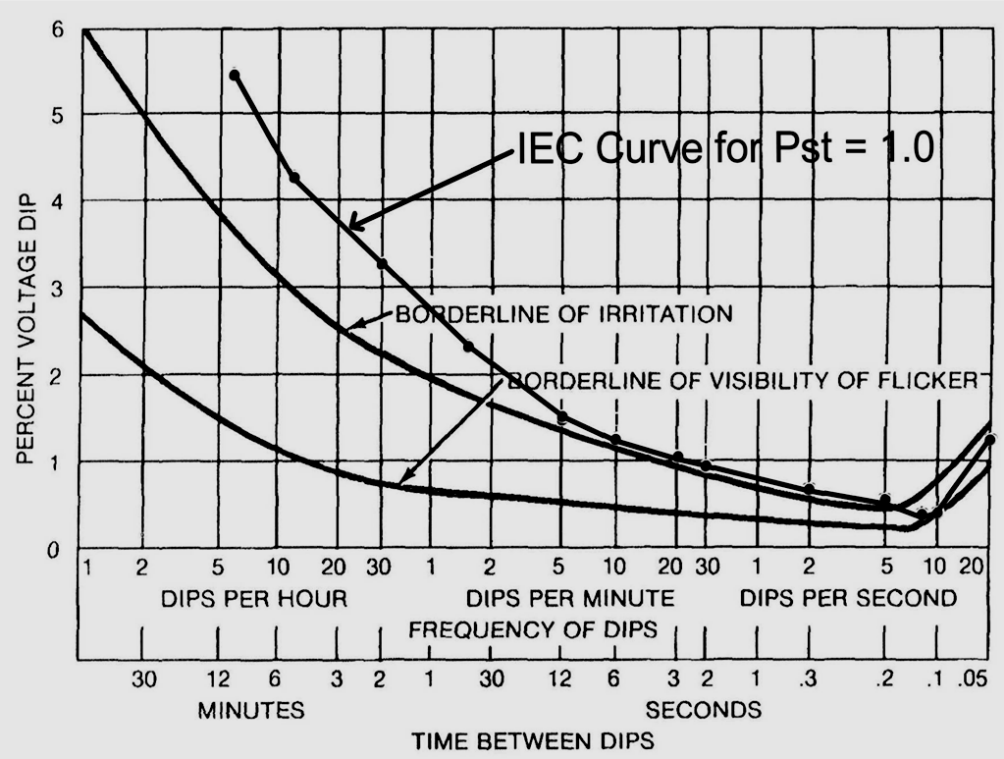


Figure 48. IEEE & IEC flicker curves

IEEE standard 1453-2004 specifies a flicker meter which can be used to measure the flicker directly [143]. The output of the flicker meter when measured at the point of common coupling (PCC) should always be less than 1 for a safe and stable electric system.

*Steady State Voltage:* Steady state voltage is the voltage of the power system over a sustained period of time. The operation of a power plant should not cause the electric network voltage to go outside the steady state limit established by the American National Standard ANSI C 84.1 [144]. According to this standard, the operation of any power plant should not cause the voltage to fluctuate by more than ±5%.

***Frequency:*** Throughout the world, the electricity is distributed through AC systems in which current constantly changes its direction and voltage its polarity. The number of these changes per second is frequency which is proportional to the rotating speed of its generators. The mismatch between the generation and the load causes the rotational speed to change, which causes a drift in the system frequency. A surplus in generation creates a frequency increase, and a shortage in generation leads to a decrease in the frequency [145]. As per IEEE std. 1547.2, the output frequency of any power producing unit should not vary by more than ±0.5% of the nominal frequency of the grid which is 60 Hz [62].

***Harmonics:*** Harmonics are frequency components of the grid voltage that are an integer multiple of the fundamental frequency. Harmonic distortions are produced by all type of nonlinear loads such as: personal computers, adjustable speed drives, power converters, etc. Harmonics increase the current in the network and cause transformers to overheat which, in turn, overheat neutral conductors. This overheating may cause erroneous tripping of circuit breakers and other equipment malfunctions.

The IEEE standard 1547-2002 has specified the limits on harmonics that can be injected at PCC and these limits are shown in Table 41 [62].

Table 41. Limitations of harmonics that can be injected at PCC (Maximum harmonic current distortion in percent of current (I))

| Individual harmonic order | h< 11 | 11≤ h ≤ 17 | 17≤ h ≤ 23 | 23≤ h ≤ 35 | 35 ≤ h | Total harmonic distortion THD |
|---|---|---|---|---|---|---|
| Percent (%) | 4.0 | 2.0 | 1.5 | 0.6 | 0.3 | 5.0 |

Based on the amplitudes (RMS values) of the harmonics present in the voltage, THD can be found as:

$$THD = 100* \sqrt{\sum_{i=2}^{n} \frac{V_i^2}{V_1^2}} \% \quad (6)$$

Where $V_i$ is the individual rms magnitude of voltage harmonics and $V_1$ is the rms magnitude of the fundamental component (60 Hz) of voltage. A similar equation can be written for the THD in the current of the system.

***Reactive Power:*** The rate at which a reactive component (capacitive and inductive elements) stores energy in its magnetic felid, and then returns it to the source, is known as reactive power. Devices which store energy by virtue of a magnetic field produced by a flow of current absorb reactive power (like an inductor) and those which store energy by virtue of electric fields generate reactive power (like a capacitor).

Since reactive power flows between the source and the load, its flow through the power meter does not affect the meter reading. However, the transfer of reactive power reduces the capacity of the lines, causes thermal losses and can, in some cases, reduce the voltage stability margin of the system. Figure 49 is the power triangle which illustrates the relation between Real, Reactive, and Apparent power.

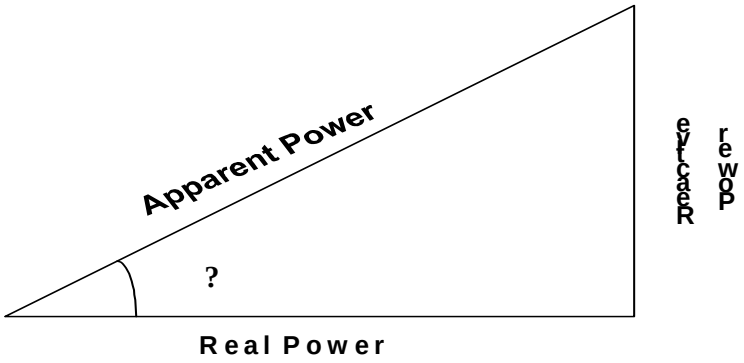


Figure 49. Power triangle

Power factor is defined as the cosine of angle θ between the apparent power and the active (real) power. The more reactive power the load needs, the lesser its power factor will be. Loads with a power factor less than 0.9 are required to install capacitors on their site to provide the required reactive power. The power factor can be calculated as:

$$\text{Power Factor} = \frac{\text{Real Power}}{\text{Apparent Power}} \tag{7}$$

### 7.1.4. Electrical Protection

Electrical protection is essential not only to secure the investment in the power plant and its equipment, but also to maintain the power quality and safety of the people involved. The IEEE Standard 1547-2003 requires several types of protection, such as [146]:

a) The interconnection system must include protection that prevents energization of the power system when it is de-energized.

b) The interconnection system must be able to detect faults and isolate the power plant.

c) The interconnection system must be coordinated with reclosers in the area electrical power system (EPS) that may isolated the feeder that connects the power plant to the electric grid. Failure to coordinate can result in damage to equipments and lead to hazards to work crews.

The overvoltage and under voltage protection and over frequency and under frequency detections are the primary means for detecting faults and other disturbances on a line. These protections should be programmed in such a way that the power plant will be quickly isolated under severe conditions, but it will be allowed for a longer operation when conditions are less severe so that unnecessary disconnection is avoided when reasonable.

In order to address the above mentioned issues, a simulation model has been created in a MATLAB/SIMULINK environment. Description of the model and results are presented in the following sections.

### 7.1.5. Simulation Model

The simulated model in Figure 50 has been created with the general components available in simulink. Based on available preliminary data, these components have been modified to reflect the proposed system.

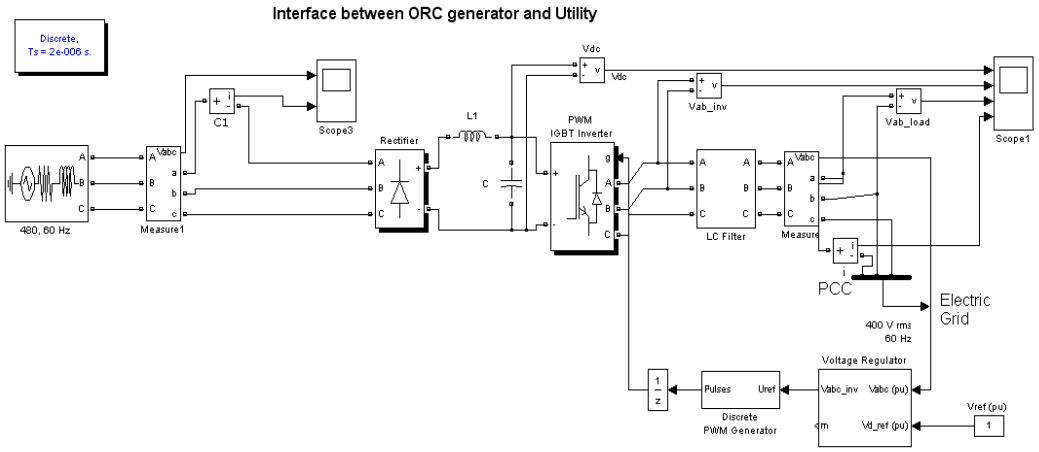


Figure 50. Interface between geothermal ORC generator and the utility grid.

The electric circuit in the simulation consists of a generator that is connected to electric grid through an AC-DC-AC converter using a rectifier, IGBT inverter, and voltage regulator. The voltage obtained from the generator of the model is first rectified by a six pulse rectifier diode bridge. The filtered DC voltage is then applied to an IGBT inverter generating 60 Hz AC voltage which is connected to the regulated grid [147].

The inverter uses PWM at a 2 kHz carrier frequency. The circuit is discretized at a sample of 2 micro second. Voltage from the IGBT inverter is regulated at 1 pu (480V rms) by a PI voltage controller using abc-to-dq and dq-to-abc transformations. The first output of the voltage regulator is a vector containing the three modulation signals used by the PWM generator to generate the 6 IGBT switching pulses.

### 7.1.6. Results

***Without Interface:*** The voltage and current obtained from the generator are shown in Figures 51 and 52, respectively. The unregulated voltage and the huge inrush current and harmonics presented in the current signal must be removed before connecting the plant to the local electric network.


Figure 51. Three phase generator voltage

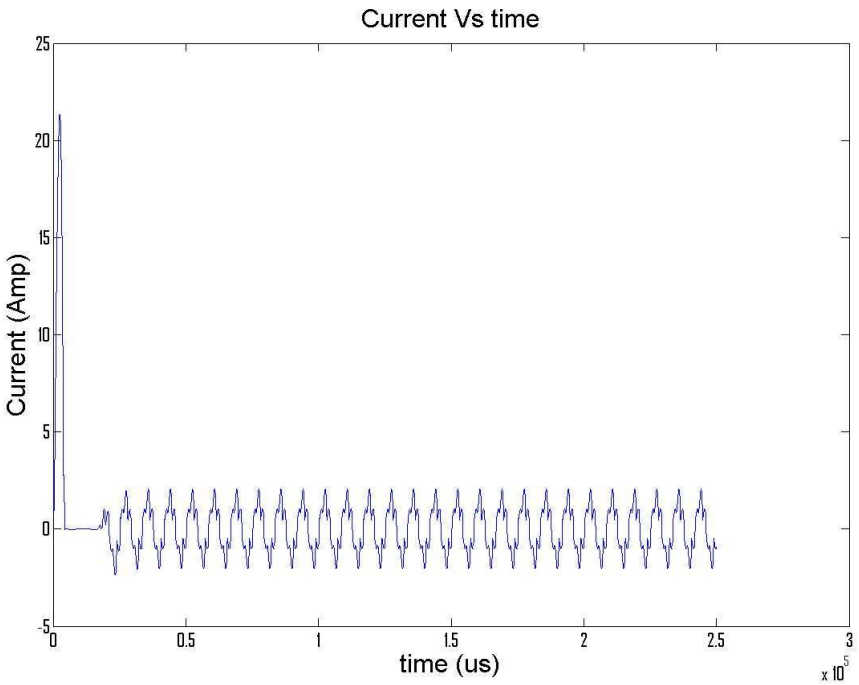


Figure 52. Generator current.

***With Interface:*** The voltage and current at the point of common coupling (PCC) are shown in Figures 53 and 54, respectively. The voltage at this point will always meet

the IEEE standard of ±5% of steady state voltage of the area network which is maintained at 480V (1 pu). Similarly, the large inrush current observed in Figure 52 has been filtered and the total harmonic distortion (THD) of the current has been lowered to the IEEE standard of less than 5%.

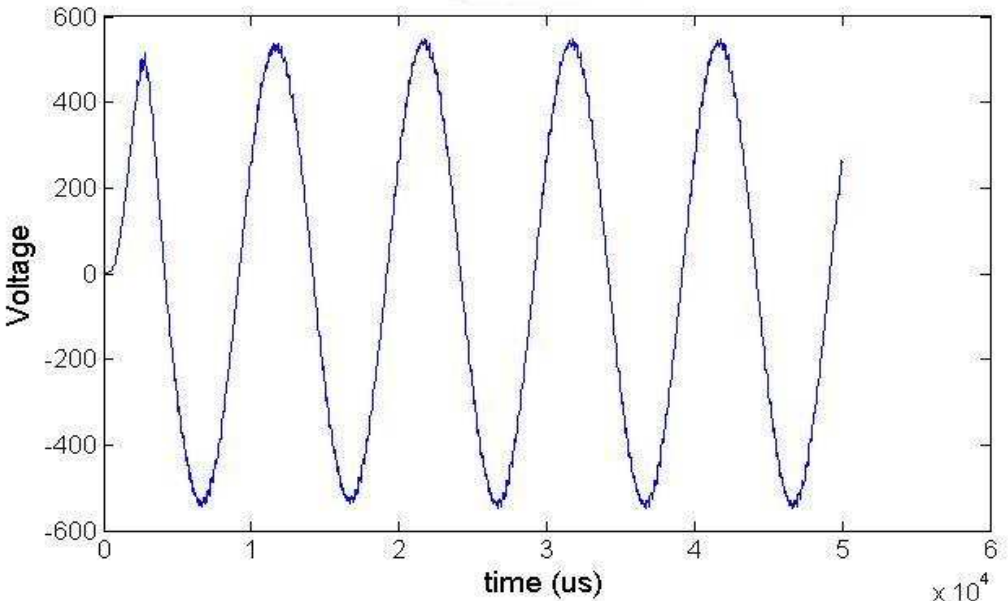


Figure 53. Regulated voltage at PCC

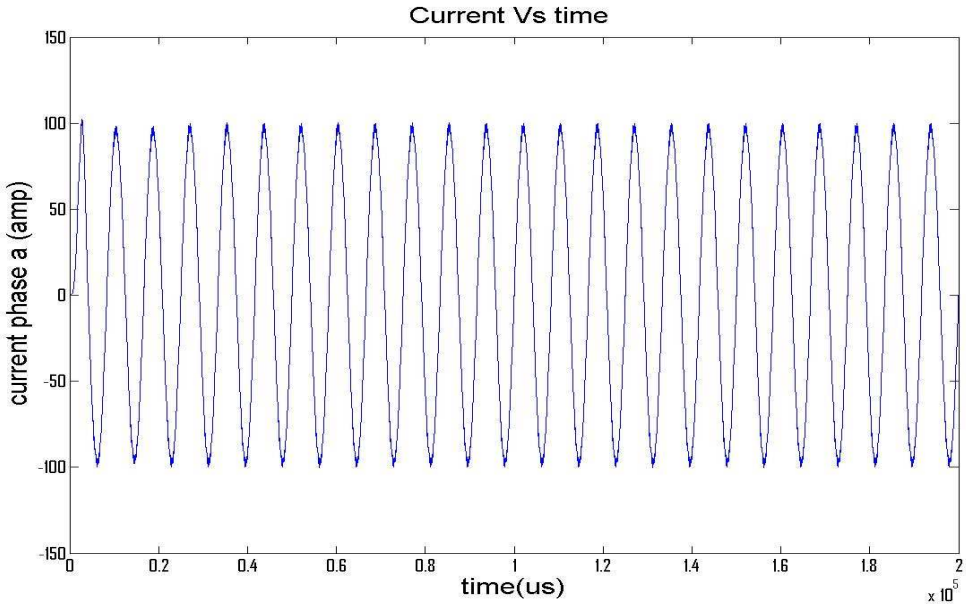


Figure 54. Current at the PCC.

### 7.1.7. Conclusion

Among renewable sources of energy, geothermal sources have the potential of supplying more than 100 gigawatts of energy at a constant base load. Hundreds of thousands of oil wells that currently exist in the US have the possibility of becoming one of the major electricity producers. Recent work on the geothermal plants has been focused on improving the efficiency of the power production. Since most of these plants will be connected to the local electric network, their effects on these networks must be studied. Issues like voltage and reactive power control, frequency control, and fault ride-through capabilities limit the energy output of the plant and for that reason local electric grid should be considered as part of the planning process. The simulation presented in this work not only highlights major issues that might cause instability in the power grid but it also looks into the electrical interface that can be used to resolve those issues. Simulation studies like that presented in this section must be conducted before connecting any power plant to the grid to reduce degradation of the power quality.

With advancements in power electronics, most of the electric generation systems today are already equipped with efficient power controllers. Hence the output of these systems meets most of the standards on power quality; but additional design and implementation of power controllers might be needed to satisfy the local utility's requirements. Attention should be given to available standards while designing, simulating and implementing power controllers.

## 7.2. Case Study: Evaluation of Geothermal Potential of Lightning Dock KGRA, New Mexico.

Lightning Dock in New Mexico currently houses the largest geothermal greenhouse complex in the United States, one of the largest aquaculture farms, and a binary geothermal power plant. With the addition of Cyrq Energy's (formerly Raser Techonologies) 10MW geothermal power plant, it will be the most utilized geothermal resource in New Mexico. This section presents an evaluation of the geothermal potentials of the area of the Lightning Dock area. The evaluation has been performed by examining the following attributes of the area: physiography, geology, tectonics and structure, water resources, infrastructure, population and target markets, other geothermal considerations, and economic considerations and available incentives. This objective has been accomplished by using a combination of literature reviews and data analyses in conjunction with the interpretation of information obtained from digitized map layers created in ArcGIS® [148].

The evaluation indicates that the Lightning Dock area has high geothermal potentials without requiring significant infrastructure additions or upgrades. Using the reported heat flow of 650mW/$m^2$, it is estimated that the 90$^o$C and 180$^o$C isotherms will be reached at depths of 0.3 km (984 ft) and 0.7 km (2,165 ft) respectively [149]. Hence, various applications including direct use and electricity production using binary power plant technology are viable in the area.

### 7.2.1. Introduction

The Lightning Dock known geothermal resource area (KGRA) is located in the Animas Valley in western Hidalgo County of New Mexico as shown in Figure 55. The area is bordered by the Pyramid and Animas Mountains in the east and the Peloncillo

Mountains in the west (Figure 56). Since its discovery in 1948 the resource has been used for greenhouse heating, aquaculture, and electric power production [150].

The Burgett geothermal greenhouses, the largest geothermally heated greenhouse complex in the U.S., have been in operation since 1977. This facility covers 426,700 $m^2$ (32 acres) and uses geothermal water with temperatures of 104 to 113$^oC$ (220 to 235$^oF$) at a maximum flow rate of 126 liters per second (l/s) (2,000 gallons per minute (gpm)). The complex uses 53,900 MW (184 billion Btu) of geothermal energy annually which amounts to cost savings of about $736,000, as compared to using propane [151]. In addition, Two PureCycle model 280 systems were installed in the complex in July 2008. These units use the geothermal water at 107$^oC$ (225$^oF$) to produce more than 500 kW which is consumed on site for the greenhouse and facility operations.

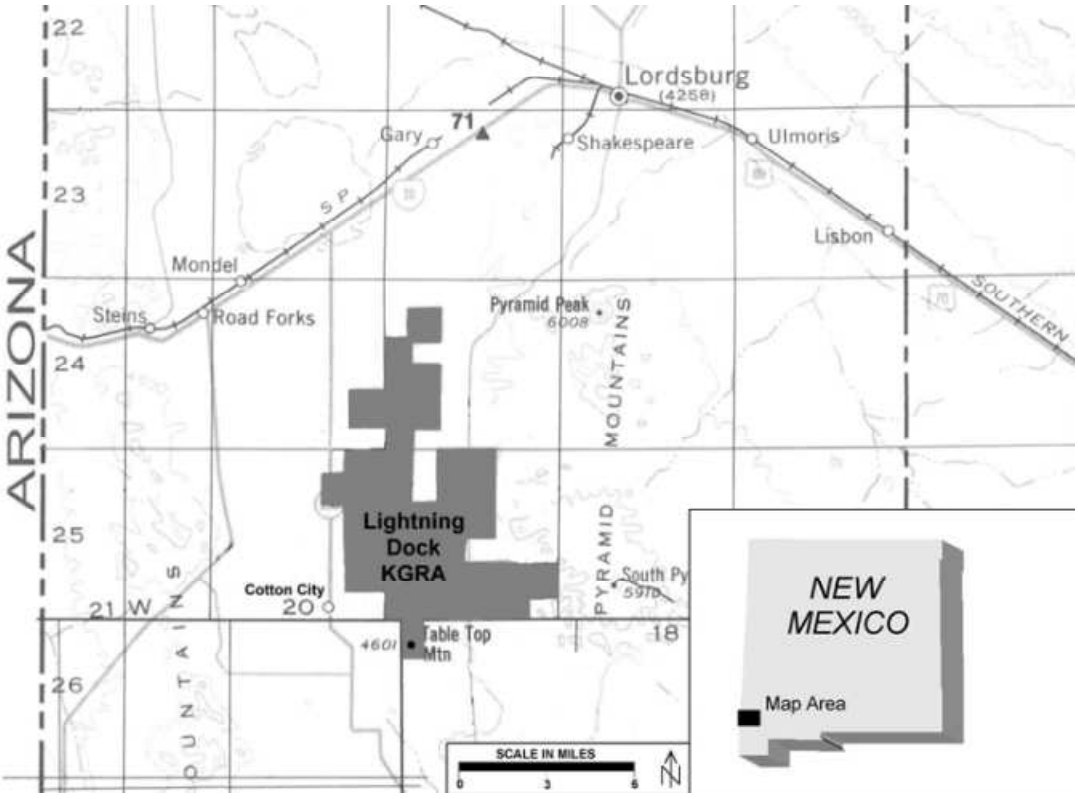


Figure 55. Location of Lightning Dock KGRA

Americulture owns and operates an aquaculture complex which uses geothermal heating to produce between four to seven million fish annually. This facility uses a down hole heat exchanger to circulate 6.3 l/s (100 gpm) of "cold water" through the 122 m (399 ft) well which has an average temperature of 110$^{o}$C (230$^{0}$F). This results in an annual energy use of 3220 MW (11 billion Btu) [151].

In May 2012, Public Service Co. of New Mexico announced its intention to enter into a 20 year Power Purchase agreement with Cryq Energy (formerly Raser Technologies) for the 10 MW Lightning Dock Geothermal Power plant which is currently under construction and that is expected to be operational by January of 2014 [152].

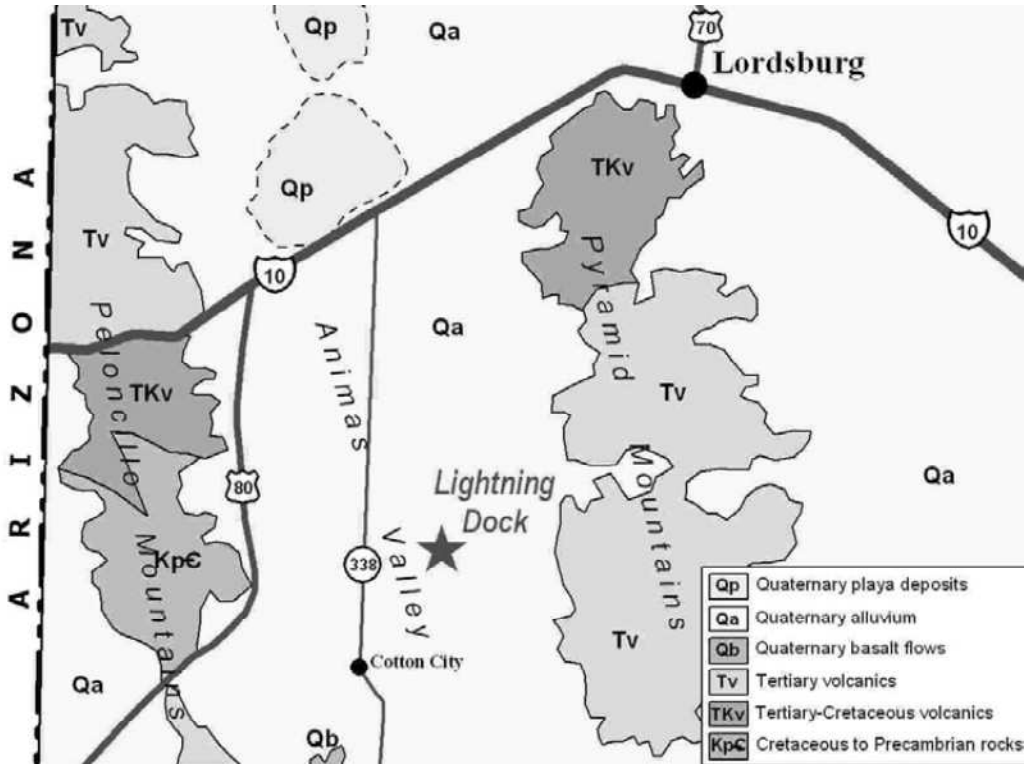


Figure 56. Map showing Animas Valley

### 7.2.2. Physiography

As mentioned above, the Lightning Dock KGRA is bordered by the Pyramid and Animas Mountains in the east and the Peloncillo Mountains in the west [153]. The elevation of the area is approximately 1,402 m (4,600 ft) above sea level [154].

Data from the Western Regional Climate Center indicates that the average temperature in the Lightning Dock KGRA area varies from 14.6$^{o}$C (58.3$^{o}$F) to -2.8$^{o}$C (27$^{o}$F) in the month of January and 34.9$^{o}$C (94.8$^{o}$F) to 17.7$^{o}$C (63.8$^{o}$F) in the month of July. The average annual temperature is 15.8$^{o}$C (60.5$^{o}$F). The average annual precipitation in the area is 27.7 cm (10.9 in.).

### 7.2.3. Geology

Lightning Dock KGRA is located in the Animas Valley which ranges in a width from 11 to 21 km (7 to 13 miles) and has a length of about 145 km (90 miles). The geothermal area lies at the foot of the Pyramid Mountains which border the Animas Valley in the east [155]. North trending Basin and Range features and a caldera ring fracture zone are the primary structures of the area. Because of the presence of small volcanic hills on the valley floor and based on the results of extensive drilling, authors in [155] conclude that the valley fill is relatively thin and mention that the "Quaternary sediments consist of alluvial fans and pediment deposits, fluvial deposits, and modern eolian and sheetwash deposits."

In [153], authors mention that during late Pleistocene and Holocene times the Animas Basin was occupied by Lake Animas which left lacustrine deposits and shoreline features. The exposed rocks found in the bordering mountains are Precambrian granodiorite, Paleozoic and Mesozoic sedimentary rocks, Tertiary/Cretaceous volcanic

rocks, Tertiary intrusive rocks, Tertiary conglomerate, Quaternary/Tertiary basalt flows, and Quaternary conglomerate [155], [156]. The Pyramid Mountains form the Muir Cauldron, a complex volcanic sequence and contain rocks that are mostly Cretaceous in age or younger.

Using the gravity and magnetic data, authors in [157] developed a model of the Lightning Dock KGRA. The authors observed the high north-south magnetic and gravity anomalies near the Burgett green house complex where Paleozoic sedimentary rock underlies volcanic rock. This layered structure reaches a low point at the west side where the limestone has a modeled depth of about 1.7 km (1.1 miles).

### 7.2.4. Tectonics and Structure

Three major regional tectonic features, a mid-Tertiary caldera ring fracture zone, a major basement structure zone, and a young incipient normal fault tip, enclose the Lightning Dock geothermal system. The upflow zone is believed to be due to the intrusion of the mid-Tertiary caldera ring fracture in the horst block of the normal fault system [151].

Authors in [153] report that the Animas Valley fault (AVF) has a surface expression with the presence of a northeasterly trending fault zone and the ring-fracture zone of the Muir cauldron. In [155], gravity data was used to conclude that the upper Animas Valley was displaced and rotated by the major lineament of the fault which strikes roughly southwest to northeast. Using the residual gravity pattern, authors in [157] identified the horst block and estimated that it is 2 km (1.2 miles) wide (Figure 57). They also concluded that the westward fault is the major horst bounding structure while the Animas Valley fault passes through the middle of the horst and with the

volcanic layer thinning on the west side of the well 55-7. Moreover, it is predicted that the uplift in the basement of Animas Valley is due to faults bounding both sides and that the mapped Animas Valley fault which runs through the previously mentioned horst does not bound the west side of the uplift. Instead, a different fault bounds the west side of the uplift and an unmapped fault bounds the east side of the uplift. Both of these faults appear to converge on the north side of well 55-7 [157].

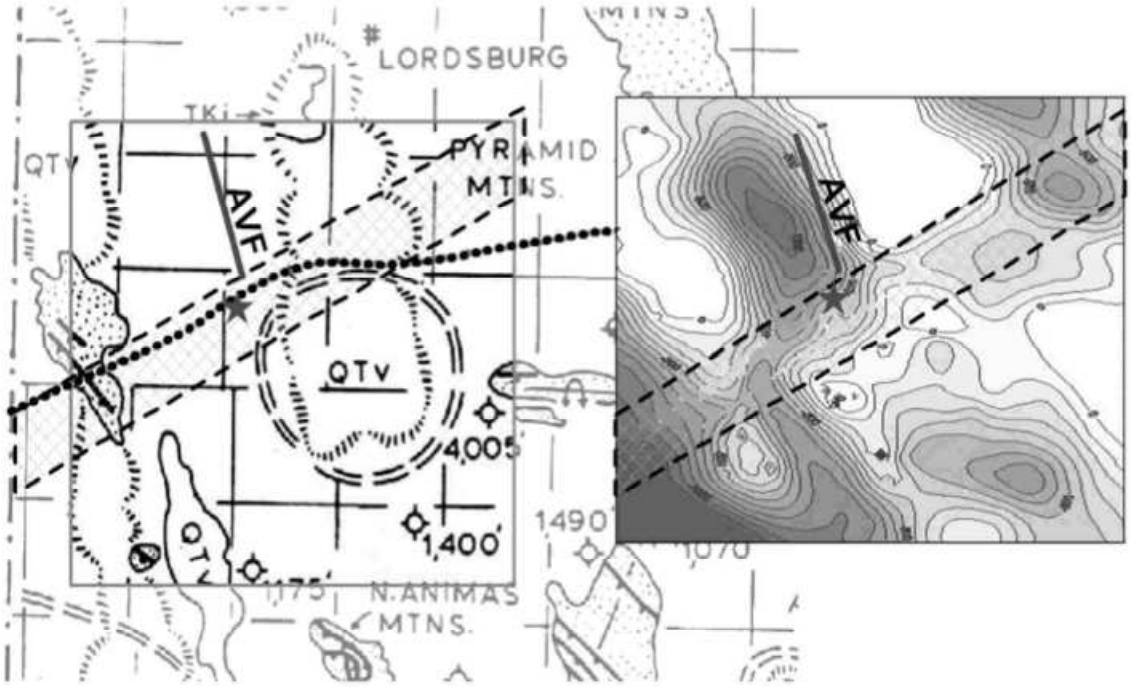


Figure 57. Integrated Regional Geology with depth to basement map generated from gravity inversion

.

### 7.2.5. Geothermal

In a study conducted by Lightning Dock Geothermal Inc. the rocks found in a recent temperature gradient hole were predominantly lakebed sediments deposited in the Pleistocene and Recent Lake Animas [149]. Unconsolidated sand and gravel beds, reported to be about two feet thick, were interbedded with thin layers of greenish clay.

Authors in [151], reported that the total natural heat loss for the geothermal system at Lightning Dock is less than $10MW_{thermal}$. They also determined the temperature of the base reservoir to be 154 to $160^{o}C$ (310 to $320^{0}F$) by using the silica geothermometer and the temperature profile of the 2,130 m (7,000 ft) deepsteam Reserve Animas 55-7 geothermal test well.

In [153], authors mention that hydrothermal alteration in the Lightning Dock KGRA occurred during the collapse of the Muir cauldron in Oligocene time and during the activity of Miocene or younger hot springs and shallow vein-forming hydrothermal fluids. From their model the authors conclude that the deep geothermal reservoir is located in fractured volcanic rocks at a depth of approximately 1.5 km (0.9 miles). They add that the northeast trending high-angle fault system intersects this reservoir. Small volumes of hot water rise through this northeast trending fault and leak into shallow aquifers near the surface. Because of the formation of highly permeable conduits in the area where a northeast trending fault intersects the Muir cauldron ring-fracture zone and a basin and range fault, large volumes of water move up into a mixing zone. In this zone, the authors postulate that water at 250°C (482°F) mixes with the cold ground water in a one to three ratio to produce mixed water at 150–170°C (302-338°F). The Riedel shear zone structurally controls the rise of this mixed water towards the aquifer located near the surface [149], [153].

Dismissing the assumption that the thermal anomaly of the Lightning Dock geothermal resource is a point source upwelling along a single fault, authors in [149] suggested that the reservoir is "either a pervasively fractured zone or a series of small faults and shears in the shallow volcanic rocks and deeper sedimentary rocks, created by

the relative recent possible lateral offset of the AVF resulting from strong tectonic extension forces. Furthermore, Cunniff and Bowers observed the depth to Precambrian bedrock to be 2.5 km (1.6 miles) and the depth interval had a measured average temperature of 145°C (293°F) [149]. They also calculated the heat flow around the area to be about 650 mW/m$^2$ (15.5 HFU). Based on this heat flow value and an annual surface temperature of 15.8°C (60.5°F), the 90°C isotherm would be encountered at a depth of approximately 0.3 km (984 ft) and the 180°C isotherm would be reached at a depth of approximately 0.7 km (2,165 ft).

### 7.2.6. Water Resources

Geothermal waters at Lightning Dock contain sodium sulfate and carbonate with TDS values around 1,100 mg/L and no detectable arsenic [151]. Very low concentrations of carbon dioxide and hydrogen sulfide have also been reported in the thermal waters. The transmissivity of the geothermal reservoir is more than 25,000 gpd/ft. Due to the relatively low elevation of the resource, it is in a favorable location for forced or advective discharge of fluid and heat from a regional bedrock groundwater flow system and the combination of Cretaceous and Tertiary uplift has facilitated non-deposition or erosional stripping of regional aquitards to create a local “geohydrologic discharge window” [151]. This system is recharged from the surrounding higher terrains, mountains and valley. Oxygen isotope analysis on the geothermal waters indicates that recharge occurs relatively quickly with an estimated age of the water from Pleistocene to Recent [153].

Authors in [151] report that “All currently producing geothermal wells at Lightning Dock area are between 107 to 183 m (350 to 600 ft) deep, and produce from the shallow

outflow plume reservoir. Well production ranges from a few hundred gpm to 1,200 gpm (76 liters/s), typically at 99 to 113°C (210 to 235°F)."

The Lightning Dock KGRA does not have an abundance of surface water resources. Lack of permanent streams and the low average annual precipitation (27.7cm (10.9 inches)) makes groundwater the primary source for irrigation and domestic needs. The groundwater for irrigation is obtained from saturated sand and gravel beds at depths ranging from 4.6 m (15 feet) in the north to 61 m (200 feet) in the south. Piezometric data indicates that the groundwater moves north towards the Gila River. The groundwater of the Animas Valley was designated as a groundwater basin and was closed for further appropriation in 1948. The average transmissivity of the aquifer is about 50,000 gpd/ft with the coefficient of storage at about 0.10 [158].

The water at the hot wells in the Lightning Dock KGRA is considered to be mixed water containing approximately 25% of deep geothermal fluid at around 250°C (482°F) [153]. As mentioned before, and as shown in Figure 58, the mixed water ascends in the area of the hot wells and then cools as it disperses in the aquifer, mainly to the north-northwest and to the southwest [155].

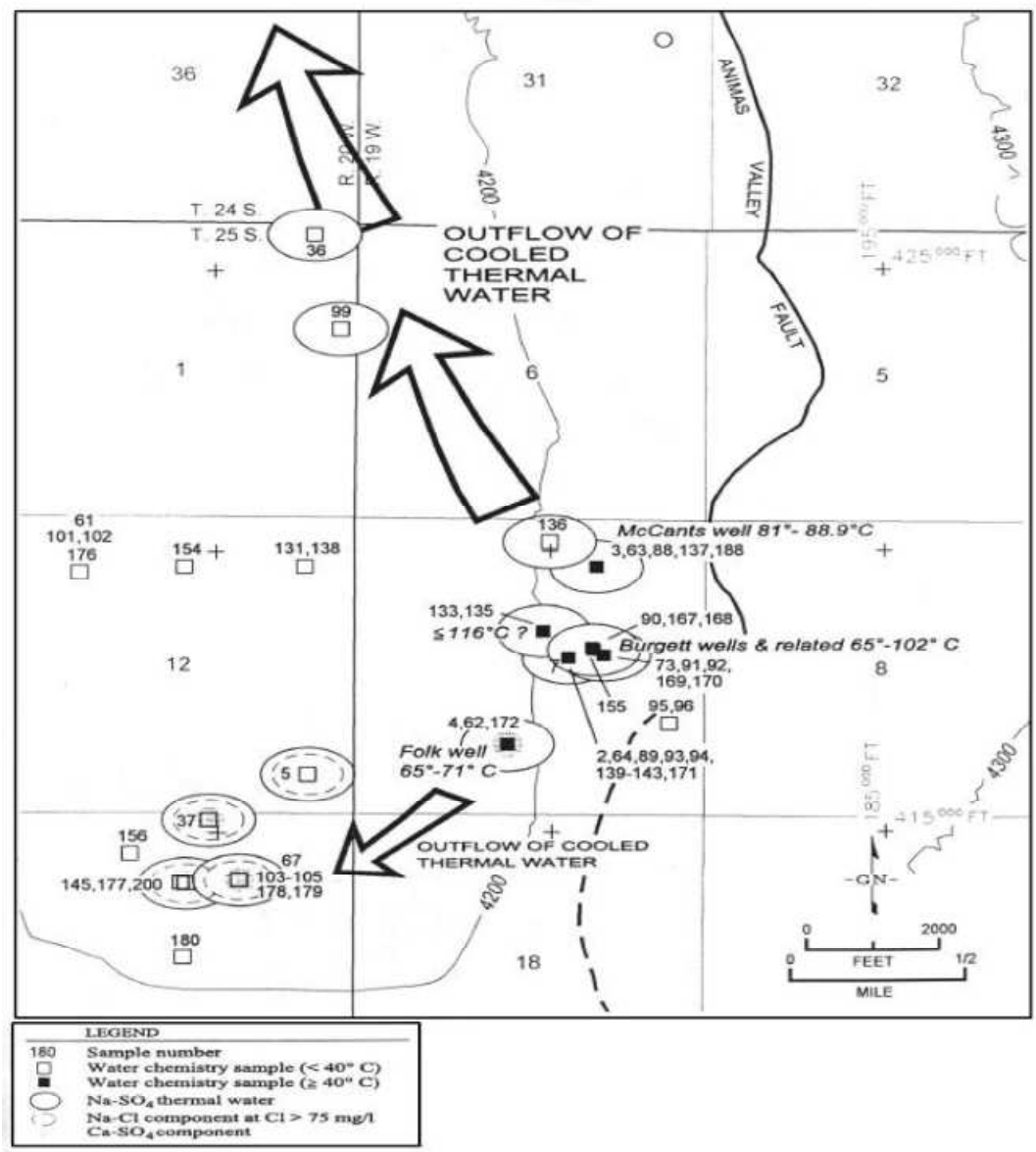


Figure 58. Flow pattern of geothermal water

Rain water that falls within the drainage area of Animas Valley is the ultimate source of recharge for the groundwater aquifer, however due to the high average annual temperature and low precipitation, only a fraction of rain water actually penetrates into the groundwater body [158]. Although the groundwater has been used extensively for agricultural and domestic purposes, there is no indication that the volume of the ground

water body has decreased. As reported by authors in [155], the water level at the hot wells was at a depth of about 21 m (70 feet), which had been maintained for about 10 years.

### 7.2.7. Infrastructure

Lightning Dock is located in western Hidalgo County of New Mexico. New Mexico Highway 338 connects Lightning Dock with U.S Interstate I-10 which is located 23 km (14 miles) north. U.S. Interstate I-10 provides access to Las Cruces located 193 km (120 miles) to the East; Tucson, 257 km (160 miles) to the west; and El Paso, 266 km (165 miles) to the southeast. The only available transmission line near the Lightning Dock area is a 69kV line which is owned and maintained by Columbus Electric Cooperative who currently provides electrical service to the area. New transmission lines must be created in order to utilize the full electrical production potential of the Lightning Dock KGRA. However, the development of 10MW geothermal power plant by Cyrq Energy may strengthen the available infrastructure, thus, eliminating the need of additional significant upgrades. Figure 59 shows the available roads and transmission lines around Lightning Dock KGRA.

### 7.2.8. Assessment and Conclusions

Geothermal resources in the Lightning Dock KGRA have long been used on a commercial scale. This area houses the largest greenhouse complex and one of the largest aquaculture farms in the U.S. Although previous attempts at producing electric power had failed, the recent developments in geothermal technology have allowed the installation of two binary power plants which produce more than 500 kW of electric power at the Burgett greenhouse. Using a previously drilled well, TFD 55-7, Cyrq Energy is planning

to install a binary power plant using 140 – 154°C (284–309°F) waters. Upon completion, this power plant is expected to produce 10 MW of electric power.

A 2005 study by Cunniff and Bowers has shown that the geothermal reservoir extends deep to the southwest of the Lightning Dock KGRA [149]. This area should be explored and studied as a potential site capable of producing electric power.

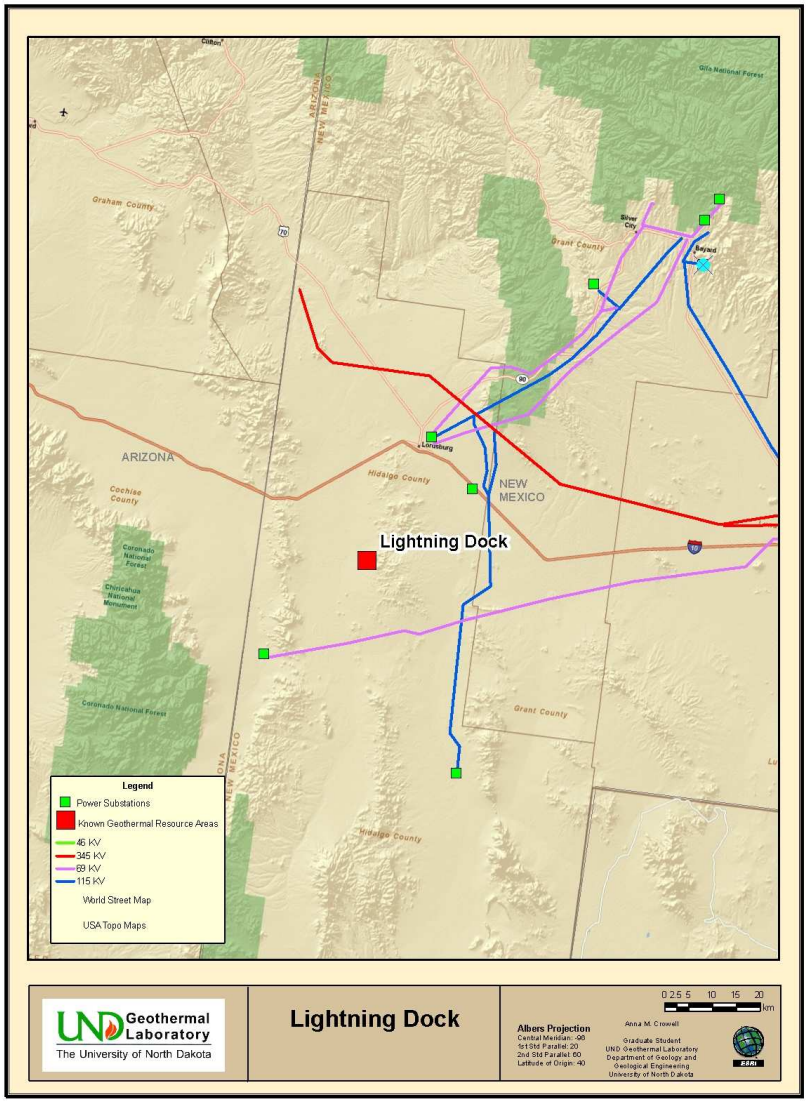


Figure 59. Infrastructure in the Lightning Dock area. (Courtesy of Anna M. Crowell)

# CHAPTER 8

# SUMMARY AND RECOMMENDATIONS

## 8.1. Summary

In recent years, the penetration of renewable energy sources has increased significantly. According to the United States Energy Information Administration (USEIA), the contribution of renewable energy sources has now reached 13% with a target of reaching 25% by 2020. Renewable sources are most commonly utilized as Distributed Generators (DGs). Implementing DGs significantly reduces the distribution system losses and improves voltage regulation, power quality, and the reliability of the power supply. However, improperly planned DGs not only increase the distribution system losses but they can de-stabilize the whole power grid. In this dissertation, several methodologies for DGs integration into distribution systems are presented. The uniqueness of the work presented in this dissertation is highlighted by the implementation of the proposed methods in multi-phase unbalanced distribution networks.

In this dissertation work, the primary objective of optimally allocating renewable DGs in multi-phase unbalanced distribution networks was accomplished through several secondary objectives as follows:

1) Investigate the impact of renewable DGs on power losses and voltage profile of distribution networks.

This objective was accomplished by first using a combination of the particle swarm optimization (PSO) technique and Newton-Raphson load flow method to determine the optimal size and location of distributed generators in balanced distribution networks. After validating the effectiveness of the proposed method in balanced distribution networks, it was then adapted to solve the optimal allocation of DGs in multi-phase unbalanced distribution network. The proposed PSO based method was implemented in MATLAB using EPRI's open source software called OpenDSS in a co-simulation environment to solve the distribution power flow and to find the optimal location and sizing of various types of distributed generators. Results from the proposed method show that if optimally sized DGs are located at their optimal locations, not only is the total power loss in the distribution system reduced significantly but the voltage profile will improve as well.

2) Improve the reliability of distribution systems via the optimal allocation of DGs.

This objective was accomplished by implementing a discrete particle swarm optimization (DPSO) based method to determine the optimal allocation of reclosers and DGs. A new reliability index named composite reliability index (CRI) was proposed by combining the two mostly used reliability indices (SAIFI and SAIDI). The proposed method was validated by comparing the results with those obtained from the ant colony system (ACS) algorithm. The robustness of the proposed method was demonstrated by solving the optimal allocation problem for both balanced and unbalanced distribution networks. Additionally, a customer interruption cost based objective function (ECOST)

for the optimal allocation of reclosers and DGs was developed. Results indicated that simultaneous optimization of reclosers and DGs provides the best system reliability.

3) Reduce the total cost incurred by utilities due to the integration of DGs in the distribution system.

This objective was accomplished by implementing a new cost benefit analysis approach combined with the application of the PSO algorithm in a co-simulation environment of MATLAB and OpenDSS software to estimate the most cost-effective DGs allocation to serve the projected peak demand. The proposed optimization model minimized the total investment cost incurred by utility by implementing various issues including investment cost, OM cost, reliability cost, pollution cost, and cost of purchasing power by utility. The intermittent nature of both DGs and load profiles were also considered in this study. Results indicated that integrating various sources of DGs results in a minimal investment. Also, base load DGs must be integrated to achieve the maximum benefit. Although DGs reduce the total distribution loss and increase the reliability of the distribution system, maximum return on the investment can be achieved when DGs are planned to meet the future load growth.

4) Develop and verify an equivalent circuit model of 1.2 kW PEM fuel cells.

This objective was accomplished by writing a program in MATLAB to determine the number of loops that can effectively characterize the impedance behavior of fuel cell stacks. This program also extracted the initial values of the circuit components which are then used in a Levengberg-Marquardt algorithm for least square curve fitting. An objective function representing the impedance behavior of the PEM fuel cell was developed. Using this objective function and the impedance behaviors of the 1.2kW

Nexa$^{TM}$ PEM fuel cell stack, obtained via EIS technique, an equivalent circuit model was proposed. This model was verified by fitting the curve to the experimentally obtained impedance measurements. Furthermore, the dynamic behavior of the proposed model was compared with the behavior of real fuel cell stack. Results showed that the proposed model behaves much like the real PEM fuel cell stack in similar operating conditions.

5) Model and simulate an electrical interface between geothermal power plants and the electric grid.

This objective was accomplished by designing and implementing an AC-DC-AC converter using a rectifier, IGBT inverter, and voltage regulator. The voltage obtained from the geothermal based power generator was first rectified by a six pulse rectifier bridge. The filtered DC voltage was then applied to an IGBT inverter generating 60 Hz AC voltage which was then connected to the regulated grid. The proposed electrical interface successfully removed the fluctuations in the output current and voltage of the geothermal power plant.

## 8.2. Recommendations for future work

Although the work presented in this dissertation provides promising methods and results for DGs integration in both balanced and unbalanced distribution networks, it can be extended in the following research directions.

- The impact of DGs on distribution system security must be evaluated. Power quality issues like frequency balance, voltage stabilization, and reactive power regulations should be addressed carefully. Appropriate control methods must be adapted to incorporate intermittent sources of renewable energy.

- The impact of DGs on reliability of the distribution systems must be conducted while taking all the economic variables into account. A thorough cost analysis including DG integration cost (capital cost, installation cost, and OM cost) and costs of protective devices must be conducted to better understand the economic impact of integrating DGs on distribution network.
- In this study, DGs were assumed to be 100% available. This assumption is flawed because DGs like wind generators and PV systems are weather and time dependent sources. Therefore, the time-dependent nature of these sources must be incorporated in the study.
- Transient behaviors of DGs which result from their connection to a local grid must be carefully studied. This can be accomplished by using the actual model of DGs rather than treating them as constant power sources. This dissertation proposed an equivalent circuit model of PEM fuel cells which can be connected to the grid to study their complete effects.
- More descriptive and complete models of geothermal power plants must be developed. This will aid in the development of more robust and effective power controllers that can be used as an interface between the geothermal power plants and the electric grid.

# APPENDICES

## Appendix A

## IEEE 69-bus Distribution Test Feeder

Table 42: System and load data for IEEE 69- bus system

| | | Line Impedance in p.u | | Loads on to-bus (p.u) | |
|---|---|---|---|---|---|
| From Bus | To Bus | R (p.u) | X (p.u) | P | Q |
| 1 | 2 | 0.000001 | 0.000001 | 0 | 0 |
| 2 | 3 | 0.000001 | 0.000001 | 0 | 0 |
| 3 | 4 | 0.000001 | 0.000002 | 0 | 0 |
| 4 | 5 | 0.000016 | 0.000018 | 0 | 0 |
| 5 | 6 | 0.000228 | 0.000116 | 0 | 0 |
| 6 | 7 | 0.000238 | 0.000121 | 0.026 | 0.022 |
| 7 | 8 | 0.000058 | 0.000029 | 4.404 | 0.3 |
| 8 | 9 | 0.000031 | 0.000169 | 0.75 | 0.54 |
| 9 | 10 | 0.000511 | 0.000039 | 0.3 | 0.22 |
| 10 | 11 | 0.000117 | 0.000147 | 0.28 | 0.19 |
| 11 | 12 | 0.000444 | 0.000212 | 1.45 | 1.04 |
| 12 | 13 | 0.000643 | 0.000215 | 1.45 | 1.04 |
| 13 | 14 | 0.000651 | 0.000218 | 0.08 | 0.055 |
| 14 | 15 | 0.00066 | 0.000041 | 0.08 | 0.055 |
| 15 | 16 | 0.000123 | 0.000077 | 0 | 0 |
| 16 | 17 | 0.000234 | 0.000001 | 0.455 | 0.3 |
| 17 | 18 | 0.000003 | 0.000068 | 0.6 | 0.35 |
| 18 | 19 | 0.000204 | 0.000043 | 0.6 | 0.35 |
| 19 | 20 | 0.000131 | 0.00007 | 0 | 0 |
| 20 | 21 | 0.000213 | 0.000003 | 0.01 | 0.006 |
| 21 | 22 | 0.000009 | 0.000033 | 1.14 | 0.81 |
| 22 | 23 | 0.000099 | 0.000071 | 0.053 | 0.035 |
| 23 | 24 | 0.000216 | 0.000154 | 0 | 0 |
| 24 | 25 | 0.000467 | 0.000064 | 0.28 | 0.2 |
| 25 | 26 | 0.000193 | 0.000036 | 0 | 0 |
| 26 | 27 | 0.000108 | 0.000007 | 0.14 | 0.1 |
| 3 | 28 | 0.000003 | 0.000098 | 0.14 | 0.1 |
| 28 | 29 | 0.00004 | 0.000082 | 0.26 | 0.186 |
| 29 | 30 | 0.000248 | 0.000014 | 0.26 | 0.186 |
| 30 | 31 | 0.000044 | 0.000072 | 0 | 0 |
| 31 | 32 | 0.000219 | 0.000176 | 0 | 0 |
| 32 | 33 | 0.000523 | 0.000352 | 0 | 0 |
| 33 | 34 | 0.001066 | 0.000064 | 0.14 | 0.1 |

Table 43. System and load data of IEEE 69-bus system (continued from Table 42)

| | | Line Impedance in p.u | | Loads on to-bus (p.u) | |
|---|---|---|---|---|---|
| From Bus | To Bus | R (p.u) | X (p.u) | P | Q |
| 4 | 36 | 0.000002 | 0.000005 | 0.06 | 0.04 |
| 36 | 37 | 0.000053 | 0.00013 | 0 | 0 |
| 37 | 38 | 0.000181 | 0.000442 | 0.79 | 0.564 |
| 38 | 39 | 0.000051 | 0.000125 | 0.79 | 0.564 |
| 8 | 40 | 0.000058 | 0.00003 | 3.847 | 2.745 |
| 40 | 41 | 0.000207 | 0.00007 | 3.847 | 2.745 |
| 9 | 42 | 0.000109 | 0.000055 | 0.036 | 0.027 |
| 42 | 43 | 0.000127 | 0.000065 | 0.0435 | 0.035 |
| 43 | 44 | 0.000177 | 0.00009 | 0.264 | 0.19 |
| 44 | 45 | 0.000176 | 0.0000089 | 0.24 | 0.172 |
| 45 | 46 | 0.000992 | 0.000333 | 0 | 0 |
| 46 | 47 | 0.000489 | 0.000164 | 0 | 0 |
| 47 | 48 | 0.00019 | 0.000063 | 0 | 0 |
| 48 | 49 | 0.000241 | 0.000073 | 1 | 0.72 |
| 49 | 50 | 0.000317 | 0.000161 | 0 | 0 |
| 50 | 51 | 0.000061 | 0.000031 | 12.44 | 8.88 |
| 51 | 52 | 0.00009 | 0.00046 | 0.32 | 0.23 |
| 52 | 53 | 0.000443 | 0.000226 | 0 | 0 |
| 53 | 54 | 0.00065 | 0.000331 | 2.27 | 1.62 |
| 11 | 55 | 0.000126 | 0.000038 | 0.59 | 0.42 |
| 55 | 56 | 0.000003 | 0.000001 | 0.18 | 0.13 |
| 12 | 57 | 0.000461 | 0.000152 | 0.18 | 0.13 |
| 57 | 58 | 0.000003 | 0.000001 | 0.28 | 0.2 |
| 3 | 59 | 0.000003 | 0.000007 | 0.28 | 0.2 |
| 59 | 60 | 0.00004 | 0.000098 | 0.26 | 0.1855 |
| 60 | 61 | 0.000066 | 0.000077 | 0.26 | 0.1855 |
| 61 | 62 | 0.000019 | 0.000022 | 0 | 0 |
| 62 | 63 | 0.000001 | 0.000001 | 0.24 | 0.171 |
| 63 | 64 | 0.000454 | 0.000531 | 0.24 | 0.17 |
| 64 | 65 | 0.000193 | 0.000226 | 0.012 | 0.01 |
| 65 | 66 | 0.000026 | 0.00003 | 0 | 0 |
| 66 | 67 | 0.000006 | 0.000007 | 0.06 | 0.043 |
| 67 | 68 | 0.000068 | 0.000086 | 0 | 0 |
| 68 | 69 | 0.000001 | 0.000001 | 0.3922 | 0.263 |

## Appendix B

## IEEE 90-bus Distribution Test Feeder

Table 44. Parameters of IEEE 90-bus distribution test feeder

| Sending Node | Receiving Node | r (p.u) | X (p.u) | Length (miles) | Receiving Node P (kW) | Receiving Node Q(KVAr) | Receiving Node customers |
|---|---|---|---|---|---|---|---|
| 1 | 2 | 0.00031 | 0.00075 | 0.010 | 0 | 0 | 0 |
| 0 | 1 | 0.00031 | 0.00075 | 0.010 | 0 | 0 | 0 |
| 2 | 3 | 0.00094 | 0.00225 | 0.010 | 0 | 0 | 0 |
| 2 | 27 | 0.00275 | 0.00674 | 0.030 | 26 | 11.16 | 5 |
| 2 | 27e | 0.00275 | 0.00674 | 0.030 | 26 | 11.13 | 5 |
| 3 | 4 | 0.01566 | 0.01834 | 0.160 | 0 | 0 | 0 |
| 3 | 35 | 0.00212 | 0.00524 | 0.020 | 414.67 | 177.6 | 55 |
| 4 | 5 | 0.22863 | 0.11630 | 2.280 | 2.6 | 1.32 | 1 |
| 5 | 6 | 0.23778 | 0.12110 | 2.380 | 40.4 | 18 | 8 |
| 6 | 7 | 0.05753 | 0.02932 | 0.580 | 75 | 32.4 | 3 |
| 7 | 8 | 0.03076 | 0.01566 | 0.310 | 30 | 13.2 | 2 |
| 7 | 40 | 0.05790 | 0.02951 | 0.580 | 40.5 | 16.98 | 8 |
| 8 | 9 | 0.51099 | 0.16890 | 5.110 | 28 | 11.4 | 5 |
| 8 | 42 | 0.10856 | 0.05528 | 1.090 | 4.35 | 2.1 | 1 |
| 9 | 10 | 0.11680 | 0.03862 | 1.170 | 145 | 62.4 | 26 |
| 10 | 11 | 0.44386 | 0.14668 | 4.440 | 145 | 62.4 | 16 |
| 10 | 55 | 0.12553 | 0.03812 | 1.260 | 18 | 7.8 | 1 |
| 11 | 12 | 0.64264 | 0.21213 | 6.430 | 8 | 3.3 | 1 |
| 11 | 57 | 0.46133 | 0.15249 | 4.610 | 28 | 12 | 1 |
| 12 | 13 | 0.65138 | 0.21525 | 6.510 | 8 | 3.3 | 1 |
| 13 | 14 | 0.66011 | 0.21812 | 6.600 | 0 | 0 | 0 |
| 14 | 15 | 0.12266 | 0.04056 | 1.230 | 45.5 | 18 | 1 |
| 15 | 16 | 0.23360 | 0.07724 | 2.340 | 60 | 21 | 5 |
| 16 | 17 | 0.00293 | 0.00100 | 0.030 | 60 | 21 | 1 |
| 17 | 18 | 0.20440 | 0.06575 | 2.040 | 0 | 0 | 0 |
| 18 | 19 | 0.13140 | 0.04343 | 1.310 | 1 | 0.36 | 0 |
| 19 | 20 | 0.21313 | 0.07044 | 2.130 | 114 | 48.6 | 3 |
| 20 | 21 | 0.00873 | 0.00287 | 0.090 | 5.3 | 2.1 | 0 |
| 21 | 22 | 0.09927 | 0.03282 | 0.99 | 0 | 0 | 0 |
| 22 | 23 | 0.21607 | 0.07144 | 2.160 | 28 | 12 | 5 |
| 23 | 24 | 0.46720 | 0.15442 | 4.670 | 0 | 0 | 0 |
| 24 | 25 | 0.19273 | 0.06370 | 1.930 | 14 | 6 | 0 |
| 25 | 26 | 0.10806 | 0.03569 | 1.080 | 14 | 6 | 1 |
| 27 | 28 | 0.03993 | 0.09764 | 0.400 | 2 | 11.16 | 1 |
| 28 | 29 | 0.24820 | 0.08205 | 2.480 | 0 | 0 | 0 |

Table 45. Parameters of IEEE 90-bus distribution test feeder (continued from Table 42).

| Sending Node | Receiving Node | r (p.u) | X (p.u) | Length (miles) | Receiving Node P (kW) | Receiving Node Q(KVAr) | Receiving Node customers |
|---|---|---|---|---|---|---|---|
| 29 | 30 | 0.04380 | 0.01448 | 0.440 | 414.67 | 177.6 | 78 |
| 30 | 31 | 0.21900 | 0.07238 | 2.190 | 0 | 0 | 0 |
| 31 | 32 | 0.52347 | 0.17570 | 5.230 | 14 | 6 | 3 |
| 32 | 33 | 1.06566 | 0.35227 | 10.660 | 19.5 | 8.4 | 3 |
| 33 | 34 | 0.91967 | 0.30404 | 9.200 | 6 | 2.4 | 1 |
| 35 | 36 | 0.05310 | 0.12996 | 0.530 | 79 | 33.84 | 8 |
| 36 | 37 | 0.18081 | 0.44243 | 1.810 | 384.7 | 164.7 | 18 |
| 37 | 38 | 0.05129 | 0.12547 | 0.510 | 384.7 | 164.7 | 78 |
| 40 | 41 | 0.20708 | 0.06951 | 2.070 | 3.6 | 1.62 | 1 |
| 42 | 43 | 0.12666 | 0.06451 | 1.270 | 26.4 | 11.4 | 4 |
| 43 | 44 | 0.17732 | 0.09028 | 1.770 | 24 | 10.32 | 1 |
| 44 | 45 | 0.17551 | 0.08941 | 1.760 | 0 | 0 | 0 |
| 45 | 46 | 0.99204 | 0.33299 | 9.920 | 0 | 0 | 0 |
| 46 | 47 | 0.48897 | 0.16409 | 4.890 | 0 | 0 | 0 |
| 47 | 18 | 0.18980 | 0.06277 | 1.900 | 100 | 43.2 | 8 |
| 48 | 49 | 0.24090 | 0.07312 | 2.410 | 0 | 0 | 0 |
| 49 | 50 | 0.31664 | 0.16128 | 3.170 | 414.67 | 177.6 | 107 |
| 50 | 51 | 0.06077 | 0.03095 | 0.610 | 32 | 13.8 | 2 |
| 51 | 52 | 0.09047 | 0.04605 | 0.900 | 0 | 0 | 0 |
| 52 | 53 | 0.44330 | 0.22580 | 4.430 | 227 | 37.2 | 62 |
| 53 | 54 | 0.64951 | 0.33081 | 6.500 | 59 | 25.2 | 4 |
| 55 | 56 | 0.00293 | 0.00087 | 0.030 | 18 | 7.8 | 0 |
| 57 | 58 | 0.00293 | 0.00100 | 0.030 | 28 | 12 | 5 |
| 65 | 66 | 0.01897 | 0.02215 | 0.190 | 24 | 10.2 | 6 |
| 28e | 65 | 0.06570 | 0.07674 | 0.660 | 0 | 0 | 0 |
| 66 | 67 | 0.00112 | 0.00131 | 0.010 | 24 | 10.2 | 1 |
| 67 | 68 | 0.45440 | 0.53090 | 4.540 | 1.2 | 0.6 | 0 |
| 68 | 69 | 0.19342 | 0.22605 | 1.930 | 0 | 0 | 0 |
| 69 | 70 | 0.02558 | 0.02982 | 0.260 | 6 | 2.58 | 1 |
| 70 | 88 | 0.00574 | 0.00724 | 0.060 | 0 | 0 | 0 |
| 88 | 89 | 0.06795 | 0.08566 | 0.680 | 39.22 | 15.78 | 4 |
| 89 | 90 | 0.00056 | 0.00075 | 0.010 | 39.22 | 15.78 | 4 |
| 27e | 28e | 0.03993 | 0.09764 | 0.400 | 26 | 11.13 | 1 |
| 48 | 88 | 0.04492 | 0.10985 | 0.450 | 0 | 0 | 0 |

## Appendix C

## IEEE 123 Node Test Feeder

Table 46. Overhead Line Configurations (Config.)

| Config. | Phasing | Phase Cond. | Neutral Cond. | Spacing |
|---|---|---|---|---|
| | | ACSR | ACSR | ID |
| 1 | A B C N | 336,400 26/7 | 4/0 6/1 | 500 |
| 2 | C A B N | 336,400 26/7 | 4/0 6/1 | 500 |
| 3 | B C A N | 336,400 26/7 | 4/0 6/1 | 500 |
| 4 | C B A N | 336,400 26/7 | 4/0 6/1 | 500 |
| 5 | B A C N | 336,400 26/7 | 4/0 6/1 | 500 |
| 6 | A C B N | 336,400 26/7 | 4/0 6/1 | 500 |
| 7 | A C N | 336,400 26/7 | 4/0 6/1 | 505 |
| 8 | A B N | 336,400 26/7 | 4/0 6/1 | 505 |
| 9 | A N | 1/0 | 1/0 | 510 |
| 10 | B N | 1/0 | 1/0 | 510 |
| 11 | C N | 1/0 | 1/0 | 510 |

Table 47. Underground Line Configuration (Config.)

| Config. | Phasing | Cable | Spacing ID |
|---|---|---|---|
| 12 | A B C | 1/0 AA, CN | 515 |

Table 48. Transformer Data

| | kVA | kV-high | kV-low | R - % | X - % |
|---|---|---|---|---|---|
| Substation | 5,000 | 115 - D | 4.16 Gr-W | 1 | 8 |
| XFM - 1 | 150 | 4.16 - D | .480 - D | 1.27 | 2.72 |

Table 49. Line Segment Data

| Node A | Node B | Length (ft.) | Config. | Node A | Node B | Length (ft.) | Config. |
|---|---|---|---|---|---|---|---|
| 1 | 2 | 175 | 10 | 42 | 43 | 500 | 10 |
| 1 | 3 | 250 | 11 | 42 | 44 | 200 | 1 |
| 1 | 7 | 300 | 1 | 44 | 45 | 200 | 9 |
| 3 | 4 | 200 | 11 | 44 | 47 | 250 | 1 |
| 3 | 5 | 325 | 11 | 45 | 46 | 300 | 9 |
| 5 | 6 | 250 | 11 | 47 | 48 | 150 | 4 |
| 7 | 8 | 200 | 1 | 47 | 49 | 250 | 4 |
| 8 | 12 | 225 | 10 | 49 | 50 | 250 | 4 |
| 8 | 9 | 225 | 9 | 50 | 51 | 250 | 4 |
| 8 | 13 | 300 | 1 | 51 | 151 | 500 | 4 |
| 9 | 14 | 425 | 9 | 52 | 53 | 200 | 1 |
| 13 | 34 | 150 | 11 | 53 | 54 | 125 | 1 |
| 13 | 18 | 825 | 2 | 54 | 55 | 275 | 1 |
| 14 | 11 | 250 | 9 | 54 | 57 | 350 | 3 |
| 14 | 10 | 250 | 9 | 55 | 56 | 275 | 1 |
| 15 | 16 | 375 | 11 | 57 | 58 | 250 | 10 |
| 15 | 17 | 350 | 11 | 57 | 60 | 750 | 3 |
| 18 | 19 | 250 | 9 | 58 | 59 | 250 | 10 |
| 18 | 21 | 300 | 2 | 60 | 61 | 550 | 5 |
| 19 | 20 | 325 | 9 | 60 | 62 | 250 | 12 |
| 21 | 22 | 525 | 10 | 62 | 63 | 175 | 12 |
| 21 | 23 | 250 | 2 | 63 | 64 | 350 | 12 |
| 23 | 24 | 550 | 11 | 64 | 65 | 425 | 12 |
| 23 | 25 | 275 | 2 | 65 | 66 | 325 | 12 |
| 25 | 26 | 350 | 7 | 67 | 68 | 200 | 9 |
| 25 | 28 | 200 | 2 | 67 | 72 | 275 | 3 |
| 26 | 27 | 275 | 7 | 67 | 97 | 250 | 3 |
| 26 | 31 | 225 | 11 | 68 | 69 | 275 | 9 |
| 27 | 33 | 500 | 9 | 69 | 70 | 325 | 9 |
| 28 | 29 | 300 | 2 | 70 | 71 | 275 | 9 |
| 29 | 30 | 350 | 2 | 72 | 73 | 275 | 11 |
| 30 | 250 | 200 | 2 | 72 | 76 | 200 | 3 |
| 31 | 32 | 300 | 11 | 73 | 74 | 350 | 11 |
| 34 | 15 | 100 | 11 | 74 | 75 | 400 | 11 |
| 35 | 36 | 650 | 8 | 76 | 77 | 400 | 6 |
| 35 | 40 | 250 | 1 | 76 | 86 | 700 | 3 |
| 36 | 37 | 300 | 9 | 77 | 78 | 100 | 6 |
| 36 | 38 | 250 | 10 | 78 | 79 | 225 | 6 |
| 38 | 39 | 325 | 10 | 78 | 80 | 475 | 6 |
| 40 | 41 | 325 | 11 | 80 | 81 | 475 | 6 |
| 40 | 42 | 250 | 1 | 81 | 82 | 250 | 6 |

Table 50: Line Segment data (continued from table 47)

| Node A | Node B | Length (ft.) | Config. | Node A | Node B | Length (ft.) | Config. |
|---|---|---|---|---|---|---|---|
| 81 | 84 | 675 | 11 | 101 | 105 | 275 | 3 |
| 82 | 83 | 250 | 6 | 102 | 103 | 325 | 11 |
| 84 | 85 | 475 | 11 | 103 | 104 | 700 | 11 |
| 86 | 87 | 450 | 6 | 105 | 106 | 225 | 10 |
| 87 | 88 | 175 | 9 | 105 | 108 | 325 | 3 |
| 87 | 89 | 275 | 6 | 106 | 107 | 575 | 10 |
| 89 | 90 | 225 | 10 | 108 | 109 | 450 | 9 |
| 89 | 91 | 225 | 6 | 108 | 300 | 1000 | 3 |
| 91 | 92 | 300 | 11 | 109 | 110 | 300 | 9 |
| 91 | 93 | 225 | 6 | 110 | 111 | 575 | 9 |
| 93 | 94 | 275 | 9 | 110 | 112 | 125 | 9 |
| 93 | 95 | 300 | 6 | 112 | 113 | 525 | 9 |
| 95 | 96 | 200 | 10 | 113 | 114 | 325 | 9 |
| 97 | 98 | 275 | 3 | 135 | 35 | 375 | 4 |
| 98 | 99 | 550 | 3 | 149 | 1 | 400 | 1 |
| 99 | 100 | 300 | 3 | 152 | 52 | 400 | 1 |
| 100 | 450 | 800 | 3 | 160 | 67 | 350 | 6 |
| 101 | 102 | 225 | 11 | 197 | 101 | 250 | 3 |

Table 51. Shunt Capacitor Data

| Node | Ph-A | Ph-B | Ph-C |
|---|---|---|---|
| | kVAr | kVAr | kVAr |
| 83 | 200 | 200 | 200 |
| 88 | 50 | | |
| 90 | | 50 | |
| 92 | | | 50 |
| Total | 250 | 250 | 250 |

Table 52. Three Phase Switch Data

| Node A | Node B | Normal | Node A | Node B | Normal |
|---|---|---|---|---|---|
| 13 | 152 | closed | 250 | 251 | open |
| 18 | 135 | closed | 450 | 451 | open |
| 60 | 160 | closed | 54 | 94 | open |
| 61 | 610 | closed | 151 | 300 | open |
| 97 | 197 | closed | 300 | 350 | open |
| 150 | 149 | closed | | | |

Table 53. Regulator Data

| | | | | | |
|---|---|---|---|---|---|
| Regulator ID: | 1 | Regulator ID: | 3 | | |
| Line Segment: | 150 - 149 | Line Segment: | 25 - 26 | | |
| Location: | 150 | Location: | 25 | | |
| Phases: | A-B-C | Phases: | A-C | | |
| Connection: | 3-Ph, Wye | Connection: | 2-Ph,L-G | | |
| Monitoring Phase: | A | Monitoring Phase: | A & C | | |
| Bandwidth: | 2.0 volts | Bandwidth: | 1 | | |
| PT Ratio: | 20 | PT Ratio: | 20 | | |
| Primary CT Rating: | 700 | Primary CT Rating: | 50 | | |
| Compensator: | Ph-A | Compenator: | Ph-A | Ph-C | |
| R - Setting: | 3 | R - Setting: | 0.4 | 0.4 | |
| X - Setting: | 7.5 | X - Setting: | 0.4 | 0.4 | |
| Voltage Level: | 120 | Voltage Level: | 120 | 120 | |
| | | | | | |
| Regulator ID: | 2 | Regulator ID: | 4 | | |
| Line Segment: | 9 - 14 | Line Segment: | 160 - 67 | | |
| Location: | 9 | Location: | 160 | | |
| Phases: | A | Phases: | A-B-C | | |
| Connection: | 1-Ph, L-G | Connection: | 3-Ph, LG | | |
| Monitoring Phase: | A | Monitoring Phase: | A-B-C | | |
| Bandwidth: | 2.0 volts | Bandwidth: | 2 | | |
| PT Ratio: | 20 | PT Ratio: | 20 | | |
| Primary CT Rating: | 50 | Primary CT Rating: | 300 | | |
| Compensator: | Ph-A | Compensator: | Ph-A | Ph-B | Ph-C |
| R - Setting: | 0.4 | R - Setting: | 0.6 | 1.4 | 0.2 |
| X - Setting: | 0.4 | X - Setting: | 1.3 | 2.6 | 1.4 |
| Voltage Level: | 120 | Voltage Level: | 124 | 124 | 124 |

Table 54. Spot Load Data

| Node | Load Model | Ph A (kW) | Ph A (KVAr) | Ph B (kW) | Ph B (KVAr) | Ph C (kW) | Ph C (KVAr) |
|---|---|---|---|---|---|---|---|
| 1 | Y-PQ | 40 | 20 | 0 | 0 | 0 | 0 |
| 2 | Y-PQ | 0 | 0 | 20 | 10 | 0 | 0 |
| 4 | Y-PR | 0 | 0 | 0 | 0 | 40 | 20 |
| 5 | Y-I | 0 | 0 | 0 | 0 | 20 | 10 |
| 6 | Y-Z | 0 | 0 | 0 | 0 | 40 | 20 |
| 7 | Y-PQ | 20 | 10 | 0 | 0 | 0 | 0 |
| 9 | Y-PQ | 40 | 20 | 0 | 0 | 0 | 0 |
| 10 | Y-I | 20 | 10 | 0 | 0 | 0 | 0 |
| 11 | Y-Z | 40 | 20 | 0 | 0 | 0 | 0 |
| 12 | Y-PQ | 0 | 0 | 20 | 10 | 0 | 0 |
| 16 | Y-PQ | 0 | 0 | 0 | 0 | 40 | 20 |
| 17 | Y-PQ | 0 | 0 | 0 | 0 | 20 | 10 |
| 19 | Y-PQ | 40 | 20 | 0 | 0 | 0 | 0 |
| 20 | Y-I | 40 | 20 | 0 | 0 | 0 | 0 |
| 22 | Y-Z | 0 | 0 | 40 | 20 | 0 | 0 |
| 24 | Y-PQ | 0 | 0 | 0 | 0 | 40 | 20 |
| 28 | Y-I | 40 | 20 | 0 | 0 | 0 | 0 |
| 29 | Y-Z | 40 | 20 | 0 | 0 | 0 | 0 |
| 30 | Y-PQ | 0 | 0 | 0 | 0 | 40 | 20 |
| 31 | Y-PQ | 0 | 0 | 0 | 0 | 20 | 10 |
| 32 | Y-PQ | 0 | 0 | 0 | 0 | 20 | 10 |
| 33 | Y-I | 40 | 20 | 0 | 0 | 0 | 0 |
| 34 | Y-Z | 0 | 0 | 0 | 0 | 40 | 20 |
| 35 | D-PQ | 40 | 20 | 0 | 0 | 0 | 0 |
| 37 | Y-Z | 40 | 20 | 0 | 0 | 0 | 0 |
| 38 | Y-I | 0 | 0 | 20 | 10 | 0 | 0 |
| 39 | Y-PQ | 0 | 0 | 20 | 10 | 0 | 0 |
| 41 | Y-PQ | 0 | 0 | 0 | 0 | 20 | 10 |
| 42 | Y-PQ | 20 | 10 | 0 | 0 | 0 | 0 |
| 43 | Y-Z | 0 | 0 | 40 | 20 | 0 | 0 |
| 45 | Y-I | 20 | 10 | 0 | 0 | 0 | 0 |
| 46 | Y-PQ | 20 | 10 | 0 | 0 | 0 | 0 |
| 47 | Y-I | 35 | 25 | 35 | 25 | 35 | 25 |
| 48 | Y-Z | 70 | 50 | 70 | 50 | 70 | 50 |
| 49 | Y-PQ | 35 | 25 | 70 | 50 | 35 | 20 |
| 50 | Y-PQ | 0 | 0 | 0 | 0 | 40 | 20 |
| 51 | Y-PQ | 20 | 10 | 0 | 0 | 0 | 0 |
| 52 | Y-PQ | 40 | 20 | 0 | 0 | 0 | 0 |
| 53 | Y-PQ | 40 | 20 | 0 | 0 | 0 | 0 |
| 55 | Y-Z | 20 | 10 | 0 | 0 | 0 | 0 |
| 56 | Y-PQ | 0 | 0 | 20 | 10 | 0 | 0 |

Table 55. Spot Load Data ( Continued from table 52)

| Node | Load Model | Ph A (kW) | Ph A (KVAr) | Ph B (kW) | Ph B (KVAr) | Ph C (kW) | Ph C (KVAr) |
|---|---|---|---|---|---|---|---|
| 58 | Y-I | 0 | 0 | 20 | 10 | 0 | 0 |
| 59 | Y-PQ | 0 | 0 | 20 | 10 | 0 | 0 |
| 60 | Y-PQ | 20 | 10 | 0 | 0 | 0 | 0 |
| 62 | Y-Z | 0 | 0 | 0 | 0 | 40 | 20 |
| 63 | Y-PQ | 40 | 20 | 0 | 0 | 0 | 0 |
| 64 | Y-I | 0 | 0 | 75 | 35 | 0 | 0 |
| 65 | D-Z | 35 | 25 | 35 | 25 | 70 | 50 |
| 66 | Y-PQ | 0 | 0 | 0 | 0 | 75 | 35 |
| 68 | Y-PQ | 20 | 10 | 0 | 0 | 0 | 0 |
| 69 | Y-PQ | 40 | 20 | 0 | 0 | 0 | 0 |
| 70 | Y-PQ | 20 | 10 | 0 | 0 | 0 | 0 |
| 71 | Y-PQ | 40 | 20 | 0 | 0 | 0 | 0 |
| 73 | Y-PQ | 0 | 0 | 0 | 0 | 40 | 20 |
| 74 | Y-Z | 0 | 0 | 0 | 0 | 40 | 20 |
| 75 | Y-PQ | 0 | 0 | 0 | 0 | 40 | 20 |
| 76 | D-I | 105 | 80 | 70 | 50 | 70 | 50 |
| 77 | Y-PQ | 0 | 0 | 40 | 20 | 0 | 0 |
| 79 | Y-Z | 40 | 20 | 0 | 0 | 0 | 0 |
| 80 | Y-PQ | 0 | 0 | 40 | 20 | 0 | 0 |
| 82 | Y-PQ | 40 | 20 | 0 | 0 | 0 | 0 |
| 83 | Y-PQ | 0 | 0 | 0 | 0 | 20 | 10 |
| 84 | Y-PQ | 0 | 0 | 0 | 0 | 20 | 10 |
| 85 | Y-PQ | 0 | 0 | 0 | 0 | 40 | 20 |
| 86 | Y-PQ | 0 | 0 | 20 | 10 | 0 | 0 |
| 87 | Y-PQ | 0 | 0 | 40 | 20 | 0 | 0 |
| 88 | Y-PQ | 40 | 20 | 0 | 0 | 0 | 0 |
| 90 | Y-I | 0 | 0 | 40 | 20 | 0 | 0 |
| 92 | Y-PQ | 0 | 0 | 0 | 0 | 40 | 20 |
| 94 | Y-PQ | 40 | 20 | 0 | 0 | 0 | 0 |
| 95 | Y-PQ | 0 | 0 | 20 | 10 | 0 | 0 |
| 96 | Y-PQ | 0 | 0 | 20 | 10 | 0 | 0 |
| 98 | Y-PQ | 40 | 20 | 0 | 0 | 0 | 0 |
| 99 | Y-PQ | 0 | 0 | 40 | 20 | 0 | 0 |
| 100 | Y-Z | 0 | 0 | 0 | 0 | 40 | 20 |
| 102 | Y-PQ | 0 | 0 | 0 | 0 | 20 | 10 |
| 103 | Y-PQ | 0 | 0 | 0 | 0 | 40 | 20 |
| 104 | Y-PQ | 0 | 0 | 0 | 0 | 40 | 20 |
| 106 | Y-PQ | 0 | 0 | 40 | 20 | 0 | 0 |
| 107 | Y-PQ | 0 | 0 | 40 | 20 | 0 | 0 |
| 109 | Y-PQ | 40 | 20 | 0 | 0 | 0 | 0 |
| 111 | Y-PQ | 20 | 10 | 0 | 0 | 0 | 0 |

Table 56. Spot Load Data (Continued from Table 53)

| Node | Load Model | Ph A (kW) | Ph A (KVAr) | Ph B (kW) | Ph B (KVAr) | Ph C (kW) | Ph C (KVAr) |
|---|---|---|---|---|---|---|---|
| 112 | Y-I | 20 | 10 | 0 | 0 | 0 | 0 |
| 113 | Y-Z | 40 | 20 | 0 | 0 | 0 | 0 |
| 114 | Y-PQ | 20 | 10 | 0 | 0 | 0 | 0 |
| Total | | 1420 | 775 | 915 | 515 | 1155 | 630 |

## Appendix D

## Snippets of Matlab and OpenDSS codes

Matlab Files

***Particle Swarm Optimization***

```
function opts = getDefaultOptions
opts.npart         = 200;
opts.niter         = 100;
opts.cbi           = 2.5;
opts.cbf           = 0.5;
opts.cgi           = 0.5;
opts.cgf           = 2.5;
opts.wi            = 0.9;
opts.wf            = 0.4;
opts.vmax          = Inf;
opts.vmaxscale     = 4;
  opts.tol         = 1e-6;


function [x, fval, exitflag, output] = pso(objfunc, nvars, options)


msg = nargchk(1, 3, nargin);
if ~isempty(msg)
   error('mrr:myoptim:pso:pso:narginerr', 'Inadequate number of input arguments.');
end

msg = nargchk(0, 4, nargout);
if ~isempty(msg)
   error('mrr:myoptim:pso:pso:nargouterr', 'Inadequate number of output arguments.');
end


if nargin==1 && ischar(objfunc) && strcmp(objfunc, 'options')
   % User desired only to access the default OPTIONS structure.
   if nargout<=1
      x = getDefaultOptions();
   else
      % The user required multiple outputs, yet only default options can be returned.
      error('mrr:myoptim:pso:pso:nargouterr', ...
         'Cannot expext more than one output when only OPTIONS are required.');
   end
else
```

```
    % If no options are specified, use the default ones.
    if nargin<3, options=getDefaultOptions(); end

    % Determination of output level, that is of amount of data to be collected in OUTPUT
structure.
    if nargout == 4
        if strcmp(options.output_level, 'none')
            if options.plot == 0
                output_level = 0;
            else
                output_level = 1;
            end
        elseif strcmp(options.output_level, 'low')
            output_level = 1;
        elseif strcmp(options.output_level, 'medium')
            output_level = 2;
        elseif strcmp(options.output_level, 'high')
            output_level = 3;
        else
            error('mrr:myoptim:pso:pso:optionserr:output_level', ...
                'Invalid value of the OUTPUT_LEVEL options specified.');
        end
    else

        if options.plot == 1
            output_level = 1;
        else
            output_level = 0;
        end
    end


    if ~all(isnan(options.vmax))

        if any(isnan(options.vmax))
            error('mrr:myoptim:pso:pso:optionserr:vmax', ...
                'VMAX option cannot have some Inf and some numerical (or Inf) values.');
        end

        if ~isnan(options.vmaxscale)
            warning('mrr:myoptim:pso:pso:optionserr:vmaxconflict', ...
                'Both relative and absolute velocity limit are specified. The relative limit is
ignored.');
        end
        if length(options.vmax) == 1
            vmax = options.vmax*ones(nvars, 1);
```

```
        elseif length(options.vmax) == nvars
            % Maximal velocity should be a column-vector or a scalar.
            if size(options.vmax, 1) ~= length(options.vmax)
                error('mrr:myopim:pso:pso:optionserr:vmax', ...
                    'VMAX option should be specified as column-vector, or as a scalar value.');
            end
            vmax = options.vmax;
        else
            error('mrr:myoptim:pso:pso:optionserr:vmax', ...
                'Inadequate dimension of VMAX option. Should be a scalar, or a column
vector with NVARS elements.');
        end
    else

        if isnan(options.vmaxscale)
            error('mrr:myoptim:pso:pso:optionserr:vmaxscale', ...
                'Either VMAX or VMAXSCALE options should be different than NaN.');
        end
        if length(options.vmaxscale) == 1
            if length(options.initspan) == 1
                vmax = options.vmaxscale*options.initspan*ones(nvars, 1);
            else
                vmax = options.vmaxscale*options.initspan;
            end
        else
            error('mrr:myoptim:pso:pso:optionserr:vmax', ...
                'Inadequate dimension of VMAXSCALE option. Must be a scalar.');
        end
    end
    vmax = repmat(vmax', options.npart, 1);

    % Initial population.
ITPOPULATION option is specified, both INITOFFSET and
    % INITSPAN options are ignored.
    if ~isnan(options.initpopulation)
        [pno, pdim] = size(options.initpopulation);
        if (pno ~= options.npart) || (pdim ~= nvars)
            error
                ['The format of initial population is inconsistent with desired population', ...
                 'size or dimension of search space - INITPOPULATION options is invalid']);
        end
        X = options.initpopulation;
    elseif (length(options.initoffset) == 1) && (length(options.initspan) == 1)
        % The same offset and span is specified for each dimension of the search space
        X = (rand(options.npart, nvars)-0.5)*2*options.initspan + options.initoffset;
    elseif (length(options.initoffset) ~= size(options.initoffset, 1)) || ...
```

```
        (length(options.initspan) ~= size(options.initspan, 1))
      error('mrr:myoptim:pso:pso:optionserr:initoffset_initspan', ...
        'Both INITOFFSET and INITSPAN options must be either scalars or column-
vectors.');
   elseif (length(options.initoffset) ~= nvars) || (length(options.initspan) ~= nvars)
      error('mrr:myoptim:pso:pso:optionserr:init', ...
        'Both INITOFFSET and INITSPAN options must be scalars or column-vectors of
length NVARS.');
   else
      initoffset = repmat(options.initoffset', options.npart, 1);
      initspan   = repmat(options.initspan', options.npart, 1);
      X = (rand(options.npart, nvars)-0.5)*2.*initspan + initoffset;


.
      if (options.trustoffset)
        X(1, :) = options.initoffset';
      end
   end

   % Initial velocities.
   % Velocities are initialized uniformly in [-VSPANINIT, VSPANINIT].
   if any(isnan(options.vspaninit))
      error('mrr:myoptim:pso:pso:optionserr:vspaninit', ...
           'VSPANINIT option must not contain NaN entries.');
   elseif isscalar(options.vspaninit)
      V = (rand(options.npart, nvars)-0.5)*2*options.vspaninit;
   else
      if (length(options.vspaninit) ~= size(options.vspaninit, 1)) || ...
        (length(options.vspaninit) ~= nvars)
         error('mrr:myoptim:pso:pso:optionserr:vspaninit', ...
           'VSPANINIT option must be either scalar or column-vector of length
NVARS');
      end
      V = (rand(options.npart, nvars)-0.5)*2.*repmat(options.vspaninit', options.npart, 1);
   end

   % Initial scores (objective values).
   % Initialization of the best personal score and position, as well as global best score and
   % position.
   Y = calcobjfunc(objfunc, X);
   Ybest = Y;                  % The best individual score for each particle - initialization.
   Xbest = X;                  % The best individual position for each particle -
                               % initialization.
   [GYbest, gbest] = min(Ybest);   % GYbest is the best score within the entire swarm.
   gbest = gbest(1);
```

```
    tolbreak = ~isnan(options.globalmin);
    foundglobal = 0;
    if tolbreak && ~isscalar(options.globalmin)
        error('mrr:myoptim:pso:pso:optionserr:globalmin', ...
            'globalmin option, if specified, option must be a scalar value equal to the global
minimum of the objective function');
    end


    if output_level >= 0
        % NONE log level
        output.itersno = options.niter;
        if output_level >= 1
            % LOW log level
            output.gbest_array = NaN*ones(options.niter+1, 1);
            output.gmean_array = NaN*ones(options.niter+1, 1);
            output.gworst_array = NaN*ones(options.niter+1, 1);
            output.gbest_array(1) = GYbest;
            output.gmean_array(1) = mean(Ybest);
            output.gworst_array(1) = max(Ybest);
            if output_level >= 2
                % MEDIUM log level
                output.gbestndx_array = NaN*ones(options.niter+1, 1);
                output.Xbest = NaN*ones(options.niter+1, nvars);
                output.gbestndx_array(1) = gbest;
                output.Xbest(1, :) = X(gbest, :);
                if output_level == 3
                    % HIGH log level
                    output.X = NaN*zeros(options.npart, nvars, options.niter+1);
                    output.X(:,:,1) = X;
                end
            end
        end
    end

    if options.verbose_period ~= 0
        disp 'PSO algorithm: Initiating the optimization process.'
    end

    % Denotes normal algorithm termination.
    exitflag = 0;

    for iter = 1:options.niter

        % Verbosing, if neccessary.
        if options.verbose_period ~= 0
```

```
    if rem(iter, options.verbose_period) == 0
      disp(['iteration ', int2str(iter), '. best criteria = ', num2str(GYbest)]);
    end
end

% Calculating PSO parameters
w = linrate(options.wf, options.wi, options.niter, 0, iter);
cp = linrate(options.cbf, options.cbi, options.niter, 0, iter);
cg = linrate(options.cgf, options.cgi, options.niter, 0, iter);


GXbest = repmat(Xbest(gbest, :), options.npart, 1);

% Calculating speeds
V = w*V + cp*rand(size(V)).*(Xbest-X) + cg*rand(size(V)).*(GXbest-X);
V = min(vmax, abs(V)).*sign(V);


X = X + V;
Y = calcobjfunc(objfunc, X);

% Calculating new individually best values
mask = Y<Ybest;
mask = repmat(mask, 1, nvars);
Xbest = mask.*X +(~mask).*Xbest;
Ybest = min(Y,Ybest);


[GYbest, gbest] = min(Ybest);
gbest = gbest(1);

if output_level >= 0
    % NONE log level
    if output_level >= 1
        % LOW log level
        output.gbest_array(iter+1)  = GYbest;
        output.gmean_array(iter+1)  = mean(Ybest);
        output.gworst_array(iter+1) = max(Ybest);
        if output_level >= 2
            % MEDIUM log level
            output.gbestndx_array(iter+1) = gbest;
            output.Xbest(iter+1, :) = X(gbest, :);
            if output_level == 3
                % HIGH log level
                output.X(:,:,iter+1) = X;
            end
```

```
            end
        end
    end

    % The code used in testing mode only.
    if tolbreak && abs(GYbest - options.globalmin)<options.tol
        output.itersno = iter;
        foundglobal = 1;
        break
    end

end

if options.verbose_period ~= 0
    disp 'Optimization process finished.'
end


x = Xbest(gbest, :); x = x(:);
fval = GYbest;

% The global moptimum has been found prior to achieving the maximal number of
iteration.
if foundglobal, exitflag = 1; end;

% Plotting the algorithm behavior at each iteration.
if options.plot
    r = 0:options.niter;
    figure
    plot(r, output.gbest_array, 'k.', r, output.gmean_array, 'r.', r, output.gworst_array,
'b.');
    str = sprintf('Best objective value : %g', fval);
    title(str);
    legend({'best objective', 'mean objective', 'worst objective'})
end

end
```

***Calculation of reliability index***

```
Pbest1=10^65;
Gbest1=10^65;
Drt = 3;
Fir = 0.22;
Wsaifi = 0.2;
Wsaidi = 0.33;
```

```
SaifiT = 1.0
Saidit = 2.2;

for Iten=1:100
   popsize=100;
   bit=20;
   upb=mybinary(ones(1,bit));
   lowb=mybinary(zeros(1,bit));
   up=50;
   low=-50;
   % vec=3;
   N=vec;
   x=randint(popsize,bit*vec,[0 1]);
   vel=rand(popsize,bit*vec)-0.5;

   ff='objective function (Drt, Fir,Wsaifi,Wsaidi,SaifiT,SaidiT)';
   vel=rand(popsize,bit*vec)-0.5;
   one_vel=rand(popsize,bit*vec)-0.5;
   zero_vel=rand(popsize,bit*vec)-0.5;

   for i=1:popsize
      xn=[];
      for j=1:N
         x1=x(i,1+(j-1)*bit:j*bit);
         x1=mybinary(x1)/(upb-lowb)*(up-low)+low;
         xn=[xn x1];
      end
      fx(i)=feval(ff,xn);
   end

   pbest=fx;
   xpbest=x;
   w1=0.5;
   [gbest l]=min(fx);
   xgbest=x(l,:);
   c1=1;
   c2=1;
   maxiter=1000;
   vmax=4;
   for iter=1:maxiter
      w=(maxiter-iter)/maxiter;
      w=0.5;
      for i=1:popsize
         xn=[];
         for j=1:N
            x1=x(i,1+(j-1)*bit:j*bit);
```

```
        x1=mybinary(x1)/(upb-lowb)*(up-low)+low;
        xn=[xn x1];
    end
    fx(i)=feval(ff,xn);
    if fx(i)<pbest(i)
        pbest(i)=fx(i);
        xpbest(i,:)=x(i,:);
    end
end
[gg l]=min(fx);
if gbest>gg
    gbest=gg;
    xgbest=x(l,:);
end

oneadd=zeros(popsize,bit*vec);
zeroadd=zeros(popsize,bit*vec);
c3=c1*rand;
dd3=c2*rand;
for i=1:popsize
    for j=1:bit*vec
        if xpbest(i,j)==0

            oneadd(i,j)=oneadd(i,j)-c3;
            zeroadd(i,j)=zeroadd(i,j)+c3;
        else

            oneadd(i,j)=oneadd(i,j)+c3;
            zeroadd(i,j)=zeroadd(i,j)-c3;
        end
        if xgbest(j)==0

            oneadd(i,j)=oneadd(i,j)-dd3;
            zeroadd(i,j)=zeroadd(i,j)+dd3;
        else

            oneadd(i,j)=oneadd(i,j)+dd3;
            zeroadd(i,j)=zeroadd(i,j)-dd3;
        end
    end
end
one_vel=w1*one_vel+oneadd;
zero_vel=w1*zero_vel+zeroadd;
for i=1:popsize
    for j=1:bit*vec
        if abs(vel(i,j))>vmax
```

```
                zero_vel(i,j)=vmax*sign(zero_vel(i,j));
                one_vel(i,j)=vmax*sign(one_vel(i,j));
            end
        end
    end
    for i=1:popsize
        for j=1:bit*vec
            if x(i,j)==1
                vel(i,j)=zero_vel(i,j);
            else
                vel(i,j)=one_vel(i,j);
            end
        end
    end


    veln=logsig(vel);

    temp=rand(popsize,bit*vec);
    for i=1:popsize
        for j=1:bit*vec
            if temp(i,j)<veln(i,j)
                x(i,j)=not(x(i,j));
            else
                x(i,j)=(x(i,j));
            end
        end
    end
end


if Gbest1>gbest
    Gbest1=gbest;
end
if Pbest1>sum(pbest)/popsize
    Pbest1=sum(pbest)/popsize;
end

end

function y=mybinary(x)

if x==0
    y=0;
else
    l=length(x);
```

```
    y=0;
    for i=0:l-1
        y=y+x(i+1)*2^(i);
    end
end
```

***Function to call OpenDSS program in Matlab.***

```
function [Start,Obj,Text] = DSSStartup

    Obj = actxserver('OpenDSSEngine.DSS');
    Start = Obj.Start(0);
    Text = Obj.Text;
```

***DSSStartup Code***

```
[DSSStartOK, DSSObj, DSSText] = DSSStartup;

if DSSStartOK
    DSSText.command='Compile (C:\opendss\IEEE123Master.dss)';
    DSSCircuit=DSSObj.ActiveCircuit;
    DSSSolution=DSSCircuit.Solution;

    DSSText.Command='New EnergyMeter.Main Line.SW1 1';

    DSSText.Command='New Monitor.FeederEnd Line.L99 1';

    Regulators = DSSCircuit.RegControls;
    iReg = Regulators.First;
    while iReg>0
      Regulators.MaxTapChange = 1;
      Regulators.Delay = 30;
      iReg = Regulators.Next;
    end

    % now set creg1a delay to 15s  so it goes first
    Regulators.Name = 'creg1a';  % Make this the active regcontrol
    Regulators.Delay = 15;

    DSSSolution.MaxControlIterations=30;

    MyControlIterations = 0;

    while MyControlIterations < DSSSolution.MaxControlIterations

        DSSSolution.SolveNoControl;
```

```
   % display the result
   disp(['Result='  DSSText.Result])

   if DSSSolution.Converged
     a = ['Solution Converged in ' num2str(DSSSolution.Iterations) ' iterations.'];
   else
     a = 'Solution did not Converge';
   end
   disp(a)

   DSSSolution.SampleControlDevices;
   DSSSolution.DoControlActions;

   if DSSSolution.ControlActionsDone, break, end

   MyControlIterations = MyControlIterations + 1;
end

DSSText.Command = 'Summary';  %show solution summary
% display the result, which should be the solution summary
disp(['Result='  DSSText.Result])

DSSText.Command = 'Export voltages';
VoltageFileName = DSSText.Result;
% read in skipping first row and first column, which are strings
MyCSV = csvread(VoltageFileName,1, 1);

Volts = MyCSV(:,3);
figure(1)
plot(Volts,'k*');      hold on

ylabel('Volts');
title('All voltages in circuit on one phase.');
hold off

DSSLoads = DSSCircuit.Loads;
iLoad = DSSLoads.First;
while iLoad>0
   DSSLoads.daily = 'default';
   iLoad = DSSLoads.Next;
end

DSSText.Command = 'set mode=daily';
DSSSolution.Solve;
DSSText.Command = 'export mon FeederEnd';
MonFileName = DSSText.Result;
```

```
MyCSV = csvread(MonFileName, 1, 0);
Hour = MyCSV(:,1);
Volts1 = MyCSV(:,3);
Volts2 = MyCSV(:,5);
Volts3 = MyCSV(:,7);
figure(2);
plot(Hour, Volts1,'-k+');
hold on
plot(Hour, Volts2,'-r+');
plot(Hour, Volts3,'-b+');
title('Daily Simulation');
ylabel('Volts');
xlabel('Hour');
hold off

DSSText.Command = 'Set number=1';

for i=1:48
   DSSSolution.Solve;
   DSSCircuit.SetActiveBus('54');
   AllVoltages = DSSCircuit.ActiveBus.puVoltages;
   Volts1(i) = abs(complex(AllVoltages(1), AllVoltages(2)));
   Volts2(i) = abs(complex(AllVoltages(3), AllVoltages(4)));
   Volts3(i) = abs(complex(AllVoltages(5), AllVoltages(6)));
end

Hour=[1:48];

figure(3);
plot(Hour, Volts1,'-k+');
hold on
plot(Hour, Volts2,'-r+');
plot(Hour, Volts3,'-b+');
title('Daily Simulation, Voltages at Bus 54');
ylabel('Volts');
xlabel('Hour');
hold off

DSSText.Command = 'New Generator.GL99 Bus1=450 kW=1000 PF=1 ';

DSSText.Command = 'Solve Mode=snapshot';
DSSText.Command = 'Set Mode=Daily Number=1';
DSSText.Command = 'Generator.GL99.enabled=no';

for i=1:12
  DSSSolution.Solve;
```

```
    end

    DSSCircuit.Generators.Name='GL99';
    ActiveElement = DSSCircuit.ActiveCktElement.Name
    DSSText.Command = 'Generator.GL99.enabled=Yes';
    for i=1:3
      DSSSolution.Solve;
    end

    DSSText.Command = 'Generator.GL99.enabled=no';

    for i=1:9
      DSSSolution.Solve;
    end

    % Export monitor
    DSSText.Command = 'export mon FeederEnd';
    MonFileName = DSSText.Result;
    MyCSV = csvread(MonFileName, 1, 0);
    Hour = MyCSV(:,1);
    Volts1 = MyCSV(:,3);
    Volts2 = MyCSV(:,5);
    Volts3 = MyCSV(:,7);
else
    a='DSS Did Not Start'
    disp(a)
end
```

***File to test new distribution system.***

```
[DSSStartOK, DSSObj, DSSText] = DSSStartup;
if DSSStartOK
    DSSText.command='Compile (C:\opendss\IEEE123Master.dss)';
    % Set up the interface variables
    DSSCircuit=DSSObj.ActiveCircuit;
    DSSSolution=DSSCircuit.Solution;

    DSSText.Command='RegControl.creg1a.maxtapchange=1  Delay=15  !Allow only
one tap change per solution. This one moves first';
    DSSText.Command='RegControl.creg2a.maxtapchange=1  Delay=30  !Allow only
one tap change per solution';
    DSSText.Command='RegControl.creg3a.maxtapchange=1  Delay=30  !Allow only
one tap change per solution';
    DSSText.Command='RegControl.creg4a.maxtapchange=1  Delay=30  !Allow only
one tap change per solution';
```

```
   DSSText.Command='RegControl.creg3c.maxtapchange=1  Delay=30  !Allow only
one tap change per solution';
   DSSText.Command='RegControl.creg4b.maxtapchange=1  Delay=30  !Allow only
one tap change per solution';
   DSSText.Command='RegControl.creg4c.maxtapchange=1  Delay=30  !Allow only
one tap change per solution';

   DSSText.Command='Set MaxControlIter=30';

   DSSSolution.SolveNoControl;
   disp(['Result='  DSSText.Result])
   if DSSSolution.Converged
      a = 'Solution Converged';
      disp(a)
   else
      a = 'Solution did not Converge';
      disp(a)
   end

   DSSText.Command='Export Voltages';
   disp(DSSText.Result)
   DSSSolution.SampleControlDevices;
   DSSCircuit.CtrlQueue.Show;
   disp(DSSText.Result)
   DSSSolution.DoControlActions;
   DSSCircuit.CtrlQueue.Show;

   DSSText.Command='Buscoords Buscoords.dat   ! load in bus coordinates';
else
   a = 'DSS Did Not Start'
   disp(a)
end
```

OpenDSS Files

***Load definition***

```
New Load.S1a   Bus1=1.1   Phases=1 Conn=Wye   Model=1 kV=2.4   kW=40.0
kvar=20.0
New Load.S2b   Bus1=2.2   Phases=1 Conn=Wye   Model=1 kV=2.4   kW=20.0
kvar=10.0
New Load.S4c   Bus1=4.3   Phases=1 Conn=Wye   Model=1 kV=2.4   kW=40.0
kvar=20.0
New Load.S5c   Bus1=5.3   Phases=1 Conn=Wye   Model=5 kV=2.4   kW=20.0
kvar=10.0
```

New Load.S6c Bus1=6.3 Phases=1 Conn=Wye Model=2 kV=2.4 kW=40.0 kvar=20.0
New Load.S7a Bus1=7.1 Phases=1 Conn=Wye Model=1 kV=2.4 kW=20.0 kvar=10.0
New Load.S9a Bus1=9.1 Phases=1 Conn=Wye Model=1 kV=2.4 kW=40.0 kvar=20.0
New Load.S10a Bus1=10.1 Phases=1 Conn=Wye Model=5 kV=2.4 kW=20.0 kvar=10.0
New Load.S11a Bus1=11.1 Phases=1 Conn=Wye Model=2 kV=2.4 kW=40.0 kvar=20.0
New Load.S12b Bus1=12.2 Phases=1 Conn=Wye Model=1 kV=2.4 kW=20.0 kvar=10.0
New Load.S16c Bus1=16.3 Phases=1 Conn=Wye Model=1 kV=2.4 kW=40.0 kvar=20.0
New Load.S17c Bus1=17.3 Phases=1 Conn=Wye Model=1 kV=2.4 kW=20.0 kvar=10.0
New Load.S19a Bus1=19.1 Phases=1 Conn=Wye Model=1 kV=2.4 kW=40.0 kvar=20.0
New Load.S20a Bus1=20.1 Phases=1 Conn=Wye Model=5 kV=2.4 kW=40.0 kvar=20.0
New Load.S22b Bus1=22.2 Phases=1 Conn=Wye Model=2 kV=2.4 kW=40.0 kvar=20.0
New Load.S24c Bus1=24.3 Phases=1 Conn=Wye Model=1 kV=2.4 kW=40.0 kvar=20.0
New Load.S28a Bus1=28.1 Phases=1 Conn=Wye Model=5 kV=2.4 kW=40.0 kvar=20.0
New Load.S29a Bus1=29.1 Phases=1 Conn=Wye Model=2 kV=2.4 kW=40.0 kvar=20.0
New Load.S30c Bus1=30.3 Phases=1 Conn=Wye Model=1 kV=2.4 kW=40.0 kvar=20.0
New Load.S31c Bus1=31.3 Phases=1 Conn=Wye Model=1 kV=2.4 kW=20.0 kvar=10.0
New Load.S32c Bus1=32.3 Phases=1 Conn=Wye Model=1 kV=2.4 kW=20.0 kvar=10.0
New Load.S33a Bus1=33.1 Phases=1 Conn=Wye Model=5 kV=2.4 kW=40.0 kvar=20.0
New Load.S34c Bus1=34.3 Phases=1 Conn=Wye Model=2 kV=2.4 kW=40.0 kvar=20.0
New Load.S35a Bus1=35.1.2 Phases=1 Conn=Delta Model=1 kV=4.160 kW=40.0 kvar=20.0
New Load.S37a Bus1=37.1 Phases=1 Conn=Wye Model=2 kV=2.4 kW=40.0 kvar=20.0
New Load.S38b Bus1=38.2 Phases=1 Conn=Wye Model=5 kV=2.4 kW=20.0 kvar=10.0
New Load.S39b Bus1=39.2 Phases=1 Conn=Wye Model=1 kV=2.4 kW=20.0 kvar=10.0

New Load.S41c Bus1=41.3 Phases=1 Conn=Wye Model=1 kV=2.4 kW=20.0 kvar=10.0
New Load.S42a Bus1=42.1 Phases=1 Conn=Wye Model=1 kV=2.4 kW=20.0 kvar=10.0
New Load.S43b Bus1=43.2 Phases=1 Conn=Wye Model=2 kV=2.4 kW=40.0 kvar=20.0
New Load.S45a Bus1=45.1 Phases=1 Conn=Wye Model=5 kV=2.4 kW=20.0 kvar=10.0
New Load.S46a Bus1=46.1 Phases=1 Conn=Wye Model=1 kV=2.4 kW=20.0 kvar=10.0
New Load.S47 Bus1=47 Phases=3 Conn=Wye Model=5 kV=4.160 kW=105.0 kvar=75.0
New Load.S48 Bus1=48 Phases=3 Conn=Wye Model=2 kV=4.160 kW=210.0 kVAR=150.0
New Load.S49a Bus1=49.1 Phases=1 Conn=Wye Model=1 kV=2.4 kW=35.0 kvar=25.0
New Load.S49b Bus1=49.2 Phases=1 Conn=Wye Model=1 kV=2.4 kW=70.0 kvar=50.0

***Transformer Definition***

new transformer.reg2a phases=1 windings=2 buses=[9.1 9r.1] conns=[wye wye] kvs=[2.402 2.402] kvas=[2000 2000] XHL=.01 %LoadLoss=0.00001 ppm=0.0
new transformer.reg3a phases=1 windings=2 buses=[25.1 25r.1] conns=[wye wye] kvs=[2.402 2.402] kvas=[2000 2000] XHL=.01 %LoadLoss=0.00001 ppm=0.0
new transformer.reg4a phases=1 windings=2 buses=[160.1 160r.1] conns=[wye wye] kvs=[2.402 2.402] kvas=[2000 2000] XHL=.01 %LoadLoss=0.00001 ppm=0.0
new transformer.reg3c like=reg3a buses=[25.3 25r.3] ppm=0.0
new transformer.reg4b like=reg4a buses=[160.2 160r.2] ppm=0.0
new transformer.reg4c like=reg4a buses=[160.3 160r.3] ppm=0.0

***Regulator definition***
new regcontrol.creg2a transformer=reg2a winding=2 vreg=120 band=2 ptratio=20 ctprim=50 R=0.4 X=0.4
new regcontrol.creg3a transformer=reg3a winding=2 vreg=120 band=1 ptratio=20 ctprim=50 R=0.4 X=0.4
new regcontrol.creg4a transformer=reg4a winding=2 vreg=124 band=2 ptratio=20 ctprim=300 R=0.6 X=1.3
new regcontrol.creg4b like=creg4a transformer=reg4b
R=1.4 X=2.6
new regcontrol.creg4c like=creg4a transformer=reg4c
R=0.2 X=1.4

***Line definations***

New linecode.1 nphases=3 BaseFreq=60
!!!~ rmatrix = (0.088205 | 0.0312137 0.0901946 | 0.0306264 0.0316143 0.0889665 )
!!!~ xmatrix = (0.20744 | 0.0935314 0.200783 | 0.0760312 0.0855879 0.204877 )
!!!~ cmatrix = (2.90301 | -0.679335 3.15896 | -0.22313 -0.481416 2.8965 )
~ rmatrix = [0.086666667 | 0.029545455 0.088371212 | 0.02907197 0.029924242 0.087405303]
~ xmatrix = [0.204166667 | 0.095018939 0.198522727 | 0.072897727 0.080227273 0.201723485]
~ cmatrix = [2.851710072 | -0.920293787  3.004631862 | -0.350755566  -0.585011253 2.71134756]

New linecode.2 nphases=3 BaseFreq=60
!!!~ rmatrix = (0.0901946 | 0.0316143 0.0889665 | 0.0312137 0.0306264 0.088205 )
!!!~ xmatrix = (0.200783 | 0.0855879 0.204877 | 0.0935314 0.0760312 0.20744 )
!!!~ cmatrix = (3.15896 | -0.481416 2.8965 | -0.679335 -0.22313 2.90301 )
~ rmatrix = [0.088371212 | 0.02992424  0.087405303 | 0.029545455 0.02907197 0.086666667]
~ xmatrix = [0.198522727 | 0.080227273  0.201723485 | 0.095018939 0.072897727 0.204166667]
~ cmatrix = [3.004631862 | -0.585011253 2.71134756 | -0.920293787  -0.350755566 2.851710072]

New linecode.3 nphases=3 BaseFreq=60
!!!~ rmatrix = (0.0889665 | 0.0306264 0.088205 | 0.0316143 0.0312137 0.0901946 )
!!!~ xmatrix = (0.204877 | 0.0760312 0.20744 | 0.0855879 0.0935314 0.200783 )
!!!~ cmatrix = (2.8965 | -0.22313 2.90301 | -0.481416 -0.679335 3.15896 )

~ rmatrix = [0.087405303 | 0.02907197 0.086666667  | 0.029924242 0.029545455 0.088371212]
~ xmatrix = [0.201723485 | 0.072897727 0.204166667 | 0.080227273 0.095018939 0.198522727]
~ cmatrix = [2.71134756  | -0.350755566 2.851710072 | -0.585011253 -0.920293787 3.004631862]

New linecode.4 nphases=3 BaseFreq=60
!!!~ rmatrix = (0.0889665 | 0.0316143 0.0901946 | 0.0306264 0.0312137 0.088205 )
!!!~ xmatrix = (0.204877 | 0.0855879 0.200783 | 0.0760312 0.0935314 0.20744 )
!!!~ cmatrix = (2.8965 | -0.481416 3.15896 | -0.22313 -0.679335 2.90301 )
~ rmatrix = [0.087405303 | 0.029924242 0.088371212 | 0.02907197   0.029545455 0.086666667]
~ xmatrix = [0.201723485 | 0.080227273 0.198522727 | 0.072897727 0.095018939 0.204166667]
~ cmatrix = [2.71134756  | 0.585011253 3.004631862 | -0.350755566 -0.920293787 2.851710072]

New linecode.5 nphases=3 BaseFreq=60

!!!~ rmatrix = (0.0901946 | 0.0312137 0.088205 | 0.0316143 0.0306264 0.0889665 )
!!!~ xmatrix = (0.200783 | 0.0935314 0.20744 | 0.0855879 0.0760312 0.204877 )
!!!~ cmatrix = (3.15896 | -0.679335 2.90301 | -0.481416 -0.22313 2.8965 )

~ rmatrix = [0.088371212 | 0.029545455 0.086666667 | 0.029924242 0.02907197 0.087405303]
~ xmatrix = [0.198522727 | 0.095018939 0.204166667 | 0.080227273 0.072897727 0.201723485]
~ cmatrix = [3.004631862 | -0.920293787 2.851710072 | -0.585011253 -0.350755566 2.71134756]

New linecode.6 nphases=3 BaseFreq=60
!!!~ rmatrix = (0.088205 | 0.0306264 0.0889665 | 0.0312137 0.0316143 0.0901946 )
!!!~ xmatrix = (0.20744 | 0.0760312 0.204877 | 0.0935314 0.0855879 0.200783 )
!!!~ cmatrix = (2.90301 | -0.22313 2.8965 | -0.679335 -0.481416 3.15896 )
~ rmatrix = [0.086666667 | 0.02907197 0.087405303 | 0.029545455 0.029924242 0.088371212]
~ xmatrix = [0.204166667 | 0.072897727 0.201723485 | 0.095018939 0.080227273 0.198522727]
~ cmatrix = [2.851710072 | -0.350755566 2.71134756 | -0.920293787 -0.585011253 3.004631862]
New linecode.7 nphases=2 BaseFreq=60
!!!~ rmatrix = (0.088205 | 0.0306264 0.0889665 )
!!!~ xmatrix = (0.20744 | 0.0760312 0.204877 )
!!!~ cmatrix = (2.75692 | -0.326659 2.82313 )
~ rmatrix = [0.086666667 | 0.02907197 0.087405303]
~ xmatrix = [0.204166667 | 0.072897727 0.201723485]
~ cmatrix = [2.569829596 | -0.52995137 2.597460011]
New linecode.8 nphases=2 BaseFreq=60
!!!~ rmatrix = (0.088205 | 0.0306264 0.0889665 )
!!!~ xmatrix = (0.20744 | 0.0760312 0.204877 )
!!!~ cmatrix = (2.75692 | -0.326659 2.82313 )
~ rmatrix = [0.086666667 | 0.02907197 0.087405303]
~ xmatrix = [0.204166667 | 0.072897727 0.201723485]
~ cmatrix = [2.569829596 | -0.52995137 2.597460011]
New linecode.9 nphases=1 BaseFreq=60
!!!~ rmatrix = (0.254428 )
!!!~ xmatrix = (0.259546 )
!!!~ cmatrix = (2.50575 )
~ rmatrix = [0.251742424]
~ xmatrix = [0.255208333]
~ cmatrix = [2.270366128]
New linecode.10 nphases=1 BaseFreq=60
!!!~ rmatrix = (0.254428 )
!!!~ xmatrix = (0.259546 )
!!!~ cmatrix = (2.50575 )

~ rmatrix = [0.251742424]
~ xmatrix = [0.255208333]
~ cmatrix = [2.270366128]
New linecode.11 nphases=1 BaseFreq=60
!!!~ rmatrix = (0.254428 )
!!!~ xmatrix = (0.259546 )
!!!~ cmatrix = (2.50575 )
~ rmatrix = [0.251742424]
~ xmatrix = [0.255208333]
~ cmatrix = [2.270366128]
New linecode.12 nphases=3 BaseFreq=60
!!!~ rmatrix = (0.291814 | 0.101656 0.294012 | 0.096494 0.101656 0.291814 )
!!!~ xmatrix = (0.141848 | 0.0517936 0.13483 | 0.0401881 0.0517936 0.141848 )
!!!~ cmatrix = (53.4924 | 0 53.4924 | 0 0 53.4924 )
~ rmatrix = [0.288049242 | 0.09844697  0.29032197 | 0.093257576  0.09844697 0.288049242]
~ xmatrix = [0.142443182 | 0.052556818  0.135643939 | 0.040852273  0.052556818 0.142443182]
~ cmatrix = [33.77150149 | 0  33.77150149 | 0  0  33.77150149]

***Bus Definitions***

New Line.L115 Bus1=149 Bus2=1 LineCode=1 Length=0.4
New Line.L1 Phases=1 Bus1=1.2 Bus2=2.2 LineCode=10 Length=0.175
New Line.L2 Phases=1 Bus1=1.3 Bus2=3.3 LineCode=11 Length=0.25
New Line.L3 Phases=3 Bus1=1.1.2.3 Bus2=7.1.2.3 LineCode=1 Length=0.3
New Line.L4 Phases=1 Bus1=3.3 Bus2=4.3 LineCode=11 Length=0.2
New Line.L5 Phases=1 Bus1=3.3 Bus2=5.3 LineCode=11 Length=0.325
New Line.L6 Phases=1 Bus1=5.3 Bus2=6.3 LineCode=11 Length=0.25
New Line.L7 Phases=3 Bus1=7.1.2.3 Bus2=8.1.2.3 LineCode=1 Length=0.2
New Line.L8 Phases=1 Bus1=8.2 Bus2=12.2 LineCode=10 Length=0.225
New Line.L9 Phases=1 Bus1=8.1 Bus2=9.1 LineCode=9 Length=0.225
New Line.L10 Phases=3 Bus1=8.1.2.3 Bus2=13.1.2.3 LineCode=1 Length=0.3
New Line.L11 Phases=1 Bus1=9r.1 Bus2=14.1 LineCode=9 Length=0.425
New Line.L12 Phases=1 Bus1=13.3 Bus2=34.3 LineCode=11 Length=0.15
New Line.L13 Phases=3 Bus1=13.1.2.3 Bus2=18.1.2.3 LineCode=2 Length=0.825
New Line.L14 Phases=1 Bus1=14.1 Bus2=11.1 LineCode=9 Length=0.25
New Line.L15 Phases=1 Bus1=14.1 Bus2=10.1 LineCode=9 Length=0.25
New Line.L16 Phases=1 Bus1=15.3 Bus2=16.3 LineCode=11 Length=0.375
New Line.L17 Phases=1 Bus1=15.3 Bus2=17.3 LineCode=11 Length=0.35
New Line.L18 Phases=1 Bus1=18.1 Bus2=19.1 LineCode=9 Length=0.25
New Line.L19 Phases=3 Bus1=18.1.2.3 Bus2=21.1.2.3 LineCode=2 Length=0.3
New Line.L20 Phases=1 Bus1=19.1 Bus2=20.1 LineCode=9 Length=0.325
New Line.L21 Phases=1 Bus1=21.2 Bus2=22.2 LineCode=10 Length=0.525
New Line.L22 Phases=3 Bus1=21.1.2.3 Bus2=23.1.2.3 LineCode=2 Length=0.25
New Line.L23 Phases=1 Bus1=23.3 Bus2=24.3 LineCode=11 Length=0.55

```
New Line.L24    Phases=3 Bus1=23.1.2.3   Bus2=25.1.2.3   LineCode=2    Length=0.275
New Line.L25    Phases=2 Bus1=25r.1.3    Bus2=26.1.3     LineCode=7    Length=0.35
New Line.L26    Phases=3 Bus1=25.1.2.3   Bus2=28.1.2.3   LineCode=2    Length=0.2
New Line.L27    Phases=2 Bus1=26.1.3     Bus2=27.1.3     LineCode=7    Length=0.275
New Line.L28    Phases=1 Bus1=26.3       Bus2=31.3       LineCode=11   Length=0.225
New Line.L29    Phases=1 Bus1=27.1       Bus2=33.1       LineCode=9    Length=0.5
New Line.L30    Phases=3 Bus1=28.1.2.3   Bus2=29.1.2.3   LineCode=2    Length=0.3
New Line.L31    Phases=3 Bus1=29.1.2.3   Bus2=30.1.2.3   LineCode=2    Length=0.35
New Line.L32    Phases=3 Bus1=30.1.2.3   Bus2=250.1.2.3  LineCode=2    Length=0.2
New Line.L33    Phases=1 Bus1=31.3       Bus2=32.3       LineCode=11   Length=0.3
New Line.L34    Phases=1 Bus1=34.3       Bus2=15.3       LineCode=11   Length=0.1
New Line.L35    Phases=2 Bus1=35.1.2     Bus2=36.1.2     LineCode=8    Length=0.65
New Line.L36    Phases=3 Bus1=35.1.2.3   Bus2=40.1.2.3   LineCode=1    Length=0.25
New Line.L37    Phases=1 Bus1=36.1       Bus2=37.1       LineCode=9    Length=0.3
New Line.L38    Phases=1 Bus1=36.2       Bus2=38.2       LineCode=10   Length=0.25
New Line.L39    Phases=1 Bus1=38.2       Bus2=39.2       LineCode=10   Length=0.325
New Line.L40    Phases=1 Bus1=40.3       Bus2=41.3       LineCode=11   Length=0.325
New Line.L41    Phases=3 Bus1=40.1.2.3   Bus2=42.1.2.3   LineCode=1    Length=0.25
New Line.L42    Phases=1 Bus1=42.2       Bus2=43.2       LineCode=10   Length=0.5
New Line.L43    Phases=3 Bus1=42.1.2.3   Bus2=44.1.2.3   LineCode=1    Length=0.2
New Line.L44    Phases=1 Bus1=44.1       Bus2=45.1       LineCode=9    Length=0.2
New Line.L45    Phases=3 Bus1=44.1.2.3   Bus2=47.1.2.3   LineCode=1    Length=0.25
New Line.L46    Phases=1 Bus1=45.1       Bus2=46.1       LineCode=9    Length=0.3
New Line.L47    Phases=3 Bus1=47.1.2.3   Bus2=48.1.2.3   LineCode=4    Length=0.15
New Line.L48    Phases=3 Bus1=47.1.2.3   Bus2=49.1.2.3   LineCode=4    Length=0.25
New Line.L49    Phases=3 Bus1=49.1.2.3   Bus2=50.1.2.3   LineCode=4    Length=0.25
New Line.L50    Phases=3 Bus1=50.1.2.3   Bus2=51.1.2.3   LineCode=4    Length=0.25
New Line.L51    Phases=3 Bus1=51.1.2.3   Bus2=151.1.2.3  LineCode=4    Length=0.5
New Line.L52    Phases=3 Bus1=52.1.2.3   Bus2=53.1.2.3   LineCode=1    Length=0.2
New Line.L53    Phases=3 Bus1=53.1.2.3   Bus2=54.1.2.3   LineCode=1    Length=0.125
New Line.L54    Phases=3 Bus1=54.1.2.3   Bus2=55.1.2.3   LineCode=1    Length=0.275
New Line.L55    Phases=3 Bus1=54.1.2.3   Bus2=57.1.2.3   LineCode=3    Length=0.35
New Line.L56    Phases=3 Bus1=55.1.2.3   Bus2=56.1.2.3   LineCode=1    Length=0.275
New Line.L57    Phases=1 Bus1=57.2       Bus2=58.2       LineCode=10   Length=0.25
New Line.L58    Phases=3 Bus1=57.1.2.3   Bus2=60.1.2.3   LineCode=3    Length=0.75
New Line.L59    Phases=1 Bus1=58.2       Bus2=59.2       LineCode=10   Length=0.25
New Line.L60    Phases=3 Bus1=60.1.2.3   Bus2=61.1.2.3   LineCode=5    Length=0.55
New Line.L61    Phases=3 Bus1=60.1.2.3   Bus2=62.1.2.3   LineCode=12   Length=0.25
New Line.L62    Phases=3 Bus1=62.1.2.3   Bus2=63.1.2.3   LineCode=12
Length=0.175
New Line.L63    Phases=3 Bus1=63.1.2.3   Bus2=64.1.2.3   LineCode=12   Length=0.35
New Line.L64    Phases=3 Bus1=64.1.2.3   Bus2=65.1.2.3   LineCode=12
Length=0.425
New Line.L65    Phases=3 Bus1=65.1.2.3   Bus2=66.1.2.3   LineCode=12
Length=0.325
```

***Normally Closed Switches Definitions:***

New Line.Sw1 phases=3 Bus1=150r Bus2=149 r1=1e-3 r0=1e-3 x1=0.000 x0=0.000 c1=0.000 c0=0.000 Length=0.001
New Line.Sw2 phases=3 Bus1=13 Bus2=152 r1=1e-3 r0=1e-3 x1=0.000 x0=0.000 c1=0.000 c0=0.000 Length=0.001
New Line.Sw3 phases=3 Bus1=18 Bus2=135 r1=1e-3 r0=1e-3 x1=0.000 x0=0.000 c1=0.000 c0=0.000 Length=0.001
New Line.Sw4 phases=3 Bus1=60 Bus2=160 r1=1e-3 r0=1e-3 x1=0.000 x0=0.000 c1=0.000 c0=0.000 Length=0.001
New Line.Sw5 phases=3 Bus1=97 Bus2=197 r1=1e-3 r0=1e-3 x1=0.000 x0=0.000 c1=0.000 c0=0.000 Length=0.001
New Line.Sw6 phases=3 Bus1=61 Bus2=61s r1=1e-3 r0=1e-3 x1=0.000 x0=0.000 c1=0.000 c0=0.000 Length=0.001

***Normally Open Switches Definitions***

New Line.Sw7 phases=3 Bus1=151 Bus2=300_OPEN r1=1e-3 r0=1e-3 x1=0.000 x0=0.000 c1=0.000 c0=0.000 Length=0.001
New Line.Sw8 phases=1 Bus1=54.1 Bus2=94_OPEN.1 r1=1e-3 r0=1e-3 x1=0.000 x0=0.000 c1=0.000 c0=0.000 Length=0.001

***Capacitors Definition***

New Capacitor.C83 Bus1=83 Phases=3 kVAR=600 kV=4.16
New Capacitor.C88a Bus1=88.1 Phases=1 kVAR=50 kV=2.402
New Capacitor.C90b Bus1=90.2 Phases=1 kVAR=50 kV=2.402
New Capacitor.C92c Bus1=92.3 Phases=1 kVAR=50 kV=2.

## REFERENCES


[1] "DSIRE: Database of Energy Efficiency, Renewable Energy Solar Incentives, Rebates, Programs, Policy." [Online]. Available: http://www.dsireusa.org/. [Accessed: 28-Apr-2014].

[2] K.-H. Kim, Y.-J. Lee, S.-B. Rhee, S.-K. Lee, and S.-K. You, "Dispersed generator placement using fuzzy-GA in distribution systems," in *IEEE Power Engineering Society Summer Meeting,*, vol. 3, pp. 1148–1153.

[3] K. Nara, Y. Hayashi, K. Ikeda, and T. Ashizawa, "Application of tabu search to optimal placement of distributed generators," in *2001 IEEE Power Engineering Society Winter Meeting. Conference Proceedings (Cat. No.01CH37194)*, 2001, vol. 2, pp. 918–923.

[4] N. Acharya, P. Mahat, and N. Mithulananthan, "An analytical approach for DG allocation in primary distribution network," *Int. J. Electr. Power Energy Syst.*, vol. 28, no. 10, pp. 669–678, Dec. 2006.

[5] D. Singh, R. K. Misra, and D. Singh, "Effect of Load Models in Distributed Generation Planning," *IEEE Trans. Power Syst.*, vol. 22, no. 4, pp. 2204–2212, Nov. 2007.

[6] F. S. Abu-Mouti and M. E. El-Hawary, "Optimal Distributed Generation Allocation and Sizing in Distribution Systems via Artificial Bee Colony Algorithm," *IEEE Trans. Power Deliv.*, vol. 26, no. 4, pp. 2090–2101, Oct. 2011.

[7] L. D. Arya, A. Koshti, and S. C. Choube, "Distributed generation planning using differential evolution accounting voltage stability consideration," *Int. J. Electr. Power Energy Syst.*, vol. 42, no. 1, pp. 196–207, Nov. 2012.

[8] D. Q. Hung and N. Mithulananthan, "Multiple Distributed Generator Placement in Primary Distribution Networks for Loss Reduction," *IEEE Trans. Ind. Electron.*, vol. 60, no. 4, pp. 1700–1708, Apr. 2013.

[9] R. S. Rao, K. Ravindra, K. Satish, and S. V. L. Narasimham, "Power Loss Minimization in Distribution System Using Network Reconfiguration in the Presence of Distributed Generation," *IEEE Trans. Power Syst.*, vol. 28, no. 1, pp. 317–325, Feb. 2013.

[10] A. Pregelj, M. Begovic, and A. Rohatgi, “Recloser Allocation for Improved Reliability of DG-Enhanced Distribution Networks,” *IEEE Trans. Power Syst.*, vol. 21, no. 3, pp. 1442–1449, Aug. 2006.

[11] C. Singh, “Reliability-Constrained Optimum Placement of Reclosers and Distributed Generators in Distribution Networks Using an Ant Colony System Algorithm,” *IEEE Trans. Syst. Man, Cybern. Part C (Applications Rev.*, vol. 38, no. 6, pp. 757–764, Nov. 2008.

[12] S. Conti, R. Nicolosi, and S. A. Rizzo, “Generalized Systematic Approach to Assess Distribution System Reliability With Renewable Distributed Generators and Microgrids,” *IEEE Trans. Power Deliv.*, vol. 27, no. 1, pp. 261–270, Jan. 2012.

[13] W. Tippachon and D. Rerkpreedapong, “Multiobjective optimal placement of switches and protective devices in electric power distribution systems using ant colony optimization,” *Electr. Power Syst. Res.*, vol. 79, no. 7, pp. 1171–1178, Jul. 2009.

[14] Z. Li, X. Yuqin, and W. ZengPing, “Research on optimization of recloser placement of DG-enhanced distribution networks,” in *2008 Third International Conference on Electric Utility Deregulation and Restructuring and Power Technologies*, 2008, pp. 2592–2597.

[15] H. Ying-yi and W. Fu-ming, “Development of three-phase Newton optimal power flow for studying imbalance / security in transmission systems,” vol. 55, pp. 39–48, 2000.

[16] A. A. Chowdhury, S. K. Agarwal, and D. O. Koval, “Reliability modeling of distributed generation in conventional distribution systems planning and analysis,” in *Conference Record of the 2002 IEEE Industry Applications Conference. 37th IAS Annual Meeting (Cat. No.02CH37344)*, vol. 2, pp. 1089–1094.

[17] R. E. Brown and L. A. A. Freeman, “Analyzing the reliability impact of distributed generation,” in *2001 Power Engineering Society Summer Meeting. Conference Proceedings (Cat. No.01CH37262)*, 2001, vol. 2, pp. 1013–1018.

[18] M. Fotuhi-Firuzabad and A. Rajabi-Ghahnavie, “An Analytical Method to Consider DG Impacts on Distribution System Reliability,” in *2005 IEEE/PES Transmission & Distribution Conference & Exposition: Asia and Pacific*, 2005, pp. 1–6.

[19] S.-Y. Yun, J.-C. Kim, J.-F. Moon, C.-H. Park, S.-M. Park, and M.-S. Lee, “Reliability evaluation of radial distribution system considering momentary interruptions,” in *2003 IEEE Power Engineering Society General Meeting (IEEE Cat. No.03CH37491)*, vol. 1, pp. 480–485.

[20] H. Falaghi and M.-R. Haghifam, “Distributed Generation Impacts on Electric Distribution Systems Reliability: Sensitivity Analysis,” in *EUROCON 2005 - The International Conference on “Computer as a Tool,”* 2005, vol. 2, pp. 1465–1468.

[21] T. E. McDermott and R. C. Dugan, “Distributed generation impact on reliability and power quality indices,” in *2002 Rural Electric Power Conference. Papers Presented at the 46th Annual Conference (Cat. No. 02CH37360)*, 2002, pp. D3–1–7.

[22] J. Kennedy, “The particle swarm: social adaptation of knowledge,” in *Proceedings of 1997 IEEE International Conference on Evolutionary Computation (ICEC ’97)*, 1997, pp. 303–308.

[23] R. C. Dugan and T. E. McDermott, “An open source platform for collaborating on smart grid research,” in *2011 IEEE Power and Energy Society General Meeting*, 2011, pp. 1–7.

[24] M. R. Rapaić, Ž. Kanović, and Z. D. Jeličić, “Discrete particle swarm optimization algorithm for solving optimal sensor deployment problem,” *J. Autom. Control*, vol. 18, no. 1, pp. 9–14.

[25] P. M. Gomadam and J. W. Weidner, “Analysis of electrochemical impedance spectroscopy in proton exchange membrane fuel cells,” *Int. J. Energy Res.*, vol. 29, no. 12, pp. 1133–1151, Oct. 2005.

[26] A. Rangathan, “The Levenberg-Marquardt Algorithm.”[Online]. Available http://www.ananth.in/Notes_files/lmtut.pdf

[27] S. Dahal and H. Salehfar, “Optimal location and sizing of distributed generators in distribution networks,” in *2013 North American Power Symposium (NAPS)*, 2013, pp. 1–6.

[28] D. (EPRI W. P. Herman, “Integrating Distributed Resources into Electric Utility Distribution System,” 2001.

[29] S. Kotamarty, S. Khushalani, and N. Schulz, “Impact of distributed generation on distribution contingency analysis,” *Electr. Power Syst. Res.*, vol. 78, no. 9, pp. 1537–1545, Sep. 2008.

[30] P. P. Barker and R. W. De Mello, “Determining the impact of distributed generation on power systems. I. Radial distribution systems,” in *2000 Power Engineering Society Summer Meeting (Cat. No.00CH37134)*, 2000, vol. 3, pp. 1645–1656.

[31] R. S. Al Abri, E. F. El-Saadany, and Y. M. Atwa, “Optimal Placement and Sizing Method to Improve the Voltage Stability Margin in a Distribution System Using

Distributed Generation," *IEEE Trans. Power Syst.*, vol. 28, no. 1, pp. 326–334, Feb. 2013.

[32] A. D. T. Le, M. A. Kashem, M. Negnevitsky, and G. Ledwich, "Control Strategy of Distributed Generation for Voltage Support in Distribution Systems," in *2006 International Conference on Power Electronic, Drives and Energy Systems*, 2006, pp. 1–6.

[33] "California ISO - Daily renewables watch." [Online]. Available: http://www.caiso.com/market/Pages/ReportsBulletins/DailyRenewablesWatch.aspx.

[34] M. A. Kashem and G. Ledwich, "Distributed Generation as Voltage Support for Single Wire Earth Return Systems," *IEEE Trans. Power Deliv.*, vol. 19, no. 3, pp. 1002–1011, Jul. 2004.

[35] C. Dai and Y. Baghzouz, "On the voltage profile of distribution feeders with distributed generation," in *2003 IEEE Power Engineering Society General Meeting (IEEE Cat. No.03CH37491)*, vol. 2, pp. 1136–1140.

[36] T. E. Kim and J. E. Kim, "Voltage regulation coordination of distributed generation system in distribution system," in *2001 Power Engineering Society Summer Meeting. Conference Proceedings (Cat. No.01CH37262)*, 2001, vol. 1, pp. 480–484.

[37] "How much electricity is lost in transmission and distribution in the United States? - FAQ - U.S. Energy Information Administration (EIA)." [Online]. Available: http://www.eia.gov/tools/faqs/faq.cfm?id=105&t=3. [Accessed: 27-Apr-2014].

[38] J. F. V. Gonzalez and C. Lyra, "Learning classifiers shape reactive power to decrease losses in power distribution networks," in *IEEE Power Engineering Society General Meeting, 2005.*, 2005, pp. 2906–2911.

[39] A. Anwar, S. Member, and H. R. Pota, "Optimum Capacity Allocation of DG Units Based on Unbalanced Three-phase Optimal Power Flow," 2012.

[40] A. Anwar, S. Member, and H. R. Pota, "Loss Reduction of Power Distribution Network Using Optimum Size and Location of Distributed Generation."

[41] Y. M. Atwa, S. Member, S. Member, M. M. A. Salama, and R. Seethapathy, "Optimal Renewable Resources Mix for Distribution System Energy Loss Minimization," vol. 25, no. 1, pp. 360–370, 2010.

[42] Soo-Hyoung Lee and Jung-Wook Park, "Selection of Optimal Location and Size of Multiple Distributed Generations by Using Kalman Filter Algorithm," *IEEE Trans. Power Syst.*, vol. 24, no. 3, pp. 1393–1400, Aug. 2009.

[43] L. F. Ochoa, C. J. Dent, and G. P. Harrison, “Maximisation of intermittent distributed generation in active networks.” pp. 1–4, 2008.

[44] H. L. Willis, “Analytical methods and rules of thumb for modeling DG-distribution interaction,” in *2000 Power Engineering Society Summer Meeting (Cat. No.00CH37134)*, 2000, vol. 3, pp. 1643–1644.

[45] C. Wang and M. H. Nehrir, “Analytical Approaches for Optimal Placement of Distributed Generation Sources in Power Systems,” *IEEE Trans. Power Syst.*, vol. 19, no. 4, pp. 2068–2076, Nov. 2004.

[46] F. S. Abu-Mouti and M. E. El-Hawary, “Heuristic curve-fitted technique for distributed generation optimisation in radial distribution feeder systems,” *IET Gener. Transm. Distrib.*, vol. 5, no. 2, p. 172, 2011.

[47] H. Hedayati, S. A. Nabaviniaki, and A. Akbarimajd, “A New Method for Placement of DG Units in Distribution Networks,” in *2006 IEEE PES Power Systems Conference and Exposition*, 2006, pp. 1904–1909.

[48] P. M. Costa and M. A. Matos, “Avoided losses on LV networks as a result of microgeneration,” *Electr. Power Syst. Res.*, vol. 79, no. 4, pp. 629–634, Apr. 2009.

[49] M. F. AlHajri, M. R. AlRashidi, and M. E. El-Hawary, “Improved Sequential Quadratic Programming Approach for Optimal Distribution Generation Deployments via Stability and Sensitivity Analyses,” *Electr. Power Components Syst.*, vol. 38, no. 14, pp. 1595–1614, Dec. 2010.

[50] H. Hamedi and M. Gandomkar, “A straightforward approach to minimizing unsupplied energy and power loss through DG placement and evaluating power quality in relation to load variations over time,” *Int. J. Electr. Power Energy Syst.*, vol. 35, no. 1, pp. 93–96, Nov. 2011.

[51] A. Pregelj, M. Begovic, A. Rohatgi, and D. Novosel, “On optimization of reliability of distributed generation-enhanced feeders,” in *36th Annual Hawaii International Conference on System Sciences, 2003. Proceedings of the*, 2003, p. 6 pp.

[52] “State Electricity Profiles - Energy Information Administration.” [Online]. Available: http://www.eia.gov/electricity/state/.

[53] N. Mithulananthan, T. Oo, and L. Van Phu, “Distributed Gener ator in Power Distribution Placement System Using Genetic Algorithm to Reduce Losses,” vol. 9, no. 3, 2004.

[54] C. L. T. Borges and D. M. Falcao, “lmpact of distributed generation allocation and sizing on reliability, losses and voltage profile,” in *2003 IEEE Bologna Power Tech Conference Proceedings,*, vol. 2, pp. 396–400.

[55] T. Griffin, K. Tomsovic, D. Secrest, and A. Law, “Placement of dispersed generation systems for reduced losses,” in *Proceedings of the 33rd Annual Hawaii International Conference on System Sciences*, vol. vol.1, p. 9.

[56] J. V. Schmill, “Optimum Size and Location of Shunt Capacitors on Distribution Feeders,” *IEEE Trans. Power Appar. Syst.*, vol. 84, no. 9, pp. 825–832, Sep. 1965.

[57] M. H. Moradi and M. Abedini, “A combination of genetic algorithm and particle swarm optimization for optimal DG location and sizing in distribution systems,” *Int. J. Electr. Power Energy Syst.*, vol. 34, no. 1, pp. 66–74, Jan. 2012.

[58] D. Q. Hung, N. Mithulananthan, and R. C. Bansal, “Analytical Expressions for DG Allocation in Primary Distribution Networks,” *IEEE Trans. Energy Convers.*, vol. 25, no. 3, pp. 814–820, Sep. 2010.

[59] S. He, J. Y. Wen, E. Prempain, Q. H. Wu, J. Fitch, and S. Mann, “An improved particle swarm optimization for optimal power flow,” in *2004 International Conference on Power System Technology, 2004. PowerCon 2004.*, vol. 2, pp. 1633–1637.

[60] P. Umapathy, C. Venkataseshaiah, and M. S. Arumugam, “Particle Swarm Optimization with Various Inertia Weight Variants for Optimal Power Flow Solution,” *Discret. Dyn. Nat. Soc.*, vol. 2010, pp. 1–15, 2010.

[61] M. S. Arumugam and M. V. C. Rao, “On the performance of the particle swarm optimization algorithm with various inertia weight variants for computing optimal control of a class of hybrid systems,” *Discret. Dyn. Nat. Soc.*, vol. 2006, pp. 1–17, 2006.

[62] “IEEE Standard for Interconnecting Distributed Resources with Electric Power Systems.” [Online]. Available: http://grouper.ieee.org/groups/scc21/1547/1547_index.html.

[63] M. E. Baran and F. F. Wu, “Optimal capacitor placement on radial distribution systems,” *IEEE Trans. Power Deliv.*, vol. 4, no. 1, pp. 725–734, 1989.

[64] “Smart Grid | Department of Energy.” [Online]. Available: http://energy.gov/oe/technology-development/smart-grid.

[65] J. y. Liserre, Marco Sauter, Thilo Hung, “Future Energy Systems: Integrating Renwable Sources into the Smart Grid Through Industrial Electronics,” vol. 4, no. March, pp. 18–37, 2010.

[66] Jiyuan Fan and S. Borlase, “The evolution of distribution,” *IEEE Power Energy Mag.*, vol. 7, no. 2, pp. 63–68, 2009.

[67] S. Bruno, S. Lamonaca, G. Rotondo, U. Stecchi, and M. La Scala, “Unbalanced Three-Phase Optimal Power Flow for Smart Grids,” *IEEE Trans. Ind. Electron.*, vol. 58, no. 10, pp. 4504–4513, 2011.

[68] T.-H. Chen, M.-S. Chen, K.-J. Hwang, P. Kotas, and E. A. Chebli, “Distribution system power flow analysis-a rigid approach,” *IEEE Trans. Power Deliv.*, vol. 6, no. 3, pp. 1146–1152, Jul. 1991.

[69] C. S. Cheng and D. Shirmohammadi, “A three-phase power flow method for real-time distribution system analysis,” *IEEE Trans. Power Syst.*, vol. 10, no. 2, pp. 671–679, May 1995.

[70] R. D. Zimmerman, “Fast decoupled power flow for unbalanced radial distribution systems,” *IEEE Trans. Power Syst.*, vol. 10, no. 4, pp. 2045–2052, Nov. 1995.

[71] A. Gomez Esposito and E. Romero Ramos, “Reliable load flow technique for radial distribution networks,” *IEEE Trans. Power Syst.*, vol. 14, no. 3, pp. 1063–1069, 1999.

[72] Y. Zhu and K. Tomsovic, “Optimal distribution power flow for systems with distributed energy resources,” *Int. J. Electr. Power Energy Syst.*, vol. 29, no. 3, pp. 260–267, Mar. 2007.

[73] W. I. Zangwill, “Minimizing a function without calculating derivatives,” *Comput. J.*, vol. 10, no. 3, pp. 293–296, Mar. 1967.

[74] “Optimization by direct search: new perspective on some classical and modern methods.” [Online]. Available: http://www.cs.wm.edu/~va/research/sirev.pdf.

[75] M. A. Abido, “Optimal power ¯ ow using particle swarm optimization,” *Int. J. Electr. Power Energy Syst.*, vol. 24, pp. 563–571, 2002.

[76] J. Kennedy and R. Eberhart, “Particle swarm optimization,” in *Proceedings of ICNN’95 - International Conference on Neural Networks*, vol. 4, pp. 1942–1948.

[77] T. Ghanizadeh and E. Babaei, “Optimal power flow using iteration particle swarm optimization,” in *2012 IEEE 5th India International Conference on Power Electronics (IICPE)*, 2012, pp. 1–6.

[78] B. Zhao, C. X. Guo, and Y. J. Cao, “Improved particle swam optimization algorithm for OPF problems,” in *IEEE PES Power Systems Conference and Exposition, 2004.*, 2004, pp. 933–938.

[79] Z.-L. Gaing and X.-H. Liu, “New Constriction Particle Swarm Optimization for Security-Constrained Optimal Power Flow Solution,” in *2007 International Conference on Intelligent Systems Applications to Power Systems*, 2007, pp. 1–6.

[80] “Distribution Test Feeders - Distribution Test Feeder Working Group - IEEE PES Distribution System Analysis Subcommittee.” [Online]. Available: http://ewh.ieee.org/soc/pes/dsacom/testfeeders/.

[81] W. H. Kersting, “Radial distribution test feeders,” *IEEE Trans. Power Syst.*, vol. 6, no. 3, pp. 975–985, 1991.

[82] “How much U.S. energy consumption and electricity generation comes from renewable sources? - FAQ - U.S. Energy Information Administration (EIA).” [Online]. Available: http://www.eia.gov/tools/faqs/faq.cfm?id=92&t=4.

[83] C. Singh, “Reliability-Constrained Optimum Placement of Reclosers and Distributed Generators in Distribution Networks Using an Ant Colony System Algorithm,” *IEEE Trans. Syst. Man, Cybern. Part C (Applications Rev.*, vol. 38, no. 6, pp. 757–764, Nov. 2008.

[84] I. Ziari, G. Ledwich, A. Ghosh, D. Cornforth, and M. Wishart, “Optimal allocation and sizing of capacitors to minimize the transmission line loss and to improve the voltage profile,” *Comput. Math. with Appl.*, vol. 60, no. 4, pp. 1003–1013, Aug. 2010.

[85] L. A. Kojovic, “Integration of distributed generation in a typical USA distribution system,” in *16th International Conference and Exhibition on Electricity Distribution (CIRED 2001)*, 2001, vol. 2001, pp. v4–13–v4–13.

[86] J. Teng and Y. Liu, “A Novel ACS-Based Optimum,” *IEEE Trans. Power Syst.*, vol. 18, no. 1, pp. 113–120, 2003.

[87] Y. M. Atwa, S. Member, E. F. El-saadany, and S. Member, “With Renewable Distributed Generation During Islanded Mode of Operation,” vol. 24, no. 2, pp. 572–581, 2009.

[88] D. H. Popović, J. A. Greatbanks, M. Begović, and A. Pregelj, “Placement of distributed generators and reclosers for distribution network security and reliability,” *Int. J. Electr. Power Energy Syst.*, vol. 27, no. 5–6, pp. 398–408, Jun. 2005.

[89] W. Chai, Y. Wen, and W. Liu, “Optimal Allocation of Switches in DG Enhanced Distribution Systems,” in *2011 Asia-Pacific Power and Energy Engineering Conference*, 2011, pp. 1–5.

[90] G. Celli and F. Pilo, “Optimal sectionalizing switches allocation in distribution networks,” *IEEE Trans. Power Deliv.*, vol. 14, no. 3, pp. 1167–1172, Jul. 1999.

[91] A. Moradi and S. Member, “Optimal Switch Placement in Distribution Systems Using Trinary Particle Swarm Optimization Algorithm,” vol. 23, no. 1, pp. 271–279, 2008.

[92] R. Bezerra, G. C. Barroso, S. Le, and R. Furtado, “Power Distribution Network Planning Application Based on Multi-Objective Binary Particle Swarm Optimization Algorithm,” pp. 258–267, 2013.

[93] R. Billinton and S. Jonnavithula, “Optimal switching device placement in radial distribution systems,” *IEEE Trans. Power Deliv.*, vol. 11, no. 3, pp. 1646–1651, Jul. 1996.

[94] K. E. Parsopoulos and M. N. Vrahatis, “Particle Swarm Optimization Method for Constrained Optimization Problems.”

[95] Y. del Valle, G. K. Venayagamoorthy, S. Mohagheghi, J.-C. Hernandez, and R. G. Harley, “Particle Swarm Optimization: Basic Concepts, Variants and Applications in Power Systems,” *IEEE Trans. Evol. Comput.*, vol. 12, no. 2, pp. 171–195, Apr. 2008.

[96] I. Ziari, G. Ledwich, a. Ghosh, D. Cornforth, and M. Wishart, “Optimal allocation and sizing of capacitors to minimize the transmission line loss and to improve the voltage profile,” *Comput. Math. with Appl.*, vol. 60, no. 4, pp. 1003–1013, Aug. 2010.

[97] E. C. Laskari, K. E. Parsopoulos, and M. N. Vrahatis, “Particle swarm optimization for integer programming,” in *Proceedings of the 2002 Congress on Evolutionary Computation. CEC’02 (Cat. No.02TH8600)*, 2002, vol. 2, pp. 1582–1587.

[98] C. A. Warren, R. Ammon, and G. Welch, “A survey of distribution reliability measurement practices in the US,” *IEEE Trans. Power Deliv.*, vol. 14, no. 1, pp. 250–257, 1999.

[99] A. A. Chowdhury and D. O. Koval, “Value-Based Distribution System Reliability Planning,” vol. 34, no. 1, pp. 23–29, 1998.

[100] A. Moradi and M. Fotuhi-Firuzabad, “Optimal Switch Placement in Distribution Systems Using Trinary Particle Swarm Optimization Algorithm,” *IEEE Trans. Power Deliv.*, vol. 23, no. 1, pp. 271–279, Jan. 2008.

[101] M. J. Sullivan, D. Ph, M. Mercurio, J. Schellenberg, and M. A. Freeman, “E RNEST O RLANDO L AWRENCE B ERKELEY N ATIONAL L ABORATORY

Estimated Value of Service Reliability for Electric Utility Customers in the United States," 2009.

[102] R. C. Dugan, T. E. McDermott, and G. J. Ball, "Planning for distributed generation," *IEEE Ind. Appl. Mag.*, vol. 7, no. 2, pp. 80–88, 2001.

[103] V. H. MendezQuezada, J. RivierAbbad, and T. GomezSanRoman, "Assessment of Energy Distribution Losses for Increasing Penetration of Distributed Generation," *IEEE Trans. Power Syst.*, vol. 21, no. 2, pp. 533–540, May 2006.

[104] W. El-Khattam, K. Bhattacharya, Y. Hegazy, and M. M. A. Salama, "Optimal Investment Planning for Distributed Generation in a Competitive Electricity Market," *IEEE Trans. Power Syst.*, vol. 19, no. 3, pp. 1674–1684, Aug. 2004.

[105] A. Keane and M. O'Malley, "Optimal distributed generation plant mix with novel loss adjustment factors," in *2006 IEEE Power Engineering Society General Meeting*, 2006, p. 6 pp.

[106] C. Singh, "Multicriteria Design of Hybrid Power Generation Systems Based on a Modified Particle Swarm Optimization Algorithm," *IEEE Trans. Energy Convers.*, vol. 24, no. 1, pp. 163–172, Mar. 2009.

[107] Y. M. Atwa, S. Member, S. Member, M. M. A. Salama, R. Seethapathy, M. Assam, and S. Conti, "Adequacy Evaluation of Distribution System Including Wind / Solar DG During Different Modes of Operation," vol. 26, no. 4, pp. 1945–1952, 2011.

[108] K. Zou, A. P. Agalgaonkar, K. M. Muttaqi, and S. Perera, "Distribution System Planning With Incorporating DG Reactive Capability and System Uncertainties," *IEEE Trans. Sustain. Energy*, vol. 3, no. 1, pp. 112–123, Jan. 2012.

[109] "EPRI | Smart Grid Resource Center > Simulation Tool – OpenDSS." [Online]. Available: http://www.smartgrid.epri.com/SimulationTool.aspx.

[110] R. Chedid and S. Rahman, "Unit sizing and control of hybrid wind-solar power systems," *IEEE Trans. Energy Convers.*, vol. 12, no. 1, pp. 79–85, Mar. 1997.

[111] "U.S. Energy Information Administration (EIA) - Source." [Online]. Available: http://www.eia.gov/forecasts/aeo/electricity_generation.cfm.

[112] " Fuel Cell Systems Explained, 2nd Edition - James Larminie, Andrew Dicks." [Online]. Available: http://www.wiley.com/WileyCDA/WileyTitle/productCd-047084857X.html.

[113] "Solvay has successfully commissioned the largest PEM fuel cell in the world at SolVin's Antwerp plant." [Online]. Available: http://www.solvaychemicals.com/EN/News/20120206_Lillo.aspx.

[114] G. Maggio, V. Recupero, and L. Pino, "Modeling polymer electrolyte fuel cells: an innovative approach," *J. Power Sources*, vol. 101, no. 2, pp. 275–286, Oct. 2001.

[115] P. Buasri and Z. M. Salameh, "An electrical circuit model for a proton exchange membrane fuel cell (PEMFC)," in *2006 IEEE Power Engineering Society General Meeting*, 2006, p. 6 pp.

[116] W. H. Zhu, R. U. Payne, R. M. Nelms, and B. J. Tatarchuk, "Equivalent circuit elements for PSpice simulation of PEM stacks at pulse load," *J. Power Sources*, vol. 178, no. 1, pp. 197–206, Mar. 2008.

[117] R. F. Mann, J. C. Amphlett, M. A. I. Hooper, H. M. Jensen, B. A. Peppley, and P. R. Roberge, "Development and application of a generalised steady-state electrochemical model for a PEM fuel cell," *J. Power Sources*, vol. 86, no. 1–2, pp. 173–180, Mar. 2000.

[118] J. M. Correa, F. A. Farret, and L. N. Canha, "An analysis of the dynamic performance of proton exchange membrane fuel cells using an electrochemical model," in *IECON'01. 27th Annual Conference of the IEEE Industrial Electronics Society (Cat. No.37243)*, 2001, vol. 1, pp. 141–146.

[119] D. Chu, R. Jiang, and C. Walker, "Analysis of PEM fuel cell stacks using an empirical current–voltage equation," *J. Appl. Electrochem.*, vol. 30, no. 3, pp. 365–370, Mar. 2000.

[120] S. Yuvarajan, "A novel circuit model for pem fuel cells," in *Nineteenth Annual IEEE Applied Power Electronics Conference and Exposition, 2004. APEC '04.*, 2004, vol. 1, pp. 362–366.

[121] C. Wang, M. H. Nehrir, and S. R. Shaw, "Dynamic Models and Model Validation for PEM Fuel Cells Using Electrical Circuits," *IEEE Trans. Energy Convers.*, vol. 20, no. 2, pp. 442–451, Jun. 2005.

[122] W. Choi, J. W. Howze, and P. Enjeti, "Development of an equivalent circuit model of a fuel cell to evaluate the effects of inverter ripple current," *J. Power Sources*, vol. 158, no. 2, pp. 1324–1332, Aug. 2006.

[123] W. H. Zhu, R. U. Payne, and B. J. Tatarchuk, "PEM stack test and analysis in a power system at operational load via ac impedance," *J. Power Sources*, vol. 168, no. 1, pp. 211–217, May 2007.

[124] X. Yuan, J. C. Sun, H. Wang, and J. Zhang, “AC impedance diagnosis of a 500W PEM fuel cell stack,” *J. Power Sources*, vol. 161, no. 2, pp. 929–937, Oct. 2006.

[125] G. Li and P. G. Pickup, “Ionic Conductivity of PEMFC Electrodes,” *J. Electrochem. Soc.*, vol. 150, no. 11, p. C745, Nov. 2003.

[126] R. Holze, “The Kinetics of Oxygen Reduction at Porous Teflon-Bonded Fuel Cell Electrodes,” *J. Electrochem. Soc.*, vol. 131, no. 10, p. 2298, Oct. 1984.

[127] N. Wagner, “Characterization of membrane electrode assemblies in polymer electrolyte fuel cells using a.c. impedance spectroscopy,” *J. Appl. Electrochem.*, vol. 32, no. 8, pp. 859–863, Aug. 2002.

[128] O. Antoine, Y. Bultel, and R. Durand, “Oxygen reduction reaction kinetics and mechanism on platinum nanoparticles inside Nafion®,” *J. Electroanal. Chem.*, vol. 499, no. 1, pp. 85–94, Feb. 2001.

[129] A. M. Dhirde, N. V. Dale, H. Salehfar, M. D. Mann, and T.-H. Han, “Equivalent Electric Circuit Modeling and Performance Analysis of a PEM Fuel Cell Stack Using Impedance Spectroscopy,” *IEEE Trans. Energy Convers.*, vol. 25, no. 3, pp. 778–786, Sep. 2010.

[130] “Nexa Power module User’s Manual, 2003.” [Online]. Available: http://my.fit.edu/~swood/Fuel Cell Manual.pdf.

[131] “Fuel Cell | Membranes and Dispersions | DuPont™ Nafion®.” [Online]. Available: http://www2.dupont.com/FuelCells/en_US/products/nafion.html.

[132] X. Yuan, J. C. Sun, M. Blanco, H. Wang, J. Zhang, and D. P. Wilkinson, “AC impedance diagnosis of a 500W PEM fuel cell stack,” *J. Power Sources*, vol. 161, no. 2, pp. 920–928, Oct. 2006.

[133] A. Lasia, “Nature of the two semi-circles observed on the complex plane plots on porous electrodes in the presence of a concentration gradient,” *J. Electroanal. Chem.*, vol. 500, no. 1–2, pp. 30–35, Mar. 2001.

[134] Y. Bultel, L. Genies, O. Antoine, P. Ozil, and R. Durand, “Modeling impedance diagrams of active layers in gas diffusion electrodes: diffusion, ohmic drop effects and multistep reactions,” *J. Electroanal. Chem.*, vol. 527, no. 1–2, pp. 143–155, May 2002.

[135] D. W. Marquardt, “An Algorithm for Least-Squares Estimation of Nonlinear Parameters,” *J. Soc. Ind. Appl. Math.*, vol. 11, no. 2, pp. 431–441, Jun. 1963.

[136] S. K. Roy, M. E. Orazem, and B. Tribollet, “Interpretation of Low-Frequency Inductive Loops in PEM Fuel Cells,” *J. Electrochem. Soc.*, vol. 154, no. 12, p. B1378, Dec. 2007.

[137] S. Kim, S. Shimpalee, and J. W. Van Zee, “The effect of stoichiometry on dynamic behavior of a proton exchange membrane fuel cell (PEMFC) during load change,” *J. Power Sources*, vol. 135, no. 1–2, pp. 110–121, Sep. 2004.

[138] J. Cho, H.-S. Kim, and K. Min, “Transient response of a unit proton-exchange membrane fuel cell under various operating conditions,” *J. Power Sources*, vol. 185, no. 1, pp. 118–128, Oct. 2008.

[139] J. W. Tester, B. J. Anderson, A. S. Batchelor, D. D. Blackwell, R. DiPippo, E. M. Drake, J. Garnish, B. Livesay, M. C. Moore, K. Nichols, S. Petty, M. N. Toksoz, R. W. Veatch, R. Baria, C. Augustine, E. Murphy, P. Negraru, and M. Richards, “Impact of enhanced geothermal systems on US energy supply in the twenty-first century.,” *Philos. Trans. A. Math. Phys. Eng. Sci.*, vol. 365, no. 1853, pp. 1057–94, Apr. 2007.

[140] “pure cycle.” [Online]. Available: http://www.purecyclewater.com/projects.html.

[141] "Organic Rankin Cycle." [Online]. Available : https://inlportal.inl.gov/portal/server.pt/community/home/255

[142] “IEEE SA - 519-1992 - IEEE Recommended Practices and Requirements for Harmonic Control in Electrical Power Systems.” [Online]. Available: http://standards.ieee.org/findstds/standard/519-1992.html.

[143] “IEEE SA - 1453-2011 - IEEE Recommended Practice--Adoption of IEC 61000-4-15:2010, Electromagnetic compatibility (EMC)--Testing and measurement techniques--Flickermeter--Functional and design specifications.” [Online]. Available: https://standards.ieee.org/findstds/standard/1453-2011.html.

[144] “American National Standard For Electric Power Systems and Equipment — Voltage Ratings ( 60 Hertz ),” 2011.

[145] I. M. de Alegría, J. Andreu, J. L. Martín, P. Ibañez, J. L. Villate, and H. Camblong, “Connection requirements for wind farms: A survey on technical requierements and regulation,” *Renew. Sustain. Energy Rev.*, vol. 11, no. 8, pp. 1858–1872, Oct. 2007.

[146] “IEEE Application Guide for IEEE Std 1547(TM), IEEE Standard for Interconnecting Distributed Resources with Electric Power Systems.” pp. 1–217, 2009.

[147] “MathWorks - MATLAB and Simulink for Technical Computing - B.” [Online]. Available: http://www.mathworks.com/.

[148] “ArcGIS - Mapping and Spatial Analysis for Understanding Our World.” [Online]. Available: http://www.esri.com/software/arcgis.

[149] R. A. Cunniff and R. L. Bowers, “Final Technical Report; Geothermal Resource Evaluation and Definitioni (GRED) Program-Phases I, II, and III for the Animas Valley, NM Geothermal Resource,” Albuquerque, NM, Aug. 2005.

[150] “Catalog of thermal waters in New Mexico (Hydrologic report): W. Kelly Summers: Amazon.com: Books.” [Online]. Available: http://www.amazon.com/Catalog-thermal-waters-Mexico-Hydrologic/dp/B0006CSA54.

[151] J. C. Witcher, J. W. Lund, and D. E. Seawright, “LIGHTNING DOCK KGRA NEW MEXICO ’ S LARGEST GEOTHERMAL GREENHOUSE , LARGEST AQUACULTURE FACILITY , AND FIRST,” *Geo-Heat Center, Oregon Ist. Technol. Quaterly Bull.*, pp. 37–41, 2002.

[152] “New Mexico Utility Files Renewable Energy Plan with Regulators.” [Online]. Available: http://geothermalresourcescouncil.blogspot.com/2012/05/usa-new-mexico.html.

[153] W. E. Elston, E. G. Deal, and M. J. Logsdon, “Geology and geothermal waters of Lightning Dock region, Animas Valley and Pyramid Mountains, Hidalgo County, New Mexico,” Jan. 1983.

[154] P. J. Lienau, “Geothermal Greenhouse Development Update,” *Geo-Heat Center, Oregon Ist. Technol. Quaterly Bull.*, no. January, pp. 5–7, 1997.

[155] D. N. Schochet and R. A. Cunnif, “Development of a Plan to Implement Enhanced Geothermal System (EGS) in Animal Valley, New Mexico,” 2001.

[156] K. M. O’Brien and W. J. Stone, “Role of Geological and Geophysical Data in Modeling a Southwestern Alluvial Basin,” *Ground Water*, vol. 22, no. 6, pp. 717–727, Nov. 1984.

[157] C. Smith, “GEOPHYSICS , GEOLOGY AND GEOTHERMAL LEASING STATUS OF THE LIGHTNING DOCK KGRA , ANIMAS VALLEY , NEW MEXICO,” *New Mexivo Geol.Soc.Guidebook, 29th F. Conf. L. Cochise*, 1978.

[158] “Ground water in Animas Valley, Hidalgo County, New Mexico, (New Mexico. State Engineer Office. Technical report): Harold O Reeder: Amazon.com: Books.” [Online]. Available: http://www.amazon.com/Hidalgo-Mexico-Engineer-Office-Technical/dp/B0007IVEKK.

[159] S. Dahal and H. Salehfar, “Impact of Distributed Generators on the Power Loss and Voltage Profile of Three Phase Unbalanced Distribution Networks”, *International Journal of Power and energy systems,* submitted

[160] S. Dahal and H. Salehfar, “Reliability Evaluation of DG Enhanced Unbalanced Distribution Networks”, in preparation.

[161] S. Dahal and H. Salehfar, “Cost Minimization Planning for Allocation of Distributed Generators in Unbalanced Distribution Network”, in preparation.

[162] S. Dahal, M. Mann, and H. Salehfar, “Development and verification of an Electrical Circuit Model of Proton Electrolyte Membrane (PEM) fuel cell using Impedance spectroscopy,” *Journal of Power Sources*, submitted.

[163] S. Dahal, H. Salehfar, W. Gosnold, and M. Mann, “Modeling and simulation of the interface between geothermal power plant based on organic rankin cycle and the electric grid,” *Geothermal Research Council transactions*, vol. 34, pp 1011-1016, Oct. 2010.

[164] S. Dahal, M. R. McDonald, and B. Bubach, “Evaluation of Geothermal Potential of Lightning Dock KGRA, New Mexico,” *Geothermal Research Council transaction,* vol. 36, Sept. 2012